



**HAL**  
open science

# Déformation et circulations de fluides dans les zones de subduction

Hugues Raimbourg

► **To cite this version:**

Hugues Raimbourg. Déformation et circulations de fluides dans les zones de subduction. Planète et Univers [physics]. Université d'Orléans, 2019. tel-02081040

**HAL Id: tel-02081040**

**<https://insu.hal.science/tel-02081040>**

Submitted on 27 Mar 2019

**HAL** is a multi-disciplinary open access archive for the deposit and dissemination of scientific research documents, whether they are published or not. The documents may come from teaching and research institutions in France or abroad, or from public or private research centers.

L'archive ouverte pluridisciplinaire **HAL**, est destinée au dépôt et à la diffusion de documents scientifiques de niveau recherche, publiés ou non, émanant des établissements d'enseignement et de recherche français ou étrangers, des laboratoires publics ou privés.

Institut des Sciences de la Terre d'Orléans

**HDR** présentée par :  
**Hugues RAIMBOURG**

soutenue le : 11/02/2019

Discipline/ Spécialité : Sciences de la Terre

**Déformation et circulations de fluides  
dans les zones de subduction**

**RAPPORTEURS :**

|                        |  |
|------------------------|--|
| <b>Martine BUATIER</b> | Professeure, Université de Franche-Comté |
| <b>Donald FISHER</b>   | Professeur, PennState University         |
| <b>François RENARD</b> | Professeur, Université de Grenoble       |

---

**JURY:**

|                        |   |
|------------------------|---|
| <b>Bruno SAILLET</b>   | Directeur de Recherche, Président du jury         |
| <b>Serge LALLEMAND</b> | Directeur de Recherche, Université de Montpellier |
| <b>Laurent JOLIVET</b> | Professeur, Sorbonne Université                   |
| <b>Holger STUNITZ</b>  | Professeur, Université d'Orléans                  |

## Avant-propos

Ce manuscrit consiste principalement en une synthèse de mes activités de recherche mises en œuvre depuis 10 ans, date de mon recrutement à l'ISTO. J'ai mis l'accent dans cette synthèse sur les questions relatives aux fluides et à la déformation dans les zones de subduction, un travail que j'ai initié en post-doc au Japon et qui concentre depuis l'essentiel de mon temps et de mon effort. Je me suis néanmoins intéressé à d'autres thèmes de recherche, qui par souci de cohérence ne sont pas abordées dans ce manuscrit.

J'ai découpé ce document en cinq chapitres. Le premier est un résumé de l'ensemble de mes activités, de mes responsabilités et de ma production scientifique en tant qu'enseignant-chercheur à l'ISTO.

Le chapitre deux consiste en une synthèse, du point de vue d'un non-spécialiste, des grands résultats issus de la géophysique concernant les zones de subduction. Même s'il est imparfait, ce travail de synthèse est rendu nécessaire par l'essor fantastique des méthodes géophysiques pour décrire les processus à l'œuvre dans les marges actives. Les résultats sont si nombreux que cette synthèse sera en partie obsolète au moment où elle sera imprimée. L'objectif de ce travail de synthèse, au-delà du résumé de travaux qui me sont étrangers et souvent en dehors de ma compétence, est aussi et surtout de mettre en lumière les grandes questions sur lesquelles la géologie de terrain et l'analyse de structures fossiles peut apporter des réponses pertinentes.

Le chapitre trois est consacré la déformation et se base sur tout le travail de terrain que j'ai réalisé dans le prisme fossile japonais depuis dix ans. Je ne décris pas ici le travail de grande échelle, qui vise à insérer les affleurements, les structures et les microstructures dans un cadre tectonique d'évolution de la marge japonaise depuis la fin du Crétacé. Ce travail de contextualisation est cependant la condition nécessaire pour que l'interprétation des structures de moyenne et petite échelle soit pertinente. Dans cette description des structures tectoniques, j'ai mis l'accent sur les processus de déformation, et notamment sur l'opposition entre structures localisées (failles, pseudotachylytes) et structures de déformation distribuée.

Le chapitre quatre est principalement consacré aux circulations de fluides, à partir de l'enregistrement des veines syn-cinématiques. Ce chapitre détaille les études que j'ai réalisées à la fois sur les quartz qui forment ces veines, ainsi que sur les inclusions fluides qu'elles

contiennent et qui sont le témoin le plus direct des fluides profonds. Je passe en revue un ensemble de propriétés chimiques de ces fluides, avec comme objectif de retracer les échelles de temps et d'espace des transferts de fluides, et leur lien éventuel avec la déformation.

Le chapitre cinq est un aperçu des différentes questions de recherche sur lesquelles je compte concentrer mes efforts dans les années futures, en m'appuyant sur mon propre travail et sur les efforts des doctorants qui m'accompagneront.

Les chapitres deux à cinq sont rédigés en anglais. Le choix de cette langue est avant tout dicté par des questions d'efficacité. En effet, le contenu de ces chapitres a vocation, pour tout ou partie, à faire l'objet de publications scientifiques.

Pour finir, les résultats obtenus jusqu'à maintenant n'auraient pas vu le jour, ou bien avec une qualité bien moindre, sans le soutien et la participation d'un ensemble de collègues et d'étudiants en thèse. Je tiens en particulier à remercier les collègues qui ont directement participé à ce travail, Vincent Famin, Romain Augier, Laurent Jolivet, Holger Stunitz, Philippe Agard, Asuka Yamaguchi et Yujin Kitamura. Les étudiants sont aussi les premiers contributeurs des résultats que je présente, et notamment tous les étudiants dont j'ai encadré la thèse : Leslie Gadenne, Giulia Palazzin, Alexandre Beaudoin, Nicolas Mansard, Lucille Nègre, Clément Montmartin, Benoît Béviard, Benjamin Moris-Muttoni. Je remercie l'ensemble des collègues du laboratoire, pour les nombreuses et enrichissantes discussions, ainsi que les responsables de l'ISTO, de l'OSUC et des différents programmes de recherche (Labex, Equipex et ERC), pour leur soutien continu à mon travail de recherche. Pour finir, un grand merci à Lise.

Hugues Raimbourg

# Table des matières

|  |    |
|--|----|
| Chapitre I : Curriculum Vitae.....   | 8  |
| A.  Eléments biographiques .....   | 8  |
| B.  Carrière universitaire.....  | 8  |
| C.  Activités de recherche .....   | 8  |
| 1.  Thèmes de recherche.....   | 8  |
| 2.  Domaines d'expertise.....  | 11 |
| 3.  Collaborations principales .....   | 11 |
| 4.  Animation de la recherche et responsabilités institutionnelles .....   | 13 |
| 5.  Conférences et séminaires.....   | 14 |
| D.  Financement de la recherche.....   | 15 |
| E.  Encadrement de thèses et postdoc.....  | 16 |
| F.  Publications .....   | 17 |
| G.  Activités d'enseignement.....  | 19 |
| Chapter II: The deformation of the subduction plate interface, from the point of view of geophysics and experiments..... | 21 |
| A.  Mechanical behavior of the plate interface in subduction zones .....   | 21 |
| 1.  A simple model: the seismogenic zone model.....  | 21 |
| 2.  Variations in coupling within the seismogenic zone .....   | 23 |
| 3.  The insights from recent mega-earthquakes .....  | 24 |
| 4.  Rapid aseismic slip along the plate interface .....  | 27 |
| 5.  Conclusion .....   | 31 |
| B.  Intrinsic factors controlling the deformation mode along the plate interface .....                                   | 31 |
| 1.  Plate roughness .....  | 31 |
| 2.  Nature of subducting material.....   | 34 |
| 3.  Geodynamical parameters.....   | 36 |
| 4.  Geophysical attributes of the plate interface: from observations to physical properties.....                         | 38 |
| 5.  Conclusion .....   | 40 |
| C.  The role of fluid pressure to the mechanical behavior of the plate interface.....                                    | 40 |
| 1.  Shallow overpressure .....   | 40 |
| 2.  Deep overpressure.....   | 44 |
| 3.  Mechanical effect of fluid pressure.....   | 47 |
| 4.  Conclusions.....   | 48 |
| D.  Summary .....  | 49 |
| Chapter III: The deformation of the subduction plate interface, from the point of view of field geology.....             | 52 |
| A.  Introduction.....  | 52 |

|    |   |     |
|----|---|-----|
| 1. | Modelling plate subduction deformation .....  | 52  |
| 2. | The natural structures that illustrate plate subduction deformation.....              | 55  |
| B. | Geological settings .....   | 58  |
| 1. | General architecture of the Shimanto Belt and investigated areas .....                | 58  |
| 2. | P-T conditions of deformation .....   | 60  |
| 3. | Geodynamical evolution and structural settings of deformation .....                   | 61  |
| C. | Deformation within mélanges .....   | 62  |
| 1. | General structure of mélange zones .....  | 62  |
| 2. | Deformation structures.....   | 63  |
| 3. | Deformation microstructures .....   | 66  |
| 4. | Deformation kinematics .....  | 68  |
| D. | Localized deformation in fault zones and pseudotachylytes.....                        | 70  |
| E. | Discussion .....  | 72  |
| 1. | Deformation microstructures attending distributed deformation in mélange .....        | 72  |
| 2. | Kinematics of mélange deformation .....   | 73  |
| 3. | Underplating process of mélange.....  | 75  |
| 4. | Model of subduction plate boundary .....  | 79  |
| F. | Conclusion .....  | 82  |
|    | Chapter IV: Fluid properties and circulation in the depth of subduction zones.....    | 86  |
| A. | Fluid sources along the plate interface.....  | 86  |
| 1. | Compaction sources .....  | 86  |
| 2. | Dehydration sources.....  | 87  |
| B. | Chemistry of subduction zone fluids .....   | 92  |
| C. | The fluid circulation at depth: in general, restricted to the very local scale .....  | 96  |
| 1. | Shallow transfers (shallower than the BPT) .....                                      | 96  |
| 2. | Deep transfers (deeper than BPT, down to HP and UHP).....                             | 99  |
| D. | Evidences for fluid transfers .....   | 102 |
| 1. | The record of fluid transfers in veins.....   | 102 |
| 2. | Our past work on veins .....  | 104 |
| E. | Chemical characteristics of the circulating fluids .....                              | 110 |
| 1. | Fluid inclusion studies .....   | 110 |
| 2. | Quartz studies.....   | 111 |
| F. | Relationship between deformation and fluid flow: the action of pressure solution. 112 |     |
| 1. | The effect of clays.....  | 114 |
| 2. | The effect of reactions .....   | 114 |
| 3. | Diffusion coefficients and the wetted structure of grain boundaries .....             | 115 |
| 4. | Conclusions.....  | 116 |
| G. | Relationship between deformation and fluid flow: slow slip events .....               | 116 |

|   |     |
|---|-----|
| Chapter V: Research Project .....   | 120 |
| A. Tectonic evolution and structure of mélangé zones .....  | 120 |
| 1. Further work on the Shimanto Belt.....   | 120 |
| 2. Extension to other case studies- Kodiak accretionary prism .....   | 121 |
| B. Fluid properties and its relationship to deformation .....   | 122 |
| 1. Fluid circulation: insights from the composition of fluid inclusions.....  | 122 |
| 2. Fluid pressure as a key factor of solid rock deformation and vein precipitation.                                   | 123 |
| 3. Relationships between fluid properties and deep SSE in fossil examples.....  | 125 |
| C. Experimental approach to rheology at seismogenic depths – smectite dehydration and its influence on friction ..... | 125 |
| References .....  | 128 |

## Liste des illustrations

|  |    |
|--|----|
| Figure 1: Worldwide distribution of earthquakes  | 21 |
| Figure 2: A) Hypocenters distribution across the Aleutian subduction zone and B) foreshocks of Mw9.0 Tohoku-Oki earthquakes                            | 22 |
| Figure 3: Seismogenic zone model in subduction margins   | 23 |
| Figure 4: Comparison of interseismic coupling and coseismic slip for the 2011 Tohoku-Oki earthquake in NE Japan and the 2010 Maule earthquake in Chile | 25 |
| Figure 5: Coseismic slip near the trench during the Mw9.0 Tohoku-Oki earthquake  | 26 |
| Figure 6: Slow slip events and tremors in the Cascadia subduction zone   | 29 |
| Figure 7: Relationship between subducting plate roughness and seismicity in western Pacific  | 31 |
| Figure 8: Distribution of seafloor topography for segments of subduction zones without rupture (yellow) and with large earthquakes (blue)              | 32 |
| Figure 9: P-wave tomography analysis above the NE Japan plate interface  | 34 |
| Figure 10: Friction experiments about the influence of lithology on slip stability (left) and on slip weakening (right)                                | 35 |
| Figure 11: Subduction zones typology   | 37 |
| Figure 12: Seismic cross-section of the Nankai accretionary prism off Kii peninsula.   | 41 |
| Figure 13: Velocity-porosity relationship for high-porosity sediments from the Nankai Trough   | 43 |
| Figure 14: Velocity-porosity relationship at low porosity  | 44 |
| Figure 15: Comparison of the anomalies in Poisson ratio (left) and $V_p/V_s$ ratio (right) in subduction zones with the experimental measurements.     | 47 |
| Figure 16: Numerical models of the earthquake cycle.   | 53 |
| Figure 17: Channel flow model of subduction zone   | 55 |
| Figure 18: Conceptual models of large-scale fault zone, in strike-slip settings  | 55 |
| Figure 19: Roof thrust fault of the Mugi mélangé, Japan  | 57 |
| Figure 20: Geodynamical settings of the Shimanto Belt, Japan   | 59 |
| Figure 21: Geological map of Shimanto Belt on eastern Kyushu.  | 59 |
| Figure 22: Distribution of mélangé units within the Shimanto Belt on Shikoku   | 60 |
| Figure 23: Structure of the Okitsu mélangé   | 63 |
| Figure 24: Deformation structures within the Okitsu mélangé (outcrop 220)  | 64 |
| Figure 25: Deformation structures within the Mugi mélangé (outcrop 342)  | 65 |
| Figure 26: Deformation microstructures in Hyuga mélangé (outcrop 147)  | 65 |
| Figure 27: Shear zone network and vein precipitation in mélangé  | 66 |
| Figure 28: Detail of a shear band cutting across elongated lenses of quartz and siltstone  | 66 |
| Figure 29: Deformation microstructures within the shear band in Figure 28  | 67 |
| Figure 30: Kinematics of deformation within the Hyuga mélangé  | 68 |
| Figure 31: Kinematics of deformation in the Okitsu mélangé unit  | 69 |

|   |     |
|---|-----|
| Figure 32: Kinematics of deformation in the Mugi mélange  | 69  |
| Figure 33: Outcrop of the Nobeoka Tectonic Line (NTL) along the eastern coast of Kyushu   | 71  |
| Figure 34: Thin section of the NTL fault core   | 71  |
| Figure 35: Model of underplating of mélangé thrust sheets   | 75  |
| Figure 36: Underplating models, with distributed (A) and localized (B) deformation  | 78  |
| Figure 37: Rates of water production in subducting sediments, resulting from the contribution of sediment compaction and smectite-to-illite reactions           | 87  |
| Figure 38: Water content of metasedimentary rocks from various metamorphic grades   | 88  |
| Figure 39: Evolution of H <sub>2</sub> O and CO <sub>2</sub> content with burial for the average sediment GLOSS and for a clay-rich marl                        | 89  |
| Figure 40: Evolution of H <sub>2</sub> O and CO <sub>2</sub> content in basalts as a function of P and T  | 90  |
| Figure 41: B and Li concentration in fluid interacting with sediments in experiments  | 94  |
| Figure 42: B and Li concentration in fluids from variable depth domains   | 94  |
| Figure 43: Compilation of salinity in fluid inclusions from metasediments and metabasites in subduction zones   | 95  |
| Figure 44: $\delta^{18}\text{O}$ and $\delta^{13}\text{C}$ of carbonate veins in terranes from the Franciscan Complex   | 98  |
| Figure 45: Whole-rock N content and $\delta^{15}\text{N}$ systematics of sediments from different subduction settings   | 100 |
| Figure 46: B, Li, K, Cs and Rb concentrations in metasediments from the Schistes Lustrés and the Catalina Schists   | 101 |
| Figure 47: Evolution of B, Li, Cs and Rb in the Catalina Schists  | 101 |
| Figure 48: Growth textures in alpine fissure quartz and associated fluid pressure   | 104 |
| Figure 49: Microstructure of veins from the Shimanto Belt revealed by cathodoluminescence   | 107 |
| Figure 50: Hydrological model of the subduction interface   | 109 |
| Figure 51: Ice melting (left) and homogenization (right) temperatures of the fluid inclusions in the veins from the Hyuga Tectonic Mélange.                     | 111 |
| Figure 52: Stress–depth diagram showing the strength predicted with pressure solution and a small transport distance in pressure solution flow laws             | 114 |
| Figure 53: Crack-seal textures in quartz veins from the Kodiak Central Belt   | 118 |
| Figure 54: Deformation and veining in Waterfall Bay mélangé from the Kodiak formation   | 121 |
| Figure 55: Comparison of the P-T record of fluid inclusions in samples corresponding to the seismogenic zone with thermal régimes from modern subduction zones. | 124 |
| Figure 56: (Left): Foliation-parallel and shear veins in the Makimine Group, Japan  | 125 |
| Figure 57: Slip instabilities onset with temperature during experimental deformation of powders of K-exchanged smectite-rich sediments                          | 126 |
| Figure 58: High-pressure vessel with a transparent window   | 127 |

# Chapitre I : Curriculum Vitae

## A. Eléments biographiques

Né le 28 Avril 1978 (Paris)  
Nationalité : française  
Pacé, 2 enfants (9 et 6 ans)  
Résidence : 51 rue Marchais 45100 Orléans  
Email : hugues.raimbourg@univ-orleans.fr

## B. Carrière universitaire

- 2009-** Maître de conférence à l'ISTO, Université d'Orléans, France  
**2008-2009** Postdoc au JAMSTEC, Yokosuka, Japon, avec Masataka Kinoshita  
"Experimental study of seismic properties of accretionary prisms"  
**2005-2007** Postdoc JSPS à l'Université de Tokyo avec Gaku Kimura  
"Microstructure evolution and localization of ductile deformation, the example of the Hidaka Main Zone, Hokkaido, Japan".  
**2001-2005** Thèse en géosciences et ressources naturelles, soutenue le 28 Octobre 2005, à l'Université Paris VI (UPMC), sous la direction de Laurent Jolivet and Yves Leroy  
"Mécanismes d'éclogitisation et conséquences pour l'exhumation des roches métamorphiques de haute-pression" (Jury : Christian Chopin, Denis Gapais, Herman Van Roermund, Giorgio Ranalli, Hakon Austrheim).  
**1998-2001** Magistère des Sciences de la Terre à l'ENS Ulm  
**2001** DEA, "Mécanique et matériaux" Ecole Polytechnique, Ecole des Mines de Paris  
**2000** Maîtrise en Sciences de la Terre, Université Paris VI  
**1999** Licence en Sciences de la Terre, Université Paris VI  
**1998** Admission à l'ENS Ulm, Paris, concours E/S

## C. Activités de recherche

### 1. *Thèmes de recherche*

Mon début de carrière s'est concentré sur l'exhumation des roches de haute pression dans des zones de subduction, à partir de l'exemple des Calédonides norvégiennes. Mon travail a combiné la géologie structurale sur le terrain avec la pétrologie métamorphique et l'analyse des microstructures afin de proposer un modèle mécanique grande échelle de zones de subduction.

Mon intérêt pour les microstructures de déformation m'a amené à poursuivre dans un postdoc au Japon sur la question de l'affaiblissement mécanique et la localisation de la déformation dans les mylonites de haute température. L'environnement scientifique au Japon, centré sur la question des tremblements de terre, m'a amené à commencer à étudier en parallèle le prisme d'accrétion Shimanto, l'un des meilleurs exemples à terre des zones de subduction. En

parallèle, un second contrat postdoctoral au Japon, au Jamstec (l'équivalent japonais de l'Ifremer), m'a permis de faire des expériences de déformation en laboratoire, avec des mesures acoustiques et mécaniques sur les sédiments de la fosse de subduction de Nankai.

Depuis mon recrutement à l'Université d'Orléans, j'ai appliqué ces différentes approches à un objet unique, les zones de subduction. Une partie de mon activité de recherche s'appuie sur le **travail de terrain (1)**, avec des missions au Japon (~1/an), et une extension de cette activité vers les Alpes depuis 2014. Le cadre géologique grande échelle fourni par ce travail de terrain permet de reconstruire un calendrier tectonique, nécessaire pour interpréter les **microstructures de déformation (2)** et les **propriétés du fluide** contemporain de cette déformation. En parallèle, j'ai développé une **activité expérimentale (3)** à Orléans, qui vise à simuler les processus de déformation tout au long de l'interface des plaques, depuis des domaines superficiels (déformation d'argiles en presse Paterson) jusqu'aux domaines profonds (déformation du quartz en presse de Griggs). Les champs de recherche relatifs à ces trois thèmes ainsi que les résultats majeurs sont décrits dans ce qui suit.

(1) Géologie de terrain et tectonique des zones de subduction/collision : j'ai réalisé au cours de plusieurs missions de terrain successives dans la zone de subduction fossile japonaise la collecte de nombreuses données structurales, concernant la cinématique de la déformation. En parallèle, l'analyse Raman de la matière organique sur des échantillons de roche m'a permis de déterminer le champ de paléo-température associé à cette déformation. A partir de ces éléments, j'ai pu reconstruire un calendrier d'évolution tectonique de la chaîne depuis la fin du Crétacé (Raimbourg et al., 2014a; Raimbourg et al., 2017a; Raimbourg et al., 2009). J'ai pu montrer en particulier que, loin de fonctionner en régime « permanent », avec des paramètres géométriques et cinématiques constants dans le temps, la zone de subduction a une histoire faite d'une succession de phases dans des régimes tectoniques très variables. J'ai notamment mis en évidence le rôle majeur joué par un court épisode de collision au début du Miocène dans la structure actuelle de la chaîne.

(2) Microstructures de déformation et circulations de fluides dans des roches naturelles: mon activité principale se concentre sur la détermination des processus de déformation à l'œuvre et des relations entre ceux-ci et les fluides. Je me suis concentré sur les domaines de mélange tectonique dans les zones de subduction, qui localisent une part importante de la déformation liée au déplacement relatif entre les plaques. Dans ces zones de mélange, la déformation est distribuée sur des épaisseurs de plusieurs centaines de mètres, à l'inverse d'une déformation localisée sur des failles (Palazzin, 2016). Cette déformation distribuée est à mettre

en parallèle du glissement asismique, cad sans séisme majeur, qui domine en moyenne les frontières de plaques en subduction. Le mécanisme élémentaire qui sous-tend la déformation distribuée est la pression-dissolution des niveaux les plus résistants, riches en quartz. La présence d'un fluide aqueux et sa capacité à transporter des éléments en solution est donc la clé de la déformation distribuée, qui se manifeste par la formation d'un réseau très dense de fentes et veines remplies de quartz précipité. En conséquence, j'ai apporté une grande attention à déterminer la nature du fluide présent et les échelles de temps et d'espace de ses cellules de circulation (Raimbourg et al., 2018; Raimbourg et al., 2014b; Raimbourg et al., 2015). J'ai ainsi pu mettre en évidence le fort contraste hydrologique entre le domaine de profondeur « sismogène » et le domaine « asismique » sous-jacent (avec une limite correspondant à l'activation avec la température de la déformation plastique du quartz). Tandis que dans le domaine asismique les circulations de fluide se font uniquement à l'échelle locale, en système hydrologiquement fermé, aux profondeurs sismogènes, le système alterne entre des phases d'équilibrage local et des phases d'ouverture, pendant lesquelles un fluide exotique pénètre et infiltre la roche. La poursuite de ce travail est de contraindre géochimiquement ce qui différencie ces deux étapes, fermée et ouverte, du cycle hydrologique, et de relier ces alternances à la déformation (notamment au cycle sismique ou aux instabilités de glissement lentes) et plus généralement au comportement macroscopique de la zone de subduction.

(3) Processus de déformation à partir d'expériences de laboratoire: En parallèle du travail sur les systèmes naturels, une part croissante de mon activité de recherche est dédiée à la compréhension des mécanismes de déformation actifs dans les roches, à partir d'expériences de déformation de laboratoire. Je me suis en particulier intéressé aux processus de déformation du quartz en présence d'eau, qui correspondent aux roches sédimentaires, très riches en eau, qui subissent lors de la subduction une augmentation de température et la transition entre déformation cassante et plastique. L'effet de l'eau sur le quartz, connu depuis plus de cinquante ans sous le nom d'adoucissement hydrolytique (Griggs, 1967), reste mal compris, autant dans ses mécanismes élémentaires que dans leur traduction en termes de lois de fluage. L'originalité de notre travail sur ce thème est de combiner déformation expérimentale et mesures par infrarouge de la distribution de l'eau, afin de mettre en lumière les rétroactions déformation-transfert d'eau. Nous avons pu notamment distinguer deux effets mécaniques distincts de l'eau : d'une part la présence d'eau rend la déformation plastique des grains plus efficace (thèse en cours de Lucille Nègre) ; d'autre part l'eau accélère la recristallisation jusqu'à des tailles de grains suffisamment petites pour que les transferts diffusifs aux joints de grains contribuent significativement à affaiblir mécaniquement la roche (Palazzin et al., 2018). L'autre volet de

ces activités expérimentales concerne la déformation des argiles, qui s'applique au glissement dans le domaine superficiel des zones de subduction. Mon travail a pour objet de combiner propriétés mécaniques et réactions diagénétiques des argiles, en particulier de la smectite. La smectite a pour particularité de pouvoir incorporer une quantité variable d'eau dans son espace interfoliaire, en fonction notamment des conditions de température. Un travail préliminaire nous a permis de montrer l'effet majeur de la température sur la stabilité frictionnelle de la smectite (Gadonne, 2015). A partir de ce travail, et en utilisant l'équipement in situ de l'ISTO, mon objectif est de contraindre expérimentalement les réactions d'hydratation/déshydratation de la smectite et de mettre en relations ces propriétés thermodynamiques avec le comportement mécanique du minéral.

## *2. Domaines d'expertise*

Le travail de terrain : l'analyse de la cinématique de la déformation, due métamorphisme et de leurs relations est l'une de mes compétences centrales, que j'ai développée depuis mon doctorat dans les Calédonides et poursuivie dans d'autres marges fossiles que sont le prisme Shimanto et les Alpes.

Caractérisation des minéraux et des fluides : Mon étude des processus de déformation s'appuie sur une expertise sur l'analyse EBSD de textures minérales. En parallèle, j'ai fait un usage intensif des techniques de microthermométrie pour analyser le fluide piégé dans des inclusions. Je me suis familiarisé avec plusieurs outils nécessaires pour caractériser les conditions de déformation : l'analyse par infra-rouge de l'eau contenu dans le quartz, l'analyse Raman de la matière organique pour dériver les paléo-températures, l'analyse thermobarométrique de phases minérales de bas grade.

La déformation expérimentale : par l'intermédiaire de mon postdoc au Japon et des deux premières thèses que j'ai encadrées à Orléans, j'ai développée une expertise de la déformation expérimentale qui est essentielle pour mon projet de recherche futur. Mon expérience couvre une large gamme de conditions de pression et de température, depuis les sédiments superficiels jusqu'à la déformation ductile des roches profondes, et un large éventail de propriétés, depuis les propriétés acoustiques jusqu'à la viscosité des roches en fluage.

## *3. Collaborations principales*

Depuis mon postdoc à l'Université de Tokyo, j'ai développée des collaborations scientifiques avec des **chercheurs japonais**.

Le premier axe concerne l'étude du **prisme d'accrétion Shimanto**, en tant que structure

fossile analogue des marges actives, avec des collaborations avec Asuka Yamaguchi (Univ. Tokyo), Arito Sakaguchi (Univ. Yamaguchi) et Yujin Kitamura (Univ. Kagoshima). Ces collaborations, qui ont abouti à la publication de 6 articles de rang A, s'appuient principalement sur des travaux de terrain au Japon (chaque année depuis 2009) et une subvention "Sakura" depuis 2016 (Programme Hubert Curien géré par le Ministère français des Affaires étrangères). Depuis 2016, nous avons étendu géographiquement notre périmètre d'étude pour y inclure les domaines externes des Alpes, en vue de comparaison avec le prisme Shimanto. J'ai également coorganisé avec Asuka Yamaguchi un workshop sur les séismes dans les zones de subduction en Octobre 2017, dans le cadre d'une conférence organisée par l'Ambassade de France au Japon.

Un autre thème de la collaboration internationale avec le Japon est la **rhéologie de mylonites**, à partir des travaux sur le terrain (Hidaka montagnes, le Japon) et la modélisation numérique, en collaboration avec Tsuyoshi Toyoshima (Univ. Niigata) et Hikaru Iwamori (Institut de technologie de Tokyo), dans le cadre du projet japonais "dynamique de la croûte terrestre" financé par la JSPS. À cette fin, j'ai été invité à donner une conférence à l'Université de Hokkaido (été 2016).

Les mêmes thèmes de recherche ont été abordés dans la période 2007-2014 par une autre collaboration, avec Toshihiro Kogure (Univ. Tokyo), sur une étude des Microstructures TEM de déformation. Pr. Kogure et moi-même étions co-PI d'un financement JSPS Kakenhi Kiban C Grant dans la période 2009-2011.

Un autre axe de collaboration s'est développé avec des chercheurs de l'Istep et de l'IPG, portant sur les **Alpes en tant que zone de subduction fossile**. Ce travail s'est d'une part focalisé sur les processus de déformation profonds, dans les domaines éclogitiques du Mont Viso (Philippe Agard et Samuel Angiboust) et ceux des Schistes Lustrés, dans le faciès des schistes bleus. Cette dernière zone d'étude fait l'objet d'une collaboration à une thèse (Benjamin Lefeuvre) en cours, encadrée par des collègues de l'Istep, concernant la caractérisation chimique de la circulation des fluides et des réactions métamorphiques de haute-pression. En parallèle, je travaille aussi avec Nicolas Bellahsen et Benoît Dubacq (Istep) sur des domaines de plus bas grade métamorphiques (flyschs à Helminthoïdes, Nappes SubBriançonnais) dans le but de reconstruire leur évolution tectonique et les circulations de fluides contemporaines de la déformation. Cette collaboration est construite autour d'un stage de master 2 en 2017-2018, avec le projet d'un dépôt de sujet de thèse dans le cadre du projet RGF (Référentiel Géologique de France), conduit par le BRGM, et portant sur les Alpes. Les Alpes constituent donc un sujet d'étude d'avenir, dans lequel ces diverses collaborations peuvent s'étendre et se développer, et

qui peut permettre de mettre en œuvre un ensemble de techniques instrumentales originales, notamment le traçage des fluides, y compris les halogènes, avec la plate-forme Ar/Ar de l'ISTO et la plate-forme LA-ICPMS LIPPS6 de l'Istep (gérée notamment par Benoît Dubacq).

Le troisième axe de collaboration est basé sur les expériences de déformation.

Le premier volet concerne la **déformation expérimentale du quartz**. Il a été initié au cours de la thèse de Giulia Palazzin et repose fortement sur l'expérience et le savoir-faire d'Holger Stünitz, qui a travaillé pendant l'essentiel de sa carrière sur des presse de Griggs et qui est maintenant à temps chercheur à mi-temps à l'ISTO. Ce thème de recherche fait l'objet de deux thèses conjointes, dans lesquelles je suis impliqué. L'une est pilotée à Orléans par Holger Stünitz et moi-même, la deuxième est encadrée par Petr Jerabek de l'Université de Prague. Ces deux thèses visent à comprendre l'effet de l'eau sur la déformation plastique du quartz.

Le deuxième volet concerne la **déformation des roches argileuses**, en particulier les argiles gonflantes de type smectite qui constituent une fraction importante des zones de failles superficielles dans les zones de subduction. Ce travail, qui a fait l'objet d'un dépôt de projet comme PI à l'ANR PRC, s'appuie sur des collaborations avec Eric Ferrage (Université de Poitiers), Benoît Dubacq (Paris 6) et Manuel Munoz (Université de Montpellier). Le projet est en outre adossé à l'Equipex Planex de l'ISTO, géré par Bruno Scaillet, dans le cadre duquel un autoclave semi-transparent, équipé d'un système de DRX in situ, va permettre l'étude des changements cristallographiques et des réactions d'hydratation/déshydratation de la smectite à haute pression et haute température, c'est-à-dire les conditions de la déformation profonde le long de l'interface de subduction sismogène.

#### ***4. Animation de la recherche et responsabilités institutionnelles***

2014 - Responsable de l'équipe « Géodynamique » (~10 permanents + ~10 doctorants)

Je suis responsable de l'équipe Géodynamique, une des cinq équipes de recherche de l'ISTO, depuis l'automne 2014. À cet égard, mon rôle principal est de promouvoir la recherche des membres du groupe, grâce à l'identification des synergies possibles entre les différentes questions abordées, la promotion de discussions scientifiques, l'incubation de projets éligibles aux différents appels à projets, le développement des collaborations avec les laboratoires partenaires sur le campus orléanais (BRGM), en France et à l'international. À la tête du groupe, j'ai été chargé de concevoir la stratégie scientifique pour les 5 prochaines années, dans le cadre de "l'évaluation quinquennale du laboratoire" par l'AERES. J'ai joué un rôle important dans la promotion de la déformation expérimentale comme un nouvel axe du groupe de recherche pour

compléter le domaine de la géologie de terrain, la compétence « historique » de l'équipe. Cette évolution, qui a été appuyé par le développement rapide des installations expérimentales en laboratoire (en particulier Griggs, Paterson, plate-forme Ar-Ar), ainsi que l'embauche de Holger Stünitz comme chercheur associé (6 mois/an), permet d'aborder des questions scientifiques nouvelles et ambitieuses, et je m'efforcerai dans un proche avenir d'accompagner le groupe de recherche en ce sens.

2012 - 2016 Membre de la section 35 du Conseil National des Universités, France

2017 - Responsable du WP1 du Labex "Voltaire"

Le Labex "Voltaire", dirigé par Bruno Scaillet, est divisé en sept volets (WPS). J'ai repris au printemps 2017 la responsabilité du WP1, ce qui est centré autour des fluides géologiques et leurs relations à la déformation. Le labex constitue l'une des sources principales de financement de la recherche de l'équipe, avec par exemple le soutien financier à deux thèses et un postdoc débutés à l'automne 2017. Conformément à la stratégie développée pour l'équipe, mon ambition est que le WP1 de Labex prenne en charge l'évolution du groupe vers une approche plus quantitative de la déformation et de transferts de fluides, notamment grâce aux apports de l'expérimental.

### ***5. Conférences et séminaires***

La valorisation de mes travaux de recherche passe par une participation récurrente à des conférences internationales, au premier rang desquelles figure l'EGU (2009, 2010, 2011, 2013, 2014, 2015, 2018).

Par ailleurs, je suis régulièrement invité à donner des séminaires à propos de mes travaux dans des laboratoires de recherche en géosciences: Université de Chiba (Japon) en 2007, l'Université de Cergy-Pontoise (France) en 2009, (JAMSTEC Yokosuka) en 2009 et 2012, l' Institut Français du Pétrole ( Rueil Malmaison, France) en 2010, l'Université Pierre et Marie Curie (Paris) en 2010, 2013, 2014, GFZ (Berlin) en 2013, l' Université de Poitiers (France) en 2015, l'Université de Hokkaido (Japon) en 2016, l'Université de Tromsø (Norvège) en 2016. Récemment, j'ai été invité comme orateur principal à une conférence spéciale dédiée au processus de subduction (SIP Conférence à Barcelone, avril 2017) ainsi qu'une conférence sur la gestion des risques à Tokyo (octobre 2017, Ambassade de France au Japon, Tokyo). Dans le cadre de cette dernière conférence, j'ai organisé aussi une session franco-japonaise sur l'enregistrement géologique des séismes, en collaboration avec mon homologue japonais Asuka Yamaguchi.

Je suis à l'origine de l'organisation d'un workshop sur "quartz et eau" à l'ISTO (2 jours en octobre 2017, 4 orateurs principaux et ~20 chercheurs extérieurs à l'ISTO, dont une majorité d'étrangers).

#### **D. Financement de la recherche**

Les projets financés dont j'ai été porteur sont énumérés ci-dessous :

| <i>Titre du projet</i>  | <i>Source de financement</i>                              | <i>Quantité (Euros)</i> | <i>Période</i> | <i>Rôle</i>  |
|---|---|-------------------------|----------------|--|
| Circulations de fluides et déformation dans les prismes d'accrétion                                       | Programme du Ministère des Affaires Etrangères ("Sakura") | ~32 000                 | 2016-2017      | Chercheur principal (avec un homologue japonais : Yujin Kitamura)  |
| Caractérisation expérimentale des propriétés physiques des sédiments au cours de la diagenèse             | Programme Syster de l'INSU, CNRS, France                  | ~15 000                 | 2010-2011      | Chercheur principal  |
| Réduction de la taille de grain et localisation de la déformation dans des mylonites de haute température | JSPS Kakenhi Kiban C                                      | ~45 000                 | 2009-2011      | Chercheur principal (avec un homologue japonais : Kogure) Tohihiro |

En outre, j'ai bénéficié, en tant que chercheur associé, de l'ERC Grant Senior dirigée par Laurent Jolivet au cours de la période 2012-2017. Comme PI, j'ai candidaté sans succès à l'ANR sur la période 2012-2016 (3 fois en tant que jeune chercheur (JCJC), 1 fois en tant que chercheur senior (PRC)). Le projet a accédé à la deuxième étape de l'évaluation en 2015. J'ai candidaté également à l'ERC Consolidator Grant en 2016, avec un projet évalué comme "B". Je suis actuellement en cours d'évaluation à l'ANR PRC, comme porteur d'un projet sur les propriétés thermodynamiques des argiles et leurs relations avec le comportement mécanique.

Je suis aussi responsable du work package 1 du Labex Voltaire porté par l'ISTO et le LPCEE (responsable Bruno Scaillet), sur un volet concernant la déformation profonde, les fluides et les minéralisations.

## **E. Encadrement de thèses et postdoc**

Dans les thèses dont je ne suis pas l'encadrant principal, j'ai estimé ma participation à l'encadrement avec un pourcentage.

Encadrement d'un post-doc (co-encadrant)

Déc 2017-mars 2018 "Processus de croissance des grains de quartz - une approche expérimentale"  
(J. Fukuda) (50 %)

Encadrement comme encadrant principal:

2011-2014 "la déformation et de la diagenèse dans des zones de subduction - influence sur le comportement mécanique" (L. Gadenne)

2012-2016 "Transition fragile-ductile dans des zones de subduction : le rôle de quartz" (G. Palazzin)

Co-encadrement :

1 thèse soutenue:

2013 -2017 "Localisation de la déformation au cours de l'exhumation: l'étude de cas du Tende, Corse" (A. Beaudoin) (20 %)

4 thèses en cours :

2015 - "Dynamique de la mylonitization : contraintes sur le terrain et modélisation numérique" (B. Bévillard) (40 %)

2016 - "Rhéologie des agrégats à deux phases : une étude expérimentale" (N. Mansard) (50 %)

Octobre 2017 - "Dynamique de la subduction de l'orogénèse varisque et relation à l'événement minéralisateur Or 300" (Cl. Montmartin) (40 %)

Octobre 2017- " Relation entre le transfert de l'eau et la déformation plastique : l'étude des mylonites à quartz " (L. Nègre)

J'ai aussi encadré, depuis mon recrutement à Orléans en 2009, 4 stages de recherche de Master 2 : Maxime Vacelet (2010-2011), Nicolas Mansard (2015-2016), Pierre Filliau (2016-2017), Antoine de Kemper (2017-2018).

Je participe par ailleurs chaque année à l'encadrement d'un ou deux stages de recherche de master 1, qui durent 6 semaines (je suis par ailleurs responsable de la coordination du module et de la distribution de ces stages).

## **F. Publications**

J'ai publié au total 31 articles dans des revues internationaux de rang A (15 comme 1<sup>er</sup> auteur + 4 en deuxième auteur derrière un de mes étudiants en thèse<sup>PhD</sup>). Les citations de ces articles s'élèvent à 486 (ResearchGate)/ 513 (Google Scholar), tandis que le h-index correspondant est de 13.

### **2018**

[31] Mansard<sup>PhD</sup>, N., **Raimbourg, H.**, Augier, R., Précigout, J. and Le Breton, N. (2018) Large-scale strain localization induced by phase nucleation in mid-crustal granitoids of the south Armorican massif. *Tectonophysics* 745, 46-65.

[30] Palazzin<sup>PhD</sup>, G., **Raimbourg, H.** Stünitz, H., J. Précigout, 2018. Rheology and transfers of water in wet quartz aggregates *J. Struct. Geol.* Vol. 114, pp. 95-110.

[29] **Raimbourg, H.**, V. Famin, G. Palazzin, et al., 2018. Fluid properties and dynamics along the seismogenic plate interface *In Geosphere: Subduction top to bottom 2* vol.14, 1-23

### **2017**

[28] **Raimbourg, H.**, Thiéry, R., Vacelet, M., Famin, V., Ramboz, C., Boussafir, M., Disnar, J.-R., Yamaguchi, A., 2017. Organic matter cracking: a source of fluid overpressure in subducting sediments. *Tectonophysics* vol. 721, 254-274.

[27] Beaudoin<sup>PhD</sup>, A., Augier, R., Jolivet, L., Jourdon, A., **Raimbourg, H.**, Scaillet, S., Cardello, G.L., 2017. Deformation behavior of continental crust during subduction and exhumation: Strain distribution over the Tenda massif (Alpine Corsica, France). *Tectonophysics* vol. 705, pp. 12-32.

[26] **Raimbourg, H.**, Famin, V., Palazzin, G., Sakaguchi, A., Yamaguchi, A., Augier, R., 2017. Tertiary evolution of the Shimanto Belt (Japan): a large-scale collision in Early Miocene. *Tectonics* vol. 36, pp. 1-21.

### **2016**

[25] Palazzin<sup>PhD</sup>, G., **Raimbourg, H.**, Famin, V., Jolivet, L., Kusaba, Y., Yamaguchi, A., 2016. Deformation processes at the down-dip limit of the seismogenic zone: The example of Shimanto accretionary complex. *Tectonophysics* vol. 687, pp. 28-43.

### **2015**

[24] **Raimbourg, H.**, Vacelet, M., Ramboz, C., Famin, V., Augier, R., Palazzin, G., Yamaguchi, A., Kimura, G., 2015. Fluid circulation in the depths of accretionary prisms: an example of the Shimanto Belt, Kyushu, Japan. *Tectonophysics* vol. 655, pp. 161-176.

### **2014**

[23] **Raimbourg, H.**, Thiery, R., Vacelet, M., Ramboz, C., Cluzel, N., Trong, E.L., Yamaguchi, A., Kimura, G., 2014b. A new method of reconstituting the P-T conditions of fluid circulation in an accretionary prism (Shimanto, Japan) from microthermometry of methane-bearing aqueous inclusions. *Geochim Cosmochim Acta* vol. 125, pp. 96-109.

[22] **Raimbourg, H.**, Augier, R., Famin, V., Gadenne, L., Palazzin, G., Yamaguchi, A., Kimura, G., 2014a. Long-term evolution of an accretionary prism: the case study of the Shimanto Belt, Kyushu, Japan. *Tectonics* vol. 33, pp. 1-24.

[21] Famin, V., **Raimbourg, H.**, Garcia, S., Bellahsen, N., Hamada, Y., Boullier, A.-M., Fabbri, O., Michon, L., Uchide, T., Ricci, T., Hirono, T., Kawabata, K., 2014. Stress rotations and the long-term weakness of the Median Tectonic Line and the Rokko-Awaji Segment *Tectonics* vol. 33, pp. 1-20.

[20] Gadenne<sup>PhD</sup>, L., **Raimbourg, H.**, Champallier, R., Yamamoto, Y., 2014. Mechanical properties and processes of deformation in shallow sedimentary rocks from subduction zones: An experimental study. *Geochim. Geophys. Geosyst.* vol. 15, pp. 5001-5014.

[19] Kogure, T., **Raimbourg, H.**, Kumamoto, A., Fujii, E., Ikuhara, Y., 2014. Subgrain boundary analyses in deformed orthopyroxene by TEM/STEM with EBSD-FIB sample preparation technique. *Earth, Planets and Space* vol. 66, pp. 1-8.

## 2013

[18] Kimura, G., Hamahashi, M., Okamoto, S.y., Yamaguchi, A., Kameda, J., **Raimbourg, H.**, Hamada, Y., Yamaguchi, H., Shibata, T., 2013. Hanging wall deformation of a seismogenic megasplay fault in an accretionary prism: The Nobeoka Thrust in southwestern Japan. *J. Struct. Geol.* vol. 52, pp. 136-147.

## 2012

[17] Angiboust, S., Agard, P., Yamato, P., **Raimbourg, H.**, 2012. Eclogite breccias in a subducted ophiolite: A record of intermediate depth earthquakes? *Geology* vol. 40, pp. 707-710.

[16] Yamamoto, Y., Chiyonobu, S., Kurihara, T., Yamaguchi, A., Hina, S., Hamahashi, M., **Raimbourg, H.**, Augier, R., Gadenne, L., 2012. Unconformity between a Late Miocene–Pliocene accretionary prism (Nishizaki Formation) and Pliocene trench-slope sediments (Kagamigaura Formation), central Japan. *Island Arc* vol. 21, pp. 231-234.

## 2011

[15] Angiboust, S., Agard, P., **Raimbourg, H.**, Yamato, P., 2011. Subduction interface processes recorded by eclogite-facies shear zones. *Lithos* vol. 127, pp. 222-238.

[14] Conin, M., Henry, P., Bourlange, S., **Raimbourg, H.**, Reuschlé, T., 2011. Interpretation of porosity and LWD resistivity from the Nankai accretionary wedge in light of clay physicochemical properties: Evidence for erosion and local overpressuring. *Geochem. Geophys. Geosyst.* vol. Q0AD07, pp. 1-17.

[13] Kameda, J., **Raimbourg, H.**, Kogure, T., Kimura, G., 2011. Low-grade metamorphism around the down-dip limit of seismogenic subduction zones: Example from an ancient accretionary complex in the Shimanto Belt, Japan. *Tectonophysics* vol. 502, pp. 383-392.

[12] **Raimbourg, H.**, Hamano, Y., Saito, S., Kinoshita, M., Kopf, A., 2011a. Acoustic and mechanical properties of Nankai accretionary prism core samples. *Geochem. Geophys. Geosyst.* vol. 12, pp. doi:10.1029/2010GC003169.

[11] **Raimbourg, H.**, Kogure, T., Toyoshima, T., 2011b. Crystal bending, subgrain boundary development, and recrystallization in orthopyroxene during granulite-facies deformation. *Contrib. Min. Petr.* vol., pp. doi:10.1007/s00410-00011-00642-00413.

[10] **Raimbourg, H.**, Ujiie, K., Kopf, A., Hisamitsu, T., Hamano, Y., Saito, S., Kinoshita, M., 2011c. The role of compaction contrasts in sediments in décollement initiation in an accretionary prism. *Marine Geology* vol. 282, pp. 188-200.

## 2010

[9] Labrousse, L., Hetenyi, G., **Raimbourg, H.**, Jolivet, L., Andersen, T.B., 2010. Initiation of crustal-scale thrusts triggered by metamorphic reactions at depth: Insights from a comparison between the Himalayas and Scandinavian Caledonides. *Tectonics* vol. 29, pp. 14.

## 2009

[8] **Raimbourg, H.**, Shibata, T., Yamaguchi, A., Yamaguchi, H., Kimura, G., 2009. Horizontal shortening versus vertical loading in accretionary prisms. *Geochem. Geophys. Geosyst.* vol. 10, pp. doi:10.1029/2008GC002279.

## 2008

[7] **Raimbourg, H.**, Kimura, G., 2008a. Non-lithostatic pressure in subduction zones. *Earth Planet. Sc. Lett.* vol. 274, pp. doi:10.1016/j.epsl.2008.1007.1037.

[6] Kimura, G., Kitamura, Y., Yamaguchi, A., **Raimbourg, H.**, 2008. Links among mountain building, surface erosion, and growth of an accretionary prism in a subduction zone- An example from southwest Japan. *GSA Spec. Pap.* vol. 436, pp. 391-403.

[5] **Raimbourg, H.**, Toyoshima, T., Harima, Y., Kimura, G., 2008. Grain size reduction mechanisms and rheological consequences in high-temperature gabbro mylonites of Hidaka, Hokkaido *Earth Planet. Sc. Lett.* vol. 267, pp. 637-653.

## 2007

- [4] **Raimbourg, H.**, Jolivet, L., Leroy, Y., 2007b. Consequences of progressive eclogitisation on crustal exhumation, a mechanical study. *Geophys. J. Int.* vol. 168, pp. 379-401.
- [3] **Raimbourg, H.**, Goffe, B., Jolivet, L., 2007a. Garnet reequilibration and growth in the eclogite facies and geodynamical evolution near peak metamorphic conditions. *Contrib. Mineral. Petr.* vol. 153, pp. 1-28.

## **2005**

- [2] Jolivet, L., **Raimbourg, H.**, Labrousse, L., Avigad, D., Leroy, Y., Austrheim, H., Andersen, T.B., 2005. Softening triggered by eclogitization, the first step toward exhumation during continental subduction. *Earth Planet. Sc. Lett.* vol. 237, pp. 532-547.
- [1] **Raimbourg, H.**, Jolivet, L., Labrousse, L., Leroy, Y.M., Avigad, D., 2005. Kinematics of syneclogite deformation in the Bergen Arcs, Norway: implications for exhumation mechanisms, in: Gapais, D., Brun, J.P., Cobbold, P.R. (Eds.), *Deformation Mechanisms, Rheology and Tectonics: from Minerals to the Lithosphere*. Geological Society, London, Special Publications, pp. 175-192.

## **G. Activités d'enseignement**

Je réalise mon service d'enseignement dans la licence et le master de sciences de la Terre, ainsi que dans une moindre mesure dans la formation au Capes SVT. Quelques modules caractéristiques de mon activité d'enseignement :

### *Licence :*

Introduction aux séismes (L1) : 24h

Stage de terrain (chaîne plissée d'avant-pays - Corbières) (L3) : 60h

### *Master :*

Introduction à la géophysique et géodynamique (M1 Capes) : ~26h

Structure et dynamique de la lithosphère (M1) : 21h

Stage de terrain (géodynamique et métamorphisme - Corse) : 24h

Géodynamique et Rhéologie (M2) : 15h

J'ai par ailleurs des responsabilités particulières dans les filières d'enseignement :

### **Gestion des projets de recherche (M1) :**

J'ai été en charge de la gestion des stages de recherche du M1 (~6 semaines de recherches, pour environ 30 élèves) depuis 2009.

### **Responsabilité de la L1 « Synergie »:**

Créé dans le cadre du projet « Edifice » (PIA), ce cursus a visé à rapprocher les lycées et l'université. J'ai été en charge de la gestion de la 1<sup>ère</sup> année de la licence Synergie au cours de l'année 2016-2017, avec un programme d'enseignement intégrant l'ensemble des domaines scientifiques et proposant une ouverture vers la recherche et les laboratoires, pour une promotion d'environ 15 élèves.

**Conception de la nouvelle licence et responsabilité à partir de Septembre 2018:**

Au cours des années universitaires 2016-2018, j'ai été chargé de superviser les discussions et la conception du squelette de la nouvelle licence, qui a été mise en œuvre à partir de Septembre 2018 et dont je suis responsable depuis cette date.

## Chapter II: The deformation of the subduction plate interface, from the point of view of geophysics and experiments

I aim in this chapter at making some overview of subduction zone mechanical properties, based principally on the study of active margins. A lot of geophysical and geodetic data has been recently acquired, enabling to get a more and more complete picture of the interface behavior. In parallel, I also reviewed some experimental and theoretical work on friction mechanics, in order to interpret the observations with small-scale models of deformation. I also detailed the observations concerning fluid, which is often considered as a major control parameters in subduction zones. In these different results, I tried to unravel the “weak” links, i.e. gaps in knowledge or convenient but relatively unsupported assumptions, which can be considered conversely as fruitful paths for future research.

### **A. Mechanical behavior of the plate interface in subduction zones**

#### *1. A simple model: the seismogenic zone model*

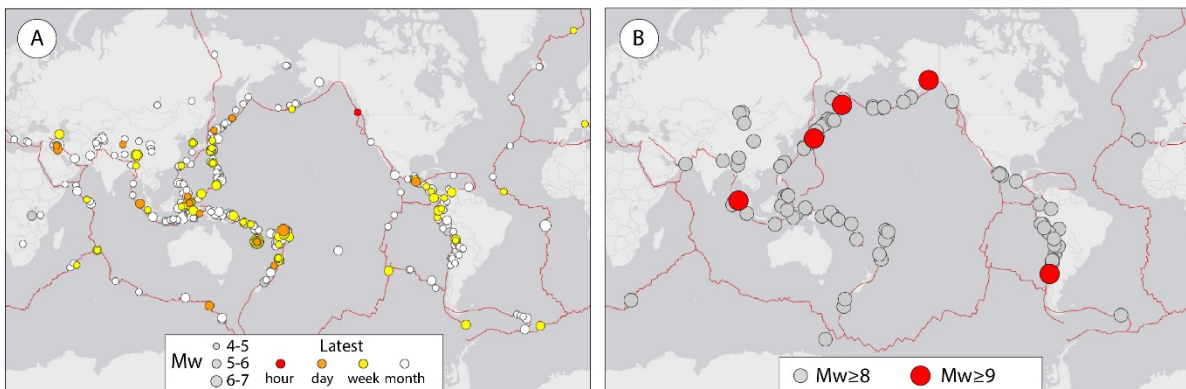


*Figure 1: A) Worldwide distribution of all earthquakes with magnitude  $M_w \geq 4.5$  in a 1 month timespan (calculated on November the 21<sup>st</sup> 2017). B) Worldwide earthquakes with  $M_w \geq 8$  since 1900. Both figures from USGS database (<https://earthquake.usgs.gov/earthquakes/>).*

The compilation of earthquakes distribution over any arbitrary time span (Figure 1) shows that most earthquakes are concentrated along subduction plate boundaries, in particular around the Pacific plate. Similarly, mega-earthquakes, with magnitude larger than 8, are also concentrated in subduction zones and they correspond to the rupture, over a very large area, of the plate interface.

The depth distribution of these earthquakes show that they distribute preferentially along a low-dipping plane, which projects geometrically to the trench (Figure 2A). This zone of concentrated seismicity is interpreted as the plate interface boundary, on the basis of its geometry and on the focal mechanisms of a large proportion of the earthquakes constituting it (Suzuki et al., 2012; Tichelaar and Ruff, 1993), as for example apparent in the earthquakes preceding the large rupture of the Mw9.0 Tohoku-Oki (Figure 2B).

The depth distribution of the earthquakes with a focal mechanism consistent with thrusting along the interplate is not homogeneous with depth (Fig. 2A) (Byrne et al., 1988; DeShon et al., 2003; Pacheco et al., 1993; Tichelaar and Ruff, 1993). Most interplate earthquakes concentrate in a restricted depth domain, with a transition to aseismic domain updip and downdip. Such depth-dependent mechanical behavior has been coined the “seismogenic zone” model (Hyndman et al., 1997; Oleskevich et al., 1999) and is widely used to describe worldwide subduction zones (Figure 3).

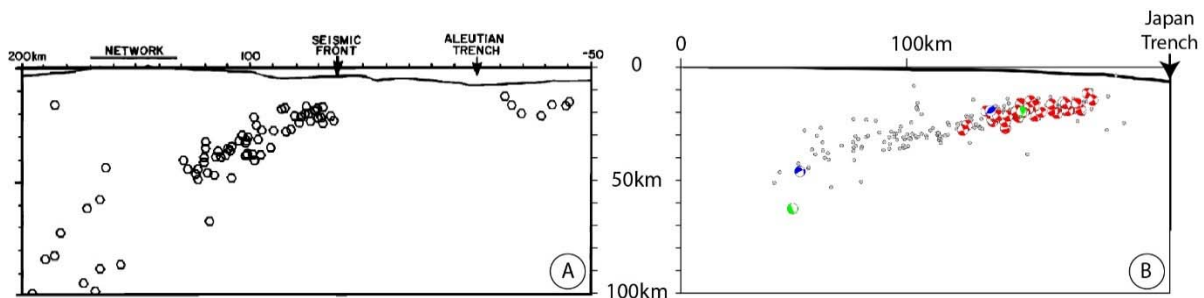


*Figure 2. A) Hypocenters distribution across the Aleutian subduction zone, for earthquakes with a magnitude larger than 4.8 in the time period 1975-1985 (Byrne et al., 1988). B) Foreshock of Mw9.0 Tohoku-Oki earthquakes, compiled from 2011 January 1<sup>st</sup> to the main shock of the 11<sup>th</sup> of March, across the Japan Trench (Suzuki et al., 2012). The red, blue and green colors of the focal mechanisms refers to low angle thrust, normal and strike-slip mechanisms, respectively.*

The depth of the downdip limit of the seismogenic zone varies to a relatively larger extent: Pacheco et al. (1993) report depths of the downdip limit in the range 30-70km. Similarly, according to Tichelaar and Ruff (1993), in most circum-Pacific subduction zones, the downdip limit is located at ~40km depth, but at larger (~50km) and smaller (~20-30km) depth in Central Chile-Hokkaido and Mexico, respectively. Their thermal modelling showed no correspondence between the downdip limit and a given isotherm. Further studies, with more sophisticated thermal modelling, provided some connection between the isotherm  $T \sim 350^{\circ}\text{C}$  and the downdip limit of the seismogenic zone in certain subduction zones, while in other ones the downdip limit was associated with the depth of the serpentinized mantle of the upper plate (Hyndman et al., 1997; Oleskevich et al., 1999). The same modeling approach resulted in the connection between the updip limit of the seismogenic zone and the  $\sim 100\text{-}150^{\circ}\text{C}$  isotherm. The seismogenic zone

model is therefore essentially thermally controlled. In turn, the transitions from aseismic to seismic sliding are accounted for by the changes in the mechanical properties of the interplate-forming minerals (Hyndman et al., 1997; Oleskevich et al., 1999; Scholz, 1998), in the framework of rate-and-state (RSF) friction laws (Dieterich, 1994; Ruina, 1983). In this framework, the transformation of smectite into illite, respectively considered as velocity-weakening and velocity-strengthening, account for the updip transition at  $\sim 100\text{-}150^\circ\text{C}$ . The downdip transition, at  $\sim 350^\circ\text{C}$ , is associated with the onset of quartz plasticity (Figure 3).

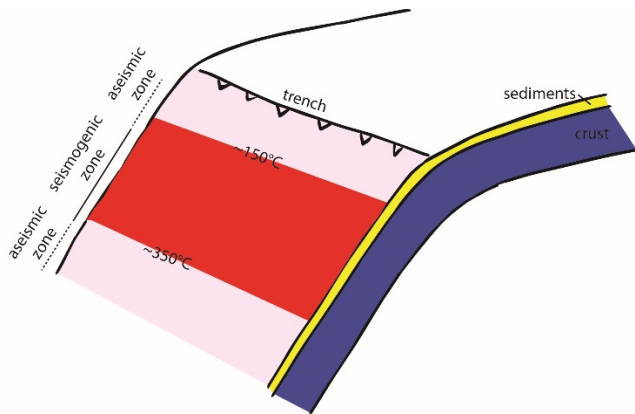


*Figure 3: Depth distribution of the mechanical behavior of the plate interface, according to the seismogenic zone model (Hyndman et al., 1997). The seismogenic portion of the plate interface is bracketed by two aseismic portions, with limits that are temperature-controlled.*

## **2. Variations in coupling within the seismogenic zone**

While the seismogenic zone model provides a very simple picture of the subduction zone behavior, a lot of geophysical data point to a much more complex distribution in space and time of the deformation along the plate interface.

On a worldwide basis, the comparison of the slip occurring during repeated earthquakes (in the timeframe 1900-1990) and the total amount of slip from plate movements show that in many subduction zones, seismic slip account for only a small fraction of total slip (Pacheco et al., 1993). Similarly, the compilation of  $M_w \geq 5.5$  earthquakes in the 1900-2007 time period reveals large difference between subduction margins, from no or rare occurrence of earthquakes (e.g. Marianna) to very frequent ones (e.g. Northern Chile or Kuriles) (Heuret et al., 2011). This dataset, collected over  $\sim 100$  yrs, span a smaller period than the recurrence time of mega-earthquake, so that, for example, the absence of earthquakes along Cascadia margin may not be a persistent feature of the margin, but a consequence of the  $\sim M_w 9$  giant earthquake in  $\sim 1700$  (Satake et al., 1996; Yamaguchi et al., 1997). In spite of this limitations, there are clear

differences in seismic coupling between subduction zones, pointing to different mechanical properties of the interface.

Similarly, GPS measurements show a contrasted behavior of the plate interface in terms of relative movement of the upper and lower plate. Along both SW and NE margins of Japan (Mazzotti et al., 2000) or along Cascadia margin (Mazzotti et al., 2003) both plates are fully coupled. The western Shumagin segment of the Alaskan subduction zone, a portion of the margin that has not experienced recent large earthquake, constitutes the other endmember, where there is no coupling of the plates across the interface (Freymueller and Beavan, 1999). The latter authors note nevertheless that the on-land GPS network is too far from the trench to determine the coupling degree in the portion of the plate interface next to the trench. In this case, the undetermined portion of the plate is actually quite large (~55km of horizontal distance from the trench, down to ~20km of depth). The lack of resolution on the slip behavior of the shallow portion of the plate interface is actually present in all margins (see below the case of NE Japan), because instrumental networks are principally located on-land.

More recent GPS studies, based on constantly improving instrumental capacities, have further supported the very large variations in the plate coupling along and across subduction margins, with locked making patches of irregular size and position (Chlieh et al., 2014; Loveless and Meade, 2010).

As a conclusion, both in terms of coseismic or interseismic strain, there is a large spatial heterogeneity in the plate interface behavior at “seismogenic” depths, between full coupling and rupture during earthquakes to null coupling and continuous creep.

### ***3. The insights from recent mega-earthquakes***

Recent mega-earthquakes in 2004 in Sumatra (Shearer and Bürgmann, 2010), 2010 in Chile (Vigny et al., 2011) or 2011 in Japan (Simons et al., 2011), recorded by broadband seismometers and geodetic networks, have provided a wealth of new data about the characteristics of the rupture and more largely on the whole seismic cycle in subduction zones. The first essential piece of information regards the correlation between interseismic and coseismic deformation. As illustrated in the case of the 2011 Tohoku-Oki earthquake, or in the case of 2010 Maule earthquake (Figure 4), the extent of the rupture zone during the mega-earthquake roughly coincides with the patch of the subduction interface that is locked during the interseismic stage (Avouac, 2011; Loveless and Meade, 2010, 2011; Moreno et al., 2010).

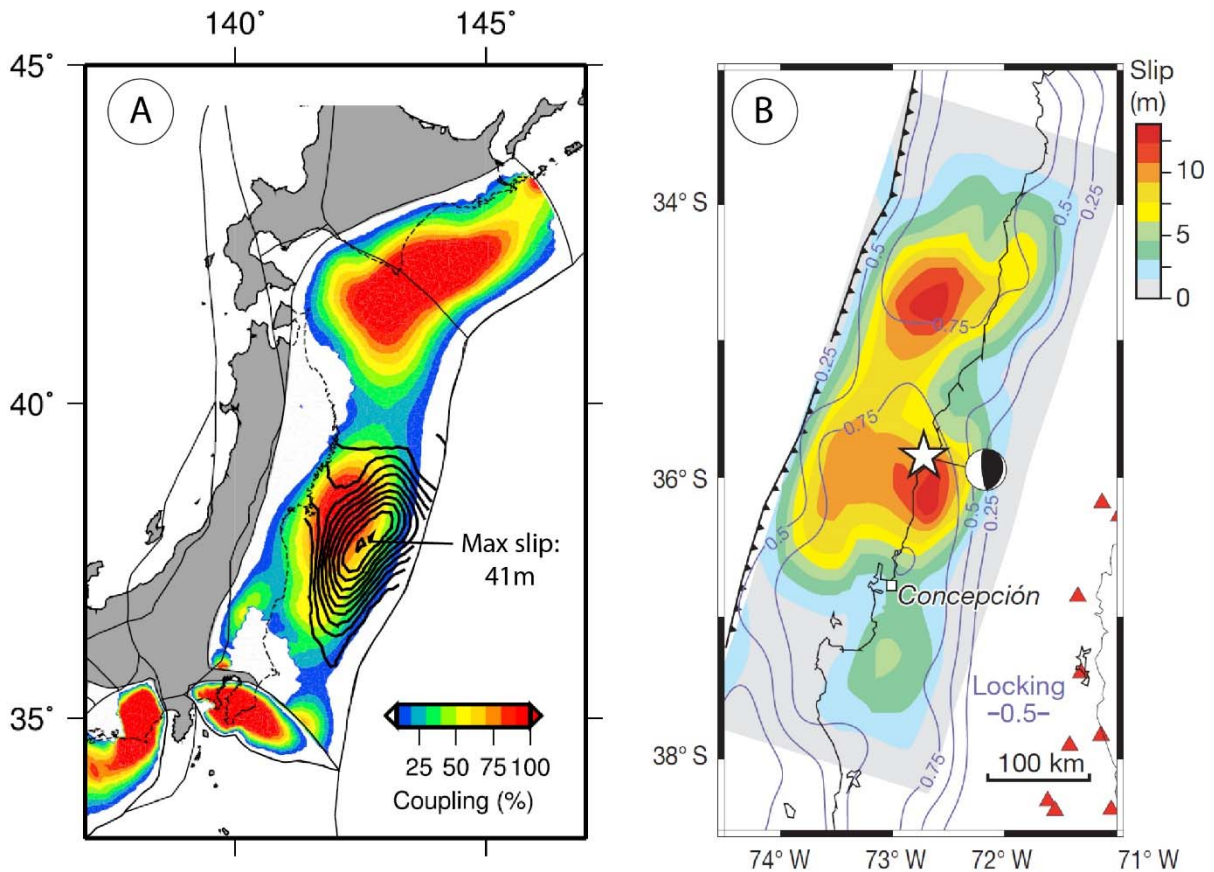


Figure 4: Comparison of interseismic coupling and coseismic slip for the 2011 Tohoku-Oki earthquake in NE Japan (Loveless and Meade, 2011) and the 2010 Maule earthquake in Chile (Moreno et al., 2010). The step in coseismic slip isolines in A) is 4m. The degree of coseismic coupling is expressed in the range 0-100% in A) and 0-1 in B).

The plate interface is therefore divided into seismic asperities, which are partially or fully locked during the interseismic stage and rupture during earthquakes, surrounded by domains of the interface with a much lower degree of coupling and which act as “barriers” to coseismic slip (Bürgmann et al., 2005; Kanamori, 2008).

This simple scheme has to be moderated by the fact that the properties of the plate interface with respect to coseismic rupture are to some extent dependent on the amplitude of earthquake and associated slip. Several slip deficit zones can be defined along the NE Japan subduction interface from GPS-monitored interseismic displacement. Within the slip deficit zone off Miyagi, several small-sized asperities were broken by Mw~7.5 earthquakes, with a recurrence time of ~40yrs and displacement of ~3m (Hashimoto et al., 2012). The rupture zone of the 2011 Tohoku-Oki earthquake occurred over a much larger area, encompassing all these smaller scale asperities and the portion in-between, with displacements of ~30m. The properties of the plate interface are different when considered from the point of view of the recurrent smaller

earthquakes or from the point of view of the mega-earthquakes. The mechanical properties of the interface are therefore strain/strain-rate dependent.

Another essential information provided by the Mw9.0 Tohoku-Oki earthquake regards the behavior of the shallow portion of the plate interface during the earthquake. The seismogenic zone model supposed that this portion of the plate interface is, in terms of frictional behavior, velocity-strengthening and therefore would resist seismic rupture (Scholz, 1998). Several models of the coseismic slip distribution of Tohoku-Oki earthquake, based on geodetic and seismic data, show large differences both in terms of slip amplitude and distribution (see the comparisons in Loveless and Meade (2011)). A large point of discrepancy regards the propagation of slip to shallow levels, even to the trench. While certain models obtained a peak in slip at very shallow levels (Lay et al., 2011), in other peak slip was at much larger distance from the trench and the slip amplitude decreased strongly towards the trench (Ozawa et al., 2011).

The propagation of slip to very shallow levels was actually demonstrated by several independent datasets, such as the displacement of ocean-bottom instruments (Figure 5 from Ito et al. (2011)) or comparative bathymetry (before and after the mega-earthquake) of the near-trench area (Fujiwara et al., 2011). In other large earthquake, the uncertainty regarding shallow slip is still very large (see for example the different models of slip distribution for the 2004 Sumatra earthquake (Shearer and Bürgmann, 2010)), so that one can wonder whether the behavior observed during Tohoku-Oki earthquake can be generalized. Nevertheless, these observation during Tohoku-Oki earthquake strongly question the postulate of the seismogenic zone model where the shallow portion of the plate interface is supposed to be aseismic.

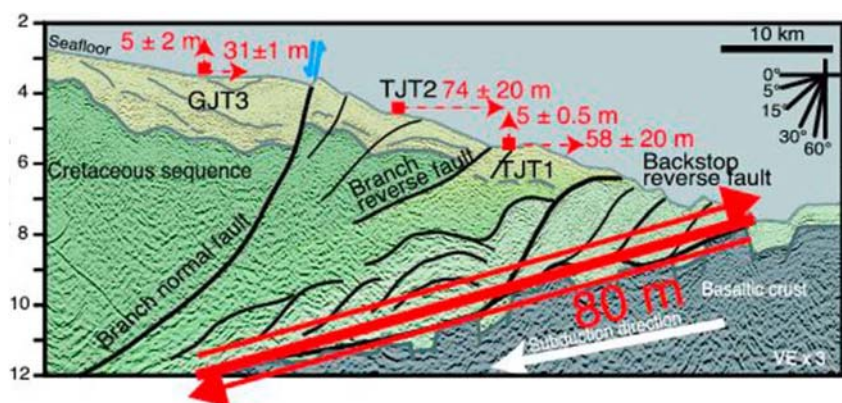


Figure 5: Coseismic slip near the trench during the Mw9.0 Tohoku-oki earthquake, as recorded by the displacement of ocean-floor pressure gauges (Ito et al., 2011). Vertical axis on the left is depth (in km).

#### ***4. Rapid aseismic slip along the plate interface***

The contrast between seismic and aseismic slip, or between coupled and uncoupled interface, enables a simple picture of the subduction zone to emerge. Yet, these behaviors are only endmembers and many intermediates exist. In particular, aseismic behavior corresponds to at least two main types of slip. First, within uncoupled domains of the plate interface, slip occurs at the same pace as the plate velocity. Second, events of rapid (i.e. larger than prescribed by plate velocity) slip have been reported along the plate interface. These events of rapid aseismic slip, described in what follows, occur as a result of earthquakes (i.e. afterslip) but also disconnected from them (slow-slip events).

##### **Afterslip**

The global estimate of the strain released by earthquakes (Pacheco et al., 1993) or the interseismic coupling (see above) point to the fact that a spatially heterogeneous but in many cases large fraction of the plate relative motion is accommodated by aseismic creep.

A first process to release strain aseismically is the post-seismic creep, or afterslip, which was studied geodetically following several large earthquakes. Along the Peru margin, the 2007 Mw8 Pisco earthquake was followed by a large after slip, which over a bit more than 1 year after the earthquake released the equivalent of ~28% of the coseismic moment (Perfettini et al., 2010). After slip occurred on two patches adjacent to the patches that were affected by large coseismic slip. Similarly, offshore the eastern coast of Kyushu, along the Philippines sea-plate boundary, post-seismic slip after two earthquakes released a moment roughly equal to the coseismic one (Yagi et al., 2001). Furthermore, zones of coseismic and postseismic slip are not overlapping but located next to each other. Off Kamtshatka, postseismic slip released as much moment as the earthquake itself. Slip preferentially localized downdip of the main rupture and extends also laterally (Bürgmann et al., 2001). Off Hokkaido, post-seismic slip is complementary to coseismic slip and occurs adjacent to it (Miyazaki et al., 2004).

These several examples tend to show that the slip occurring after large earthquakes, due to the redistribution of stresses, is significant with respect to coseismic slip. The other important feature of the afterslip in these examples is its distribution, in many cases not coinciding, but adjacent to the coseismic slip area. Counter-examples exist, for example off Tohoku, where a series of Mw~7 earthquakes occurred in the 10-yr time period preceding Tohoku-oki event (Suito et al., 2011). For each of these four afterslip events, which released a moment of the order or even larger than coseismic one, the slip distribution in this case overlaps the coseismic slip.

Excepting this case, the complementarity of coseismic and afterslip spatial distribution point to a contrast in the mechanical property of the plate interface. Indeed, relationship between stress and velocity  $\frac{d\tau}{d\ln(V)}$  indicates, although other solutions are possible, that afterslip occurs along a velocity-strengthening portion of the plate interface (Miyazaki et al., 2004). The same conclusion was obtained by (Perfettini et al., 2010) from the evolution of slip with time. Such velocity-strengthening behavior, prone to afterslip, stands in contrast to the velocity-weakening portion of the plate interface, which would rupture during large earthquakes (Scholz, 1998).

### **Deep slow slip and low frequency earthquakes**

Episodic tremor and slip (ETS) are the combination of slow slip events (SSE) and non-volcanic tremor, detected respectively by GPS and seismometers, occurring simultaneously along the subduction plate interface (Figure 6). They have been recently unraveled in the Cascadia (Gomberg and Cascadia 2007 and Beyond Working Group, 2010; Rogers and Dragert, 2003) and the SW Japan subduction zones (Hirose and Obara, 2006; Obara, 2002; Obara et al., 2004). Their correlated occurrence in space and time, as well as the focal mechanisms of very-low-frequency earthquakes constituting the tremor burst (Shelly et al., 2007), point to slip along the plate interface as a common process to seismic tremor and slow slip.

Slow-slip event last for a few days and release a significant proportion of the relative slip between upper and lower plates. For example, the SSE analyzed by (Dragert et al., 2001) along Cascadia released  $\sim 1/2$  year of relative slip and was equivalent to a Mw6.7 earthquake. Similarly, along the Hikurangi subduction zone in New Zealand, SSE release a major fraction of accumulated moment (Wallace and Beavan, 2010).

Modelling slow slip event with dislocations (Okada, 1992), the slipping portion of the plate interface has a shallow limit at depths  $\sim 30$ km along the Cascadia subduction zone (Dragert et al., 2001; Gomberg and Cascadia 2007 and Beyond Working Group, 2010),  $\sim 40$ km along SW Japan (Obara et al., 2004) or  $\sim 25$ km in Hikurangi (Wallace and Beavan, 2006). In other words, ETS occur near or below the downdip limit of the seismogenic zone, i.e. at the transition between seismic and aseismic behavior.

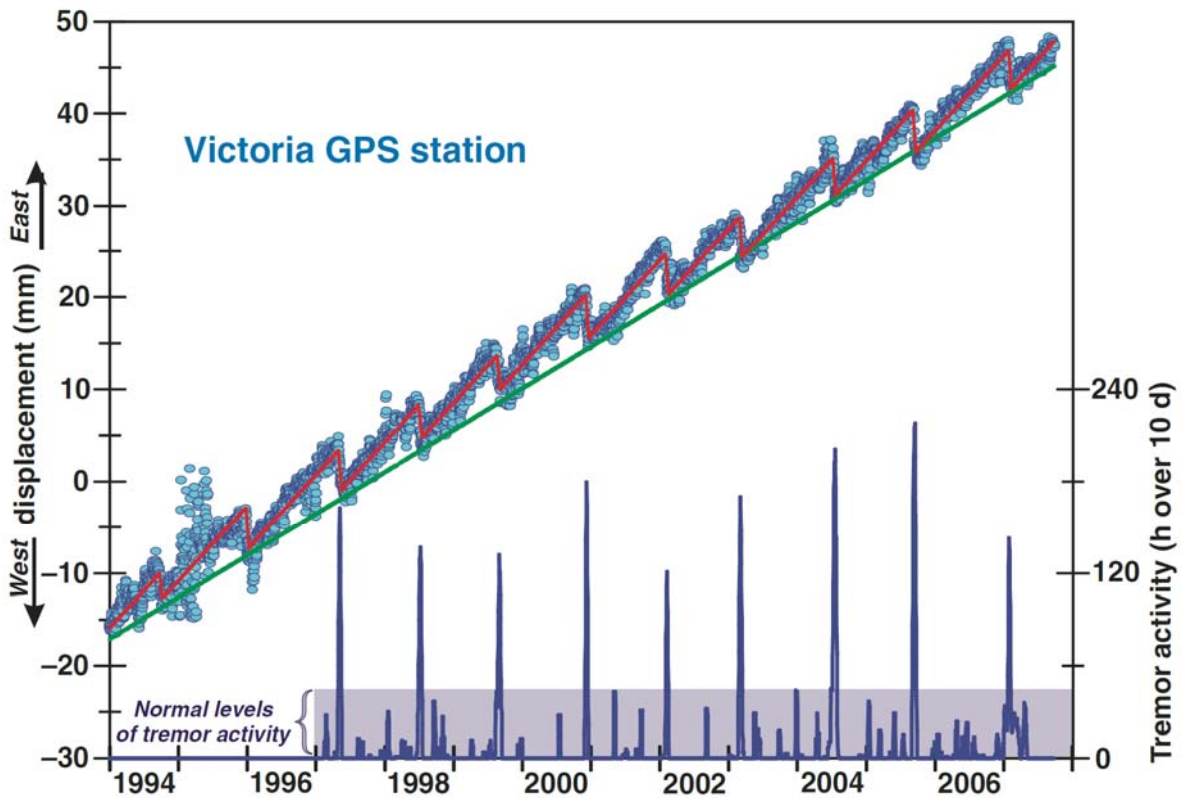


Figure 6: The horizontal displacement of a GPS station above the Cascadia subduction zone has a saw-tooth pattern, with regular events of westward displacement, interpreted as slow slip events at depth along the plate interface, superimposed on a displacement towards the east at constant rate. Slow slip events coincide in time with an increase in the generation of seismic tremors (Gomberg and Cascadia 2007 and Beyond Working Group, 2010; Rogers and Dragert, 2003).

Their segmentation along strike could be associated with upper plate geology and with the properties of the seismogenic zone, such as its segmentation into seismic asperities and creeping portions (Brudzinski and Allen, 2007) or the variations in the depths of its downdip limit (Wallace and Beavan, 2010).

From the discovery of SSE on, a potential relationship with high fluid pressure has been frequently raised (Kodaira et al., 2004; Obara, 2002), on the basis of mechanical models of slip as well as geophysical imaging of fluid pressure near the plate interface.

The mechanical condition to generate SSE have been investigated using the theoretical tools of rate-and-state friction laws (Dieterich, 1994; Ruina, 1983). Considering the temperature/depth dependence of friction parameters, SSE form spontaneously in domains of transition from slip-weakening to slip-strengthening behavior (Liu and Rice, 2005), which is supposed to coincide with the downdip limit of the seismogenic zone (Oleskevich et al., 1999) and where actual SSE occur. Focusing on this mechanical transition (transition from  $a-b > 0$  to  $< 0$ ), (Rubin, 2008) reached the conclusion that the law that is the most relevant to experiments cannot satisfactorily account for the large number of occurrences of SSE. There is a need, to stabilize slip, for an

additional process to increase the fracture energy upon slip increase and the authors invoke the effect of fault dilatancy (Segall and Rice, 1995), a mechanism all the more efficient as the pore fluid pressure is high. The role of high pore pressure is also emphasized as it increases the nucleation length (of earthquakes), which constitutes an upper bound below which SSE can be generated. Another argument in favor of high pore fluid pressure is given in the model of (Liu and Rice, 2007), as SSE duration is correlated with effective stress, and typical durations of a few days imply very low effective stress, of the order of a few MPa (Liu and Rice, 2007).

A potential link between pore fluid pressure and SSE is also provided by their preferential occurrence in domains where seismic attributes, such as  $V_p/V_s$  ratio, suggest high pore fluid pressure. This is for example the case in SW Japan, where SSE preferentially occur in zones of high  $V_p/V_s$  near Kii Peninsula (Kodaira et al., 2004) or along the Bungo channel in the west of Shikoku (Shelly et al., 2006).

### **Shallow slow slip**

SSE events are actually not restricted to the downdip limit of the seismogenic zone and some slip events have been reported in the shallow portion of the plate interface. For example, shallow SSE at depth  $\sim 10$ km along the plate interface in Ecuador, which triggered a swarm of small earthquakes (Vallée et al., 2013). The SSE occurred in the downdip portion of a shallow locked asperity.

SSE occurred also regularly on the eastern domain of the Boso Peninsula, near Tokyo. The depth of the slip zone is 10 to 20km, in the vicinity of a strongly coupled asperity, which in this area is relatively shallow (less than 20km depth) (Ozawa et al., 2007; Sagiya, 2004). It triggered small earthquakes around the downdip domain of the zone of slow slip.

Saffer and Wallace (2015) made a comprehensive review of these shallow slow slip events, which seem to be occurring in many subduction zones. These slow slip events occurs updip (Costa Rica and Nankai) or even within the zone of slip of historical large earthquakes. SSE have a long time rise and a characteristic linear seismic moment-duration relationship ( $M_0 \propto T$ ) different from normal earthquake ( $M_0 \propto T^3$ ) (Ide et al., 2007).

According to the same review paper, SSE are associated with very large fluid pressure, mostly accounted for by sediment compaction rather by clay dehydration reactions. Mechanical tests on material drilled in active or fossil faults equivalent to the décollement fault show a complex behavior, velocity-weakening at slow slip rate ( $< 1$ mm/s) and velocity strengthening at larger slip rate, which could promote slow slip.

## 5. Conclusion

From the initially simple seismogenic zone model, the recent observations of slip in subduction zones summarized above have brought up a much higher level of complexity. First, there is a large range of deformation behavior, including slip during earthquakes, slow slip at plate velocity, rapid, aseismic transient slip. Second, these slip behavior are not temperature/depth dependent, so that the mechanical behavior evolves along strike. Finally, the mode of slip of a given portion of the plate interface may vary as a function of the imposed slip conditions: Barriers to small earthquakes may break during larger ones. Similarly, the ordinarily aseismic portion of the plate interface may be affected, during very large earthquakes, by large coseismic slip.

### **B. Intrinsic factors controlling the deformation mode along the plate interface**

#### *1. Plate roughness*

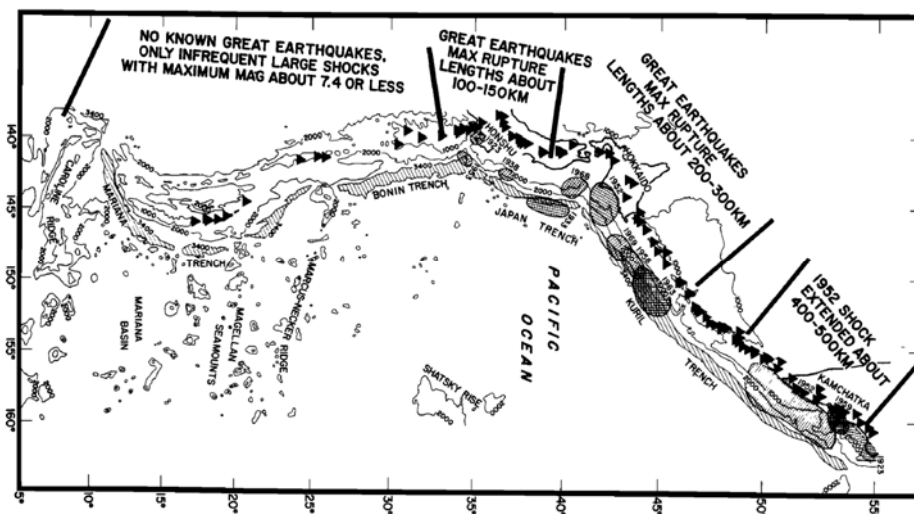


*Figure 7: Relationship between subducting plate roughness and large earthquakes in western Pacific (Kelleher and McCann, 1976). North is to the right of the figure.*

The roughness of the lower plate interface, which can host topographic highs such as seamounts or ridges, is potentially a control factor on the seismic character of the plate interface. The comparison, at a very large scale, of the distribution of lower plate roughness with the distribution of great earthquakes (e.g. in the western Pacific area, see Figure 7) suggest that a relatively flat and smooth seafloor favors large ruptures (Kelleher and McCann, 1976). This analysis has been further substantiated by recent statistical analysis of world-wide subduction zones, showing that very large ( $M_w \geq 8.5$ ) earthquakes are preferentially hosted in domains of

smooth oceanic plates, while large ( $7.5 \leq M_w \leq 8.5$ ) earthquakes are much less influenced by plate roughness (Lallemand et al., 2018; Van Rijsingen et al., 2018) (Figure 8).

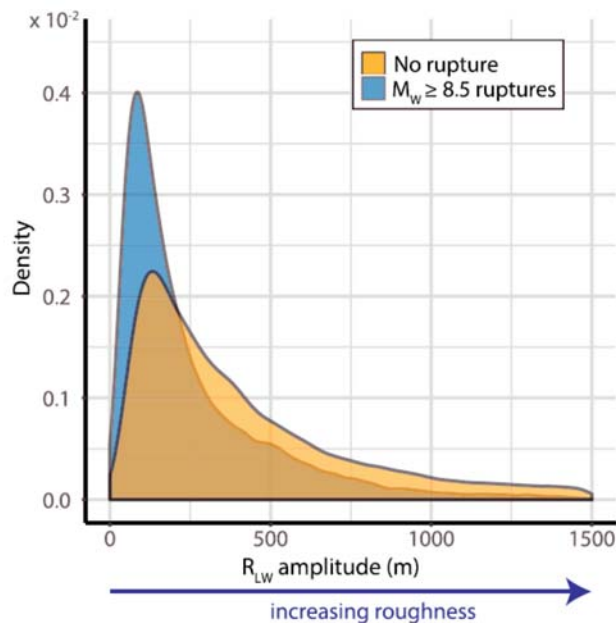


*Figure 8 : Distribution of seafloor topography for segments of subduction zones without rupture (yellow) and with large earthquakes (blue), from (Van Rijsingen et al., 2018). Segments where large rupture occur are much smoother, at the wavelength of topography considered ( $R_{LW} = 80-100\text{km}$ ).*

From the observation that large earthquakes are generated preferentially in domains of thick trench-fill (Ruff, 1989), Cloos and Shreve (1996) argue in a rather opposite direction about the role of seamounts. They developed their subduction channel theory to propose that subducted seamounts, when they are preserved from shallow truncation by their thick sediment cover, act at depth as seismic asperities to generate large earthquakes, because of their hypothetical strong coupling to the upper plate.

The role of the relief of the subducting plate on seismicity is rather controversial, in particular because the set of observations is to some extent contradictory. Off the Nicoya Peninsula of Costa Rica, subducted seamounts coincide with the rupture zone of the 1990 Mw7 (Husen et al., 2002) or 1999 Mw6.9 (Bilek et al., 2003) earthquakes. Seamounts are therefore assimilated to the seismic asperity that broke during the earthquakes. Similarly, In Central Ecuador, high interseismic locking correlates with the subduction of an oceanic relief with a limited sediment cover (Collot et al., 2017). Another example can be found along Java, where the 1994 Mw7.6 earthquake, associated with a large tsunami, is interpreted as caused by slip on a seamount locked at depth along the plate interface (Abercrombie et al., 2001).

On the other hand, in Ecuador, a low coupling zone is aligned with bathymetric highs of the Carnegie Ridge (Chlieh et al., 2014). Further south, in Peru, the Nazca ridge appears also as a barrier to rupture during large earthquakes (Perfettini et al., 2010). Along Japan Trench, weak

coupling above subducting seamounts, including Daiichi-Kashima, is advocated (Mochizuki et al., 2008) on the basis of micro-earthquake distribution.

A recent contribution (Wang and Bilek, 2016) was dedicated to try to reconcile these different observations into a unified view. Their analysis of source time function of large earthquakes in domains of subducting seamounts show a very complex pattern, reflecting the rupture of multiple fractures/seismic patches. Such behavior is considered as unfavorable to the propagation of the rupture over hundreds of kms, as is observed during mega-earthquakes, and is in agreement with the observations by Kelleher and McCann (1976) and the statistical analysis of (Lallemand et al., 2018; Van Rijsingen et al., 2018).

The main process of seamount deformation in Wang and Bilek (2016) model is aseismic slip, resulting from damaging in the hanging wall and slip on a relatively wide network of fractures, as suggested in upper margin features and sandbox modeling experiments (Dominguez et al., 1998; Dominguez et al., 2000; Lallemand and Le Pichon, 1987; Lallemand et al., 1992). Such a model hardly accounts for the moderate and up to large ( $M_w \sim 7$ ) earthquakes reported above. The dataset on the behavior of seamounts shows actually a large variability, from no to complete coupling, so large that it seems difficult to reduce it to a “single” property.

Another possible role of subducting plate topography is to drag sediments and water to large depths. Hypocenters of  $M_w 9.0$  Tohoku-Oki-related earthquakes (foreshocks, main rupture and aftershocks) along NE Japan margins are located in a zone of high-V above the plate interface (Figure 9), in between two zones of low-V (Zhao et al., 2011). The northern, low-V zone corresponds also to a domain of low seismic coupling (Yamanaka and Kikuchi, 2004). Such domain is correlated with domains of horst-and-graben in the subducting plate (Tsuru et al., 2000), and Yamanaka and Kikuchi (2004) make the hypothesis that these topographic features bring water down the subduction zone, which would eventually inhibit large seismic slip.

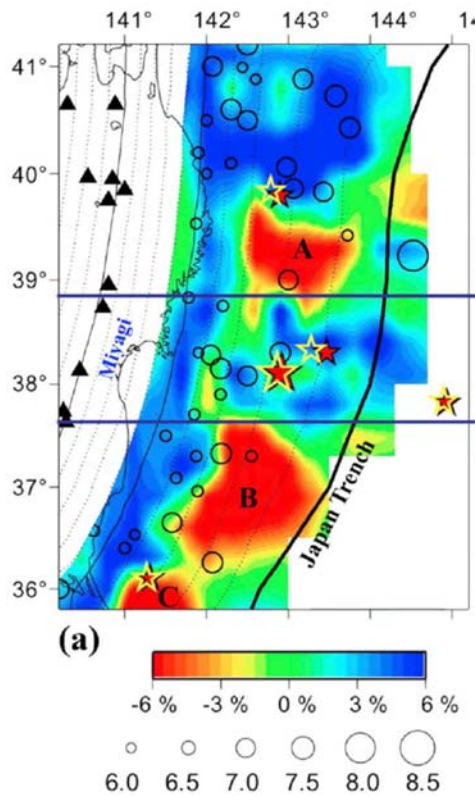


Figure 9 : P-wave tomography analysis above the plate interface (Zhao et al., 2011). The Mw9.0 Tohoku-Oki hypocenter is shown as a red star, large foreshock/aftershock with smaller stars, while the two blue line delimit roughly the domain of the plate interface where coseismic slip was larger than 25m.

## 2. Nature of subducting material

The mechanical behavior of the plate interface is also controlled to some extent by the nature of the material constituting the décollement, i.e. the actual zone of slip. In many instances, the décollement localizes in a stratigraphic horizon rich in smectite (Vrolijk, 1990), an argument that was later on used to connect the frictional properties of the plate interface with the smectite-to-illite reaction (Hyndman et al., 1997). The abundance of smectite in the slipping horizon was recently shown in the Mw9.0 Tohoku-Oki earthquake, where the décollement contains up to 90% of smectite (Kameda et al., 2015). The effect of smectite to decrease strength is extremely large (Ujiie et al., 2013), in agreement with the earlier friction work on clays (Byerlee, 1978; Morrow et al., 1992; Tembe et al., 2010; Wang et al., 1980).

On the other hand, the frictional stability of smectite is incompatible with the generation at shallow depths of slip instabilities such as SSE (Ikari and Saffer, 2011). Furthermore, there is no fundamental difference, in terms of frictional stability, with illite (Saffer et al., 2008), so that the updip limit of the seismogenic zone remains unexplained.

A potential solution, to generate slip instability in smectite-rich gouges, was proposed by (Ikari et al., 2013), who described, instead of the classical (a-b) rate dependence (Figure 10), the

evolution of the slope of the friction coefficient as a function of slip  $\eta = \frac{d\mu}{dx}$ , which is negative (i.e. slip-weakening) in the range of velocity step tested. This proposition, if attractive, makes actually the problem much more complex: If the friction coefficient depends not only on slip velocity (as in rate-and-state friction laws, including, with parameter b, the evolution with slip after each velocity step) but also on slip (with the slip-weakening law), then the material constitutive laws are dependent on the slip history of the material. In such case, it is much questionable what do mean tests with powdered then remolded material, as carried out for most samples in (Ikari et al., 2013; Ikari and Saffer, 2011). Furthermore, the slip weakening described is extremely large: Converting slip into strain, slip-weakening of  $-10^{-2}$  implies a decrease in friction coefficient of 0.1, i.e.  $\sim 25\text{-}50\%$  of overall friction coefficient, for a slip of 10mm, equivalent to strain of  $\sim 6$ . The actual strain on décollement or slip zones within the accretionary prism is much larger, hence the slip-weakening trend derived from experiment cannot be a steady-state feature of the natural slip zones. The applicability of this slip-weakening concept and value is therefore very arguable.

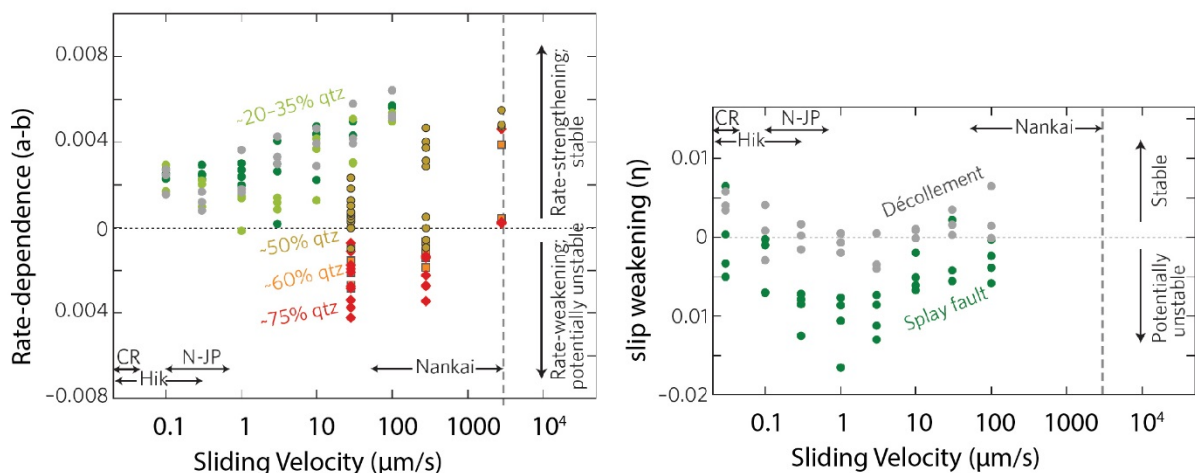


*Figure 10 : Friction experiments results in Saffer and Wallace (2015), compiling results from Ikari et al. (2013) and Saito et al. (2013). (Left): In the traditional rate-and-state framework, the addition of quartz to clay mixture results in rate-weakening behavior. (Right): using a new formulation accounting for the decrease in friction coefficient with slip, the maximum of instability coincides with slip velocities of  $1\text{-}10\mu\text{m/s}$ , i.e. the same magnitude as slow slip shown with double arrows. Grey and green points from (Ikari et al., 2013), orange and red ones from (Saito et al., 2013).*

Another line of thought, to account for the transition aseismic-seismic transition at shallow depths, relies on variations in lithology with depth, in particular quartz. In friction experiments, quartz has been shown to promote slip instability (Ikari et al., 2011; Logan and Rauenzahn, 1987; Tembe et al., 2010). Saffer and Wallace (2015) propose that there is an increase in quartz content of the décollement zone as a result of preferential quartz veining and cementation,

which would result in an evolution towards velocity-strengthening behavior. This evolution is nevertheless poorly documented: First, on a recent study of a fault zone in the Shimanto Belt in Okinawa, fault breccia is shown to be richer in quartz than foliated fault rocks or host rock (Saito et al., 2013). But in this study, only a single sample in each structure is analyzed (while there is very large variability in mineralogy within a given unit, e.g. (Fukuchi et al., 2014)) and while no mention is made of the volume of the material is analyzed, the host rock is a relatively coarse-grained turbidite with levels of sandstone, so with an intrinsically large variability in quartz content. The second reference provided refer to a thrust zone in the Franciscan Complex, injected by a dense network of calcite veins (Meneghini and Moore, 2007), a case that is often found in deformed horizons from exhumed accretionary prisms (Raimbourg et al., 2015). Nonetheless, geochemical evidences point rather to local redistribution of elements, rather than to a net influx of quartz or calcite, and there is to our knowledge no well-documented example where the fault zone is shown to be richer in quartz than foot- and hanging wall. The idea that the quartz or calcite proportion increases along with burial within the slip zone is therefore unsupported by data.

In summary, the pattern emerging from experimental work on friction is confusing irrespective of the depth domain considered. On the one hand, the velocity-strengthening behavior of clays, across the smectite-to-illite transformation, is difficult to reconcile with the SSE or the large rupture within the seismogenic zone. On the other hand, lithological variations with depth, such as an increase in quartz in slip zones, invoked to account for the onset of slip-weakening at depth, are so far not supported by a sufficient amount of data.

### ***3. Geodynamical parameters***

Different statistical studies have tried to classify the different subduction zone worldwide, in an attempt to connect their mechanical properties to geometrical and kinematic ones. For example, the classical work by Uyeda and Kanamori (1979) define two end-members, the “Chilean type”, with a low dip of the lower plate, compression in the upper plate and large earthquake, and the “Mariana type”, with a large dip, tension in the upper plate and absence of large earthquakes (Figure 11). The authors connect these configurations to several parameters, such as the age of the subducting plate, or the motion of the lower plate with respect to asthenosphere or deep mantle.

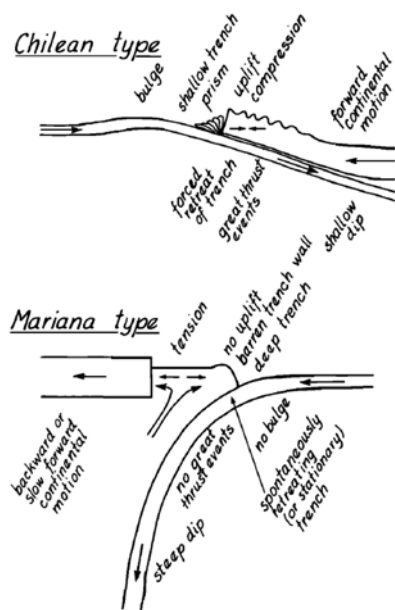


Fig. 7. Two kinds of subduction boundaries.

*Figure 11: Early attempt at classifying subduction zone according to their geometry (in particular dip angle), tectonic régime in the upper plate and potential to generate large earthquakes (Uyeda and Kanamori, 1979).*

This first attempt provided the basis for several posterior studies on the correlation between the many parameters characteristic for subduction zones, with contrasted or even contradictory results. In Pacheco et al. (1993) no clear correlation is found between seismic coupling and other parameters of the plate (age, subduction velocity) or sediments nature/thickness, seafloor topography. A much larger dataset was used in (Heuret et al., 2011) for their statistical analysis of parameter correlation. They found first that no correlation exist between the maximum magnitude recorded across a subduction segment and the age of the slab, on the contrary to the early proposition by Ruff and Kanamori (1980). Similarly, there is no correlation between the maximum magnitude and the slab dip, in contradiction with the Chilean-Mariana dichotomy proposed above. In terms of mechanical behavior, several conclusions emerged in Heuret et al. (2011). First, the best correlation with the seismic characters of a subduction zone (seismic rate, maximum magnitude or moment release rate) is found for the subduction velocity. Second, the largest earthquakes are associated with a neutral stress state in the upper plate (and not with a compressive state, as proposed by Uyeda and Kanamori (1979)). The statistical compilation is also at variance with the proposition by (Scholz, 1995, 1998) of a control on seismic coupling of the plate interface by the normal stress across the interface. Based on a stability criterion derived from friction laws, (Scholz, 1995, 1998) predicted that the seismic/aseismic character of the interface was related to a large/low normal stress across the interface, which in turn could be correlated at first order with trenchward/opposite to trenchward motion of the upper plate. The data compiled in (Heuret et al., 2011) show actually no correlation between upper plate

velocity and the seismic features of the subduction interface, discarding (Scholz, 1995, 1998) model, which integrated too many simplifying hypotheses in the large-scale force model elaborated to estimate the normal stress across the interface.

Overall, the statistical correlations with seismic features are relatively small (Heuret et al., 2011), i.e. no single, or combination of the large-scale parameters considered can be considered as a very good control on the mechanical properties of the plate interface. Said conversely, the plate interface behavior is too complex and multifactorial to be reducible to a single or a few large-scale kinematic or geometric parameters. Furthermore, if some correlations emerge, as for example with the subduction velocity or the state of stress in the upper plate, no mechanistic model is proposed to relate these parameters with the mechanical behavior of the plate interface.

#### ***4. Geophysical attributes of the plate interface: from observations to physical properties***

The most direct source of information about the properties of the material along the plate interface is given by geophysical studies. The observation of the slip distribution and seismic wave radiation during earthquakes and rapid aseismic slip provides indeed a dynamic image of the interface behavior. In both cases, the difficulty is then to interpret such geophysical attributes in terms of physical properties.

##### **a) Seismic slip**

The depth variations of earthquake rupture processes provide insights into the mechanical properties of the surrounding material. In particular, the variations in the duration of slip, for a given magnitude, is related to the shear modulus of the rock along the ruptured domain (Bilek et al., 2012; Bilek and Lay, 1999; Bilek et al., 2004). Along the subduction plate interface, the shallower (down to ~10-20km depth) portion of the plate interface is characterized in several subduction zones by a larger duration (normalized to magnitude), interpreted by the authors as reflecting the lower shear modulus of the rocks composing it compared to the deeper portion of the seismogenic depth interval.

Similarly, the seismic attributes of tsunamigenic earthquakes are a long duration, a small stress drop, often interpreted as reflected slip in the near-trench area through low-strength material (Bilek et al., 2016). Indeed, the depth distribution of the frequency of the seismic wave radiated during the Mw9.0 Tohoku-Oki earthquakes show that the shallower portion of the rupture area, where slip was very large (Lay et al., 2011), had a weak component of high-frequency, in contrast to the downdip portion of the rupture area (Koper et al., 2011).

The interpretation of such seismic attributes in terms of material physical properties geometrical properties of the rupture, is nevertheless not straightforward. The decrease in slip duration

observed in several subduction zones could as well result from a larger slip area, for constant rigidity (Bilek and Lay, 1999). Due to the number of unknowns, it is difficult to get univoqual properties solely from the seismic attributes.

The properties of the plate interface can also be deduced from the evolution in time of the distribution of aftershocks over the rupture area of large earthquake. (Tajima et al., 2013) connect a strong/weak coupling on the interface to limited/large propagation of the aftershock swarms with time (by comparison of the 1 day and 1 year period of time after the main shock). The properties of NE Japan interface are nevertheless ambiguous in this respect, as recurrent M7 events and the 2011 M9 events are characterized by propagating and non-propagating aftershocks, respectively.

#### **b) Aseismic slip (afterslip and slow slip)**

Fitting of afterslip after large earthquakes is a powerful approach to the mechanical properties of the plate interface. Afterslip on the two patches that crept after the 2007 Mw8 Pisco earthquake (Perfettini et al., 2010) can be successfully carried out with rate-strengthening laws, yielding parameters describing the rate dependence  $\frac{d\tau}{d\log(\dot{U})}$  in the range 0.1-1MPa.

Similarly, in the zone of afterslip of the 2003 M8.0 Tokachi earthquake, (Miyazaki et al., 2004) use the simple, unidimensional spring-slider model to interpret the slip vs stress evolution as reflecting velocity-strengthening behavior with  $(a-b)\sim 10^{-3}$ .

In another modelling approach to SSE, (Liu and Rice, 2005) observed the spontaneous generation of slow slip events in the domain of transition of frictional behavior, near the downdip limit of the seismogenic zone. The transition from velocity-weakening to velocity-strengthening with slip velocity is also advocated by (Saffer and Wallace, 2015) as a potential factor for slow slip generation. Similarly, (Rubin, 2008) proposes a process of stabilization of fault slip through an increase in fracture energy with slip velocity, revolving around dilation and pore fluid pressure reduction.

These models also provide theoretical arguments in favor of large fluid pressure, either through the recurrence of SSE (Liu and Rice, 2007), nucleation length (Rubin, 2008) or the stress levels required to trigger the slip events (Liu and Rice, 2007; Rubinstein et al., 2007).

Therefore, these different approaches to slow slip converge towards a vision of the plate interface properties where the material is either frictionally stable or at the transition stable-unstable, in a context of large fluid pressure.

## 5. Conclusion

There is no intrinsic properties that can be singled out to account for the diversity of the mechanical behavior observed in subduction zones. The image of seamount acting as asperities scratching the upper plate and triggering large earthquakes is in most cases not supported by the data. In contrast, the homogeneity of the subducting plate is rather a condition for large rupture areas. Another favorable conditions for seismic deformation of the plate interface are a high velocity of the subducting plate and a neutral state of strain in the upper plate. Still, these large-scale correlations do not pinpoint the mechanisms at stake to control the deformation mode. Attempts to interpret these correlations rely on geometrical factors (deformation through a fault network favoring aseismic slip in subducting seamounts) or on fluid (dragging down of water within horst and grabens), but lack supporting evidence. The deterministic approach to subduction mechanics relies solely on friction laws. So far, there is no convincing result to account for the seismic vs. aseismic transition. The generation of slow slip events is possible in this framework and in many models involves large fluid pressure.

### **C. The role of fluid pressure to the mechanical behavior of the plate interface**

While lithological parameters cannot so far explain the diversity of deformation modes along the plate interface, fluid properties, in particular its pressure, are commonly raised as the main controlling factor. Indeed, while the rocks properties are fixed, or change slowly along with the diagenetic and metamorphic reactions, fluid pressure may vary over a much smaller time-scale. In addition, friction laws are often cast in terms of effective pressure, where the fluid pressure counterbalances the lithostatic pressure (Dahlen, 1990; Hubbert and Rubey, 1959).

#### ***1. Shallow overpressure***

In the relatively shallow (~a few km below seafloor) domain of accretionary prism, the décollement appears in many cases as a well-defined seismic reflector (Figure 12), for example in Nankai (Bangs and Gulick, 2005; Park et al., 2002; Tobin and Saffer, 2009), Barbados (Moore, 2000) or Costa Rica (Shipley et al., 1990). In Nankai, the reflector has a negative polarity and the modelling of the associated waveform shows that the material below the décollement has lower density/higher porosity than the material above (Bangs et al., 2009).

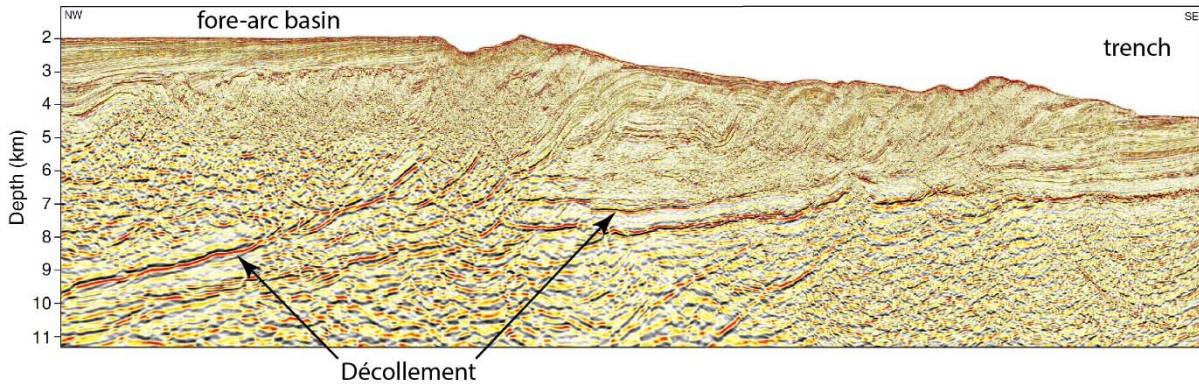


*Figure 12: Seismic cross-section of the Nankai accretionary prism off Kii peninsula. The décollement, separating underthrust from accreted sediments, appears as a sharp reflector, with a negative polarity, interpreted as the result of impedance contrast between lower-velocity-higher-porosity underthrust sediments and higher-velocity-lower-porosity accretionary prism sediments (Moore et al., 2009).*

Such a contrast is confirmed in drilling across the décollement in the vicinity of the trench: there is for example a drop in both velocity and density (hence an increase in porosity) across the décollement, towards the underthrust material, observed in Nankai (e.g. site 1174 (Shipboard Scientific Party, 2001)), Costa Rica (e.g. site 1040 (Shipboard Scientific Party, 1997)) or even Barbados (sites 1044 and 1045 (Moore et al., 1998)), even if in the latter case the porosity anomaly is focused on the décollement zone itself and not over the entire underthrust section.

From these observations, the general hydrological model of the prism is based on the idea that the material below the décollement is underconsolidated, i.e. it cannot expel water and compact at the pace it is buried (Kastner et al., 1991; Le Pichon et al., 1993; Saffer and Tobin, 2011). Water in the pore of subducted sediments acts therefore as a source of water and the fluid pressure field is the result of the equilibrium of fluid production by compaction and fluid expulsion towards the surface by Darcian flow (Bekins and Dreiss, 1992; Saffer and Bekins, 2006).

Beyond this qualitative model, the next step is to derive, from seismic properties, the amplitude of fluid overpressure along the décollement and in the underthrust section. It requires several calibrated relationships. First, seismic velocity have to be converted into porosity, on the basis principally of experimentally calibrated laws, such as provided in (Erickson and Jarrard, 1998), (Hoffman and Tobin, 2004), or our own work (Raimbourg et al., 2011). Second, one has to assume that compaction in basins in the settings of vertical, uniaxial load, can apply to any compaction setting, i.e. there is a unique porosity-fluid pressure relationship for a given material. Under this hypothesis, compaction laws (e.g. (Baldwin and Butler, 1985; Bray and Karig, 1985; Issler, 1992; Velde, 1996)) can be applied to underthrust material to convert porosity into fluid and effective pressure.

The application of such an approach can be found in Tobin and Saffer (2009), where in the Nankai Trough, off Muroto Peninsula, low seismic velocity towards the base of the accretionary prism and in the underthrust sediments are interpreted in terms of abnormally high (with respect to the fluid drained conditions) porosity and fluid pressure.

Anomalies in fluid pressure can then be compared with the mechanical behavior of the plate interface. For example, in Hikurangi subduction zones, along strikes variations in fluid pressure are derived from contrast in seismic velocity (Basset et al., 2014), and fluid-pressurized zones in the northern domain of the subduction zone coincide with anomalously shallow downdip limit of the locked portion of the plate interface, as well as shallow SSE. In their review of shallow SSE and low-frequency earthquakes, Saffer and Wallace (2015) propose that these phenomena correlate with domains where the fluid pressure is extremely high, with examples cited in northern Hikurangi, northern Japan, Nankai and Costa Rica.

The hypothesis of high fluid pressure is rather attractive, and the compilation of four different cases makes the argument rather compelling, but when considered in detail there are very strong limitations to the four cases studied.

In Costa Rica, the pore pressure profile at depth is constrained by a parametric, hydrological model, with only very shallow data (pore pressure and chloride profile in drilled hole 1040, shallower than 1000mbsf) (Spinelli et al., 2006).

In Nankai, the pore pressure level is constrained to very high values by mechanical considerations on the level of stress before and after Tohoku-Oki, or on the critical state of the prisms, but on the hypothesis of normal friction of 0.6 in the décollement (Kimura et al., 2012). Later work has shown that the décollement of NE Japan runs through very weak, smectite-rich material, with a much lower friction coefficient (0.1 to 0.3), so that estimated fluid pressure are much smaller (Ujiie et al., 2013).

The two other cases raised by Saffer and Wallace (2015) are based on the interpretation of seismic velocity profiles in terms of fluid pressure, hence they rely on  $V_p$ -porosity-effective pressure calibrated laws, as exposed above.

The first difficulty arises, in high-porosity rocks, from the fact that there are multiple  $V_p$ -porosity relationships, as well as multiple compaction curves, reflecting for example the variable lithology of the compacting material or the state of stress (uniaxial, vertical loading or horizontal shortening in accretionary complexes) (Figure 13).

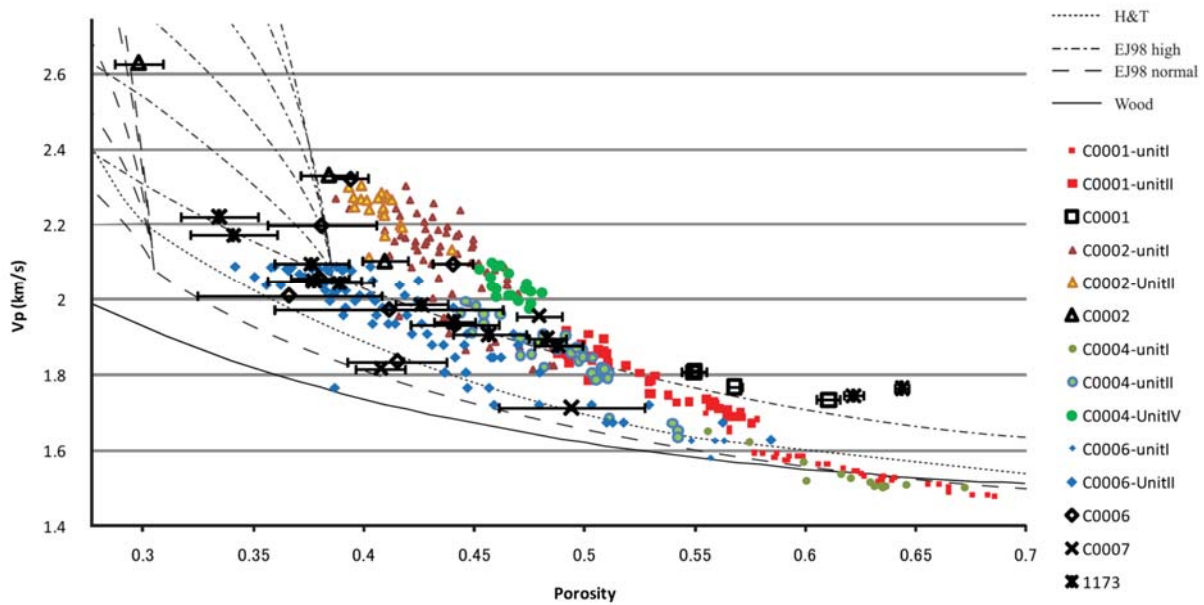


Figure 13: Velocity-porosity points in the Nankai Trough area, from logging data and experimental measurements on core samples (Raimbourg et al., 2011). Superimposed laws include (Hoffman and Tobin, 2004), (Erickson and Jarrard, 1998) for normal (basin) and high (accretionary prisms) contexts, and (Wood, 1941). Around 40% porosity, variations ~20% are observed. Larger variations are predicted at smaller porosity, according to the material composition and tectonic settings (Erickson and Jarrard, 1998).

The problem worsens with increasing depth and decreasing porosity. This can be observed in all the dataset compiled by Erickson and Jarrard (1998), where below 20% porosity scatter in velocity increases strongly. For sedimentary rocks with a porosity lower than 10-5%, there is no single relationship  $V_p$ -porosity-fluid pressure that can be fit to the data. It can be readily shown in the Figure 14, where the single curve fit to velocity-porosity relationship is good for low-porosity rocks, but becomes meaningless for the metamorphic samples with a low porosity, as a result of the combination of texture development, mineral reactions and cementation. Given the very strong decrease in porosity with depth, and the low temperature conditions for diagenetic reactions to start (e.g. 40-60°C for opal-to-quartz reactions (Spinelli et al., 2007)), the interpretation of velocity anomalies becomes difficult deeper than a few km below seafloor.

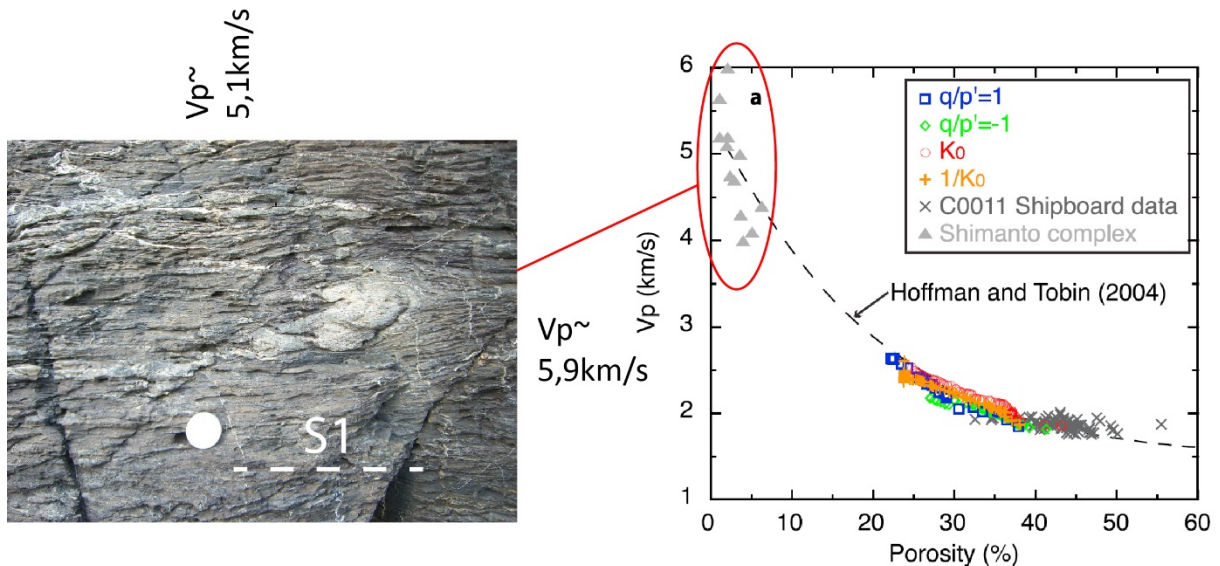


Figure 14: The  $V_p$ -porosity relationship, well-defined for porosity above 20% (Kitajima and Saffer, 2012), breaks down for rocks with a porosity lower than ~5-10%. The low-porosity data points, from (Tsuji et al., 2006), comes from low-grade metamorphic rocks in the Shimanto Belt. The large variations in  $P$ -wave velocity is correlated with structural and textural parameters: foliation-parallel  $V_p$  is higher, by ~20%, than foliation  $V_p$ . In this low-porosity range, there is no longer a unique relationship between porosity and velocity.

As a result, the quantitative estimation of the overpressure in the Northern Hikurangi by (Basset et al., 2014) is highly questionable, as they consider depth in the range 2-10km and porosity in the range 10-30%. Consequently, if there are many arguments (velocity anomalies, taper angle, hydrological models), raised for example in (Saffer and Tobin, 2011), so far the quantification of the amplitude of the overpressures remains rather elusive. Accordingly, it is difficult to correlate fluid state with mechanical behavior.

## 2. Deep overpressure

Considering now deeper overpressure, they are inferred principally from low-velocity or high  $V_p/V_s$  anomalies. Large variations in  $P$ - and  $S$ -wave velocities are observed in the upper plate above the interface along NE Japan margin (Tajima et al., 2013; Zhao et al., 2011). Rupture zones of several large earthquakes, including the M9 Tohoku-Oki, are principally located below high- $V$  areas of the upper plate (Figure 9). Similarly, along the Chile margin, the distribution of high seismic coupling seems to correlate with areas of lower fluid pressure along the plate interface (Moreno et al., 2014). Nonetheless, in this example, the variations in inferred fluid pressure are relatively small, while the average fluid pressure is extremely high, close to lithostatic values.

The amplitude of fluid pressure has also raised a lot of attention with respect to deep slow slip generation. Large  $V_p/V_s$  domains have been observed in the subducting crust roughly coinciding with SSE generation in the SW Japan subduction zone across central Japan, in the

depth range 15-40km (Kodaira et al., 2004). Similarly, the subducting crust was imaged as a low velocity layer, with high  $V_p/V_s$  ratio, interpreted as reflecting large fluid overpressure, in Cascadia, at depth  $\sim$ 20-40km (Audet et al., 2009; Nicholson et al., 2005). The authors note that the anomaly in velocity or velocity ratio terminates at  $\sim$ 45km depth, and interpret this fact as a result of onset of eclogitization of downgoing crust. The anomaly in  $V_p$  or  $V_p/V_s$  ratio is tentatively interpreted as a result of large fluid overpressure (Abers et al., 2009; Audet et al., 2009) and is shown to coincide with the zone of generation of ETS. In Costa Rica, along-strike segmentation of the margin in terms of slip behavior is correlated with  $V_p/V_s$  ratio in the subducting crust and overlying fore-arc: high  $V_p/V_s$  ratio in crust and even more in the fore-arc are identified where slow slip events were generated (Audet and Schwartz, 2013). The authors interpret in this case also the seismic signature as being related to fluid pressure.

Another independent evidence for large fluid pressure comes from the generation of LFE near the downdip limit of the plate interface. Some LFE in Cascadia area were generated as a result of the propagation of Love waves associated with very small stress changes ( $\sim$ 45kPa) (Rubinstein et al., 2007), which suggest that in the pre-LFE stress state the effective stress is very small and the fluid pressure close to lithostatic (although near-critical, but not necessarily small, stress could be an alternative explanation). A similar reasoning is proposed in (Liu and Rice, 2007): non volcanic tremor, occurring during the time period of the SSE in the Cascadia area, have hypocenters principally localized in the spatial domain corresponding to a release of stress for a vertical fracture. From this observation, the authors propose that the SSE created conduits for fluids that triggered the tremor. This model implies that the pre-SSE has a near-lithostatic fluid pressure, so that the small decrease in stress due to the SSE ( $\sim$ a few hundredths of MPa) is sufficient to open fracture.

In their detailed review of the worldwide relationship between deep slow slip event and seismic signature of the subduction, (Audet and Kim, 2016) note that, if deep SSE and tremor are associated to zone of low velocity interpreted as resulting from high fluid pressure, the velocity anomaly within the downgoing crust extends well updip (i.e. within the zone of classical earthquakes) and downdip from the area where slip is generated. Therefore, the relationship between fluid overpressure and mechanical behavior is not straightforward and overpressure are considered as necessary, but not sufficient condition for ETS occurrence.

Furthermore, (Audet and Kim, 2016) note the relationship in Cascadia and Costa Rica between the geological features of the subduction zone and the generation of deep ETS, which hints at some control by the rock nature/structure (including its permeability behavior). Another interesting prospect evoked in this paper is raised by seismic anisotropy characterization near ETS source, which in turn may be related to the anisotropic texture of rocks resulting from

shearing along the plate interface. Such seismic attribute could enable to image structural features and their potential relationship with active deformation processes.

An interesting point to note with respect to the interpretation of seismic anomalies in terms of fluid overpressure is the paucity of experimental data. In SW Japan (Kodaira et al., 2004), Cascadia (Audet et al., 2009), Coasta Rica (Audet and Schwartz, 2013) or Chile (Moreno et al., 2014), the effect of pore fluid pressure on seismic velocity is based on experimental measurements on basalts and dolerite (Christensen, 1984) and on sandstone (Christensen and Wang, 1985).

In the former article, no permeability measurements provide the evidence that the time lapse is sufficient for the sample to equilibrate with surrounding fluid pressure. We recalculated characteristic timescale of fluid pressure pulse propagation through the sample (Appendix 1) and the hypothesis of equilibration seems reasonable, with respect to basalt/dolerite permeability range. On the other hand, the interpretation of velocity anomaly in terms of very large fluid pressure, close to lithostatic values, is disputable. In the original study (Christensen, 1984) to which the seismic studies refer to, two types of material were tested, one sample of basalt with a porosity of 4% and one sample of dolerite with a porosity of 1%. At several tens of kilometers of depths where the  $V_p/V_s$  ratio are detected, the low-porosity dolerite seems to be a much more appropriate material than the basalt with a large porosity. On the dolerite, the effect of pore fluid pressure variations, even to 0.05kbars of effective pressure ( $P_{eff}=P_c-P_f$ ), is relatively limited (Figure 15):  $V_p/V_s$  increases from 1.81 to 1.84 over a 1.5kbar range in  $P_{eff}$ . These variations are first much smaller than the variations due to lithological changes: the largest change occurs between dunite and serpentine, with  $V_p/V_s$  ratio of 1.75 and 2.05 (Christensen, 1996). Second, the  $P_{eff}$ -related variations are much smaller than the amplitude of the anomalies detected in the subduction zones, with  $V_p/V_s$  commonly in the range 2 to 3.

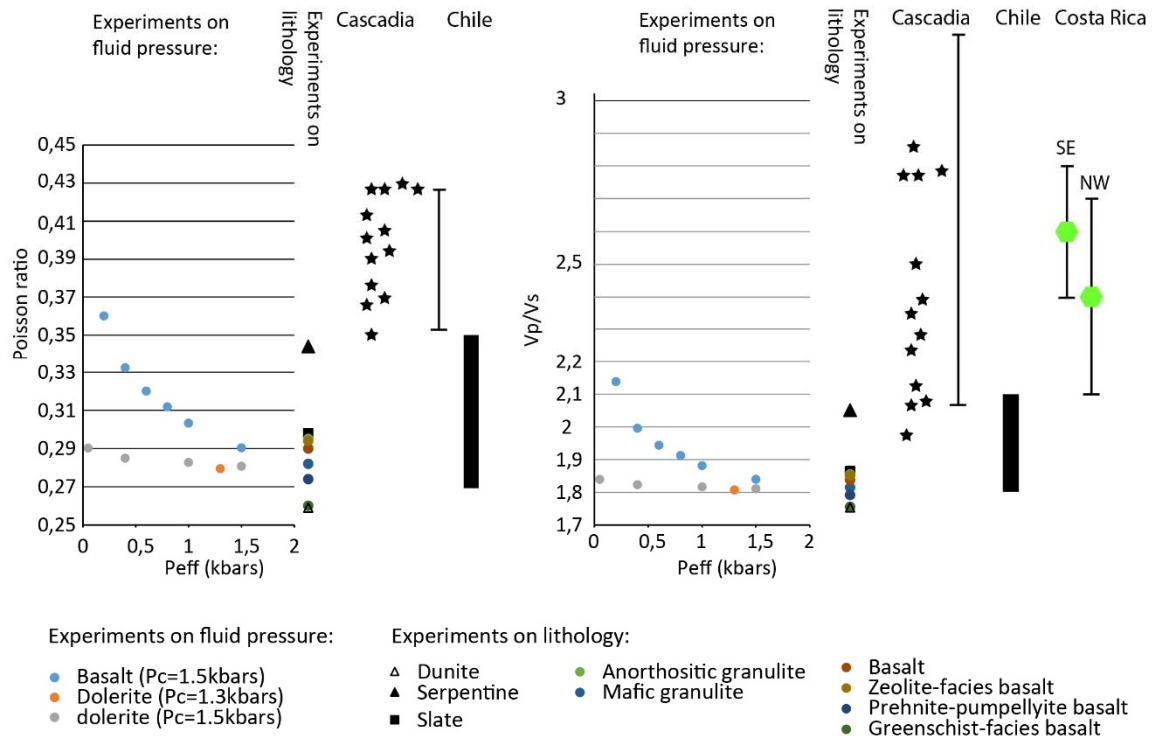


*Figure 15: Comparison of the anomalies in Poisson ratio (left) and  $V_p/V_s$  ratio (right) in subduction zones with the experimental measurements. Experiments include the effect of effective pressure (Christensen, 1984) and of the lithology (Christensen, 1996). Seismic anomalies in subducting slab from Cascadia (Audet et al., 2009), Chile (Moreno et al., 2014) and Costa Rica (Audet and Schwartz, 2013). One can note the very small effect of the effective pressure on  $V_p/V_s$  or Poisson ratio in dolerite (comparable to deeply subducted oceanic crust) compared to the anomalies actually observed in subduction zones.*

From these experimental data, the interpretation of the extremely high anomalies in  $V_p/V_s$  and Poisson ratios is not clear. High fluid pressure may contribute to it, but to an unknown extent, so that the link between very large fluid pressure and slow slip gets more difficult to establish.

### 3. Mechanical effect of fluid pressure

The interactions between the pore fluid and the surrounding solid have been defined in the framework of the poro-elastic formulation (Biot, 1941; Rice and Rudnicki, 1979). (Rice and Rudnicki, 1979) describe how the presence of fluid can help stabilize slip, through two distinct processes. First, fluid-saturated rocks, which form the surrounding of the fault, have a stiffness that varies depending on the speed of loading, and during rapid (coseismic) loading, the stiffness is maximum (undrained case), which stabilizes the slip. The second effect is related to the creation of porosity at the tip of the cracks through its progression, reducing the pore pressure and increasing the effective pressure. Such dilatant strengthening would also tend to prevent runaway propagation of the rupture. A similar effect of dilatancy (i.e. increase in porosity upon increase in slip velocity) has also been demonstrated in friction experiments on gouge material

(Marone, 1998; Marone et al., 1990) representative of more mature faults. A converse effect of the fluid on slip is considered at high velocity, when heat dissipated during slip results in an increase in fluid pressure (Lachenbruch, 1980; Sibson, 1973). Considering the balance between shear heating along the fault and the dissipation of the pressure generated by Darcian flow into the wall rock, shear heating is proposed to play a major role late in the nucleation process, for slip velocity of the order of  $\sim 1$  mm/s (Segall and Rice, 2006).

The processes mentioned above correspond to the effect of a fluid phase wetting the rock pores when considering rupture, but they are active irrespective of the absolute level of the pore fluid pressure. The influence of the fluid pressure can be highlighted when considered stability criteria for slip, e.g. in (Scholz, 1990, 1998):

$$\bar{\sigma}_c = \frac{kL}{-(a - b)}$$

where  $L$ ,  $a$  and  $b$  are parameters of the friction law, describing the critical slip distance and the amplitude of friction variations upon a velocity step, respectively, and  $k$  is the stiffness of the surrounding medium. Instability occurs when the effective normal stress  $\bar{\sigma} > \bar{\sigma}_c$ , i.e. a decrease in the effective stress, for example through an increase in the pore fluid pressure, moves the system towards stable slip. Similarly, considering a more complex behavior involving variations in porosity upon changes in slip velocity, the effective pressure must exceed some threshold for slip instabilities to be generated (Segall and Rice, 1995). Conversely, on modelling slip along the plate interface, slow slip events are generated spontaneously when the effective pressure is extremely low (Liu and Rice, 2007).

#### **4. Conclusions**

Deep fluid overpressure have been largely advocated to account for the occurrence of shallow (Saffer and Wallace, 2015) and deep (Audet and Kim, 2016) rapid aseismic slip events. In contrast, rupture zone of large earthquakes seem to correlate with domains of more limited fluid overpressure, even if the dataset is still too small to draw firm conclusions. These observations are at first order consistent with stability analysis in friction laws, which show that a very large fluid pressure drive the system towards stable slip.

Nonetheless, a striking feature of the seismic studies is that fluid pressure is considered as the only factor on the seismic velocity and  $V_p/V_s$  ratio. This assumption is rather simplistic, as many other processes, including metamorphic deformation and deformation (through texture development), have an effect on the seismic velocities (Figure 13). Furthermore, concerning  $V_p/V_s$  ratio, there is a large discrepancy between the experimental effect of fluid pressure and the actual measurement in subducted material (Figure 14). In both cases, the experimental

dataset on velocities in low porosity material is extremely limited and appears as the limiting point to make further progresses in the understanding of the material properties at depth and its relationship with fluid pressure.

#### **D. Summary**

The great deal of geophysical and geodetic data collected recently in subduction zones has considerably improved our image of subduction zones, adding a lot of complexity to the simple seismogenic zone mode. Slip along the plate interface occurs in many different ways, including the two endmembers rapid coseismic slip and aseismic slip at plate velocity, but also other modes of transient, rapid aseismic slip events. The distribution of these modes of deformation is also complex: in space, as the “seismogenic” depth range covers actually very different modes of deformation, from full coupling (hence slip during earthquakes) to no coupling (hence continuous aseismic creep); in time, as depending on the loading conditions, aseismically creeping portions of the plate interface may break during large earthquakes.

The deformation processes behind these macroscopic modes of slip are systematically considered in the framework of rate-and-state friction (RSF) laws, where velocity-strengthening, -weakening and neutral, are associated with aseismic creep, seismic slip and slow slip portions of the plate interface, respectively. Nevertheless, if RSF laws are a powerful theoretical tool, there is so far no clear interpretation, in terms of material properties or structure, to account for the supposed variations in frictional properties along the plate interface. In this topics, the insights from deformed zones in fossil subduction zones constitutes an alternative to the experimental approach of plate interface mechanics. For this purpose, we describe in **chapter III** our observations of fossil structures and interpret them in terms of mechanical behavior of the plate interface.

In parallel, correlations between the deformation mode and macroscopic variables of the subduction zone have been investigated. The absence of topography of the lower plate is a factor favorable for large earthquakes to occur, although in some examples a coincidence between subducted seamounts and large earthquakes is present. Besides, a high subduction velocity and a neutral state of stress in the upper plate are statistically correlated with the generation of large earthquakes. No clear causal link is provided between the role of these macroscopic factors and the deformation processes along the plate interface.

Fluid pressure plays also possibly a role, with large fluid overpressure favoring SSE generation, as can be inferred from observations and theoretical models of slip using RSF laws. The interpretation of the different macroscopic modes of slip along the plate interface in terms of

fluid pressure is severely hampered by the large uncertainty in the estimation of the fluid pressure amplitude at depth. The experimental data to relate seismic velocity or velocity ratio to fluid pressure are too scarce for a clear picture of the fluid pressure distribution at depth to emerge. In this topics, the record of natural structures, such as veins and fluid inclusions, provides some additional information regarding fluid properties at depth. We describe in **chapter IV** our own results obtained in natural examples concerning the geometry of the fluid circulation, composition and pressure in the depths of subduction zones.

## Appendix

The experimental data of sonic velocity on basalts and dolerite (Christensen, 1984) were carried out with samples with a porosity of ~4 and 1%, respectively, of a relatively large size (~50mm in height x 25mm in diameter). Confining and pore fluid pressure were varied over a relatively large range and for each set of imposed conditions ( $P_c$ ,  $P_p$ ), compressional and shear wave velocities were measured after 12hrs of equilibration. No detail is given about the way pore fluid pressure equilibrates within the sample over this period and one can actually wonder to which extent the internal pore fluid pressure asymptotically approaches the externally-imposed fluid pressure

Within a porous sample, the transmission of a pore fluid pressure variation is given by a mass conservation equation similar to a diffusion equation (Jaeger et al., 2007), which can be written as, for no variation in confining pressure:

$$\frac{\partial P_p}{\partial t} = \frac{kBK}{\alpha\mu} \nabla^2 P_p$$

where  $k$  is the permeability ( $m^2$ ),  $B$  is the Skempton coefficient,  $K$  is the bulk modulus (Pa),  $\alpha$  is the Biot coefficient,  $\mu$  is the fluid viscosity (Pa.s). The coefficient  $D = \frac{kBK}{\alpha\mu}$  is the hydraulic diffusivity, in  $m^2/s$ . The bulk modulus varies as a function of the effective pressure: for example, in experiments on a basalt core,  $K$  increases from ~10GPa to ~50GPa as the effective pressure is raised from a few MPa to 200MPa (Adelinet et al., 2010). Because of the lack of data, we consider for the poroelastic coefficient  $B$  and  $\alpha$  the values of 0.55 and 0.27 in (Jaeger et al., 2007) for another crystalline material, granite. The range of variations of these variables is small and does not affect the order of characteristic time of the problem. Water viscosity is  $\sim 0.8 \cdot 10^{-3}$  Pa.s (Wagner and Pruss, 2002). The largest source of variation lies within the permeability. For the basalts, permeability shows a large range of values,  $10^{-19} - 10^{-13} m^2$  in (Jaeger et al., 2007),  $10^{-15} m^2$  in (Adelinet et al., 2010),  $10^{-18} - 10^{-11} m^2$  in (Saar and Manga, 1999), depending

on porosity and textures of voids and vesicles. For gabbros, the permeability range is much lower, from  $10^{-22} - 10^{-18}\text{m}^2$ , depending on the effective pressure. Variations in hydraulic diffusivity are therefore controlled, at first order, by the permeability variations.

The solutions to pressure diffusion equation above, for a semi-infinite space, are of the form  $\text{erf}\left(\frac{x}{2\sqrt{Dt}}\right)$ . So if the characteristic diffusion length is 12.5mm (from core surface to axis), the characteristic time, given by  $\frac{x^2}{4D}$ , is at most 4hrs (corresponding to a permeability of  $10^{-22}\text{m}^2$ ), so well below the 12hrs time lapse of equilibration before each velocity measurement.

## **Chapter III: The deformation of the subduction plate interface, from the point of view of field geology**

From the review exposed in the preceding chapter, it appears that the plate interface is principally envisioned by the geophysics and rock mechanics community, as a fault plane, governed by friction laws. We develop in this chapter the point of view of field geology, based on field studies and microstructural works carried out in various worldwide examples of exhumed subduction zones. Our own work has focused on one of those fossil examples, the Shimanto Belt in Japan. We have described, in a series of papers, the large-scale tectonic evolution of the whole SW Japan margin over Cenozoic time and the associated growth of the accretionary prism (Raimbourg et al., 2014a; Raimbourg et al., 2017a; Raimbourg et al., 2009). In parallel of this large-scale work, we have also focused on describing the small-scale processes of deformation and the factors that may influence them (Palazzin et al., 2016; Raimbourg et al., 2018; Raimbourg et al., 2017j; Raimbourg et al., 2014b; Raimbourg et al., 2015). The work exposed hereafter integrates some of these earlier results, but is built principally as a new contribution (in the form of a journal article), to present the features of deformation as they can be analyzed in natural structures, from thin-section to outcrop-scale, and the interpretation that can be drawn about the deformation processes at depth along the plate interface.

### **A. Introduction**

#### ***1. Modelling plate subduction deformation***

##### **Regular earthquakes**

The description of stick-slip processes in deformation experiments (Brace and Byerlee, 1966) has opened the way to study earthquake generation using friction experiments. The standard description of friction processes relies on rate-and-state friction laws (e.g. (Dieterich, 1994; Ruina, 1983)), which integrate a dependence of shear stress on velocity (the parameter  $a$ ) and on the state of the sliding surface (the parameter  $b$ ). Using the simple spring-slider model, the stability/instability of the system is shown to depend critically on the sign of  $a-b$  (Gu et al., 1984; Scholz, 1990, 1998). Earthquake cycles on strike-slip (Lapusta and Rice, 2003; Tse and Rice, 1986) or subduction faults (Kato and Hirasawa, 1997; Stuart, 1988) have been successfully modelled (Figure 16) using imposed depth variations of  $(a-b)$ . In these 1-D or 2-D models, the fault has a prescribed geometry and is surrounded by an elastic medium. More sophisticated numerical models have integrated, through an elasto-visco-plastic formulation,

the competition between the different deformation mechanisms (van Dinther et al., 2013). Without prescribing a fault plane, they can successfully reproduce the occurrence of earthquakes along the subduction plate interface and the downdip transition to aseismic slip for  $T$  in the range  $\sim 350\text{-}450^\circ\text{C}$ . In all these models the variations in the slip behavior are controlled through factors intervening in the friction laws: the amplitude and sign of (a-b), the critical slip distance, the friction drop from static to dynamic, or the pore fluid/effective pressure (Lapusta and Rice, 2003; van Dinther et al., 2013). Even in the elasto-visco-plastic formulation (van Dinther et al., 2013), the role of viscous deformation is restricted to the large temperatures of the downdip limit of earthquake rupture. At seismogenic depths, i.e. for temperature of the order of  $200^\circ\text{C}$ , the viscosity of sediments, modelled by wet quartzite dislocation flow law (Ranalli, 1995) in (van Dinther et al., 2013), is larger than  $10^{24}\text{Pa}\cdot\text{s}$  (for high shear stress values of  $100\text{MPa}$ ), hence they cannot any significant fraction of the strain resulting from plate differential motion.

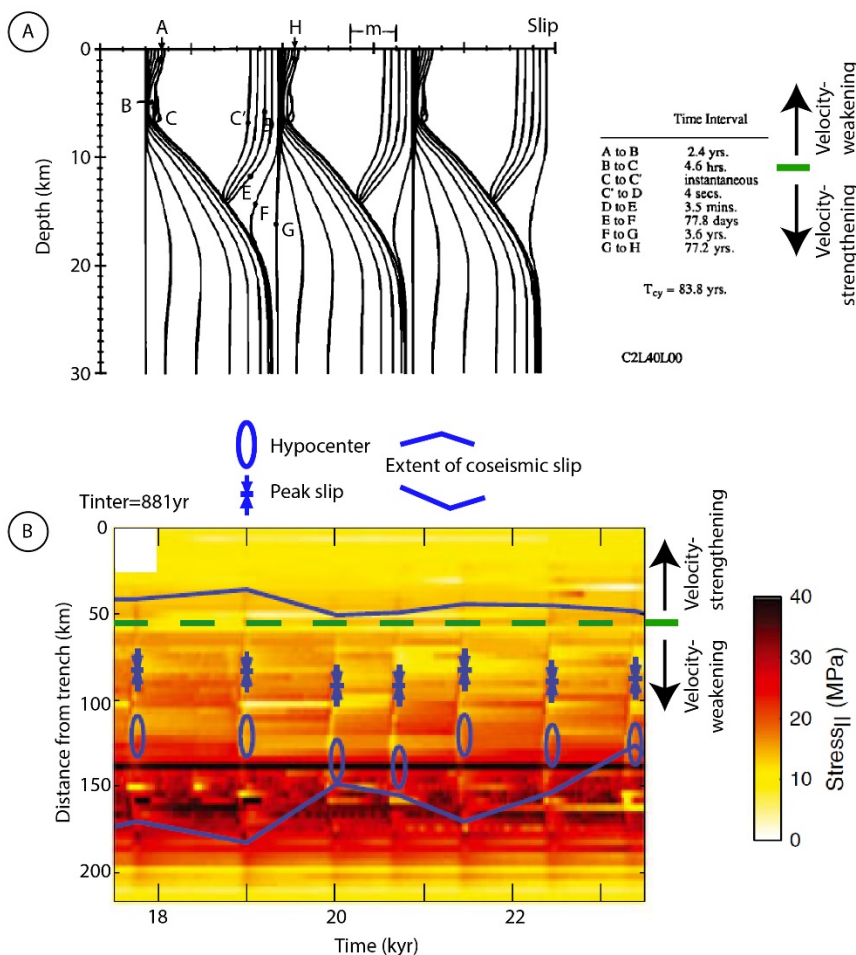


Figure 16: Numerical models of the earthquake cycle. a) 1-D model of a strike slip fault, with a transition from velocity-weakening (above) to velocity strengthening (below) at 11km depth, from (Tse and Rice, 1986). Each curve corresponds to the slip at a constant time. Note that the time interval between two adjacent curves varies. Coseismic slip (C to C') occurs over the velocity-weakening portion of the fault and extends also slightly below.

*(b) Second invariant in the stress over time, calculated along the subduction interface, in the 2-D model of (van Dinther et al., 2013). Coseismic rupture is visible in the discontinuities in stress. In this model, the thrust plane is not prescribed, but is defined as the highest strain zone.*

### **Slow-slip events**

Similarly to these models, slow slip events (SSE), which occur towards the shallow or deep domain of the seismogenic zone (e.g. (Dragert et al., 2001; Obara et al., 2004; Ozawa et al., 2007; Saffer and Wallace, 2015)), are commonly envisioned in the mechanical framework of friction. For example, assuming a transition from velocity-weakening to velocity-strengthening behavior towards the downdip limit of the seismogenic zone results in the spontaneous generation of SSE in this transition zone (Liu and Rice, 2005, 2007). In an alternative approach, SSE can also form if slip is stabilized by processes such as fault zone dilation and pore pressure decrease during slip (Rubin, 2008). At shallow depths, one possible process accounting for the generation of SSE revolves not around velocity-weakening processes, but on slip-weakening (Ikari et al., 2013). From mega-earthquakes to SSE, the plate interface is therefore usually modelled as a frictional interface down to the temperatures of  $\sim 350\text{-}450^\circ\text{C}$  where viscous processes are thermally activated (Hyndman et al., 1997; Oleskevich et al., 1999).

On the other side of the modelling spectrum, the plate interface has also been modelled as a subduction channel (Figure 17), where viscous deformation is broadly distributed within a channel of several hundreds of meters of thickness, composed of the incoming sedimentary sequence (or a fraction of it) between two rigid walls (Cloos, 1982; Cloos and Shreve, 1988a, 1988b; England and Holland, 1979; Mancktelow, 1995; Raimbourg et al., 2007b; Shreve and Cloos, 1986). This model was originally developed to account for the formation of metamorphic *mélange* in the Central *Mélange* Belt of the Franciscan Complex (Cloos, 1982), which involved the return flow, from various depths down to eclogite-facies conditions, of blocks and their mixing in a pelitic matrix, contemporaneously with subduction. The subduction channel models accounts for (1) mixing of blocks with very contrasted metamorphic facies, (2) the strong and distributed deformation observed in *mélange* and (3) underplating at depth. The assumptions concerning the rheology are nevertheless questionable. Underplating is attributed to an increase in viscosity due to dewatering with burial, a process which may not be relevant below a few km depth. Furthermore, rheology is assumed as Newtonian viscous flow, with viscosity either considered as constant (Cloos, 1982; Cloos and Shreve, 1988a, 1988b; Shreve and Cloos, 1986) or increasing down to the onset of plastic deformation (Mancktelow, 1995). This choice of Newtonian rheology is made for the sake of simplicity but its relevance is questionable and actual constraints on the values of the effective viscosity or of its variations with depth are very

limited. In addition, the choice of a viscous flow of material, designed to account for geological and petrological observations, does not account for brittle behavior and earthquake occurrence.

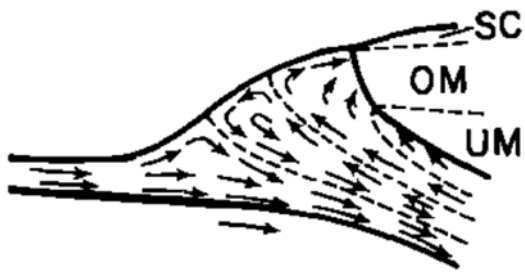


Figure 17: Channel flow with particle velocities shown as arrows (Shreve and Cloos, 1986). Several configurations are possible, the one shown here corresponds to the case where metamorphosed rock from the downgoing plate are uplifted within an upward-directed flow in the upper section of the channel. Shear deformation occurs as a result of the strong velocity gradient across the channel, while the mixing of metamorphic facies results from particle dispersal within the flow and circular motion in the central section of the channel.

## 2. The natural structures that illustrate plate subduction deformation

In correspondence to a model of the plate interface as a frictional surface, the natural structures where deformation is extremely localized are faults, which have been thoroughly studied and described in transcurrent settings (Chester and Logan, 1986; Faulkner et al., 2010; Faulkner et al., 2003; Sibson, 2003; Wibberley and Shimamoto, 2003). Common models of faults revolve around a single or a small number of high-strain fault cores or fault gouge bands, surrounded by a damage zone (Figure 18). The thickness of the principal slip zones, which accommodate most of the strain, depends on the nature of the wall rock (Faulkner et al., 2010; Faulkner et al., 2003), but it is thinner than a few meters and in many cases restricted to a dm- to cm-thick layer of gouge or ultracataclasite (Sibson, 2003; Wibberley and Shimamoto, 2003).

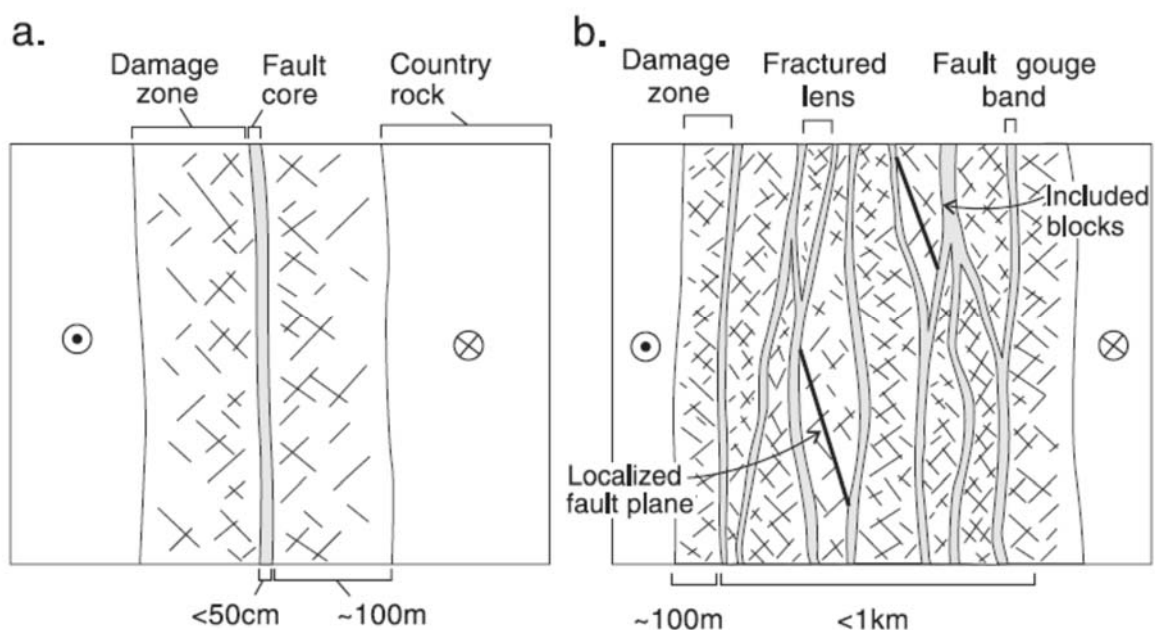
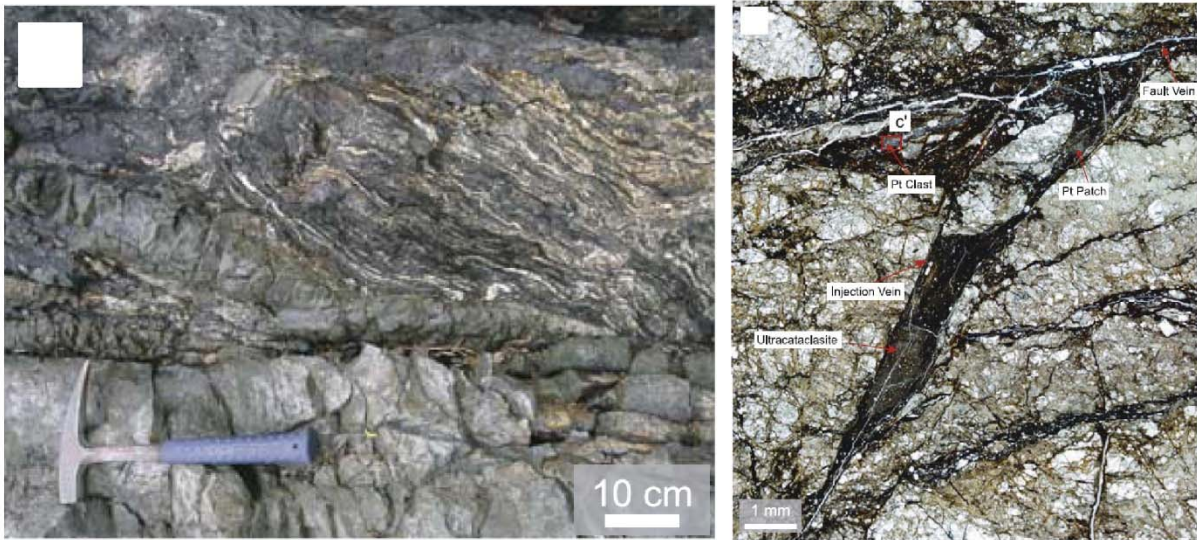


Figure 18: Two conceptual models of large-scale fault zone, in strike-slip settings (Faulkner et al., 2010). The fault is composed of one (a) or several (b) high-strain

*layers (fault core or fault gouge bands), surrounded by a damage zone. The thickness of the high-strain zone ranges from a few meters in case (b) to a few dm or cm in case (a), while the damage zone extends over hundreds of meters.*

In subduction zones, seismic discontinuities interpreted as plate boundary décollement have been drilled at relatively shallow depths (<1km below seafloor). In the NE Japan margin (Chester et al., 2013), the Nankai Trough (Shipboard Scientific Party, 1991, 2001) or Barbados (Maltman et al., 1997), décollement consist in a ~5-30m thick zone concentrating, with respect to surrounding rocks, abundant deformation structures such as breccia and faults (Nankai Trough), or clay scaly fabrics (Barbados and NE Japan). Observations at larger depths are beyond the reach of active margin drilling and rely on fossil structures. In the Shimanto Belt, the Cretaceous to Mesozoic accretionary prism bordering SW Japan, the NTL is a large-scale, out-of-sequence fault that accommodated tens of km of displacement (Raimbourg et al., 2014a). Even if a damage zone is observable in the footwall, all the displacement is localized on a cataclastic fault core of a few cm of thickness (Kondo et al., 2005; Mukoyoshi et al., 2009). A network of sharp faults, with thickness of the principal slip zones less than 10mm and displacement larger than a few kilometers, has also been recognized in the same belt on Shikoku island (Mukoyoshi et al., 2006). In the Kodiak accretionary prism in Alaska, several cataclastic zones have been described near Pasagshak Point (Byrne, 1984; Fisher and Byrne, 1987; Meneghini et al., 2010; Rowe et al., 2011; Rowe et al., 2005). These cataclasites have a variable texture (absence/presence of a foliation, proportion of matrix vs. clasts) and a thickness that varies between 7 and 31m (Rowe et al., 2011). In addition to the cataclasites, very-fine grained, black fault rocks form a dm-thick horizon traceable over kms, interpreted as an ancient pseudotachylyte (Meneghini et al., 2010; Rowe et al., 2005). In the Shimanto Belt, similar cm-thick pseudotachylytes have been described (Figure 19), either forming tectonic boundaries or crosscutting preexisting boundaries (Ikesawa et al., 2003; Mukoyoshi et al., 2006; Ujiie et al., 2007).



*Figure 19: Roof thrust fault of the Mugi mélange, constituted of a ~1m thick fault zone (left). Towards the base of the fault zone, a thin pseudotachylyte layer, with injection structures (right), is present. From (Kitamura et al., 2005)*

In contrast to these very narrow zones of deformation, in Alaska, the Shimanto Belt, the Franciscan Complex, the Apennines or the Otago Schists, tectonic units constituted of disrupted strata, called tectonic mélangé (Connelly, 1978; Fagereng and Sibson, 2010; Kimura and Mukai, 1991; Meneghini et al., 2009; Moore and Wheeler, 1978; Wakabayashi, 2011), coexist with the cataclastic zones described above. Tectonic mélanges have a block-in-matrix structure resulting from pervasive deformation and they contain various deformation structures, such as cataclastic bands and shear zones, pressure solution foliation and mineralized veins (e.g. (Fisher and Byrne, 1987, 1990; Kimura and Mukai, 1991; Kitamura and Kimura, 2012)). Their thickness is larger than 1km in Alaska (Byrne and Fisher, 1990; Fisher and Byrne, 1987) and reaches ~500-1000m in the Shimanto Belt examples of Hyuga Tectonic Mélange (called Mikado Unit in the 1:50,000 maps (Imai et al., 1975; Okumura et al., 2010; Saito et al., 1996)), Okitsu mélangé (Sakaguchi et al., 2006) or Mugi mélangé (Ikesawa et al., 2005; Kitamura et al., 2005). Another example of tectonic mélangé is present in the Apennines (Vannucchi et al., 2010) and described as a “shallow” (up to temperatures of the order of 150°C), ~500m-thick, subduction channel between the Adria and European plates, following the model by (Shreve and Cloos, 1986). A deeper subduction channel (T in the range ~150-400°C) is exposed in the Northern Alps, at the plate boundary between Penninic and Austro-Alpine domains (Bachmann et al., 2009), with a thickness ranging from a few tens of meters to more than 2km.

Tectonic mélanges constitute therefore thick deformation zones, where deformation is distributed over hundreds of meters of thickness, contrasting with the narrow deformation zones, cataclastic faults or pseudotachylytes, where deformation is focused on mm- to m-thick layers. A major question concerns therefore the relationship between these contrasted

deformation modes. One possible view on this question is to interpret all deformation structures as connected. In their description of plate boundary at depth (Rowe et al., 2013) integrate into a unique fault zone a large range of structures, from the several hundreds of meter thick, low strain, total fault zone to the mm-thick, high strain principal slip surface. In such a model, tectonic *mélange* (=low strain zones) as well as pseudotachylytes (=principal strain zones) are part of a single deformation zone, and the *mélange* is interpreted as a large damage zone subsidiary to the principal slip zone, which concentrates most of the slip. Along the same line of thought, Alaskan *mélanges* were interpreted as shear below a master *décollement* (Byrne and Fisher, 1990; Fisher and Byrne, 1987, 1990), or the Hyuga Tectonic *mélange* on eastern Kyushu coast was interpreted as the damage zone of the Nobeoka Tectonic Line, a sharp fault constituting its roof thrust (Kondo et al., 2005).

In this work we reexamine this interpretation of tectonic *mélanges* as low-strain zones within a plate boundary fault, using new structural and microstructural data acquired through several tectonic *mélange* from the Shimanto Belt in Japan. Compiling these structural data, we show that the deformation recorded within *mélange* corresponds to layer-parallel extension during underthrusting and a new mode of underplating, involving distributed strain. In contrast, most of the very sharp unit-bounding faults are late-stage features, postdating underplating. Variations in strain intensity are therefore not interpreted as coeval, but successive stages of deformation during accretionary prism evolution. Consequently, strain during burial is accommodated principally over the whole thickness of the *mélange*, through non-seismic slip.

## **B. Geological settings**

### ***1. General architecture of the Shimanto Belt and investigated areas***

The Shimanto Belt is an accretionary prism forming the southwestern border of Japan and extending seaward into the active Nankai Trough margin (Kimura et al., 2016) (Figure 20). Biostratigraphic ages range from Cretaceous to Miocene and show a general younging trend from north to south (Taira, 1981; Taira et al., 1988; Taira et al., 1980a; Taira et al., 1980d). The Belt is schematically divided into a northern, Cretaceous and a southern, Cenozoic subbelts, separated by a large-scale fault, the Nobeoka Tectonic Line (NTL) on Kyushu and the Aki Tectonic Line (ATL) on Shikoku. The Shimanto Belt is principally a sedimentary wedge, mostly composed of sandstones and mudstones, in variable proportions. Other deep seafloor lithologies, such as red shales, cherts and basalts are volumetrically much less abundant. Most of these sediments preserve their sedimentary bedding, defining “coherent” units, in contrast with less abundant units of tectonic *mélanges*, showing a high degree of stratal disruption and a “block-in-matrix” structure (e.g. (Hashimoto and Kimura, 1999; Kitamura et al., 2005; Onishi

and Kimura, 1995; Taira et al., 1980a)). The general architecture of the wedge is an imbrication of km-scale units, separated by sharp contacts most often not visible, with an overall dip to the north or northwest. The dip is larger on Shikoku, where most units are close to vertical, than on Kyushu, where dip is commonly around 30° or less, especially in the Northern Belt and in the Hyuga mélangé underneath (Raimbourg et al., 2017a).

The tectonic mélanges from the Shimanto Belt analyzed here are the Hyuga tectonic mélangé (Palazzin et al., 2016; Raimbourg et al., 2014a; Raimbourg et al., 2017a) on eastern Kyushu (Figure 21), the Okitsu and Kure mélanges on western Shikoku (Ikesawa et al., 2003; Mukoyoshi et al., 2006; Sakaguchi, 1999a, 2003; Sakaguchi et al., 2006; Taira et al., 1988), the Mugi mélangé on eastern Shikoku (Ikesawa et al., 2005; Kitamura et al., 2005) (Figure 22). All these mélanges have a highly disrupted fabrics, with lenses of sandstone and basalts (and minor red shales) in a pelitic matrix. The biostratigraphic ages of the mélangé matrix are Late Eocene to Early Oligocene (Sakai et al., 1984) and Campanian (for the youngest shales) (Taira et al., 1988), for the Hyuga and Shikoku mélanges, respectively.

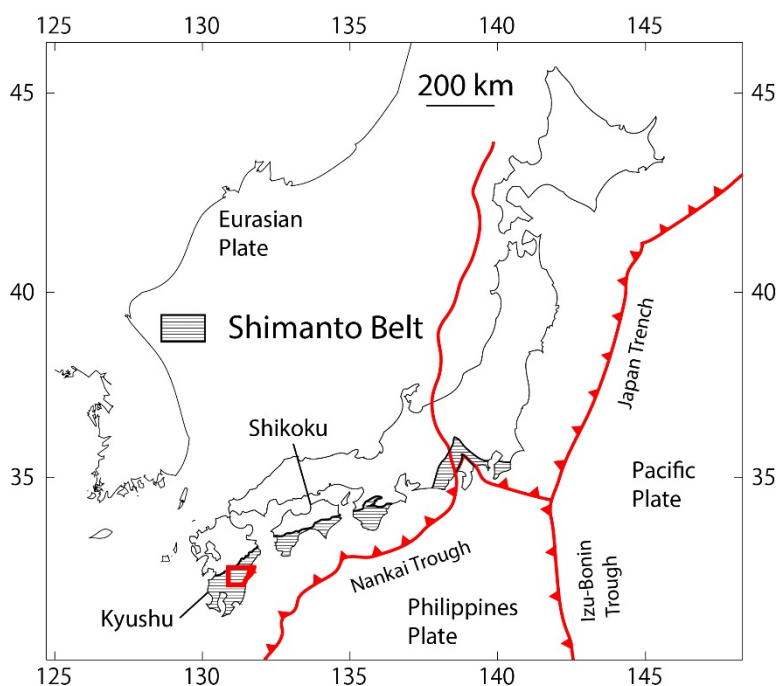


*Figure 20: Geodynamical settings of the Shimanto Belt, along the southwestern border of Japan (Kimura et al., 2016). The mélangé units analyzed are located on Kyushu and Shikoku islands. The red polygon on Kyushu corresponds to Figure 21.*

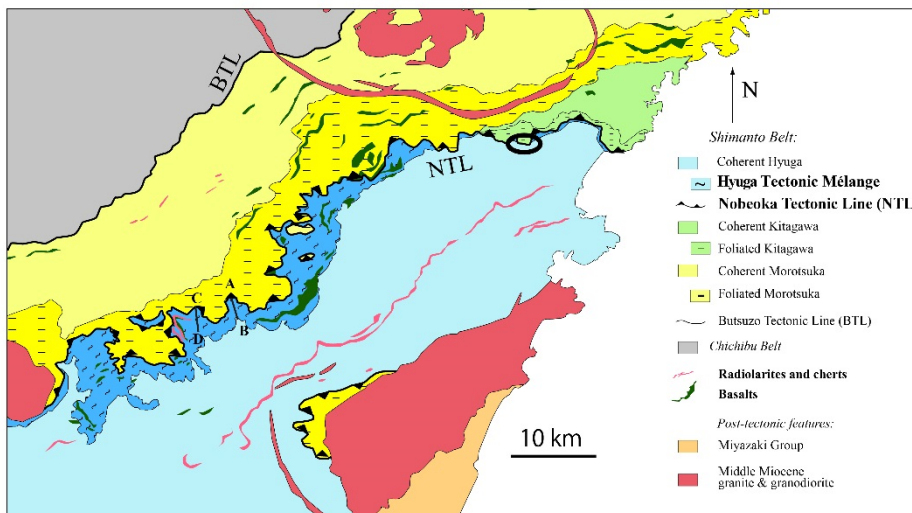


Figure 21: Geological map of Shimanto Belt on eastern Kyushu. The NTL is a large-scale, low-angle, out-of-sequence thrust separating the Northern from the Southern Shimanto Belt, with a significant metamorphic gap. The Hyuga mélangé unit is located below the NTL over most, but not all the map (e.g. black ellipse). The Hyuga mélangé incorporates, in addition to strongly sheared sedimentary rocks, sheets of basalts and to a lesser extent of red shales. Adapted from (Murata, 1997). Cross-sections A-B and C-D in Figure 30.

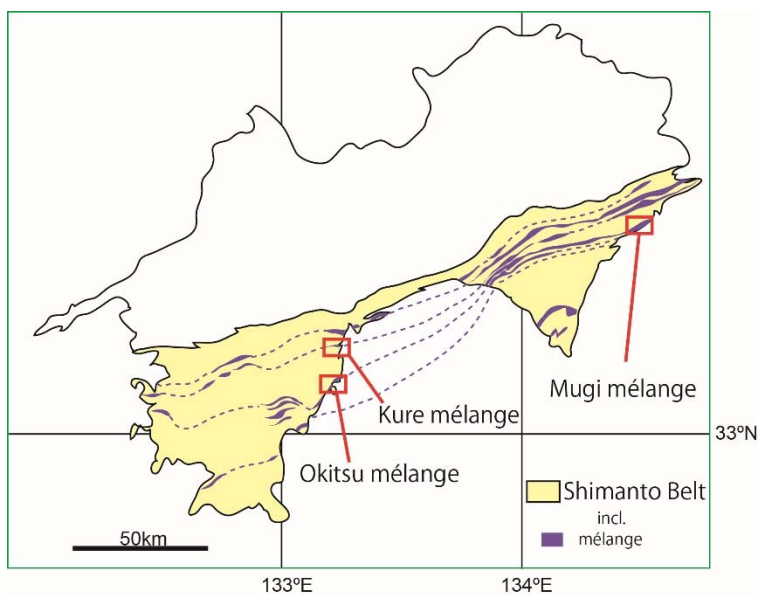


Figure 22: Distribution of mélangé units within the Shimanto Belt on Shikoku, adapted from (Taira et al., 1988).

## 2. P-T conditions of deformation

Metamorphic temperatures of the Hyuga tectonic mélangé, from vitrinite reflectance, illite crystallinity and Raman spectra of carbonaceous matter (RSCM), are of the order of 200-270°C (Hara and Kimura, 2008; Kondo et al., 2005; Mukoyoshi et al., 2009; Raimbourg et al., 2017a) (Table 1). On Shikoku, rock paleotemperatures are of the order of 185°C (Mukoyoshi et al., 2006) and 215-230°C (this study, (Sakaguchi, 1999b)) in the Kure and Okitsu mélangés, respectively. The Mugi mélangé is divided, on the basis of paleotemperatures, between a “hotter” upper and “colder” lower section (Ikesawa et al., 2005). Although the methods to

derive temperature give slightly different values, both vitrinite reflectance and RSCM show that maximum temperatures are, in descending order, Hyuga, Okitsu, Kure and Mugi (lower section).

The estimation of pressure, loosely constrained by metamorphic assemblages prehnite–pumpellyite in greenstones, is of the order of 3-5kbars on Huyga mélange (Toriumi and Teruya, 1988). Estimates of pressure in Shikoku mélange, are first based on coexisting methane-rich and water-rich fluid inclusions and on the hypothesis of their equilibrium/coeval trapping (e.g. (Matsumura et al., 2003). This hypothesis was shown to be invalid in the Hyuga mélange (Raimbourg et al., 2014b) or in the Okitsu mélange (Sakaguchi, 1999a), so that such pressure estimates are not reliable. As an alternative method, the sole water-rich fluid inclusions in syn-tectonic veins, such as stretched and boudinaged sandstone lenses in the mélange (e.g. (Kondo et al., 2005; Matsumura et al., 2003)), or foliation parallel extension veins with trails of inclusions perpendicular to the lineation (Raimbourg et al., 2015), give an estimate of the minimum temperature and fluid pressure that attended deformation. The comparison of maximum temperature of deformation in the rock (from RSCM, vitrinite reflectance or illite crystallinity) and minimum temperature in the fluid (the temperature of homogenization of water-rich fluid inclusions) give very similar values, which is best explained if deformation (including veining and fluid inclusion trapping) occurred at or near peak burial conditions. The second consequence is that the pressure that can be deduced from the water-rich fluid inclusions is systematically very low, which we interpreted as the result of either (i) cycles of fluid pressure and precipitation of the veins/fluid inclusion trapping at low points of the cycles or (ii) reequilibration of the fluid inclusions during uplift (Raimbourg et al., 2018).

### ***3. Geodynamical evolution and structural settings of deformation***

The general architecture of the Shimanto Belt, with younging trend in stratigraphic ages towards the south (Sakai et al., 1984; Taira et al., 1988; Taira et al., 1980a; Taira et al., 1980d), is the main argument in favor of a model of progressive accretion and growth from Cretaceous to Miocene. Such a model was disputed by the recognition of a collision stage in Early Miocene (Charvet, 2013; Charvet and Fabbri, 1987; Sakai, 1988; Sakai, 1985; Sakamoto, 1977; Tanaka, 1977), whose influence on the structure of the Belt and on its internal deformation is unclear. Principally based on the existence of a belt-wide unconformity, our recent work has shown that this collision was also responsible for the development of a vertical foliation, as a result of horizontal shortening, in the Cenozoic part of the belt on western Shikoku (Raimbourg et al., 2017a). This work also suggested that this collision stage also affected more internal domains

of the belt, through for example the movement on the NTL on Kyushu or tilting of tectonic units on Shikoku.

Most studies focused on *mélange* units have so far considered that the deformation they recorded was contemporaneous with their burial (Ikesawa et al., 2005; Ikesawa et al., 2003; Kimura and Mukai, 1991; Onishi and Kimura, 1995; Ujiie, 1997; Ujiie et al., 2007), so they implicitly discarded a possible influence of the Miocene collision, which occurred at a much later stage than subduction. This issue is in fact not so easy to solve, as tectonic influence of the collision is unambiguously present in the southern part of the Belt. In addition, ages of deformation obtained in pseudotachylytes from faults bounding the Mugi (Tonai et al., 2016) or the Okitsu (Honda et al., 2011) *mélange* support post-subduction activity, possibly related to the collision.

The main argument in favor of simultaneous *mélange internal* deformation and subduction is the fact that this deformation is almost absent in nearby coherent units. This very strong contrast in deformation style and intensity between *mélange* units and adjacent coherent units suggests that *mélange* internal deformation was achieved relatively early in its history, at least before *mélange* units were stacked upon adjacent coherent units. In contrast, the Miocene collisional event is relatively recent (Charvet, 2013) and should have affected the whole tectonic pile made of *mélange* units sandwiched between coherent units. On the other hand, the very localized deformation between units, in particular the occurrences of “out-of-sequence” thrusts, such as the NTL (Kondo et al., 2005) or the fault network cutting across Kure *mélange* and adjacent units (Mukoyoshi et al., 2006), could well be the expression, at least to some extent, of posterior later collision phase. The amplitude of this collisional phase is unclear, as there is no remaining exposed evidence of the colliding microblock. For these reasons, in the following section, we consider that all deformation distributed within the *mélange* is coeval with subduction, while the timing of faulting, either during subduction or during later collision, is unclear.

## **C. Deformation within *mélanges***

### ***1. General structure of *mélange* zones***

Tectonic *mélanges* are defined by a block-in-matrix structure. In most of the volume, the *mélange* is strictly made of sedimentary material, with blocks made principally of sandstone and to a smaller extent tuff layer in a pelitic matrix. Locally, lenses of basalt are present, along with lenses of deep seafloor sediments such as cherts or red shales (see maps in Figure 21), in a pelitic matrix. The blocks of sandstone have a variable size, from mm- to m-scale. The basalts, which show in some instances such as Mugi, pillow lava structures, form larger lenses, from m- to tens-of-meters sized.

In some mélangé occurrences, the recognition of ocean-floor stratigraphy (i.e. the succession of pillowed basalts, radiolarian cherts, red pelagic clays and varicolored hemipelagic shales (Taira et al., 1988)), and to the description of fault zones along the basal (i.e. southern) boundaries of basalt layers (e.g. (Kitamura et al., 2005)) has led to interpret mélangé zone as a stack of several thrust sheets, each of them soled by a layer of basalt. As a result, three thrust sheets are described in the Okitsu mélangé (Sakaguchi, 2003) (Figure 23), five thrust sheets in the Mugi mélangé (Kitamura et al., 2005), while the internal division of the Hyuga mélangé is unclear but several distinct lenses of basalts are present in the tectonic pile.

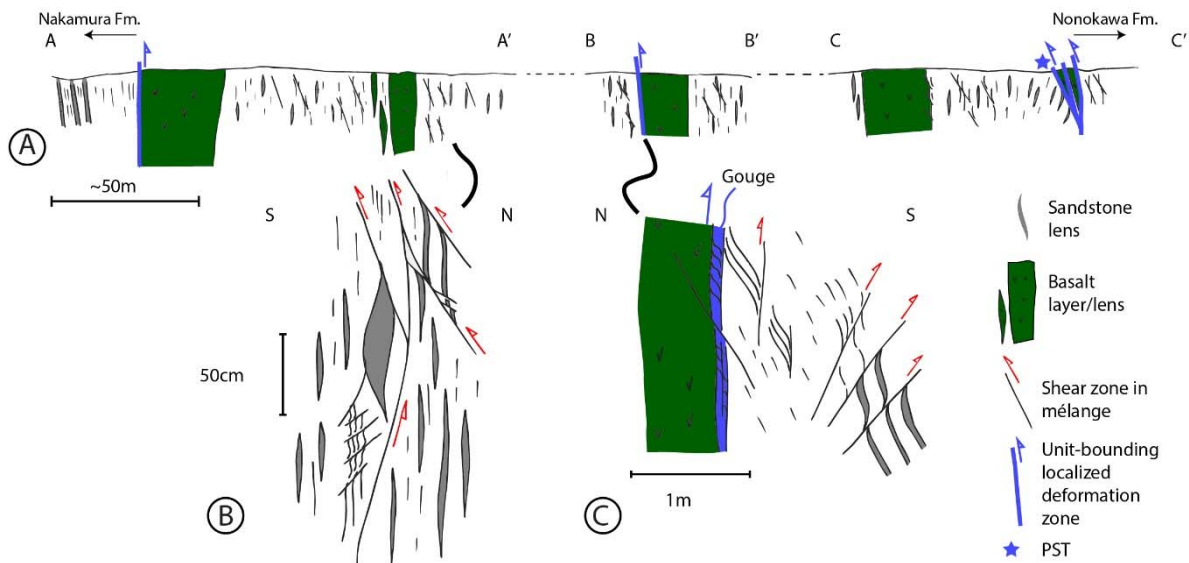


*Figure 23: A) Cross-section of the stack of units constituting the Okitsu mélangé, along the profile defined in Figure 31. Basalt is present in thick layers, preserving their pillow structure, and locally in lenses embedded and deformed within the mélangé. B) The pervasive deformation of the mélangé is visible in its sedimentary layers, with a dense network of top-to-the-south mineralized shear zones deflecting the foliation and offsetting sandstone lenses. C) More localized zones of deformation are present along the boundaries of the basalt lenses, including the pseudotachylyte-bearing one. Note that because of the actual orientation of the outcrop, in the field drawing in C) the orientation of the profile is reversed with respect to A) and B).*

## 2. Deformation structures

The deformation is first apparent in the presence of a pervasive foliation (S1) in the pelitic matrix. Sandstone lenses are preferentially flattened within this foliation. Lineation is difficult to observe on the foliation, except locally in the Hyuga mélangé, which has been affected by the highest temperature conditions of deformation (Table 1). The macroscopic deformation is principally accommodated by the formation of a network of shear bands (Figure 23, Figure 24 and Figure 25) deflecting the shale matrix foliation and the lenses of sandstone. The spacing between adjacent shear bands is variable, from ~1m to a few cms (see below). Some shear bands contains thin lenses of precipitated quartz (Figure 24-B and Figure 25) while in other cases the shear bands are not mineralized (Figure 24-A). Another conspicuous feature of deformation

within the mélangé is the large number of cracks filled with quartz within the sandstone lenses, especially in the necked domains towards the tips of the sandstone lenses or in the vicinity of the shear bands (Figure 24-A).

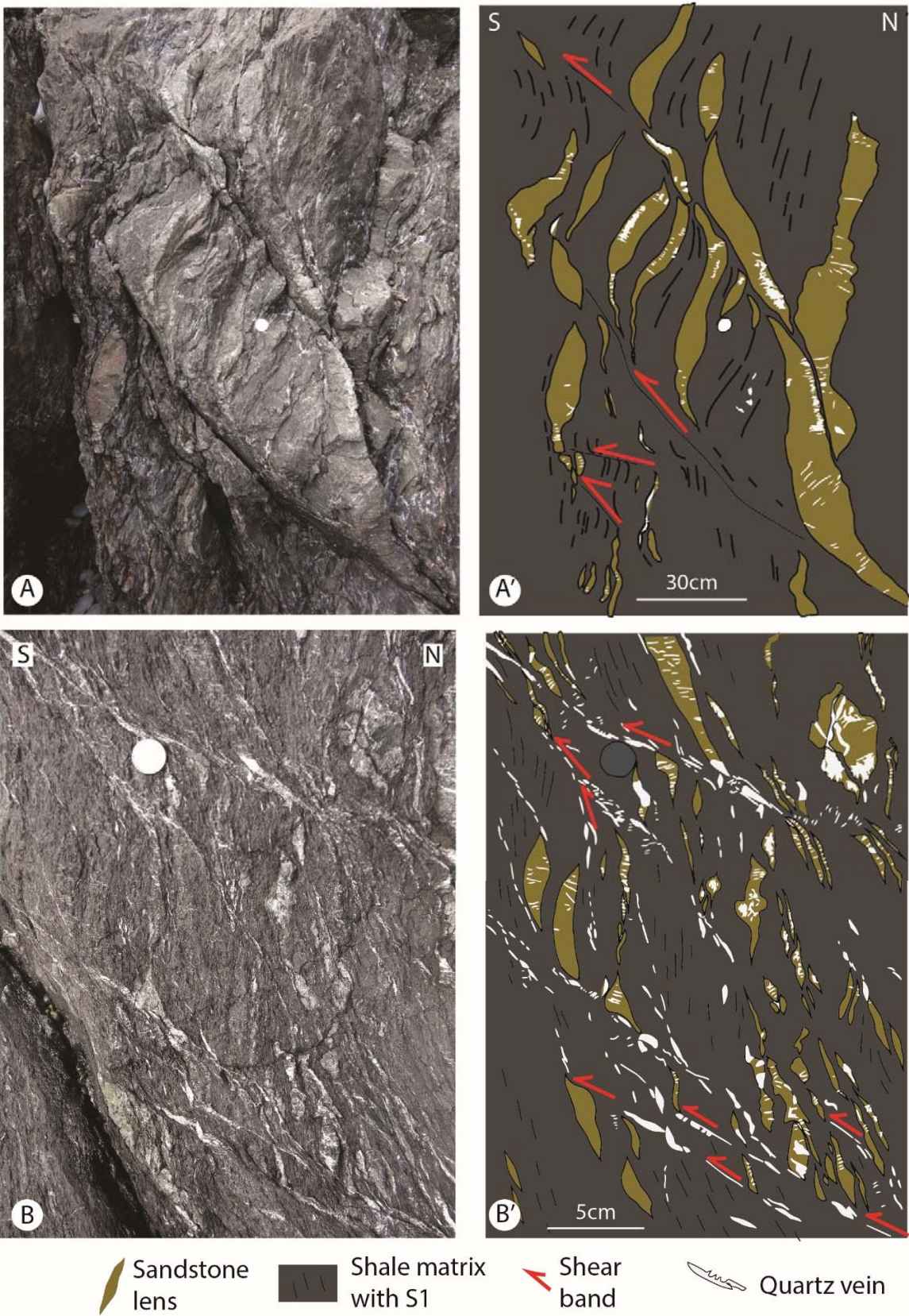


Figure 24: Deformation structures within the Okitsu mélangé (outcrop 220). The vertical foliation, composed of elongated sandstone lenses embedded in a shale matrix, is crosscut

by a dense network of shear bands with-to-the-south sense of shear. Quartz precipitation is in A) mostly distributed within fractures cutting across the sandstone lenses. Alternately, in B), quartz precipitation is much more intense and quartz also precipitates along and in the vicinity of the shear bands.

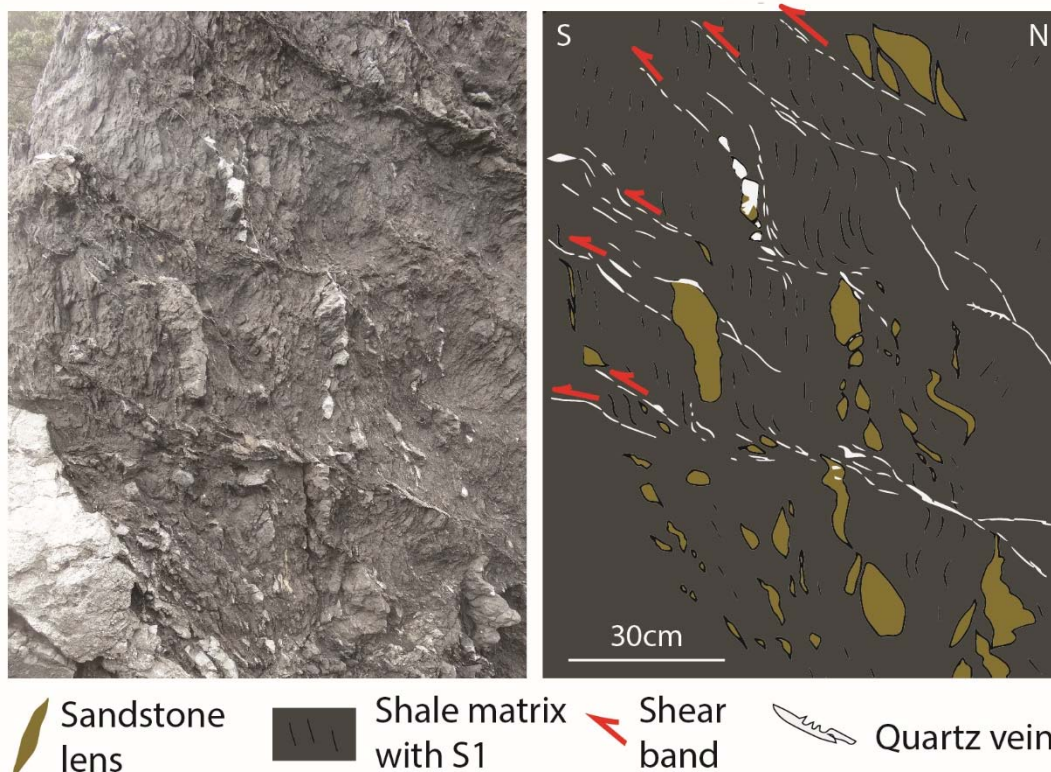


Figure 25: Network of shear bands deflecting the vertical sandstone lenses and the foliation of the shale matrix within the Mugi mélangé (outcrop 342). Most of the shear bands are filled with quartz.

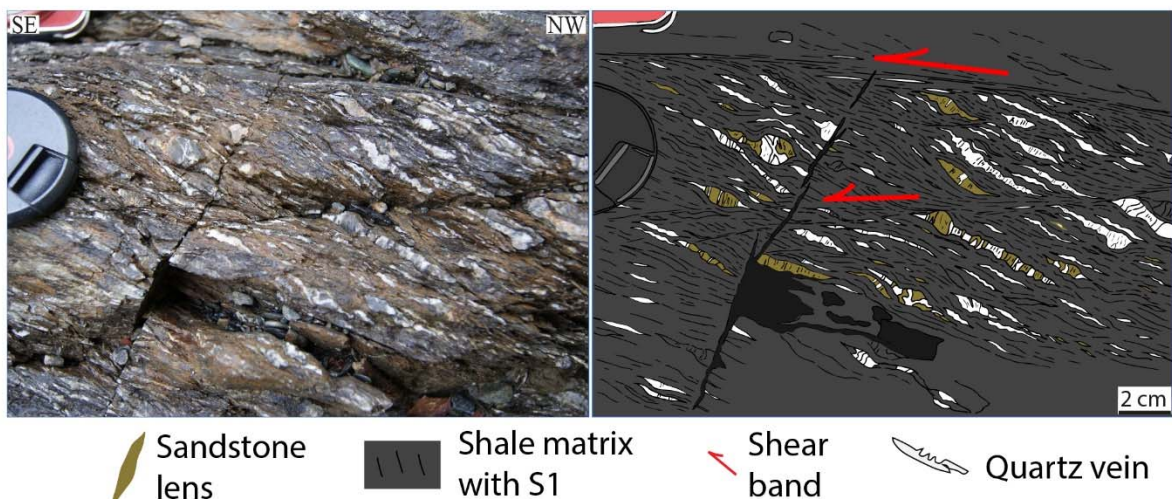


Figure 26: Deformation microstructures in Hyuga mélangé (outcrop 147). Lenses of sandstone, elongated parallel to the foliation within the pelitic matrix, are boudinaged. Quartz precipitated as foliation-parallel lenses and in tension cracks forming the necks of sandstone lenses. Both quartz and sandstone lenses are deflected by top-to-the-SE shear bands.

### 3. Deformation microstructures

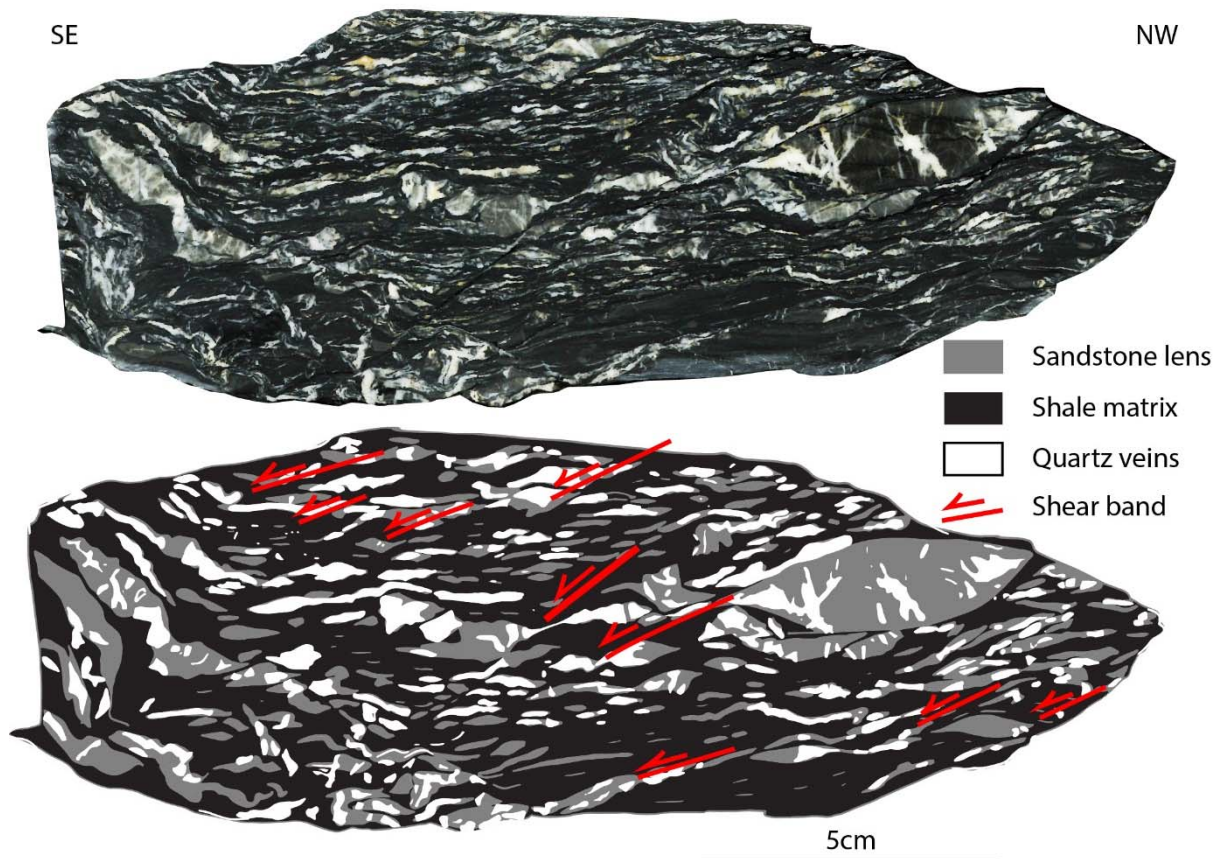


Figure 27: Deformation within the mélange is accommodated by a distributed network of shear zones, affecting lenses of sedimentary material as well as precipitated quartz (“quartz veins”). Quartz precipitation occurs (i) in fractures cutting across sandstone lenses, (ii) in the neck of boudinaged sandstone lenses and (iii) in lenses elongated parallel to the main foliation (sample HN299).

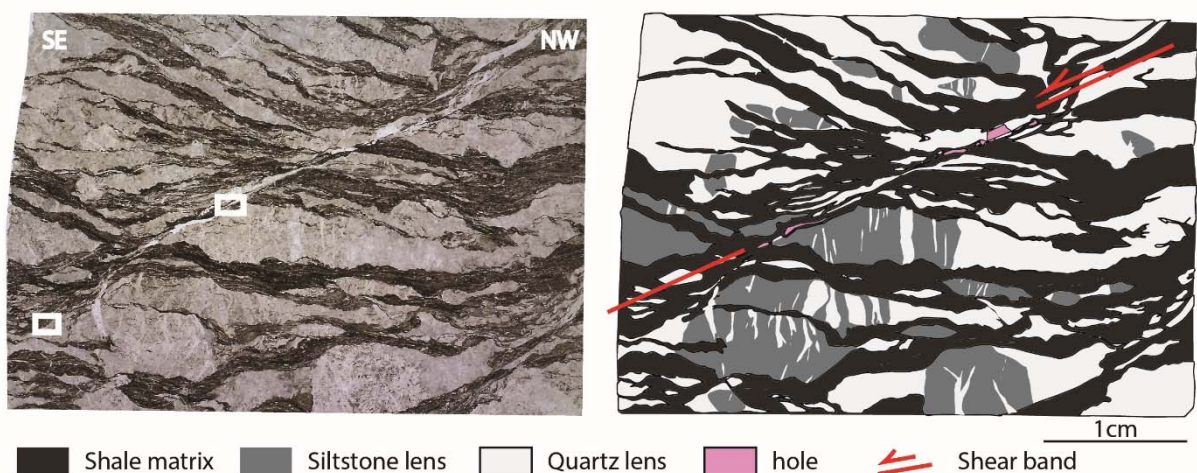
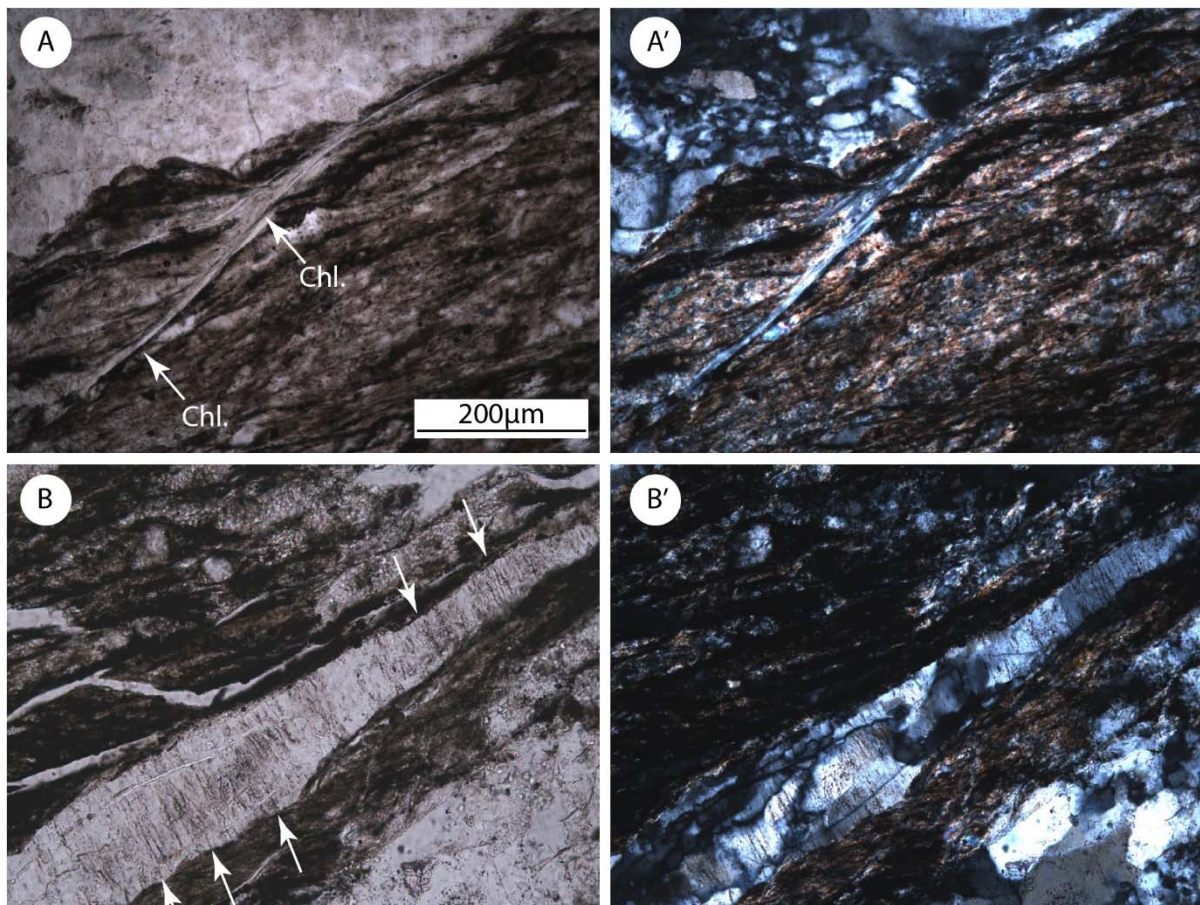


Figure 28: Detail of a shear band cutting across elongated lenses of quartz and siltstone, within the Hyuga mélange (sample HN299). Quartz lenses are continuous across the shear band and deflected by it. Most of the lenses in this pervasively deformed sample are not composed of sedimentary, coarser-grained siltstone, but rather of lenses of precipitated quartz. The two rectangles in the left picture correspond to Figure 29.

The patterns of deformation observed at outcrop-scale are transposable to the smaller scales of the hand-scale or thin-section-scale. Small lenses embedded within the shale matrix are truncated by a dense array of quartz-filled fractures and deflected by shear bands (Figure 26, Figure 27, Figure 28). These lenses are constituted of sand- or siltstone, but also of precipitated quartz forming boudins elongated within the foliation. Quartz precipitation is therefore (i) polyphased, as several successive events of veins, with crosscutting relationship, can be observed, and (ii) massive, as in Figure 28, where precipitated quartz domains are volumetrically larger than inherited sedimentary material.

Quartz lenses are most often continuous across the shear bands (Figure 27 and 2. Figure 28), even if sometimes their thickness is much reduced by local high strain (see the necking structures in the central part of Figure 27 and Figure 28).

At the mineral scale, the shear bands have a composite structure, incorporating a network of chlorite-filled shear zones (Figure 29-A) and elongated domains of precipitated quartz (Figure 29-B). In the latter quartz domains, abundant healed microcrack planes, visible as they contain secondary planes of fluid inclusions, are orientated perpendicular to the local stretching direction (Figure 29-B).



*Figure 29: Deformation microstructures within the shear band in Figure 28. A-A') A network of microscale, chlorite-filled shear zones ("Chl.") develop within the main shear zone. B-B') Quartz lenses elongated within the shear band are pervasively affected by*

microcracking, apparent in the dense array of fluid inclusion planes, shown as arrows, oriented perpendicular to the stretching direction. Quartz crystals (B') are elongated preferentially parallel to the stretching direction. Optical microscope photographs, without (A, B) and with (A', B') crossed-nicols.

#### 4. Deformation kinematics

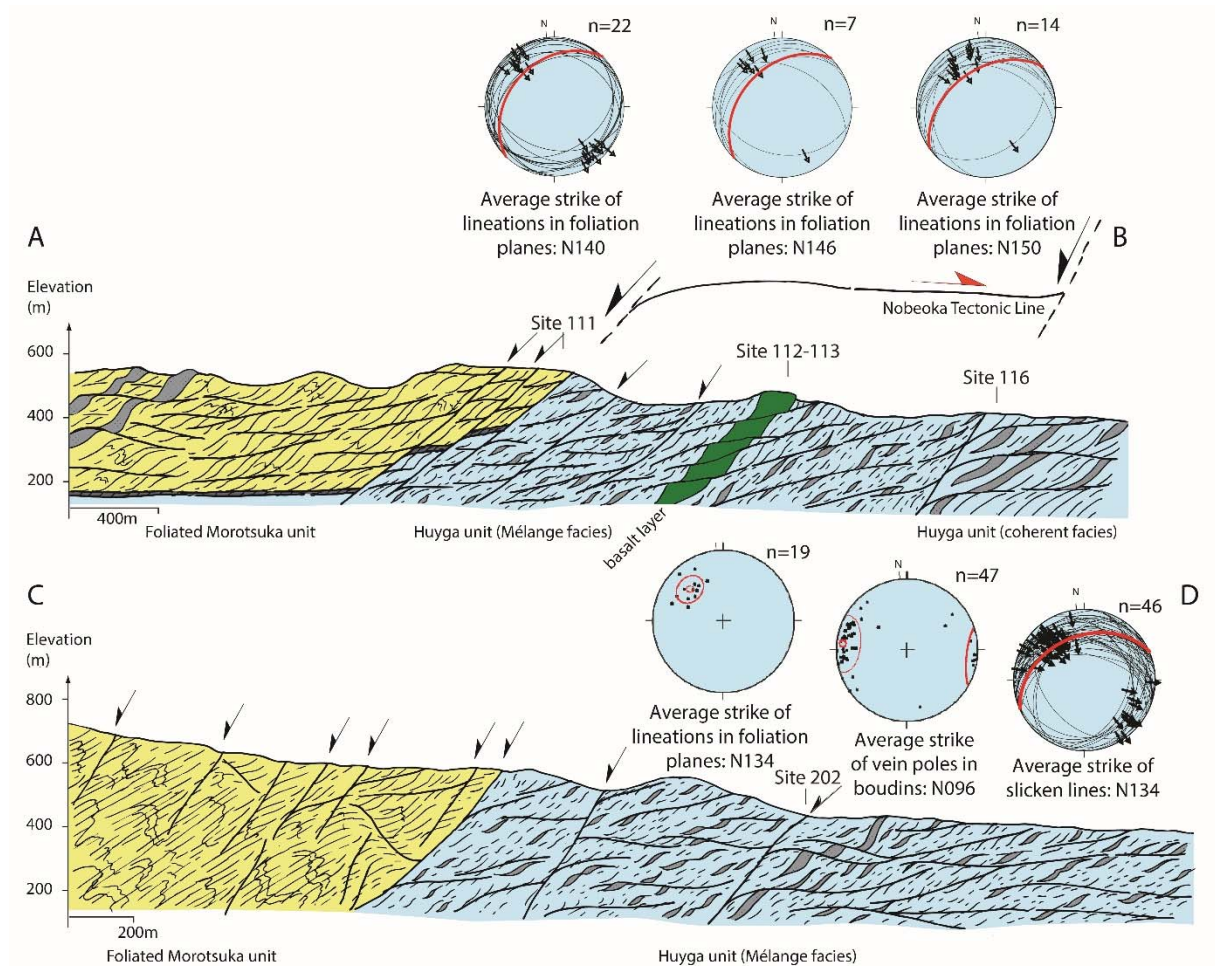


Figure 30: Kinematics of deformation within the Hyuga mélange. Foliation is shown as the red circle, while planes with arrows correspond to shear bands. Cross-section location refer to Figure 21.

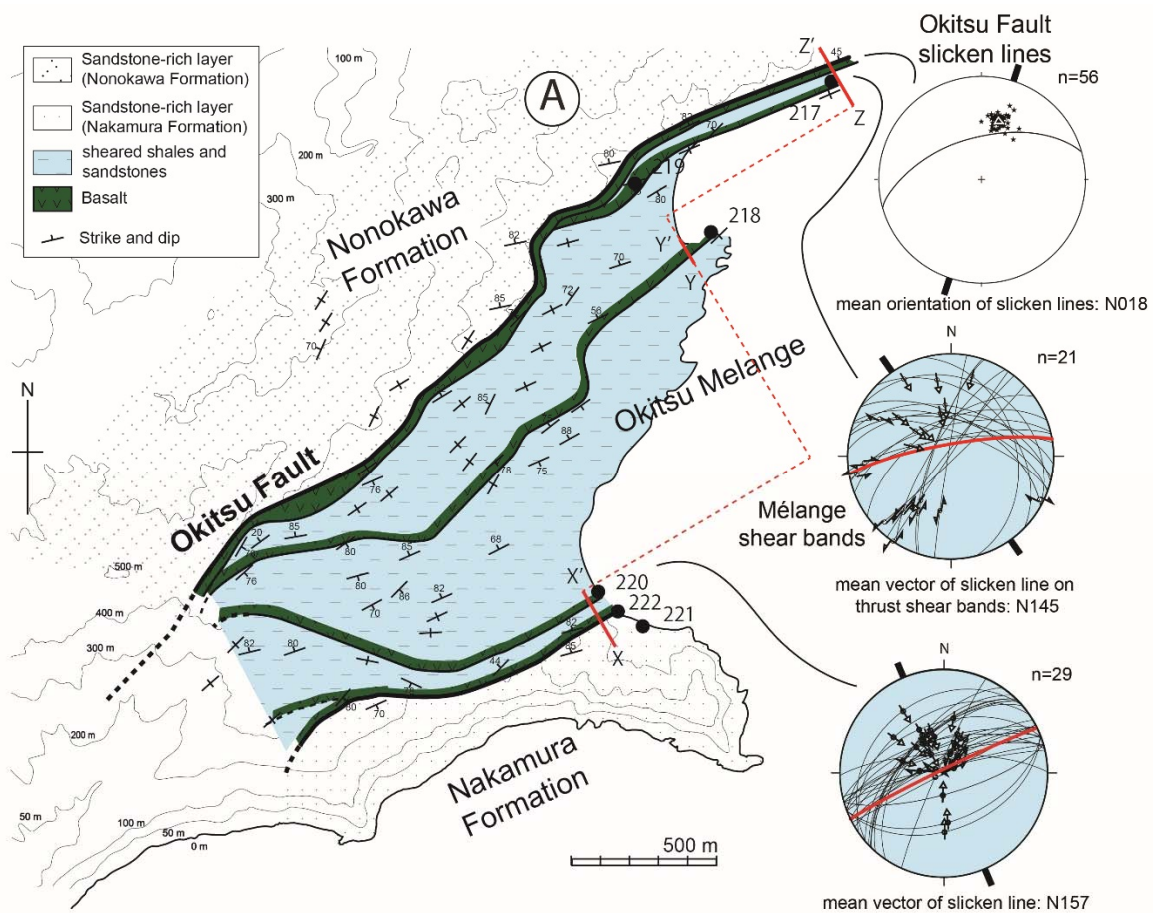


Figure 31: Kinematics of deformation in the Okitsu mélangé unit. The pseudotachylite-bearing fault zone along its northern boundary is associated with top-to-the-SSE thrust motion. Abundant shear zones in the mélangé indicate top to the SE thrusting. A-B, C-D, E-G profiles in Figure 23. Kinematic data on fault zone from (Sakaguchi, 2003).

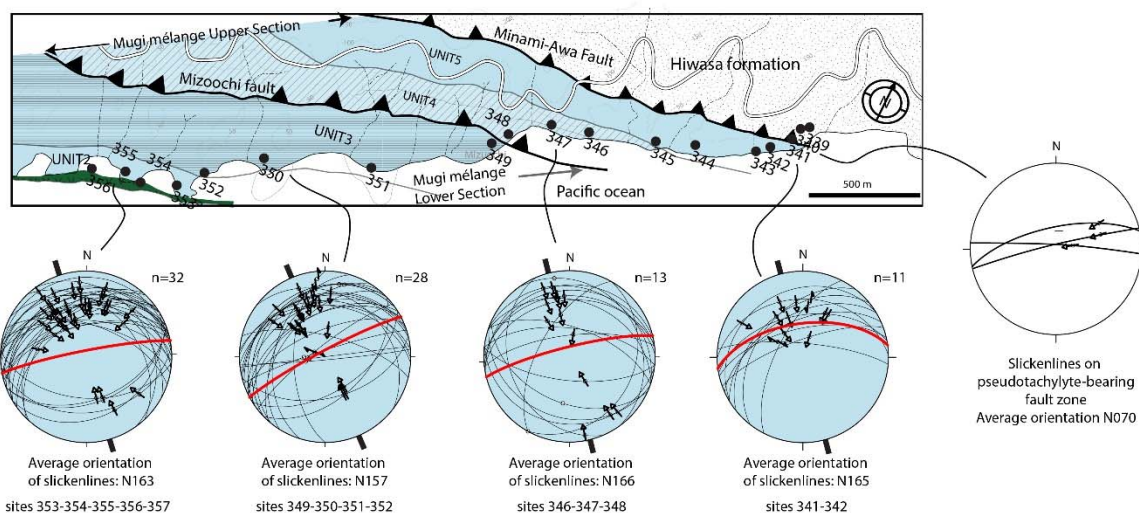


Figure 32: Kinematics of deformation in the Mugi mélangé (stereoplots with blue font). On each stereographic plot, the red circle corresponds to average foliation. The white stereoplot on the right shows the data of the pseudotachylite-bearing fault zone of Minami-Awa, which makes the upper boundary of the Mugi mélangé unit (Kitamura, 2006; Kitamura et al., 2005) The numbers on the map refer to outcrops.

Deformation kinematics of the connected network of shear bands is similar in each of the *mélange* units studied (Figure 30, Figure 31, Figure 32). First, macroscopic quartz-filled crack veins in boudins are nearly perpendicular to the foliation plane for the three *mélanges* (Figure 10). In the case of the Hyuga *mélange* for which a lineation is available, quartz-filled cracks are oriented N006 on average, i.e. nearly perpendicular to the average direction of transport (N134). Second, the shear bands correspond to a top-to-the-SE sense of shear, with slickenlines oriented N134 – N150, in Hyuga, N145 – N157 in Okitsu, and N157 – N166 in Mugi. This top-to-the-SE sense of shear is consistent with the overall convergence direction in the whole Shimanto Belt and the asymmetry of the subduction. Third, the shear bands have a lower averaged dip than the *mélange* foliation, both in cases where *mélange* foliation is steeply (Okitsu and Mugi) or gently (Hyuga) dipping. Finally, the slickenlines of the major pseudotachylyte-bearing faults, observable at the boundary of the Okitsu and Mugi *mélanges*, are oriented N018 and N070 on average in the former and latter case, respectively. The kinematics of these faults is thus not compatible with the direction of motion observed in *mélange* shear zones.

#### **D. Localized deformation in fault zones and pseudotachylytes**

In addition to distributed deformation, fault zones are also present within the *mélange* zones studied here. In particular, fault zones constitute in Mugi and in Okitsu (Kitamura, 2006; Kitamura et al., 2005; Sakaguchi, 2003), as well as in Hyuga (Mukoyoshi et al., 2009) the northern boundaries of the whole *mélange*. In some instances, such as Mugi, fault zones also form the boundaries between individual thrust sheets within the *mélange* unit.

Fault zones have overall a thickness of the order of ~1 to 10 meters (Kitamura et al., 2005; Kondo et al., 2005; Sakaguchi, 2003; Ujiie et al., 2007). Strain is very heterogeneous within the fault zone, and one or several cm- to dm-thick layers of cataclasites or ultracataclasites are present (Figure 33). In the case of Mugi and Okitsu, evidences of melting have been found within the ultrafine-grained layers, considered therefore as pseudotachylytes (Ikesawa et al., 2005; Ikesawa et al., 2003; Kitamura et al., 2005; Sakaguchi, 2003). The microstructure of the cataclasites and ultracataclasites is much different from the *mélange*, as it is composed of rounded clasts of variable sizes embedded in a very fine-grained, dark matrix (Figure 34)



Figure 33: Outcrop of the NTL along the eastern coast of Kyushu. The fault zone is principally composed of a ~15cm-thick layer of cataclasite.

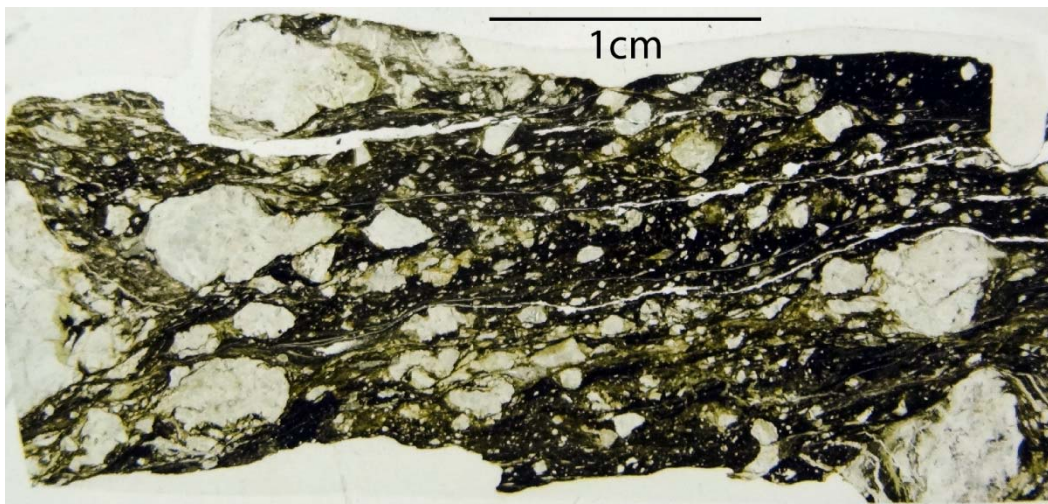


Figure 34: Thin section of the NTL fault core, composed of relatively rounded clasts within a very-fine-grained, dark matrix.

## **E. Discussion**

### ***1. Deformation microstructures attending distributed deformation in mélanges***

Foliation-parallel veins are a conspicuous feature of tectonic mélanges in the Shimanto Belt. The orientation of healed microcracks (Figure 29B) and the crystallographic-preferred orientation of quartz shows that these veins grew through successive events of fracturing perpendicular to the stretching direction (Palazzin et al., 2016). Quartz-filled cracks in sandstone lenses, perpendicular to foliation, and veins parallel to the foliation (Figure 24 to Figure 26) are therefore kinematically consistent, in spite of their different orientation and were formed contemporaneously. Foliation-parallel veins have also been reported in the Franciscan Complex in the USA, in the Kodiak Complex in Alaska, in the Chrystalls Beach Complex in New Zealand, and in the Internal Ligurian Units in Italy (Fagereng and Harris, 2014; Fagereng et al., 2011; Meneghini et al., 2009; Mittempergher et al., 2018). In these examples as well as in Shimanto, foliation-parallel veins are interpreted as extensional shear veins and record increments of deformation in crack-seal textures (Fagereng and Harris, 2014; Fagereng et al., 2011; Fisher and Byrne, 1990; Fisher and Brantley, 1992, 2014; Fisher et al., 1995). Conditions of formation of such veins span a large temperature range. They can be found at low temperatures (~150°C) in the Mugi mélanges lower and “colder” thrust sheets (Kitamura et al., 2005), in the relatively shallow subduction channel of the Apennines (Mittempergher et al., 2018; Vannucchi et al., 2010), in unlithified to semi-lithified rocks from the Internal Ligurian Unit (Meneghini et al., 2007) and during the very shallow (40-70°C) stage of burial of InfraHelvetic Flysch units of the Alps (Dielforder et al., 2015). Nevertheless, veins were also formed at higher temperatures (250-300°C) in the Hyuga Tectonic mélanges (Palazzin et al., 2016; Raimbourg et al., 2015), in the Otago Schists (Fagereng and Harris, 2014) or in Kodiak (Vrolijk et al., 1988) (see also the compilation of temperatures in (Raimbourg et al., 2018)). Additionally, at thin section scale, a network of microscale shear bands, forming an anastomosed network parallel to the foliation, contain a large proportion of preferentially-oriented chlorite plates (Figure 29A Figure 28), as was reported on other mélanges examples (e.g. Meneghini et al. (2009)). Bulk rock deformation at depth, for temperature conditions in the range ~150-300°C, is therefore the result of combined microfracturing, solution precipitation of quartz and slip on chlorite plates.

The other conspicuous deformation feature we observed in the different mélanges of the Shimanto Belt are macroscopic shear bands (Figure 24 to Figure 26) at a low angle to the foliation. Shear bands of similar geometry are also present in many tectonic mélanges, such as in Kodiak (Fisher and Byrne, 1987), or in the subduction channel exposed in the Northern Alps

(Bachmann et al., 2009), for T that range from 150-400°C. There, deformation involves a combination of distributed shear zones and extension fractures (principally oriented parallel to the foliation), which increase in abundance with depth along the subduction channel.

The chronology of the deformation structures is similar between Okitsu, Mugi and Hyuga mélanges zones. The first stage of deformation involves layer-parallel extension, which results in the development of necking of sandstone lenses, formation of tension cracks perpendicular to foliation and foliation parallel veins (which themselves are to a large extent the result of repeated tension microcracking, Figure 29B and Palazzin et al. (2016)). The elongated and fractured sandstones lenses and foliation-parallel veins are then deflected by macro- (Figure 24 to Figure 26) and microshear zones (Figure 27 to Figure 29), developed in a second stage.

A further indication on the relative timing of microstructures with respect to the mélange tectonic evolution is provided by the comparison between Mugi, Okitsu and Hyuga, which experienced increasing peak T conditions. Only in the western domain of Hyuga, where the metamorphic temperatures were the highest (ca. 240-270°C), a clear mineral lineation is visible, suggesting that lineation developed for maximum temperature conditions. The direction of motion indicated by the shear zones is parallel to the lineation (Figure 30), which shows that the shear bands themselves were active for the highest T conditions, at peak burial. Furthermore, in the Hyuga mélange, poles to tension veins (N096) and direction of slip on shear bands (N134) are close, which suggests that veins and shear bands developed during the same framework of burial, but probably at different depths.

## ***2. Kinematics of mélange deformation***

The foliation is well-developed in the three mélange units studied here, whereas the lineation is well-defined only in the western domain of the Hyuga Tectonic mélange (Figure 4, see also Raimbourg et al. (2014a)). In the rest of mélange exposures (eastern part of Hyuga, Okitsu and Mugi areas), where temperatures did not reach 240°C, it is therefore unclear whether the lenses of sandstone within the foliation formed by flattening, pure or simple shear.

This evolution of finite strain markers with temperature is further supported by anisotropy of magnetic susceptibility (AMS) data. Sandstones lenses from the two sections of Mugi mélange shows a magnetic fabrics corresponding to a flattening régime (Kitamura and Kimura, 2012), with a well-defined foliation and magnetic lineations scattered in the magnetic foliation plane. In contrast, in the higher temperature (~340°C, i.e. Palazzin et al. (2016)) of the Makimine mélange, the magnetic fabrics change towards a 3-dimensional shape (Kitamura and Kimura, 2012) and the magnetic lineations are clustered around NNW-SSE direction, parallel to the stretching lineation (Raimbourg et al., 2014a). The same magnetic fabrics was described in

Okinawa islands, also belonging to the Shimanto Belt, in an underplated *mélange* unit (Ujiie et al., 2000). In parallel to the AMS fabrics, analysis of the 3D shape of radiolarians in the higher-grade units of the Shimanto Belt ( $T \sim 350^\circ\text{C}$ ) has also revealed a preferred elongation direction, parallel to the shear direction (Kimura and Mukai, 1991; Toriumi and Teruya, 1988).

Extension parallel to the underthrusting direction is therefore revealed by the development of a clear stretching lineation, or the AMS or shape fabrics of radiolarites in the higher-temperature examples of *mélanges*, while in the lower temperature example the strain ellipsoid is more ambiguous, partly because of a lack of strain markers.

In addition, in the examples treated here, the clearest microstructures, in terms of kinematics, are the macroscopic shear bands that develop within the *mélanges*, with directions oriented NW-SE in Hyuga and NNE-SSW in Okitsu and Mugi. These shear bands indicate consistently top-to-the-SE shear deformation. This sense of shear is consistent with burial and underthrusting of the *mélange* below Eurasia in Early Cenozoic times (Raimbourg et al., 2014a; Sakaguchi, 1999b). Furthermore, as shear band dip is lower than the main foliation (Figure 30 to Figure 32), when the latter is restored back to underthrusting attitude (i.e. with a low landward dip), the shear bands become extensional structures.

Similar to these Shimanto case studies, the most commonly reported kinematic indicator in worldwide examples of *mélange* reflect layer parallel coaxial extension, top-to-the-trench shearing or both. In most cases, these kinematics are interpreted as the result of shear along or near a master *décollement* (Byrne and Fisher, 1990; Fisher and Byrne, 1987, 1990). In the Uyak Complex in Alaska, conjugate normal faults are reported, with the set of normal faults synthetic with subduction-related shear dominant over the other one (Byrne and Fisher, 1990). In the Marin Headlands of the Franciscan Complex (Meneghini and Moore, 2007) or in the Mugi *mélange* of the Shimanto Belt (Kitamura and Kimura, 2012), structures are interpreted in terms of Y-P-R brittle fabrics and the abundant R planes are similar, geometrically and kinematically, to the extensional shear bands described in our work. In the northern Apennines, extensional shear bands and faults are also reported, but two conjugate sets seem to be present (Vannucchi et al., 2010). In the subduction channel in the Northern Alps, shear bands are widely distributed, some of them with S-C geometry, and the senses of shear are synthetic with the master shear on the *décollement* during subduction (Ring et al., 1989). Therefore the general pattern is that extensional shear bands, sometimes conjugate but in most cases synthetic with underthrusting-related shear, dominate the deformation in *mélanges*.

### 3. Underplating process of *mélange*

*Mélange* units in the Shimanto Belt have a relatively constant structure, with the imbrication of individual sheets composed of a basaltic sole below a thicker sequence of tectonic *mélange* composed of sedimentary material (and minor, in terms of volume, occurrences of other ocean-floor lithologies such as cherts or red and black shales) (Figure 23). In addition, some of the basalt lenses or layers are associated with fault zones, for example in Mugi (Ikesawa et al., 2005; Kitamura et al., 2005) or Okitsu *mélange* (Ikesawa et al., 2003; Sakaguchi, 2003; Sakaguchi et al., 2006). The imbricated structure and the presence of faults led to the model of underplating, to account for the stacking of *mélange* sheets to the upper plate (Fisher and Byrne, 1990; Ikesawa et al., 2005; Kimura and Mukai, 1991; Onishi et al., 2001; Sample and Fisher, 1986). In this model, each individual thrust sheet is underplated at the base of the overlying plate as a result of the stepdown of the décollement to the upper levels of the basalt of the subducting plate. The resulting structure, after successive events of décollement step-down, is a stack of imbricated thrust sheets (Figure 35).

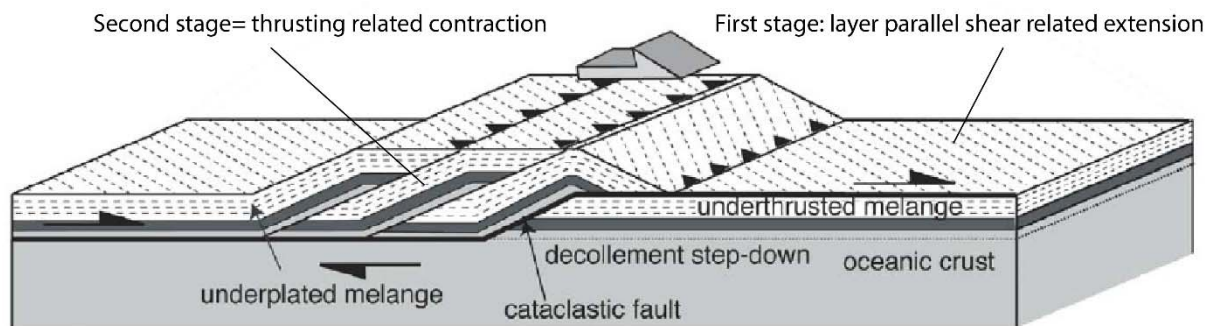


*Figure 35: Model of underplating of *mélange* thrust sheets, resulting from successive stages of décollement step-down. Two distinct stages of deformation are recorded in the *mélange*, first shear-related extension, during burial, then thrusting-related contraction, during underplating. Adapted from (Onishi et al., 2001) and (Ikesawa et al., 2005).*

Such a model of imbrication during underplating share many similarities with fold-and-thrust belts, which have been widely studied in the external domains of collisional orogens (Bally et al., 1966; Chapple, 1978). Kinematics of deformation in fold-and-thrust belts has for example been derived from passive strain markers (e.g. oolites) in the Northern Mountains, in the Appalachians, showing that within thrust sheets the shortening axis of finite strain is close to the parallel to the transport direction (Evans and Dunne, 1991). Microtectonic analysis, applied to fold-and-thrust belts, has shown similarly that meter-scale faults record the same pattern of horizontal shortening as can be deduced from imbrication of thrust sheets over a main thrust, as for example in Taiwan (Angelier et al., 1986; Angelier et al., 1990; Barrier and Angelier, 1986; Chang et al., 2000), the French Jura Belt (Homberg et al., 2002).

Accordingly, even if most of strain is localized on a master fault, the model of localized underplating (Figure 36B) involves evidence for contractional deformation within the stacked thrust sheets. Contractional deformation has indeed been described in some *mélange* examples. For instance, deformation within the Kodiak *mélange* is divided into two stages, D1 related to shearing during burial, D2 related to fold and thrusting and to the formation of a slaty cleavage, during underplating and imbrication (Fisher and Byrne, 1990; Sample and Fisher, 1986; Sample and Moore, 1987). Contraction during underplating is also described in the *mélange* along Akamatsu river in eastern Shikoku, Japan (Kimura and Mukai, 1991). Similarly, although the subduction channel in the Alps is restricted to relatively shallow depths and temperatures (below  $\sim 150^{\circ}\text{C}$ ), early extensional structures are overprinted by compressional structures (Vannucchi et al., 2008).

A major ambiguity still regards the timing of the folds and thrusts that characterize the contractional deformation recorded in accretionary prisms such as Kodiak or the Shimanto Belt. Instead of having formed during underplating, it may as well result from a posterior stage of deformation, within the accretionary wedge itself. In the Shimanto Belt, a large-scale collision stage has been described, which has largely reworked the whole structure and may correspond to most or all mesoscale contractional structures (Charvet, 2013; Charvet and Fabbri, 1987; Raimbourg et al., 2017a). Furthermore, the first-order faults, such as the Nobeoka Tectonic Line (Kondo et al., 2005), are out-of-sequence features, formed within the wedge after accretion. In the Alaskan case, the transition between underplating and later-stage intra-wedge shortening is rather unclear. As a consequence, it is difficult to assign contractional deformation unambiguously to underplating.

Furthermore, contractional deformation structures recorded in the three *mélange* zones investigated here are an uncommon feature and most of the deformation results from shear and non-coaxial extension. In the other examples from the Shimanto Belt, distributed shortening is either limited to the vicinity of large-scale faults (Kimura and Mukai, 1991) or not observed (Hashimoto and Kimura, 1999).

A consistent model of *mélange* underplating should therefore incorporate both the repetitive formation of faults to stack thrust sheets one upon another, and the dominance of extensional deformation distributed in the volume of *mélange* units. Rather than a succession of two stages, a possible model could consider that extension recorded in shear bands actually results from, and not predates underplating (Figure 36A).

Assume that, as an initial stage, *mélange* absorbs all, or a large fraction, of the relative displacement between the subducting and overriding plates. Such a description is closely related to the “subduction channel” model, where viscous deformation is broadly distributed within a

channel of several hundreds of meters of thickness, composed of the incoming sedimentary sequence (or a fraction of it) between two rigid walls (Cloos, 1982; Cloos and Shreve, 1988a, 1988b; England and Holland, 1979; Mancktelow, 1995; Raimbourg et al., 2007b; Shreve and Cloos, 1986; Vannucchi et al., 2012). The material flowing within the channel is neither part of the lower or upper plate; its velocity varies between null on top and plate convergence rate at the bottom of the channel (in upper plate reference frame). This kinematic role of *mélange* is suggested by the abundance of deformation microstructures (tension cracks, network of shear zones at all scales, stretching lineation, shape of rigid lenses), even if no strain markers enables to evaluate the absolute strain. In addition, the subduction channel model also postulates that there is no major, actively deforming fault bounding the sediment-filled channel. This point, discussed in the following section, is supported by the fact that the faults that limit the *mélange* in its present geometry were not active contemporaneously.

Assume also that at some point, for example because of strain- or metamorphic-hardening, shear is more easily accommodated within a localized fault running through the subducting basalts than within the sediment pile. This scenario is required to form the internal architecture of *mélange* units, with a stack of several basalt-soled sheets (Figure 31 and Figure 32). After formation of such a fault within the oceanic crust, further subduction of the deforming *mélange*, connected to a more localized slip zone within the basalts, results in thinning the subducting sediment pile. This is readily apparent when comparing the velocity profiles across several sections at different depths. In the model, conservation of material is imperative. Therefore, if the channel walls are fixed, the flux through any section of the channel must be equal. Conversely, if the fluxes vary along the channel length, then motion of the walls are required. Conservation of the material implies therefore that when the deforming zone is thinner than incoming thickness, the roof boundary of the “channel” is necessarily pushed upwards, to accommodate a larger influx of material than what is flowing in (Figure 36A'4). As a result, the “nose” of the channel gets longer (at a velocity equal to burial) and its opening angle gets smaller with time (Figure 36A2 to A'4). The material flowing through it accommodates this thinning by the formation of synthetic extensional shear zones. Eventually, as the shear strain rate increases towards the tip of the channel (because the material is flowing in a thinner channel), at some point a new fault forms within the underlying basalts, and a new thrust sheets starts forming.

Unlike models of “localized” underplating, where material is strong and deformation is localized on faults, such a model of “distributed” underplating considers the *mélange* as soft and deformable, thus accommodating most of underplating-related strain.

The advantages of this model is that it accounts for the lack of shortening deformation within mélangé units and the concomitance of extension and underplating, in contrast to the examples of fold-and-thrust belts cited above. It also enables the connection between mélangé deformation (distributed within the whole subducting pile) and fault formation during underplating, while localized models of underplating consider that slip occurs principally on the décollement (Fisher and Byrne, 1990; Ikesawa et al., 2005; Kimura and Mukai, 1991; Onishi et al., 2001; Sample and Fisher, 1986), which is equivalent to completely disregarding, in terms of strain accommodation, mélangé distributed deformation. Finally, it also accounts for the thinning of the sedimentary pile (geometrically necessary because of the distributed extensional shear bands), which is not incorporated in other underplating models.

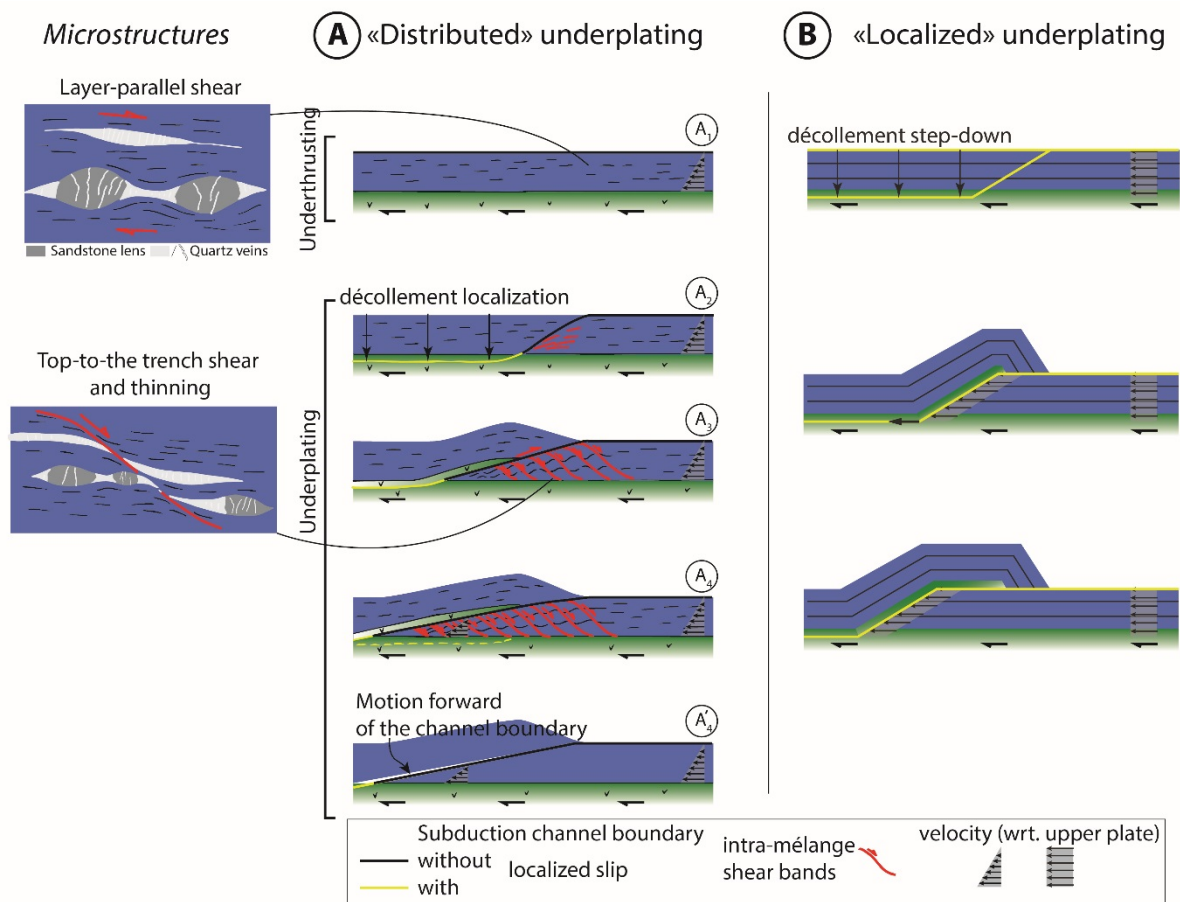


*Figure 36: Underplating models, with distributed (A) and localized (B) deformation. For the “distributed underplating” model, in an initial stage (A<sub>1</sub>), all the plate relative motion is accommodated within the mélangé. Because of strain or metamorphic hardening of the mélangé, a localized slip zone forms within the basalt of the subducting plate (A<sub>2</sub>) and connects to the upper boundary of the mélangé to form a wedge-shape zone. In the resulting evolution (A<sub>3</sub> and A<sub>4</sub>), this wedge of mélangé stretches, to account, because of mass conservation, for the difference in flow resulting from thinner section in the wedge (velocity profiles in A<sub>4</sub>’, corresponding to stage A<sub>4</sub>). Mélangé flowing through the wedge accommodates the geometrical thinning through the development of pervasive extensional shear zones, similar to the ones recorded in fossil mélangé examples. Two successive stages of deformation are recorded in the mélangé (model A), first layer-parallel shear (far from underplating zone), then extensional shear (during underplating).*

#### **4. Model of subduction plate boundary**

##### **a. Relationship between localized and distributed deformation**

Evidences for adjacent brittle deformation features, including pseudotachylytes (Ikesawa et al., 2003; Kitamura et al., 2005; Meneghini et al., 2010; Rowe et al., 2011; Rowe et al., 2005; Rowe et al., 2013) and distributed deformation in *mélange* has led to a model of plate interface incorporating simultaneously zones of highly localized slip and domains of more distributed slip (Rowe et al., 2013). This generic fault zone, forming the plate boundary, follows the fault zone model by (Faulkner et al., 2010; Faulkner et al., 2003) composed of a ~100m-1km-wide “damage” zone, ~1-5m-wide fault core and ~mm-to-cm-thick slip zones.

The coexistence, of distributed deformation and localized slip features, such as pseudotachylytes, in Kure (Mukoyoshi et al., 2006), Okitsu (Sakaguchi, 2003; Sakaguchi et al., 2006), Mugi (Ikesawa et al., 2005) or Hyuga (Kondo et al., 2005) *mélange* areas within the Shimanto Belt, might suggest that they were active at the same time, but a closer examination of their features rather show that they are disconnected.

Disconnection is in some cases geometrical, i.e. fault zones and pseudotachylytes are late-stage, or “out-of-sequence” faults, cutting across tectonic contacts and distributed deformation formed during underthrusting. For example, the faults zones (including a pseudotachylyte-bearing fault) present in the Kure *mélange* (Mukoyoshi et al., 2006) cut across the boundary between the *mélange* and the adjacent tectonic unit, so these faults were formed posterior to the deformation within the *mélange* acquired during underthrusting. This two-staged evolution is confirmed by age relationship: although underthrusting age is imprecise, the Kure *mélange* is contained within the Cretaceous Belt (Taira et al., 1988). In contrast, radiometric ages on the pseudotachylyte yielded much younger ages of 18Ma (Honda et al., 2011), which were interpreted as reflecting a post-subduction stage of collision in Early Miocene (Raimbourg et al., 2017a). Similarly, the pseudotachylyte-bearing ultracataclasite forming the roof thrust of the Mugi *mélange* was dated by K-Ar radiochronology at ~23-29Ma, while authigenic illite formed synchronously with burial and deformation within the *mélange* yielded ages older by at least several millions years (Tonai et al., 2016). In Okitsu, the maximum temperature, revealed by vitrinite reflectance, is larger in the *mélange* by ~30-50°C than in the overlying unit (Sakaguchi, 1999b; Sakaguchi et al., 2006). As discussed in (Ujiie et al., 2007), the boundary thrust, including the pseudotachylyte-bearing fault, is therefore interpreted as an out-of-sequence thrust, cutting across the thermal structure inherited from subduction/underthrusting stage. Similarly, the large-scale tectonic structure of the Cenozoic Shimanto Belt on Kyushu shows that the large-scale fault NTL is a late-stage feature cutting across a number of tectonic

units and their internal deformation, including the Hyuga Tectonic mélange (HTM) (Murata, 1996, 1997, 1998; Raimbourg et al., 2014a). The NTL constitutes the roof thrust of the HTM on the eastern coast, but further on-land the NTL cuts across the lower limit of the HTM, so that the footwall of the NTL is there constituted of the coherent turbiditic formation underlying the HTM (Figure 21). As a consequence, the penetrative deformation within the HTM is not interpreted as a damage zone associated with the thrusting movement on the NTL (Kondo et al., 2005) but rather as a distinct, earlier deformation.

In these many examples, the mélange deformation within the thrust sheets, interpreted as related to underthrusting, predates more localized deformation on faults, associated in most cases with a distinct, later-stage event. In the classical model of mélange underplating (Fisher and Byrne, 1990; Ikesawa et al., 2005; Kimura and Mukai, 1991; Onishi et al., 2001; Sample and Fisher, 1986), there is also a clear disconnection between the mélange-forming deformation, during burial, and slip on thrust sheets-bounding faults, during underplating. In the alternative model we propose in Figure 36, distributed deformation in the mélange during underplating, and repeated events of slips on faults within basalts, are coeval, although they occur at different locations along dip. But irrespective of the model of underplating, there is no configuration such as proposed in (Rowe et al., 2013) where localized and distributed slip act in parallel. Furthermore, as for the different examples from the Shimanto Belt, in most instances the most localized features, that is the pseudotachylytes, are a later-stage event occurring within the wedge, posterior to mélange emplacement at depth.

#### ***b. Seismic vs. aseismic slip along the interface – rheological models***

Although it is difficult to quantify it, mélange zones do accommodate a fraction of the strain resulting from plate relative motion, in a distributed fashion incompatible with large-scale earthquakes. Mélange can therefore be considered as a possible candidate for the aseismic deformation observed along plate boundaries in active margins, in other words to non-coupled portions of the plate interface (e.g. (Loveless and Meade, 2010; Moreno et al., 2010)). From this hypothesis on, the major issues are the reasons why deformation is distributed in the mélange and what rheological model is best representative of such deformation.

In Fagereng and Sibson (2010), mélange rheology is considered as controlled by the proportion of competent blocks (sandstone, chert, basalt), which deform by localized shear, with respect to the clay matrix that deform by distributed strain. Accordingly, clay-rich mélange would deform by aseismic creep, while domain rich in more competent blocks would act as larger seismic asperities along the subduction interface, up to the very large-scale of subducted seamounts jamming the plate interface. The interpretation of the competence contrast between

the clay matrix and the blocks is actually questionable, as the rheology of the different material change with burial and metamorphic reactions and little is known about the rheological properties of phyllosilicates for in situ conditions of P and T. For example, recent friction experiments on clay-rich material has shown a transition from velocity-strengthening to velocity-weakening for an increase in T from 50 to 150°C (Sawai et al., 2017). Moreover, the model of rigid seamount jamming the interface and acting as large seismic asperities is actually somehow invalidated by the data (Wang and Bilek, 2016). Finally, the occurrences of the most extreme type of deformation localization, the pseudotachylytes, are so far systematically associated with tectonic mélanges (e.g. in the Kodiak Complex (Meneghini et al., 2010) or the Shimanto Belt (Ikesawa et al., 2003; Kitamura et al., 2005)), which are relatively rich in clay with respect to other domains of paleoaccretionary prism containing massive sandstones. The competent vs. incompetent, clay matrix -rich vs. block-rich dichotomy is therefore too simplistic a dichotomy to account for the diversity of deformation style. The Shimanto Belt examples of tectonic mélanges described in here show actually a succession of stages, distributed shear during burial, then more localized strain during underplating, which point to time-variations in strength in a given material incompatible with a model solely controlled by the proportion of competent blocks in the matrix.

Assessing the rheology of clay-rich mélange zones require to analyze the microprocesses of deformation. In all examples of mélanges, pressure solution is a major mechanism (Fisher and Byrne, 1987, 1990; Onishi and Kimura, 1995; Palazzin et al., 2016), accounting for the formation of the foliation, but also, along with microfracturing, to the precipitation of quartz in veins (Fagereng and Harris, 2014; Fisher and Brantley, 2014; Raimbourg et al., 2018) (Figure 27, Figure 28, Figure 29, Figure 36). Another essential micromechanism for deformation is the development of a mm-scale network of phyllosilicates-shear bands or microfaults, involving in particular chlorite (Figure 29) (Fisher and Byrne, 1987; Meneghini et al., 2009). The rheology of the whole rock involves therefore slip on phyllosilicate shear band network, accommodated by the deformation by dissolution and precipitation of the quartz-rich lenses in between the boudins. Assuming that in this chain of processes, dissolution and precipitation of quartz is the rate-limiting process, then bulk rock rheology is controlled by the rate at which transport of silica can be achieved at the small scale, as all geochemical and textural evidences point to local transfers (Palazzin et al., 2016; Raimbourg et al., 2018).

The possibility to localize slip on a mm- to cm-thick plate boundary fault, rather than distribute strain within a hundreds of meters-thick mélange corresponds to the strength contrast between the fault and the mélange rheology, hence on the efficiency of pressure solution transfers within the mélange (Fagereng and Den Hartog, 2017). In such a model, the abundance of water, mostly

related to its production through clay diagenetic reactions (Saffer and Tobin, 2011), as well as transfer distances, a critical parameter of pressure solution flow laws (Gratier et al., 2009), possible related to stress heterogeneity, are essential to determine mélange strength. Aseismic portions of the plate interface could correspond to domains where the sediments on top of the subducting plate deform for very low stresses, preventing significant stress transfer across the interface and inhibiting seismic ruptures. In any case, mélange deformation is a geological evidence that plate boundary deformation cannot be modelled only on the basis of friction laws.

## **F. Conclusion**

The comparative study of several tectonic mélange units within the Shimanto Belt revealed common features, providing insights into the processes at stake along the subduction plate boundary at depth. Several conclusions can be drawn from mélange micro- and macrostructures of deformation, regarding the processes of underplating and distributed vs. localized character of deformation:

- 1) Distributed deformation, at the origin of the formation of the block-in-matrix structure of the mélange, results from slip on a pervasive network of shear bands, ranging from meter-scale, quartz-filled structures to microscopic, chlorite-filled ones. Deformation on shear bands is accompanied by pervasive veining, either in cracks formed perpendicular to extension in more competent sandstone or quartz lenses, or in extension veins parallel to foliation.
- 2) Kinematics of deformation, as it can be deduced from the slip on shear bands, is consistently top-to-the-trench shear deformation. As shear bands have in average a lower dip than foliation, they are interpreted as extensive structures.
- 3) Underplating is required by the repetition of several mélange thrust sheet units. Nonetheless, the absence of contractive structures within the mélange leads to propose a new model, where distributed extension within the mélange occurs during underplating. This model of “distributed” underplating, contrasting with usual “localized” underplating models, is in accordance with the low viscosity of the mélange material, flowing in-between more rigid material.
- 4) Localized deformation on faults, including pseudotachylytes, occurs in many instances *after* underplating, as intra-wedge deformation, while mélange deformation occurs *before* (i.e. underthrusting) and *during* underplating. There is no evidence for a structure of plate boundary comprising a roof thrust and underlying mélange deforming simultaneously.
- 5) Mélange distributed deformation constitutes a candidate for the aseismic slip observed along certain portions of active subduction plate interfaces. Plate interface rheology can be envisioned as the result of the competition between localized, frictional slip on a master fault, and

distributed shear of a hundreds-of-meters-thick *mélange* zone. Distributed deformation involves a complex interplay between slip on phyllosilicate-rich shear zone network and pressure solution of quartz. The latter process is likely to be the limiting process, therefore controlling the bulk rheology of *mélange*.

| Area                       | Method                | Sample      | Location        |  | Number of analyses |                               | Average T (°C)   |  | Reference  |                                  |                                 |
|----------------------------|-----------------------|-------------|-----------------|--|--------------------|-------------------------------|------------------|--|--|----------------------------------|---------------------------------|
| Hyuga mélange              | RSCM                  |             | Longitude       | Latitude   |                    | $RA1=(D1+D4)/(D1+D2+D3+D4+G)$ | Equivalent T(°C) | Stand. Dev. on T                                     | Raimbourg et al., Tectonics 2017                                 |                                  |                                 |
|                            |                       | HN 54       | 131,73098       | 32,59126   | 10                 | 0,540                         | 207              | 11   |  |                                  |                                 |
|                            |                       | HN 64       | 131,46297       | 32,59442   | 9                  | 0,565                         | 238              | 6  |  |                                  |                                 |
|                            |                       | HN 65       | 131,40357       | 32,54517   | 10                 | 0,567                         | 240              | 6  |  |                                  |                                 |
|                            |                       | HN 68       | 131,39923       | 32,54939   | 10                 | 0,587                         | 264              | 22   |  |                                  |                                 |
|                            |                       | HN 75       | 131,24460       | 32,41619   | 10                 | 0,570                         | 244              | 11   |  |                                  |                                 |
|                            |                       | HN 77       | 131,24460       | 32,41619   | 10                 | 0,585                         | 261              | 27   |  |                                  |                                 |
|                            |                       | HN 85       | 131,31481       | 32,42867   | 10                 | 0,569                         | 242              | 11   |  |                                  |                                 |
|                            |                       | HN 91       | 131,24250       | 32,41610   | 10                 | 0,561                         | 233              | 8  |  |                                  |                                 |
|                            |                       | HN 93       | 131,58203       | 32,60445   | 10                 | 0,570                         | 244              | 16   |  |                                  |                                 |
|                            | HN 94                 | 131,57563   | 32,60837        | 10   | 0,563              | 235                           | 13               |  |  |                                  |                                 |
|                            |                       |             |                 |  |                    |                               | <b>243</b>       |  |  |                                  |                                 |
|                            | Vitrinite reflectance |             |                 | In the vicinity of the NTL, on eastern coast of Kyushu |                    |                               | R0max            | Equivalent T(°C)                                     | Stand. Dev. on Rmax  | Kondo et al. Tectonics 2005      |                                 |
|                            |                       | NBO3        |                 |  |                    |                               | 2,75             | 205  | 0,26   |                                  |                                 |
|                            |                       | NBO1        |                 |  |                    |                               | 2,72             | 204  | 0,16   |                                  |                                 |
|                            |                       | NBO16       |                 |  |                    |                               | 2,73             | 204  | 0,22   |                                  |                                 |
|                            |                       | NBO8        |                 |  |                    |                               | 2,58             | 200  | 0,09   |                                  |                                 |
|                            |                       | NBO18       |                 |  |                    |                               | 2,69             | 203  | 0,11   |                                  |                                 |
|                            |                       |             |                 |  |                    |                               | <b>203</b>       |  |  |                                  |                                 |
|                            | Illite crystallinity  |             |                 |  |                    |                               | Mean IC value    | Equivalent T(°C)                                     | Standard deviation on IC value                                   | Hara and Kimura, Island Arc 2008 |                                 |
|                            |                       |             |                 | western area of Miyazaki-ken                           | 32                 |                               | 0,370            | 277  | 0,04   |                                  |                                 |
|                            |                       |             |                 | just below the NTL, throughout its outcropping area    | 8                  |                               | 0,424            | 266  | 0,07   |                                  |                                 |
|                            |                       |             |                 |  |                    |                               | <b>271</b>       |  | Mukoyoshi et al. 2009  |                                  |                                 |
|                            | Fluid inclusions      |             |                 |  |                    |                               |                  | T homogenization                                     | Type of vein   | Kondo et al. Tectonics 2005      |                                 |
|                            |                       | NB22        |                 | just below the NTL, throughout Miyazaki-ken            | 23                 |                               |                  | 180  | Type 1 veins, i.e. tension cracks in boudinaged sandstone blocks |                                  |                                 |
|                            |                       | NB27        |                 |  | 20                 |                               |                  | 175  |  |                                  |                                 |
|                            |                       | NB30        |                 |  | 21                 |                               |                  | 295  |  |                                  |                                 |
|                            |                       | NB31        |                 |  | 12                 |                               |                  | 305  |  |                                  |                                 |
|                            |                       | Ve11        |                 |  | 15                 |                               |                  | 220  |  |                                  |                                 |
|                            |                       |             |                 |  |                    |                               |                  | <b>235</b>   |  |                                  |                                 |
|                            |                       | HN48a site1 | 32,40899        | 131,25497  | 15                 |                               |                  | 227  | 33   |                                  | Extension veins and microcracks |
|                            |                       | HN74        | 32,49138        | 131,37704  | 22                 |                               |                  | 245  | 24   |                                  |                                 |
| HN51b site2                |                       | 32,41610    | 131,24250       | 82   |                    |                               | 224              | 35   |  |                                  |                                 |
| HN75 site3                 | 32,52284              | 131,38497   | 17              |  |                    | 200                           | 19               |  |  |                                  |                                 |
|                            |                       |             |                 |  |                    | <b>224</b>                    |                  | This study and Raimbourg et al., Tectonophysics 2015 |  |                                  |                                 |
| Kure mélange               |                       |             |                 |  |                    | Rmax                          | Equivalent T     | Mukoyoshi et al. EPSL 2006                           |  |                                  |                                 |
|                            |                       |             | Along the coast |  |                    | 2,3                           | 191              |  |  |                                  |                                 |
|                            |                       |             |                 |  |                    | 2,1                           | 184              |  |  |                                  |                                 |
|                            |                       |             |                 |  |                    | 2,1                           | 184              |  |  |                                  |                                 |
|                            |                       |             | 2km onland      |  |                    | 2,3                           | 191              |  |  |                                  |                                 |
|                            |                       |             |                 |  |                    | 1,8                           | 173              |  |  |                                  |                                 |
|                            |                       |             |                 |  |                    |                               | <b>185</b>       |  |  |                                  |                                 |
| Okitsu mélange             | RSCM                  | Sample      | Longitude       | Latitude   | Number of analyses | $RA1=(D1+D4)/(D1+D2+D3+D4+G)$ | T mean (°C)      | Stand. Dev. on T                                     | This study   |                                  |                                 |
|                            |                       | HN321       | 33,21362        | 133,24004  | 12                 | 0,546                         | 214              | 21   |  |                                  |                                 |
|                            |                       | HN323       | 33,20323        | 133,23441  | 11                 | 0,550                         | 219              | 8  |  |                                  |                                 |
|                            |                       | HN325       | 33,20200        | 133,23532  | 10                 | 0,563                         | 235              | 25   |  |                                  |                                 |
|                            |                       | HN329       | 33,16339        | 133,18384  | 10                 | 0,577                         | 252              | 9  |  |                                  |                                 |
|                            |                       |             |                 |  |                    |                               | <b>230</b>       |  |  |                                  |                                 |
|                            | Vitrinite reflectance |             |                 |  |                    |                               | Rmax             | Equivalent T   | Sakaguchi, Island Arc 1999                                       |                                  |                                 |
|                            |                       | OK521       |                 |  |                    |                               | 3,21             | 216  |  |                                  |                                 |
|                            |                       | OK801       |                 |  |                    |                               | 3,02             | 212  |  |                                  |                                 |
|                            |                       | OK805       |                 |  |                    |                               | 3,45             | 222  |  |                                  |                                 |
|                            |                       | OK831       |                 |  |                    |                               | 2,96             | 210  |  |                                  |                                 |
|                            |                       |             |                 |  |                    |                               | <b>215</b>       |  |  |                                  |                                 |
|                            | Fluid inclusions      |             |                 |  |                    |                               |                  | T homogenization                                     | Calcite veins  | Sakaguchi, Island Arc 1999       |                                 |
|                            |                       |             |                 | 115  |                    |                               | <b>210</b>       |  |  |                                  |                                 |
| Mugi mélange Lower section | RSCM                  | Sample      | Longitude       | Latitude   | Number of analyses | $RA1=(D1+D4)/(D1+D2+D3+D4+G)$ | T mean (°C)      | Stand. Dev. on T                                     | This study   |                                  |                                 |
|                            |                       | HN452       | 33,67394        | 134,45467  | 18                 | 0,500                         | 163              | 39   |  |                                  |                                 |
|                            |                       | HN454       | 33,67394        | 134,45467  | 20                 | 0,540                         | 206              | 46   |  |                                  |                                 |
|                            |                       | HN456       | 33,67233        | 134,45231  | 23                 | 0,525                         | 189              | 34   |  |                                  |                                 |
|                            |                       | HN457       | 33,67122        | 134,45139  | 18                 | 0,516                         | 176              | 35   |  |                                  |                                 |
|                            |                       |             |                 |  |                    |                               | <b>184</b>       |  |  |                                  |                                 |
|                            | Vitrinite reflectance |             |                 |  |                    |                               | R0max            | Equivalent T   |  |                                  |                                 |
|                            |                       |             |                 |  |                    |                               | 1,40             | 154  |  |                                  |                                 |
|                            |                       |             |                 |  |                    |                               | 1,50             | 159  |  |                                  |                                 |
|                            |                       |             |                 |  |                    |                               | 1,55             | 162  |  |                                  |                                 |
|                            |                       |             |                 |  |                    | 1,05                          | 133              |  |  |                                  |                                 |
|                            |                       |             |                 |  |                    | 1,00                          | 129              |  |  |                                  |                                 |

|               |                       |  |  |   |                  |              |  |                                      |                                     |
|---------------|-----------------------|--|--|---|------------------|--------------|--|--------------------------------------|-------------------------------------|
|               |                       |  |  |   | 1,05             | 133          |  |                                      | Ikesawa et al., Tectonophysics 2005 |
|               |                       |  |  |   | 1,00             | 129          |  |                                      |                                     |
|               |                       |  |  |   | 1,40             | 154          |  |                                      |                                     |
|               |                       |  |  |   | 0,85             | 117          |  |                                      |                                     |
|               |                       |  |  |   | 1,30             | 149          |  |                                      |                                     |
|               |                       |  |  |   | 1,05             | 133          |  |                                      |                                     |
|               |                       |  |  |   | 1,00             | 129          |  |                                      |                                     |
|               |                       |  |  |   | <b>140</b>       |              |  |                                      |                                     |
|               | Fluid inclusions      |  |  | n | T homogenization |              |  |                                      | Matsumura et al. Geology 2003       |
|               |                       |  |  |   | 2                | 195          |  | Extension veins in sandstone boudins |                                     |
|               |                       |  |  |   | 6                | 125          |  |                                      |                                     |
|               |                       |  |  |   | 13               | 165          |  |                                      |                                     |
|               |                       |  |  |   | 16               | 185          |  |                                      |                                     |
|               |                       |  |  |   | 20               | 175          |  | Veins in basalts near thrust zone    |                                     |
|               |                       |  |  |   | 2                | 245          |  |                                      |                                     |
|               |                       |  |  |   | 10               | 135          |  |                                      |                                     |
|               |                       |  |  | 8 | 205              |              |  |                                      |                                     |
|               |                       |  |  |   | <b>179</b>       |              |  |                                      |                                     |
| Upper section | Vitrinite reflectance |  |  |   | R0max            | Equivalent T |  |                                      | Ikesawa et al., Tectonophysics 2005 |
|               |                       |  |  |   | 2,90             | 209          |  |                                      |                                     |
|               |                       |  |  |   | 3,15             | 215          |  |                                      |                                     |
|               |                       |  |  |   | 2,80             | 206          |  |                                      |                                     |
|               |                       |  |  |   | 2,65             | 202          |  |                                      |                                     |
|               |                       |  |  |   |                  | <b>208</b>   |  |                                      |                                     |

Table 1: P-T conditions of deformation within the mélangé units.

## **Chapter IV: Fluid properties and circulation in the depth of subduction zones**

In this chapter I review the different approaches focusing on the fluid transfers at depth in subduction zones. The problem can be considered at the very large-scale, through fluid budgets of the different material that are being subducted (sediments, oceanic crust and mantle, the two latter ones being partially hydrated prior to burial), considering their progressive dehydration by mechanical (compaction) and chemical (metamorphic reactions) processes. Alternately, the geochemistry of rocks subducted to variable depths then exhumed provides another clues as to the extent of elemental and fluid transfers at depth. Finally, the question can also be considered from the point of view of the veins that were formed at depth, as they constitute the most direct record of the deep circulation. My own work focused on these veins, and some results I obtained are shown here, concerning the mineral forming the veins as well as the fluid trapped in fluid inclusions. Finally, I discuss of the relation between the fluid and the contemporaneous deformation processes, in particular fluid-mediated pressure solution.

### **A. Fluid sources along the plate interface**

#### ***1. Compaction sources***

The flux of fluid along the plate interface and in overlying accretionary prism has been extensively studied in the shallow domain (i.e. less than a few km depth) of subduction zones in the framework of deep-sea drilling campaigns. Based on direct observations or measurements of venting (e.g. (Henry et al., 1992) or hydrological models (e.g. (Bekins and Dreiss, 1992)), the general model of shallow fluid circulation is that water dragged passively down in pores of buried sediments is expelled by compaction and flows upward along permeable horizons such as faults and a master décollement (Kastner et al., 1991; Le Pichon et al., 1993; Saffer and Tobin, 2011). This source of water is restricted to a few kilometers of depth, as the pore volume fraction diminishes along with compaction (Figure 37), and is replaced by water produced by dehydration reactions (Saffer and Tobin, 2011).

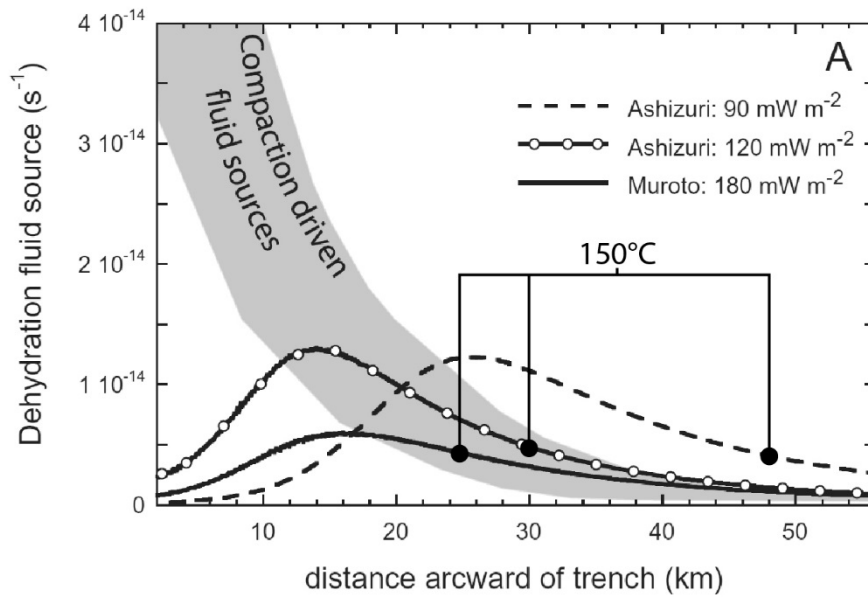


Figure 37: Rates of water production in subducting sediments, resulting from the contribution of sediment compaction (gray area) and smectite-to-illite reactions (the three curves), modified from (Saffer et al., 2008). The clay reaction rates are calculated in the Nankai subduction zone, bordering the SW Japan, along two transects (Muroto and Ashizuri), for different thermal models. The source is given as  $\frac{V_{fluid}}{V_{bulk}}$  ( $s^{-1}$ ), where  $V_{bulk}$  is the total volume of sediment entering the subduction zone per second.

## 2. Dehydration sources

### a. Sediments

Considering the deep seafloor material entering the subduction zones, the largest source of water involves clay minerals, abundant in buried sediments (Moore and Saffer, 2001; Saffer et al., 2008). In particular, smectite is a large carrier of water in subducted sediments, and releases water as it is progressively transformed into illite with the temperature rise in the range ~50-150°C (Freed and Peacor, 1989; Kastner et al., 1991; Pytte and Reynolds, 1989; Velde and Vasseur, 1992).

At larger depths, the estimation of the water fluxes is first based on the evolution of the water budget that can be stored in metamorphic minerals. Extensive geochemical studies of metamorphic series spanning a large range of burial conditions have been carried out in the Franciscan Complex and in the Alps (Bebout, 1995, 2007; Bebout et al., 2013a; Sadofsky and Bebout, 2001, 2003, 2004), providing essential clues as regards volatile mobility in subducting material.

The release of water with subduction is in average attested by the decrease in loss on ignition of metamorphosed sediments compared to their unmetamorphosed equivalents (Figure 38). In the series of Franciscan Complex Terranes, from “Coastal Belt” to “Pacheco Pass”, there is nevertheless not a clear trend of decreasing water with increasing burial depth (Sadofsky and

Bebout, 2003). In the Catalina Schists series, a clearer decrease in water content is apparent when considering increasing temperature conditions (Bebout, 1995) (note that the water content for low-grade Catalina schists in (Bebout, 2007) are to some extent discrepant with the data in (Bebout, 1995), possibly because of the measurement method). Nonetheless, these units correspond to distinct P-T paths during subduction, from “colder” (lawsonite-albite, lawsonite blueschist) to “hotter” subduction paths (epidote-blueschist, epidote-amphibolite then amphibolite). Increasing devolatilization across this suite of terranes does not correspond to the evolution with burial of a given terrane, but rather to different conditions of subduction.

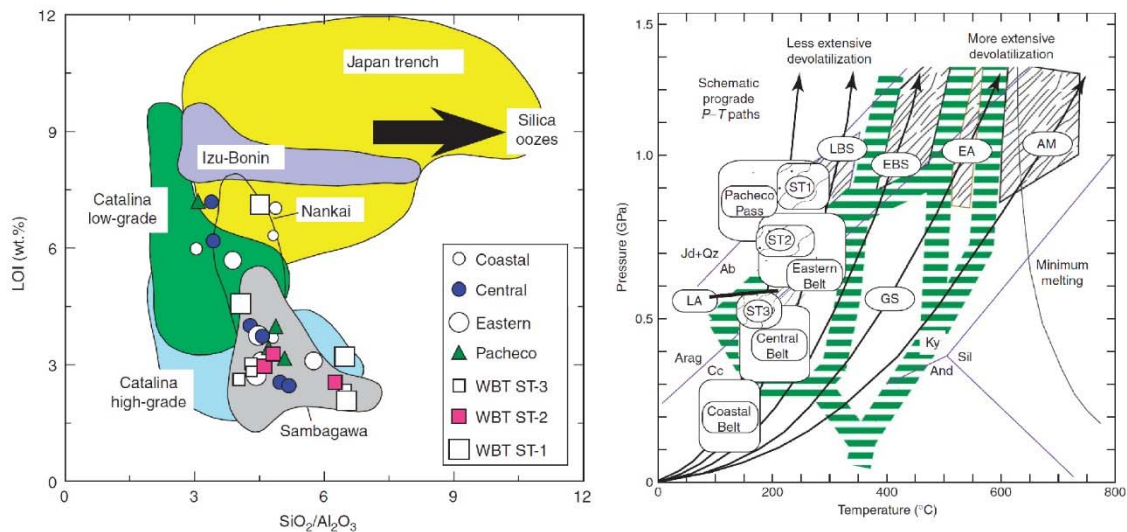


Figure 38: Evolution in water content of metasedimentary rocks across various metamorphic grades, from (Bebout, 2007). (Left): All points or domains refer to metasediments, but for Izu-Bonin, Japan Trench, Nankai and silica oozes, which correspond to modern sediments. (Right): P-T conditions in from the Franciscan Complex (“Coasta”, “Central”, “Eastern” Belts and “Pacheco Pass”, see (Sadofsky and Bebout, 2003)) and in the Catalina Schists (parageneses shown with ellipses, LA=lawsonite albite, LBS=lawsonite blueschist, EBS=epidote blueschist, EA=epidote amphibolite, AM=amphibolite).

Another approach on the question revolves not on actual rock composition but on the theoretical evolution of rocks of a given composition with burial, based on petrogenetic grids and on thermomechanical models that constrain the evolution in P and T of subducting material.

The average composition of the sediments entering subduction zones is named GLOSS and its composition was derived from the worldwide database established by Plank and Langmuir (1998). GLOSS contains  $\sim 7.3 \pm 0.4$  wt% of mineral-bound H<sub>2</sub>O. In addition, in their study of subduction-related devolatilization, (Kerrick and Connolly, 2001a) consider also a clay-rich marl, akin to the metamorphosed pelites from the Shimanto Belt, with an initial water content of  $\sim 12\%$ , siliceous limestones and carbonaceous oozes. Up to the conditions of the Lawsonite-blueschists ( $\sim 1$ GPa,  $300^\circ\text{C}$ , see Figure 38), there is a limited decrease in the amount of mineral-bound H<sub>2</sub>O, for all lithologies (including the average GLOSS) except for the clay-rich sediment,

whose water concentration decreases from original ~12wt% to slightly more than 4wt% (Figure 38).

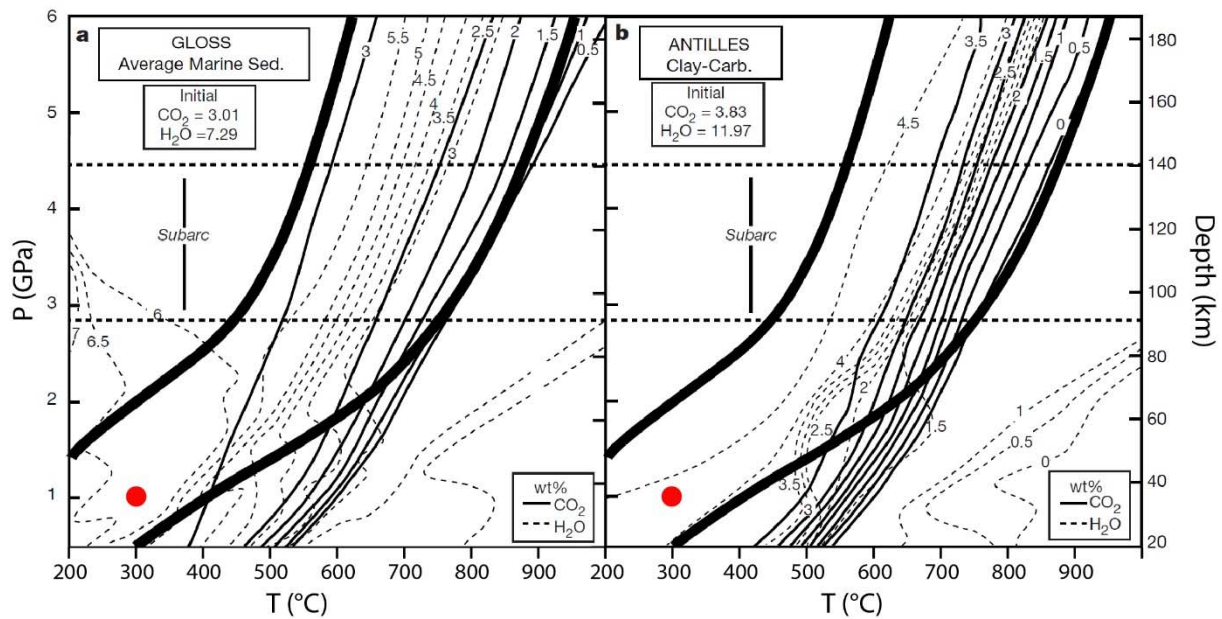


Figure 39: Evolution of H<sub>2</sub>O and CO<sub>2</sub> content with burial for the average subducted sediment GLOSS (Plank and Langmuir, 1998), and for a clay-rich marl, modified from (Kerrick and Connolly, 2001a). The red point at 1GPa and 300°C corresponds to the Lawsonite-blueschist facies in Figure 38. Realistic P-T path are bracketed by the two thick lines.

The Antilles sediments used in (Kerrick and Connolly, 2001a) are part of unit 6 site in DSDP site 543 (Shipboard Scientific Party, 1984), which is composed principally of calcareous ferruginous claystone. Lithology analyzed by XRD is composed of clays for 60 to 80%, of which more than 50-60% is smectite, the rest being illite (~10%), kaolinite (about 20-30%), and palygorskite (formed after smectite) (Pudsey, 1984). On the other hand, the mineralogy predicted at 1GPa and 300°C is composed of chlorite, aragonite, white mica, paragonite, lawsonite and dolomite (Kerrick and Connolly, 2001a). Dehydration reactions, associated with the destabilization of smectite and kaolinite, are therefore the source of fluid production during burial down to 1GPa. It is nevertheless not clear what the amount of water in original clay-rich sediment from the Antilles corresponds to. Its water-bound content is determined by loss on ignition, on sample that have been crushed and heated at 110°C (Plank and Ludden, 1992), hence on smectite without interlayer water. The ~12wt% of original water content is therefore probably underestimated, when considering that actual sediments carry down an extra amount of water stored as smectite interlayer water (smectite contains up to 20wt% of water (Spinelli and Saffer, 2004)).

The 4-5wt% water left in the clay-rich sediments, as predicted by petrogenetic grids, is well in agreement with estimates on metasediments buried to conditions up to 1GPa (Figure 38). If

there is an uncertainty on the amount of water carried down from the surface, the remaining water at 1GPa is relatively well constrained independently by thermodynamic models and geochemistry of metasediments.

Considering the evolution of metasediments deeper than 300°C-1GPa, for an increase in P-T conditions similar to the Schistes Lustrés in the Alps (from P-T conditions of ~320°C-13kbars (Fraiteve) to ~500°C-20kbars (Finestre) (Agard et al., 2001)), i.e. along a cold gradient, and with a lithology of clay-carbonate, there is a decrease in water-bound minerals from ~4wt% to ~2wt%. Therefore, most of the water release occurs shallower than 300°C, and the remaining evolution is characterized but much more limited dehydration.

### *b. Metabasites*

The same approach of petrogenetic grids was adopted to study devolatilization of metabasalts (Kerrick and Connolly, 2001e). Along the cold gradients, there is a very limited loss of water (Figure 40) down to 180km depth, while for any realistic gradient the is no devolatilization below 400°C.

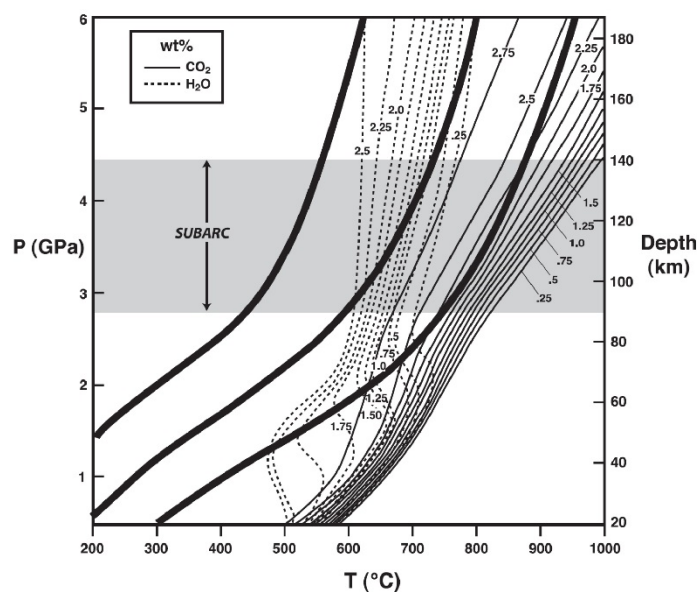


*Figure 40 : Evolution of H<sub>2</sub>O and CO<sub>2</sub> content in basalts as a function of P and T, from (Kerrick and Connolly, 2001e). The three thick lines correspond to different geotherms along the subduction plate interface.*

On another thermodynamic modelling approach, (Hacker, 2008; Hacker et al., 2003) considered excess H<sub>2</sub>O to calculate the different equilibrium parageneses within the P-T field. Such an approach yields much larger amounts of structurally-bound water than (Kerrick and Connolly, 2001e). For example, in the lawsonite-blueschist paragenesis, there is slightly more than 5wt% of water-bound mineral (including 3wt% in the very abundant lawsonite). Similarly, high P and T experiments with excess H<sub>2</sub>O predict for 1GPa and 300 to 400°C around 4 to 6wt% of mineral-bound water in metabasalts (Schmidt and Poli, 1998). In the thermodynamic models and

experiments with excess water, there is a significant decrease in water content for any subduction case, even if the devolatilization is strongly enhanced in warm subduction case (Hacker, 2008).

As for the metasediments, the evolution shallower than 1GPa and 300°C is strongly dependent on the extent of seafloor alteration of the basalts. The protolith used in (Kerrick and Connolly, 2001e) are defined on the basis of a study on DSDP cores of the Atlantic oceanic crust (Staudigel et al., 1989) and on a very thick section in the eastern equatorial Pacific (Alt and et. al., 1996), which served as a reference site to study the effect of alteration on oceanic crust. In both cases, although widespread alteration is observed in the volcanites on top of the oceanic crust (in particular with the presence of saponite, a type of smectite), the mineral-bound water is 2.7wt% in the former and mostly below 2wt% in the latter study. A more recent IODP drilling campaign on a basalt section in the Cocos Plate yielded also very low mineral-bound water, below 1wt% throughout the column ((Scientists, 2006), page 184). In contrast, (Jarrard, 2003) converted core measurement of bulk density into alteration (with saponite and celadonite). Most alteration is restricted to the ~600m thick layers of extrusive on top of oceanic crust. The total amount of water, recalculated for a 80Ma-old crust, amount to 6 and 4wt%, for upper and lower levels of extrusives, and decreases to 1.8 and 0.8wt% in the sheeted dykes complex and in gabbros. There is therefore a large uncertainty on the extent of alteration, and therefore on the amount of mineral-bound H<sub>2</sub>O, in the oceanic crust, as confirmed by the compilation of DSDP and ODP drilled section of oceanic crust ((Scientists, 2006) page 121). But in any case alteration is restricted to the uppermost levels of extrusives of the oceanic crust, and structurally bound water in underlying basalts and gabbros is very small.

Basalts exhumed within accretionary and subduction complexes have a high content in water, as reported in (Bebout, 1995): above 10wt% for the un-metamorphosed equivalent to metabasalts from the Catalina Schists. Furthermore, in the same study, the basalts metamorphosed in lawsonite-albite and lawsonite blueschist facies conditions contain ~3 and ~5wt% of water, i.e. more than the values of the few examples of altered basalts sampled on the seafloor reported in (Alt and et. al., 1996).

There seems to be therefore a large variability in initial water content in the oceanic crust, controlled by the extent of alteration. If in average altered basalts from incoming oceanic plate contain around 2wt% water, then lawsonite-blueschist basalts are able to incorporate more water, in other words there is a possibility to hydrate the oceanic crust at depth if water is made available from adjacent lithology. If the starting material basalts contain ~5-6wt% of water, this amount is sufficient to form the hydrated parageneses rich in lawsonite at 1GPa and 300°C. Further evolution is in any case associated with dehydration.

The key issue is therefore the initial extent of alteration. An additional complexity rises in the fact that alteration occurs not only at the ridge but also during slab bending on the shallow levels of subduction (Ranero et al., 2003), which promotes faulting and water penetration into the slab. As a result, it is therefore difficult to precisely constrain the entering flux of H<sub>2</sub>O in oceanic crust.

### *c. Serpentine and peridotites*

Finally, serpentines are also a possible way to carry water to depths and to release it during burial. Phase diagrams calculated by Hacker et al. (2003) show that most reactions are at first order controlled by isotherms. For most gradients, the first reaction occurs for T~500°C, with the destabilization of brucite, then around 600-700°C all antigorite is destabilized to olivine. These reactions, studied in metamafic rocks in the Western Alps and the Betic Cordilleras (Scambelluri et al., 2004a), confirm this two-step dehydration process, even if there is some disagreement on the relative amount of water released (the largest source of fluid is predicted to be the first reaction in (Hacker et al., 2003) and the second one in (Scambelluri et al., 2004a)). The total amount of water produced is potentially very large, as serpentine contain initially 12-15wt% of water (Hacker et al., 2003), most of which is released upon destabilization of serpentine minerals.

Serpentinites follow therefore the same pattern as sediments and altered oceanic crust and devolatilize potentially large volumes of water upon burial. As for the oceanic crust, the flux of water released depends on the pre-subduction state of alteration of the oceanic lithosphere, potentially very variable.

As a conclusion, the general model of water cycling in subduction zones is at first order a progressive release of water by the oceanic lithosphere upon burial. In this general model, the shallow (down to ~300°C) portion of subduction zones is somehow specific in several respects: (1) the largest source of water comes from the dehydrating clays. There is a limited release of water from other types of sediments. (2) The subducted crust contains a variable, but in many cases low, concentration in water. There is therefore a possibility to hydrate the crust by transferring water from dehydrating sediments above.

## **B. Chemistry of subduction zone fluids**

The result of the release of “fresh” water by shallow diagenetic reactions of opal-CT or clays is to decrease the chlorinity of pore fluids in subducting sediments (Kastner et al., 1993; Kastner et al., 1995). In addition to this “freshening” effect, rock-water interactions at low T (<300°C) strongly modify the chemistry of the pore fluids. Sampling of fluids in the mud volcanoes of the Mariana Trench gives an account of these interactions (Mottl et al., 2004). The sampling

sites are located at different distances from the trench, hence the fluid originates from different depths along the plate interface, allowing to analyze the evolution of fluid-rock interactions with variable T. K, Rb and Cs are leached from the rock into the fluid at  $T > 150^\circ\text{C}$ , while they are taken up into the rock at  $T < 80^\circ\text{C}$ . B is leached into the fluid for low T ( $\sim 60^\circ\text{C}$ ), which confirms experimental studies of sediment-rock interaction (You et al., 1996; You and Gieskes, 2001). In addition, all the pore water are depleted in Mg, Si, Li, F compared to sea-bottom water (Mottl et al., 2004). Such a behavior of Li is discrepant with respect to hydrothermal experiments, which showed a removal of Li from the rock for  $T \sim 300^\circ\text{C}$  (You et al., 1996; You and Gieskes, 2001).

B and Li focus a lot of attention as they are mobile elements that are used to trace fluid transfers, from incoming material down to UHP conditions and then up to arc magmas (Bebout, 1995; Scambelluri et al., 2004e). In the above experiments, the behavior of B and Li varies across the T range. B is removed from very low T (below  $150^\circ\text{C}$ ) on, while Li leaching from the rock is efficient above  $150^\circ\text{C}$  (You and Gieskes, 2001; You et al., 1995) (Figure 41). The B removal is interpreted as a two-staged process, acting at low T (below  $150^\circ\text{C}$ ) on the adsorbed fraction in the interlayer space then at higher T on the lattice bound fraction (corresponding to 20 and 80%, respectively) (Spivack et al., 1987; You and Gieskes, 2001). The contrasting behavior of Li and B is also revealed in an experimental study of the uptake of Li and B during smectite to illite reaction, showing that Li is adsorbed in the interlayer space preferentially over B during crystal growth (Williams and Hervig, 2005). This further supports the preferential release of adsorbed B from clay during prograde metamorphism. Finally, experimental compaction of clays has shown that shear strain also promotes the release of B (and Li to a smaller extent) from smectite, even at ambient T (Hüpers and Kopf, 2012).

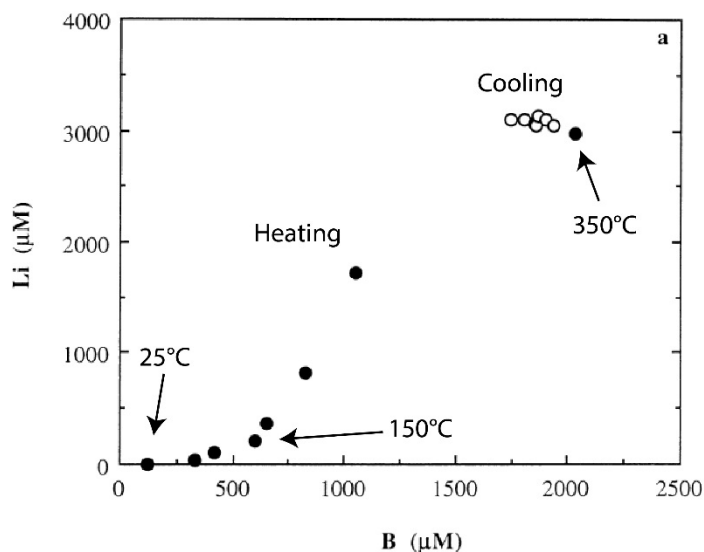


Figure 41 : B and Li concentration in fluid interacting with sediments in hydrothermal experiments (You and Gieskes, 2001). Black/empty circles correspond to heating and cooling stage, respectively. During the heating stage, B removal from the rock starts from  $T < 150^{\circ}\text{C}$ , while Li removal starts to be efficient for  $T$  above  $150^{\circ}\text{C}$ .

The evolution of Li and B at larger depths can be deciphered from the study of fluid inclusions trapped in higher-grade rocks. In a suite of metamorphic rocks from the Sambagawa Belt in Japan, syn-metamorphic fluids were analyzed by crush-leaching of fluid inclusions in quartz (Yoshida et al., 2015) (Figure 42). All metamorphic fluids show an enrichment in Li and B (with respect to Cl) with prograde metamorphism. Furthermore, in this prograde evolutionary trend, diagenetic fluids produced by clay dehydration, corresponding to low-P fluids, are relatively enriched in B with respect to Li, while high-P fluid are richer in Li. One can further note that there is no clear signature of the protolith at high-pressure conditions: eclogite-facies fluid inclusions from meta-serpentinite, metabasites or metasediments have relatively similar concentrations in B, Li and Cl (Scambelluri et al., 2004a; Scambelluri and Philippot, 2001; Yoshida et al., 2015).

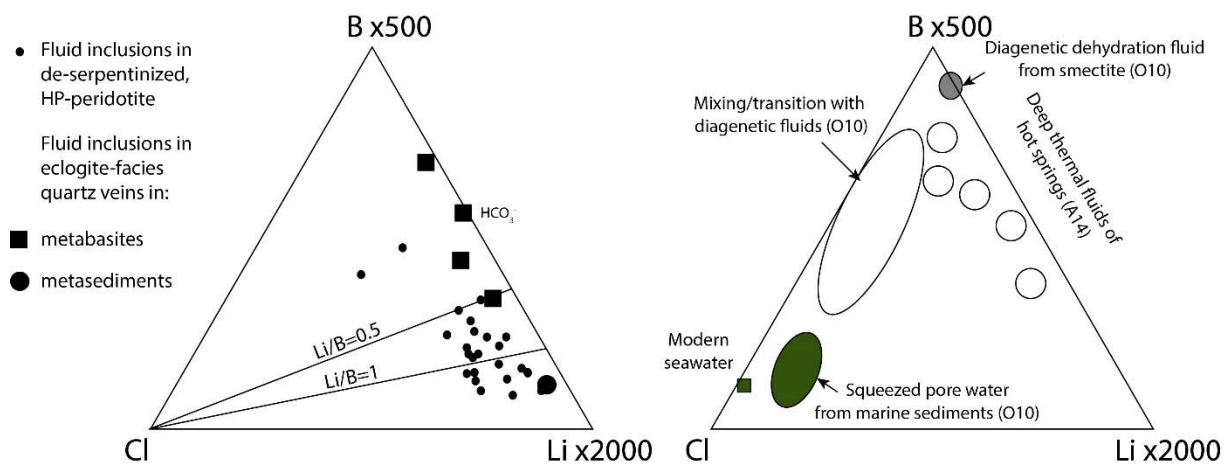


Figure 42 : B and Li concentration in fluids from variable depth domains, down to eclogite-facies conditions, adapted from (Yoshida et al., 2015). In the left diagram, corresponding to high pressure domain, fluids were analyzed in fluid inclusions in olivine by LA-ICP-MS (small circles) (Scambelluri and Philippot, 2004), and in eclogite-facies quartz veins by crush-leached technique (Yoshida et al., 2015). In all fluid inclusions, except for the one labelled “ $\text{HCO}_3^-$ ”, the principal anion is Cl. The right diagram shows the geochemical signature of shallower fluids and modern seawater. O10 and A14 refer to (Ohsawa et al., 2010) and (Amita et al., 2014), respectively. Note that the shallow evolution of metamorphic fluids is towards an enrichment in B, while deeper evolution follows a trend of enrichment in Li.

The salinity of fluid inclusions is another potential signature of subduction fluids. We have compiled in Raimbourg et al. (2018) salinities across a large range of metamorphic grades in subduction zones. There is a strong contrast between low-grade (shallower than the brittle-plastic transition (BPT)) and high-grade (deeper than BPT) rocks. The salinity in low-grade rocks is systematically low, of the order of seawater, while in high-grade rocks the salinity is

much more variable (Figure 43), even when the analysis is restricted to metasediments. In other words, highly saline fluid inclusions appear only in the depth domain deeper than the BPT, and coexist with lower-salinity inclusions. This trend of variable enrichment in solutes is visible in the transect across grade carried out in the Alps (Mullis et al., 1994), where salinity is lower than seawater in the shallower CH<sub>4</sub>-H<sub>2</sub>O zone and higher in the deeper H<sub>2</sub>O zone. The transition corresponds to T~270°C (Tarantola et al., 2007), hence coincides roughly with the BPT.

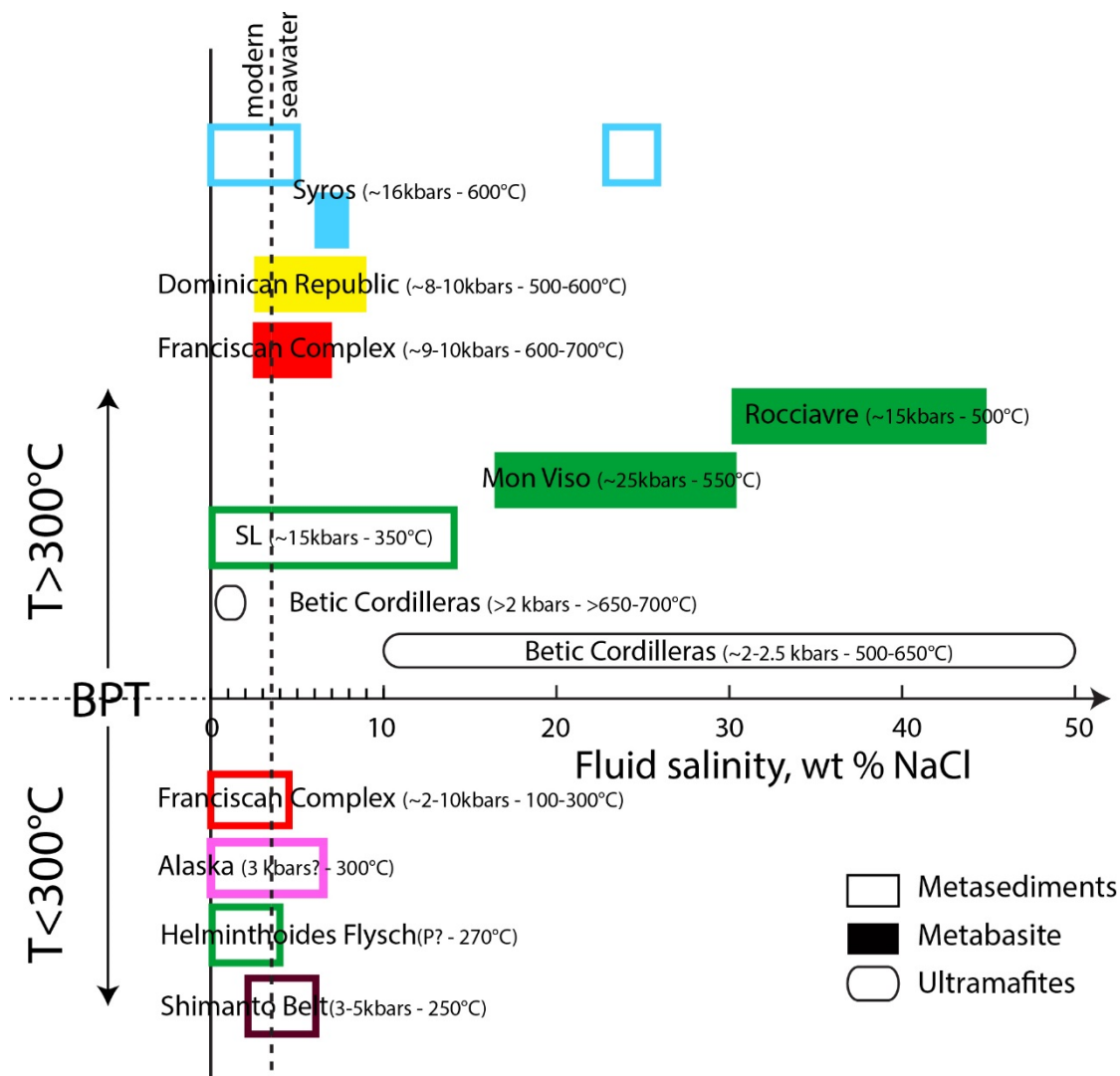


Figure 43: Compilation of salinity in fluid inclusions from metasediments and metabasites in subduction zones. The P-T conditions within brackets correspond to host rock. References: Syros - Barr (1990), Dominican Republic/ Franciscan Complex (deeper than BPT)- Giaramita and Sorensen (1994), Mon Viso/Rocciavre - (Angiboust et al., 2012; Philippot et al., 1998; Pognante, 1989), SL - (Agard et al., 2000), Betic Cordillera - (Scambelluri et al., 2004a; Scambelluri and Philippot, 2004) for , Alaska - (Brantley et al., 1997; Vrolijk, 1987), Franciscan Complex (shallower than BPT) - (Sadofsky and Bebout, 2004), Shimanto Belt - (Raimbourg et al., 2014b; Toriumi and Teruya, 1988), this study. The processes to increase the salinity in subduction settings are proposed to be progressive hydration reactions of the protolith, which consume a fraction of the water present and increase the salinity of the fluid left (Yardley and Graham, 2002). Such a process was for example

proposed for the transformation from dry granulite into eclogite in the continental subduction of Mt Emilius in the Alps (Scambelluri et al., 1998; Scambelluri and Philippot, 2001). High-salinity fluid inclusions were also described from Mon Viso eclogites, in Fe-Mg metagabbros on top of a slice of oceanic crust (Philippot and Selverstone, 1991). The interpretation of the high-salinity as resulting from consumption of the water by eclogite-facies reactions is unsatisfactory, as (i) the eclogitic paragenesis comprises solely anhydrous minerals and (ii) the metagabbro is a lens in a wide shear zone comprising abundant serpentinite and talcschists, which could provide water at the conditions of eclogitization (~550°C (Angiboust et al., 2012)). High-salinity inclusions formed at HP conditions in serpentine have a different origin (Scambelluri and Philippot, 2004), as the serpentine minerals carry down a large stock of Cl from the oceanic stage (Scambelluri et al., 2004e).

An additional source of solutes is the increased solubility at high P and T. For example, solubility of Si into an aqueous fluid reaches, at 500°C and P between 1 and 2 GPa, 1 to 1.35wt% (Manning, 1994), while experimental works show even higher concentrations in solutes (see the review of experimental data in (Scambelluri and Philippot, 2001)). In a review paper, (Frezzotti and Ferrando, 2015) describes a transition in the nature of the fluid around 600-650°C, with water-rich fluids with variable halide content below and complex aluminosilicate-rich aqueous fluid, with much larger solute concentrations, above. For subduction zones, below 600-650°C, enhanced elemental solubility may therefore explain part of the salinity increase, but the very large (up to 50wt% eq. NaCl) salinity observed in some examples require additional processes of enrichment in solute. Hydration/dehydration reactions (Scambelluri et al., 1997) may also play a role, but such an effect is somehow in contradiction with the general trend of increasing salinity with depth (Figure 43) in parallel of dehydration reactions (Figure 39).

### **C. The fluid circulation at depth: in general, restricted to the very local scale**

We consider here the subduction zone as divided in two distinct domains, shallower and deeper than the brittle plastic-transition, which occurs at T~300-350°C, a transition also coinciding with the downdip limit of earthquakes (Hyndman et al., 1997; Oleskevich et al., 1999).

#### ***1. Shallow transfers (shallower than the BPT)***

At shallow depths, i.e. below 150°C, the principal diagenetic reaction is the smectite transformation to illite. The result of smectite destabilization is a “freshening”, i.e. a decrease in salt concentration, of the pore water (which was initially seawater). The release, at the

seafloor, of water with a salinity lower than seawater, is therefore considered as an evidence for fluid transfer from the domain where diagenetic reactions start to be active up to the seafloor (Kastner et al., 1991; Moore and Saffer, 2001). Other evidences for a transfer, up to seafloor, of “deep” fluids, include the  $\delta^{13}\text{C}$  of dissolved methane in Barbados (Vrolijk et al., 1990), the presence of propane (Morris and Villinger, 2006) or the isotopic signature of Li in Costa Rica (Chan and Kastner, 2000). In the two former case, the deep source of the fluid corresponds to the domain of thermogenic cracking of buried organic matter (i.e. 100-150°C (Baudin et al., 2007)), while in the latter case it is attributed to clays reaction, in particular smectite-to-illite transformation.

At larger depths in modern margins, where direct sampling is not possible, indirect information is provided by cold seeps of fluids sampling the deep plate interface. Cold springs through serpentine mud volcanoes in the Mariana Trench (Mottl et al., 2004) display systematic geochemical trends with distance from the trench, showing that the fluid circulations along the subducting plate are limited, for temperatures of the order of 150°C.

In parallel of the analysis of modern subduction zones, information can also be retrieved from low-grade subduction rocks in fossil terranes, for example in the Alps, the Franciscan Complex or the Shimanto Belt. In metamorphic rocks, fluid transfers can be inferred from evidences of disequilibrium, including (i) spatial heterogeneities in the nature of the fluid(s) trapped and (ii) chemical disequilibrium between the fluid and the host rock. The first type of evidence may in some cases involve the infiltration of an exotic fluid, contrasting with a local one (but it may also reflect variations with time of the physico-chemical conditions). The second type of evidence may also reflect the penetration of an external fluid in disequilibrium with the host rock (but it may also be the result of local disequilibrium because of slow kinetics). In any case, the evidences for fluid transfers are there always relatively indirect in fossil structures.

In fluid inclusions from synkinematic quartz veins from worldwide fossil examples, our compilations of the salinity (Figure 43) and of the nature of the dissolved gas, down to the BPT, show that in general the fluid is composed of water with a low salinity (of the order or lower than seawater) and dissolved  $\text{CH}_4$  (Raimbourg et al., 2018; Raimbourg et al., 2014b). This homogeneity might suggest that down to the depths of the BPT the fluid is well-mixed, irrespective of the lithology and the metamorphic grade. It may also reflect the fact that metamorphic reactions are too limited to imprint the inherited, local fluid, which was originally composed of seawater trapped in the pores of the sediment. Therefore, neither salinity nor dissolved gas are really conclusive as regards the extent of fluid circulations.

Isotopes of oxygen and carbon are another potential tools to track the fluid circulations. In the Franciscan Complex, calcite veins have  $\delta^{18}\text{O}$  and  $\delta^{13}\text{C}$  that are in general in agreement with

host-rock buffering hypothesis (Figure 44)(Sadofsky and Bebout, 2004), even if locally high  $\delta^{18}\text{O}$  point to transfers from deeper fluids. In the same metamorphic suites, mobile trace elements are preserved in the rocks irrespective of the metamorphic grade (Sadofsky and Bebout, 2003), which also confirms the absence of large-scale transfers of elements.

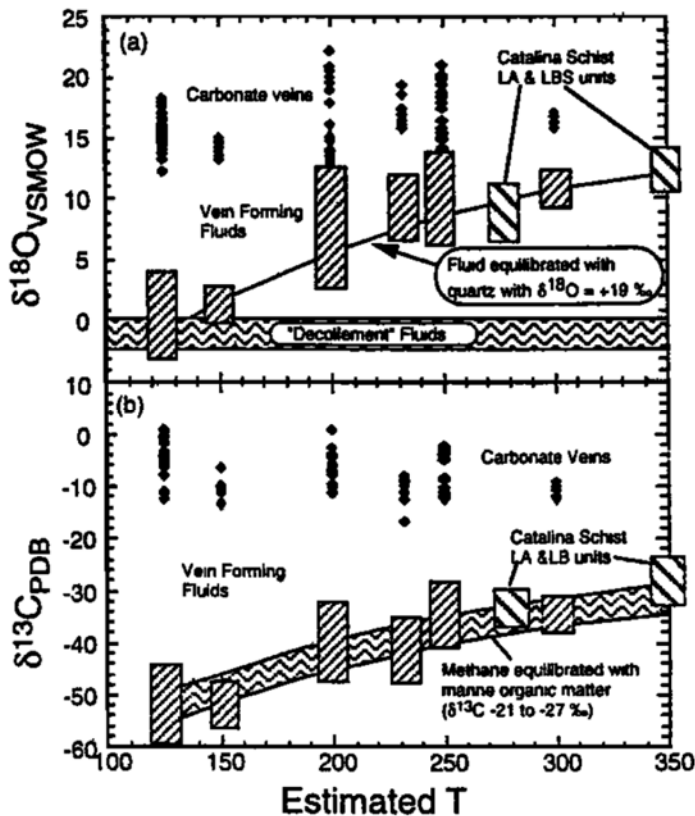


Figure 44 :  $\delta^{18}\text{O}$  and  $\delta^{13}\text{C}$  of carbonate veins in several terranes from the Franciscan Complex, spanning a large range of burial T conditions, as well as the low-T units of the Catalina Schists, in (Sadofsky and Bebout, 2001). The isotopic composition of the veins is in general agreement with equilibration with host rock (clastic sediments with quartz with  $\delta^{18}\text{O}=+19\text{‰}$ , marine organic matter with  $\delta^{13}\text{C}=-21$  to  $-27\text{‰}$ ).

In the Murotohanto subbelt of the Shimanto Belt, on Shikoku island, quartz veins formed after accretion during the thickening of the prism at T conditions of  $\sim 230^\circ\text{C}$  have  $\delta^{18}\text{O}$  (Lewis and Byrne, 2003) in the range  $+15.5$ - $17\text{‰SMOW}$ , very similar to host-rock values. In quartz veins formed during subduction from the Shimanto Belt on Kyushu, we observed a larger range of variation of  $\delta^{18}\text{O}$  of the vein quartz, between  $+16$ - $20\text{‰SMOW}$  (Raimbourg et al., 2015), but still within the range of host-rock values. The same conclusion of oxygen isotopic buffering with host rock was also reached in quartz vein studies in the Alps (Mullis et al., 1994), and in the Kodiak accretionary complex (Vrolijk, 1987), even if slightly enriched values in tectonic mélanges, compared to coherent terranes, point to a possible infiltration of deeper fluids.

Oxygen isotopes are therefore in general host-rock buffered. As we discussed in Raimbourg et al. (2015), this point may reflect not simply the absence of circulation of fluid, but also the rapid

local reequilibration of the fluid in terms of  $\delta^{18}\text{O}$ , because of the vigor of dissolution-precipitation, the rapid kinetics of isotopic exchange and the large size of the exchangeable reservoir of oxygen in the host-rock. Therefore, oxygen might not be the most reliable tracer of fluid exchanges at depths shallower than BPT.

## ***2. Deep transfers (deeper than BPT, down to HP and UHP)***

Deeper transfers, related to devolatilization reaction with prograde metamorphism (see above), are analyzed on the basis of geochemical budgets in various volatile elements. One possible approach consists in comparing elemental concentrations or concentration ratios between the unmetamorphosed protolith and its metamorphic equivalent. If transfers are limited in volume, or restricted to a scale smaller than the sampling size, then concentrations or ratios are not affected by metamorphic reactions. Another approach revolves on the comparison between veins and their host rock. If veins have a composition in elements or isotopes which is not in equilibrium with the host rock, then the parageneses within the veins is interpreted as reflecting the precipitation from an exotic, advected fluid.

The subduction complexes in the Alps and in the west of the USA are two prominent examples, where many geochemical studies provide clues as to elemental mobility at HP and UHP conditions.

Subducted serpentines in the Alps, release, upon antigorite breakdown reaction, a significant fraction of their B and Cl stock, while they are slightly enriched in Li (without a clear interpretation for the latter aspect) (Scambelluri and Philippot, 2004). The HP veins concomitant with antigorite breakdown reactions share the same mineralogy and trace elements patterns as their host rocks, suggesting closed-system behavior (Scambelluri et al., 2001). Oxygen isotopes show similarly a range of  $\delta^{18}\text{O}$  of high-pressure ultramafic rocks that coincide with the range for oceanic serpentine, attesting of limited reequilibration at high-pressure conditions.

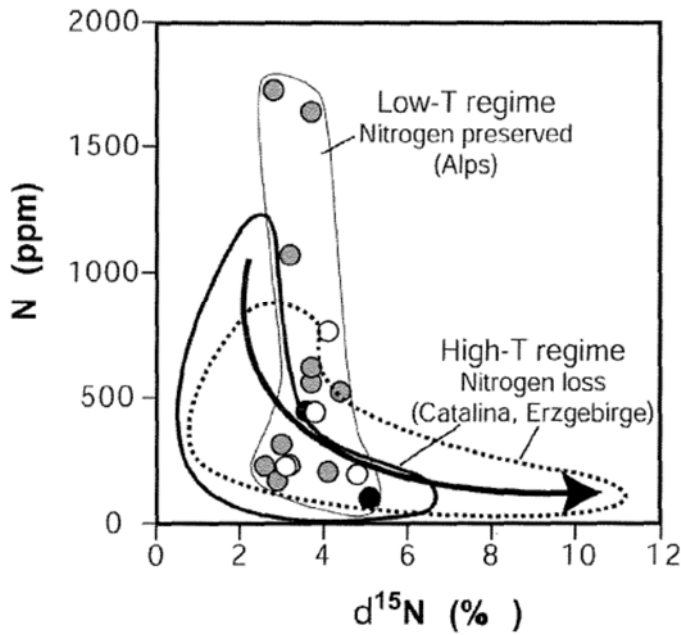
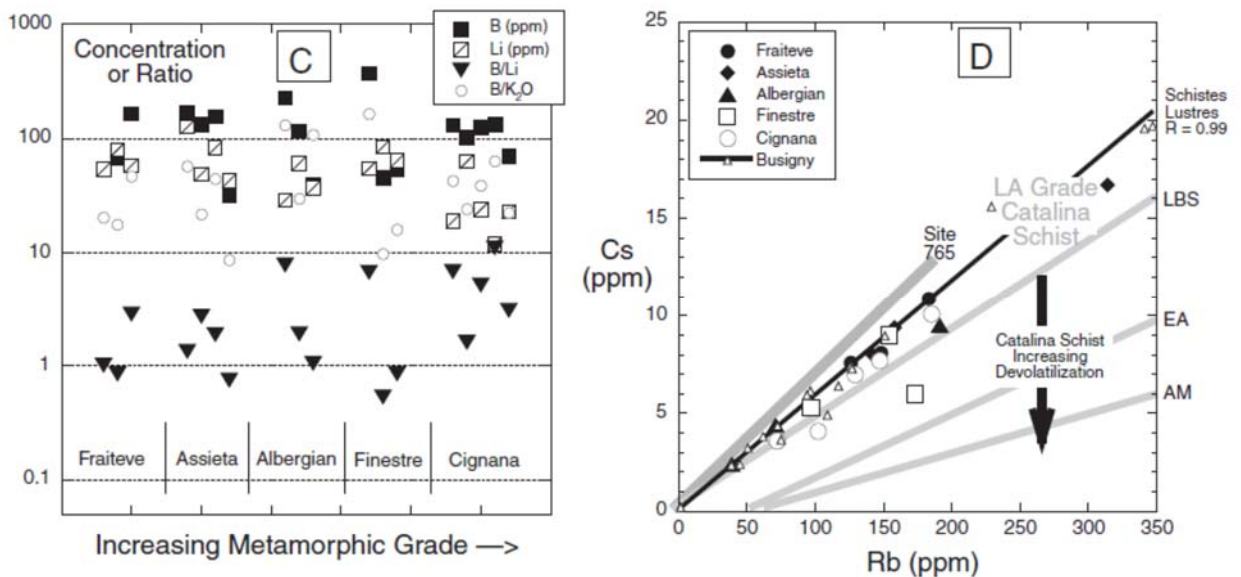


Figure 45 : Whole-rock N content and  $\delta^{15}\text{N}$  systematics of unmetamorphozed (circles), HP (grey circles) and UHP (black circles) sediments in the Alps, from (Busigny et al., 2003), and metasediments from the Catalina Schists (Bebout and Fogel, 1992) and Erzgebirge Schists (Mingram and Bräuer, 2001). The figure was copied from (Scambelluri and Philippot, 2004).

Sediments buried to HP conditions along a cold gradient act also as a closed system behavior, as attested by their N- $\delta^{15}\text{N}$  systematics (Figure 45) and their Cs/K and Cs/Rb ratios (Bebout and Fogel, 1992; Busigny et al., 2003; Mingram and Bräuer, 2001; Scambelluri and Philippot, 2004). This is the case for the “colder” facies of the Catalina Schists (Bebout, 2007) as well as the Schistes Lustrés metasediments (Bebout et al., 2013c), which show constant elemental concentration in B, Li and ratio B/K and Cs/Rb (Figure 46), from P-T conditions of  $\sim 320^\circ\text{C}$ -13kbars (Fraiteve) to  $\sim 500^\circ\text{C}$ -20kbars (Finestre) (Agard et al., 2001).



*Figure 46: B, Li, K, Cs and Rb concentrations in the metasedimentary units of the Schistes Lustrés, with increasing P-T conditions from Fraiteve to Cignana (Bebout et al., 2013c). There is no evolution of the mobile element concentration with metamorphic grade. For comparison, the Catalina Schists higher grade facies are affected by a decrease in Cs/Rb ratio, indicating significant loss through a fluid phase.*

In contrast, “hotter” gradients in the Catalina Schists studied extensively by (Bebout, 1995, 2007; Bebout et al., 2013a) show that from lawsonite-blueschist facies towards higher temperature gradients, there is a decrease in B and Cs and an increase in Li in the bulk rock (Figure 47).

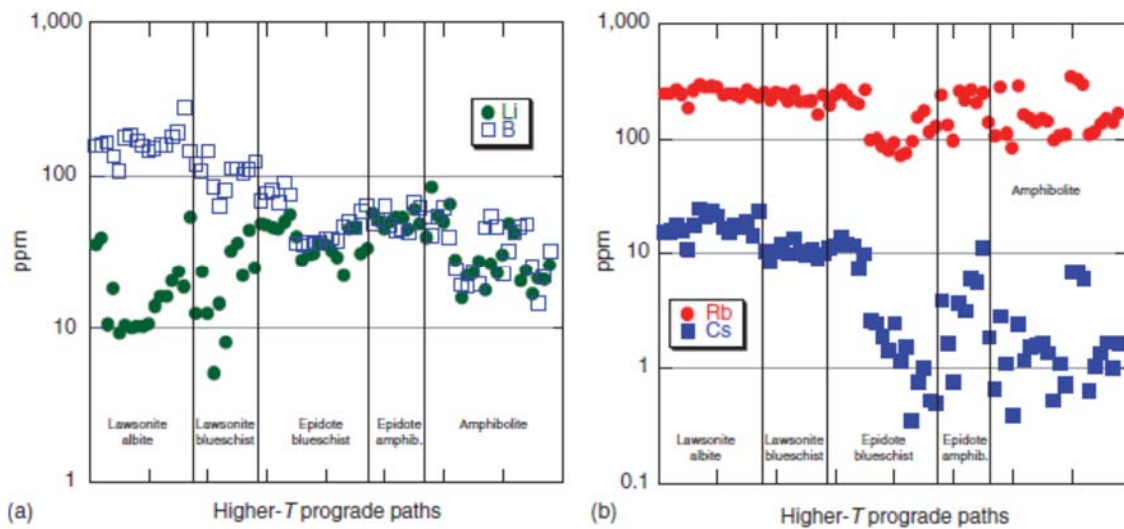


*Figure 47: Evolution of B, Li, Cs and Rb in the Catalina Schists, showing the increasing devolatilization loss towards units affected by higher P-T gradients (Bebout, 2007).*

Finally, the salinity of fluid inclusions and the  $\delta^{18}\text{O}$  of oceanic crust buried to large depths in subduction show very large variability, which is interpreted as reflecting pre-subduction heterogeneity (Philippot et al., 1998). This interpretation is somehow in contradiction with the relatively homogeneous salinity of rocks shallower than the BPT (Figure 43).

Nonetheless, all the elemental and isotopic tracers point to a closed-system behavior of the fluid at HP and UHP conditions.

**Conclusion:** Throughout the subduction zone, all elemental and isotopic studies point to a rather local-scale of the transfers. This does not necessarily implies that fluid does not circulate over larger-scale. Petrogenetic grids point unambiguously towards a progressive loss of water with prograde metamorphism and the fluid that is produced escapes towards the mantle wedge above or along the subduction channel. Still these water transfers are not accompanied by sufficient transfers in terms of elements or isotopes, to be traceable, probably because the amount of transferred water is too small and the solute concentrations are too low to have an imprint on the host rocks.

## **D. Evidences for fluid transfers**

Even if elemental and isotopic budgets point to host-rock buffering or transfers restricted to the very local scales, other studies have shown that some strongly deformed domains may focus the flow to such an extent as to leave a chemical imprint.

One example is the shallow ( $T \leq 150^\circ\text{C}$ ) subduction channel in the Apennines, where  $\delta^{18}\text{O}$  of calcite veins are lower by  $\sim 2\%$  than the host rock (Vannucchi et al., 2010). At larger temperatures, but still shallower than the BPT, in Kodiak Complex, a shift in  $\delta^{18}\text{O}$  towards higher values is observed in strongly sheared rocks (i.e. *mélange* rocks) compared to coherent units (Vrolijk, 1987). A similar shift is described in (Sadofsky and Bebout, 2001) and interpreted as reflecting the influx of a deeper fluid superimposed on the general pattern of host-rock buffering.

Although pertaining to the collisional, and not subduction stage of the alpine orogeny, the Glarus Thrust in the Alps is a similar structure in terms of geometry and kinematics (shallow dipping fault zone accommodating large-scale displacement) and temperature ( $T \sim 300^\circ\text{C}$ ) to the décollement zone or to strongly sheared tectonic *mélanges* in subduction zones. Calc-mylonites within the Glarus thrust show a large shift in Sr and O isotopes with respect to the initial protolith of the rocks, which is attributed to intense water-rock interactions, although the origin of the fluid is uncertain (Burkhard et al., 1992). In contrast, veins in the thrust nappes are reequilibrated, in terms of C and O isotopes, with their host rock, pointing to closed-system behavior (Burkhard and Kerrich, 1988).

These different studies show that isotopes can indeed show disequilibrium with the host rock and point out at fluid circulations and associated elemental/isotopic transfers. Nonetheless, in all these studies, the origin of the isotopic shift is always enigmatic. The shift in  $\delta^{18}\text{O}$  is positive in Kodiak and Franciscan Complex, negative in the Apennines and in the Alps. The interpretation is in both cases a mixture with a deeper fluid, either reequilibrated with quartz at higher T (positive shift) or with phyllosilicates (negative shift). There are therefore many possible interpretations to the isotopic signatures, which makes it difficult to clearly determine the fluid circulation characteristics (sources and spatial extent).

### ***1. The record of fluid transfers in veins***

While isotopic signatures point in some examples of strongly sheared material to disequilibrium (with respect to host rock), potentially related to focused fluid flow, another conspicuous feature of the deformed zones calls for active flow. Tectonic *mélanges* are indeed systematically associated with a high density of veins, for example in Kodiak (Fisher and Byrne, 1990; Fisher and Brantley, 1992, 2014; Fisher et al., 1995), the Franciscan Complex and the Apennines

(Meneghini et al., 2007; Meneghini and Moore, 2007) or the Shimanto Belt (Palazzin et al., 2016; Raimbourg et al., 2018; Raimbourg et al., 2015). The timing of the formation of those veins is constrained by their geometry as contemporaneous with deformation during subduction (Fagereng and Harris, 2014; Fagereng et al., 2011; Palazzin et al., 2016; Raimbourg et al., 2015), so that they provide direct insight into the fluid circulation along the plate interface.

In these veins, evidence for disequilibrium includes principally the record of fluid inclusions. For example, many examples of accretionary prisms, such as Kodiak (Vrolijk, 1987; Vrolijk et al., 1988) or the Shimanto Belt (Kondo et al., 2005; Raimbourg et al., 2014b; Sakaguchi, 1999a), includes two types of fluid inclusions, one with an aqueous fluid with little dissolved CH<sub>4</sub>, and the other type containing mostly CH<sub>4</sub>. These two types of inclusions are not at equilibrium with each other (Raimbourg et al., 2014b), although they coexist in the same quartz crystals, so that they correspond to variations in the conditions of trapping, most likely fluid pressure conditions.

Furthermore, one type of compositionally homogeneous fluid may record changing variations of P and T. Methane-rich fluid inclusions in a quartz-crystal from the Kodiak accretionary prism showed large variations in density, which were interpreted as reflecting variations in the fluid pressure at the time of entrapment (Vrolijk, 1987). A link with seismicity, through the fault valve model (Sibson, 1994), was postulated, but the lack of any time constraint on the pressure variations makes this link difficult to ascertain. We adopted a similar approach in Raimbourg et al. (2017j), on methane-rich fluid inclusions contained in secondary planes (=healed fracture planes) in synkinematic quartz, to estimate the amplitude of fluid pressure variations from the variations in density in the fluid inclusions from a single plane, as it corresponds to a single fracturing event (hence a short duration). In Vrolijk (1987) and in our case, the amplitude of the pressure variations is of the order of ~50-100MPa and ~100-150MPa, respectively. Similarly, variations in the P-T conditions recorded in the fluid inclusions have been interpreted as reflecting earthquake-related variations in fluid pressure (Boullier and Robert, 1992; Mullis, 1988a; Parry and Bruhn, 1990; Robert et al., 1995). Although attractive, this interpretation of variations in *in-situ* pressure recorded by fluid inclusions can somehow be disputed by experiments on synthetic fluid inclusions reproducing the effect of exhumation from peak burial. In most examples, there is partial reequilibration in the density of the inclusion, caused by internal over- or underpressure (Bodnar, 2003; Sterner and Bodnar, 1989), resulting in the a spread in microthermometric properties, including density, of a set of fluid inclusions with originally the same density. In fact, in any microthermometric study with a very large number of fluid inclusions, sufficient for a statistical overview on data scatter, it seems that there is a

relatively large dispersion of the microthermometric data (e.g. (Bodnar and Beane, 1980)), whose origin principal source is post-entrapment reequilibration

The most convincing case is made by quartz where the variations in density are correlated with different growth textures, such as in (Mullis, 1988a). There, the lower pressure associated with certain growth rims supports the idea of time-dependent variations in pressure during the growth of the crystal (Figure 48).

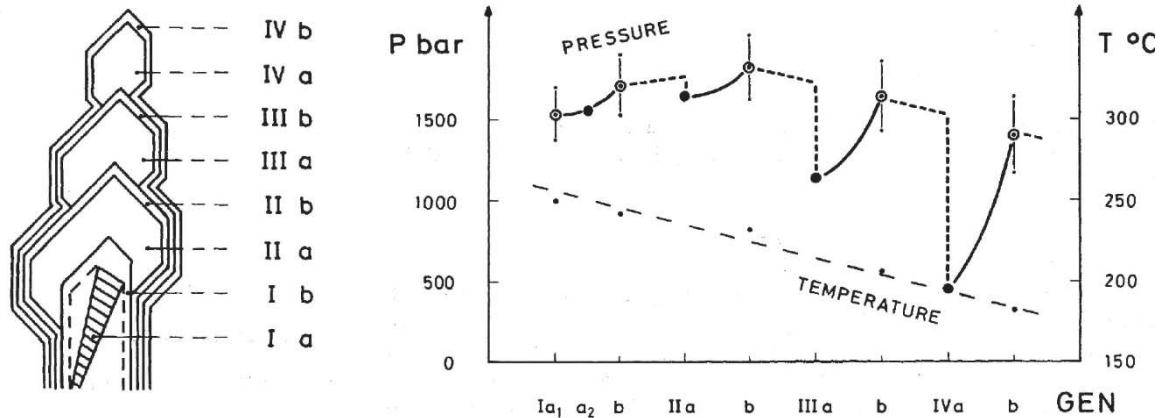


Figure 48 : The different textures of quartz crystal growth, in alpine fissure quartz from Val d'Illiez (Mullis, 1975) (left), with corresponding P-T conditions (right). A very similar pattern can be found in a study in the Appennines (Mullis, 1988d). Note that the scatter in homogenization temperature (vertical error bars in the right picture) is smaller than the fluid pressure drops. Black circles refer to CH<sub>4</sub>-rich inclusions, empty circles to H<sub>2</sub>O-rich ones.

Chemical disequilibrium can also be observed in veins and interpreted as a result of fluid transfers or in relation with deformation events. In calcite veins from fault zones near the Nobeoka Thrust in the Shimanto Belt, there is a change from reducing (syn-faulting veins) to oxidizing (extension veins = post-faulting) conditions of the fluid, in relation to brittle deformation (Yamaguchi et al., 2011). There is nevertheless no clear conclusion as to whether this change in redox conditions is associated with the advection of a deep fluid. In another study on the same structures, Yamaguchi et al. (2012) show an increase by several ‰ in  $\delta^{18}\text{O}$  (an a smaller increase in  $^{87}\text{Sr}/^{86}\text{Sr}$ ) for the fluid equilibrated with the fault vein calcite with respect to the fluid equilibrated with the calcite extension veins more distributed in the rock, akin to “post-faulting” veins.

## 2. Our past work on veins

Our studies, based on natural fossil structures from the Shimanto Belt and the Alps, build on these studies to try to decipher the fluid circulations at depth, as well as the changing conditions of pressure and temperature of the fluid (and possible link with deformation and seismicity). The studies above show that different information can be retrieved independently from the veins

itself (its geometry and kinematics with respect to host rock), the minerals (and its isotopic and elemental composition) that form the veins, and the fluid inclusions that are contained within the veins. The ideal situation is to combine mineral and fluid information in a tectonic framework well constrained by the veins. In what follows, we describe our results obtained on veins from the Alps and in the Shimanto Belt. The synthesis of this work is given in (Raimbourg et al., 2018) and relies on microstructural and geochemical results exposed in (Palazzin et al., 2016; Raimbourg et al., 2017j; Raimbourg et al., 2014b; Raimbourg et al., 2015), while the large-scale tectonic framework is given in (Raimbourg et al., 2014a; Raimbourg et al., 2017a; Raimbourg et al., 2009).

We have focused in the two cases studies on syn-kinematic veins, i.e. veins that form contemporaneously with deformation. The veins form (1) in fractures in competent lenses or beds, composed of sandstone or previously precipitated veins, orientated perpendicular to elongation direction and (2) as “extensional veins” (Fagereng et al., 2011), i.e. at low angle to the foliation, with elongated grains parallel to the stretching direction. These kinematic features, when interpreted on the basis of the large-scale architecture of the accretionary prism, led to interpret the vein formation as contemporaneous with burial, while the P-T conditions of homogenization of the fluid inclusions in the veins, when compared to maximum P-T conditions recorded in the host rock, enables to attribute veining to the deeper stage of underthrusting or underplating at the base of the accretionary prism. The kinematic features of the veins in the Flysch à Helminthoïdes is much more unclear, as the syn-subduction transport direction is not well known, and as the early-stage, syn-subduction deformation is to a large extent obliterated by late-stage alpine collision. The timing of veining in the Flysch à Helminthoïdes is therefore unclear, we attribute it to subduction stage because (1) veining of the sandstones beds predates their isoclinal folding, which is itself interpreted as slip along a master décollement and (2) fluid inclusions homogenization temperatures are only slightly lower than host rock temperatures and (3) veins form perpendicular to sandstone beds and do not propagate in the surrounding pelitic matrix, mimicking the geometry observed in the Shimanto Belt.

These veins contain only quartz in the Shimanto Belt, and a mixture of quartz and calcite in the Flysch à Helminthoïdes. The veins contain many fluid inclusion trails formed perpendicular to the stretching direction (see Chapter III), therefore attributed to the same kinematic stage. The joint study of the vein structures and microstructures, the vein-filling quartz composition (trace elements and isotopes), as well as the fluid inclusions enclosed in the veins, provide therefore insights into the nature, the physico-chemical conditions, and the geometry of the circulation of the deep fluid that wetted the rock during the deep stages of underthrusting.

The principal piece of information we have obtained in our study of the veins was provided by cathodoluminescence, which revealed the existence of two-types of quartz in the veins and their respective geometry (Figure 49). The two types of quartz are found as fracture-filling material, or as growth rims on large crystals. Mutually cross-cutting relationships, in the case of fractures, and alternation of CL-blue and CL-brown growth rims show that the two types of quartz formed alternatively in the rock at depth and do not correspond to two distinct tectonic stages.

The question is therefore to decipher the factors that control the precipitation of one or the other type of quartz and for this purpose their respective microstructure is informative. The CL-blue veins form the macro-veins, at least ten of microns thick, cutting across the sandstone and siltstone lenses. In contrast, the CL-brown quartz fills the micro-veins, which are much thinner (often micron-wide) and affect former CL-blue large veins. When several generation of large CL-blue quartz veins can be recognized, the older the vein, the larger its reworking by small micro CL-brown fractures. Finally, some of the domains of the veins are affected by plastic deformation. In such a case, the quartz forming the plastically deformed domain acquires a homogeneous CL-brown color.

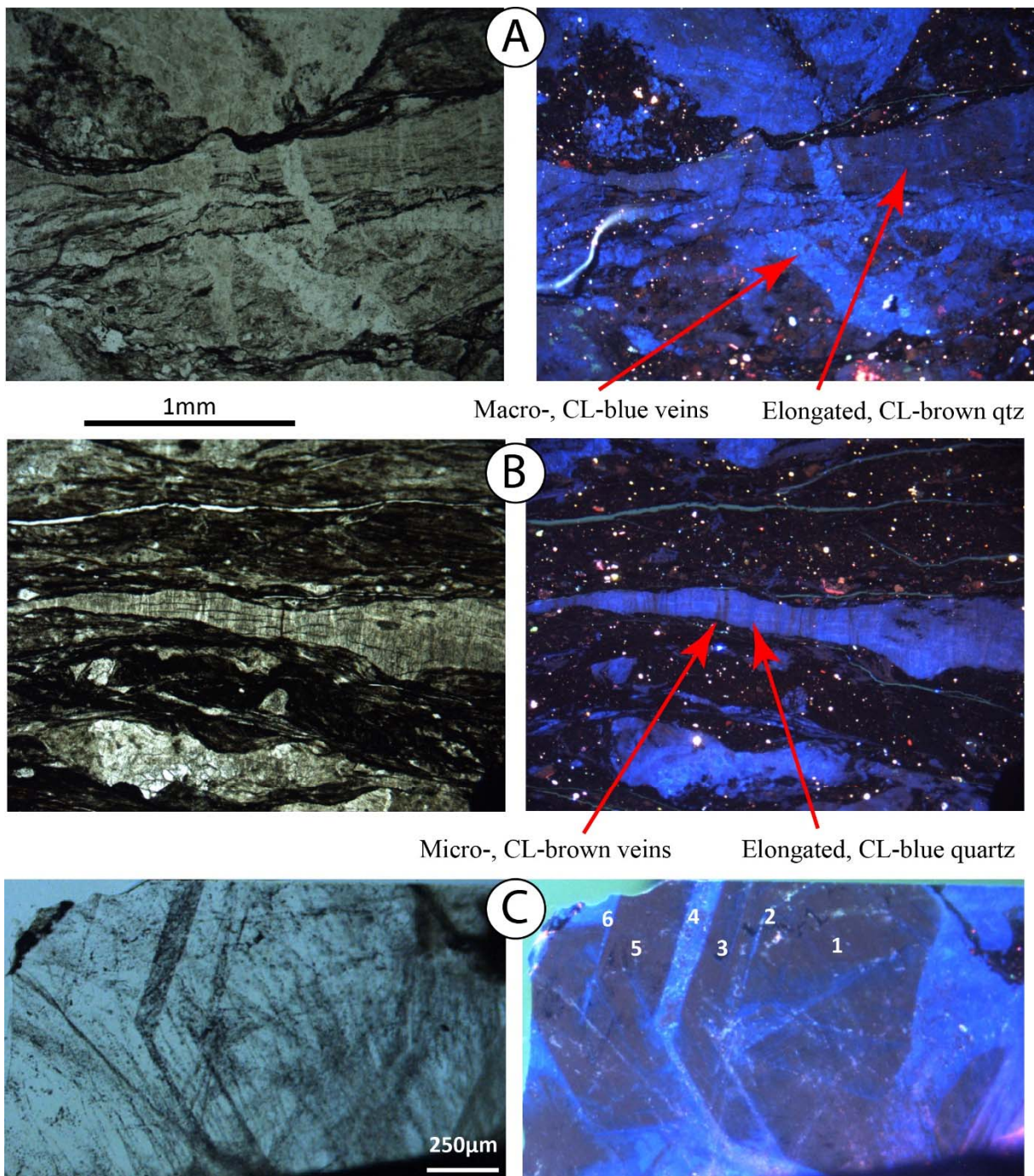


Figure 49: Microstructure of veins from the Shimanto Belt, revealed by cathodoluminescence. (A, B): In veins elongated parallel to the foliation, fractures filled by one type of CL-quartz cut across a domain filled by the other type, precipitated in a pre-dating stage. Note that the CL-blue fractures are much larger than CL-brown ones. (C) Growth rim textures, where alternating rims of CL-brown and CL-blue quartz precipitate. Note the larger abundance of fluid inclusions in CL-blue rims. Left-optical microscope, Right-cathodoluminescence.

Because the characteristic length-scales of microfracturing and chemical reequilibration during plastic deformation are very small, we attribute the CL-brown quartz to precipitation in presence of a locally reequilibrated fluid. In contrast, the CL-blue quartz is attributed to the

infiltration of an exotic fluid, enabled by the transient formation of a permeable network of larger fractures where the CL-blue quartz precipitates.

These microstructural arguments, in addition to the cyclic character of the precipitation of the two quartz, led us to propose a model of fluid circulation at seismogenic depth. Fluid circulation alternates stages in closed-state, where permeability is low and the fluid is locally reequilibrated, with stages in open state, where an external fluid penetrates the rock.

While such a behavior is proposed for quartz veins formed at temperatures below the brittle-plastic transition (BPT) at  $\sim 300^{\circ}\text{C}$  (in the Hyuga Tectonic mélange in the Shimanto Belt and the Flysch à Helminthoïdes in the Alps), veins from units deformed at higher temperature conditions, where plastic deformation is fully active (The Foliated Morotsuka in the Shimanto Belt and the Schistes Lustrés in the Alps), are formed only of CL-brown quartz. Deeper than the BPT, the hydrological behavior is much simpler, with only local equilibrium. Local reequilibration in the plastic realm, as attested by CL-color of quartz, is fully in agreement with all the geochemical argument exposed earlier.

The hydrological model of the subduction interface comprises therefore two distinct compartments, limited by the BPT (Figure 50). Shallower than the BPT, where plastic deformation is not yet activated and deformation proceeds as a result of fracturing and pressure-solution, the fluid alternates stages of local, small-scale circulation to stages of larger-scale circulation, as a result of the formation of a permeable network of fractures, eventually sealed by precipitation. Deeper than the BPT, brittle fracturing is to a large extent suppressed and fluid circulation is restricted to a local scale.

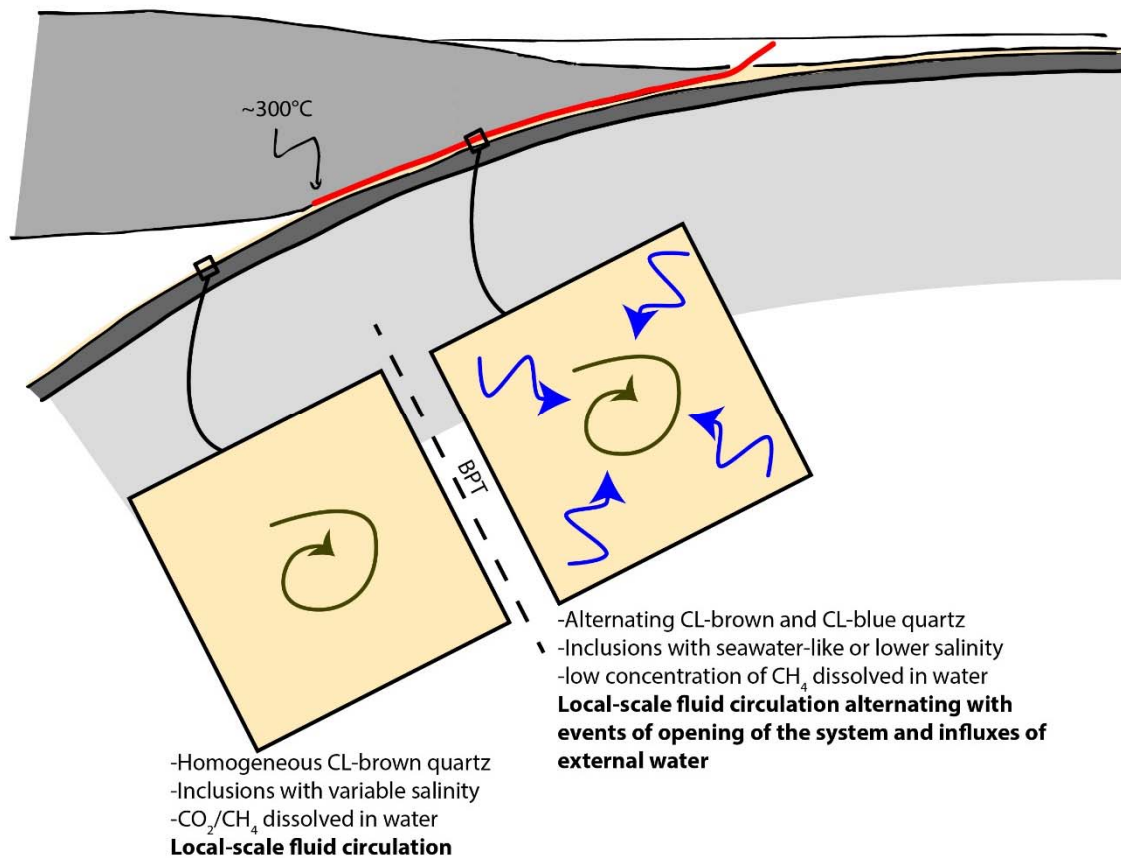


*Figure 50 : Hydrological model of the subduction interface, divided into two compartments by the brittle-plastic transition (BPT). Shallower than the BPT, stages of opening of the system, with infiltration of an external fluid through a network of fractures, alternates with closed-system stages, where the fluid circulation is local and the fluid reequilibrated with the host rock.*

Several questions arise from these observations and this model. **The first question regards the fluid and concern the origin of the exotic fluid, hence the scale of the fluid circulation.** Answering those implies to characterize geochemically the two types of fluids, and it is developed hereafter.

**The second question regards the relationship between fluid circulation and solid rock deformation.** As the penetration of the exotic fluid involves the creation of a network of fractures, one can wonder what conditions control this fracturing stage and how such fluid infiltration events relate to bulk deformation. In particular, one can wonder to which extent fluid circulation is the passive consequence of fracturing (as could result from large earthquakes) or whether the fluid itself (for example through a large fluid pressure) is not at the origin of fracturing and controls events of solid rock deformation. The question is particularly relevant in the case of the slow-slip events that occur near the base of the seismogenic zone, and which are often interpreted as resulting from large fluid pressure.

## **E. Chemical characteristics of the circulating fluids**

To decipher the origin of the fluid attending the precipitation of the CL-blue quartz, we analyzed the composition of the quartz itself and the fluid inclusions it contains in both types of quartz.

### ***1. Fluid inclusion studies***

The fluid trapped in fluid inclusions in both types of quartz is composed principally of water, with a small concentration of salt. In addition, it contains also a small fraction of dissolved methane (Raimbourg et al., 2014b). Another type of inclusions, much rarer, is rich in methane (Raimbourg et al., 2017j; Raimbourg et al., 2014b) and has already been described elsewhere in the Shimanto Belt (Kondo et al., 2005; Sakaguchi, 1999b). We interpreted this methane-rich fluid as resulting from exsolution of methane from the water, in the cases where organic matter cracking produces local concentration of methane exceeding solubility in water. But because of the low concentration in organic matter in the sediment (Raimbourg et al., 2017j), this methane-rich fluid is volumetrically minor with respect to the water-rich fluid, which is confirmed by the scarcity of the corresponding fluid inclusions.

The salinity of the water-rich fluid is in general lower than seawater, in agreement with the low salinity of the shallow fluid sampled in active margins (Kastner et al., 1991; Le Pichon et al., 1993). The interpretation of such low salinity is a freshening of seawater trapped in the sediment pores by pure water produced by clay dehydration. While both CL-blue and CL-brown quartz have the same salinity, lower than seawater, in the Flysch à Helminthoïdes, in the Hyuga Tectonic Mélange from the Shimanto Belt, the inclusions contained in the CL-blue quartz have a salinity significantly higher than in the CL-brown quartz, and slightly above seawater salinity (Raimbourg et al., 2015) (Figure 51). The simplest interpretation of this high salinity, following the discussion above about the salinity variations with depth, is to attribute it to deep metamorphic fluid circulating upward along the subduction interface, without further detail on their origin.

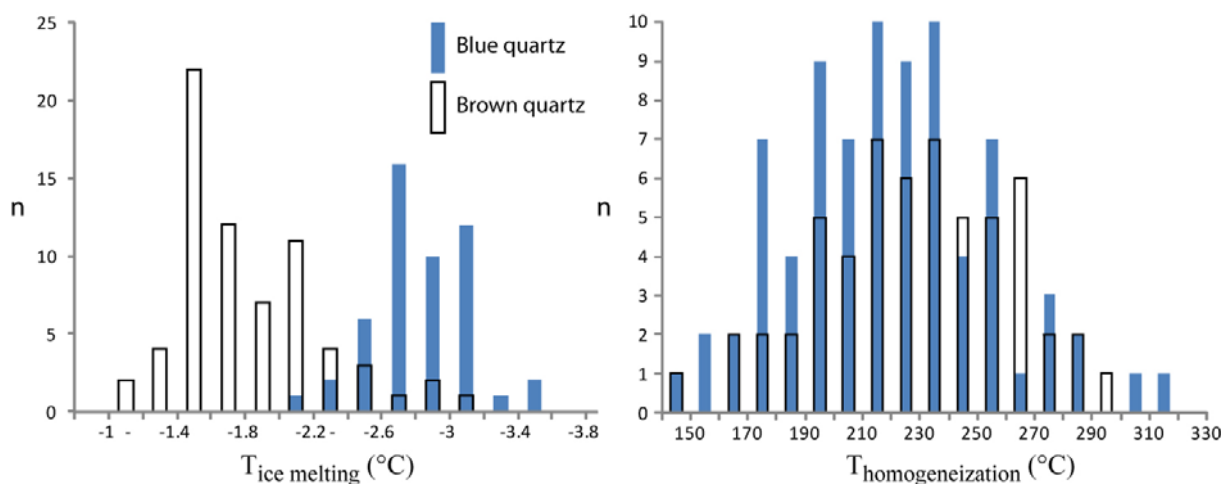


*Figure 51 : Ice melting (left) and homogenization (right) temperatures of the fluid inclusions in the veins from the Hyuga Tectonic Mélange. Similar homogenization temperatures between CL-blue and CL-brown quartz point to a formation at similar conditions of P and T, in agreement with the model of alternating precipitation. In contrast, there is significantly larger salinity of the fluid trapped in the CL-blue quartz. Early Miocene seawater salinity corresponds to ice melting temperature of -2.6°C, hence some of the inclusions in the CL-blue quartz have a salinity larger than seawater.*

To get further insights into the fluid origin, we have recently carried out LA-ICP-MS analyses of fluid inclusions in the quartz, following the method used to study fluid inclusions in olivine, related to antigorite break-down (Scambelluri et al., 2004e). These results are nevertheless in course of treatment and do not provide a clear picture yet.

## **2. Quartz studies**

The origin of the fluid can also be indirectly deciphered from the quartz itself, using its isotopic and trace element concentrations. We analyzed the  $\delta^{18}\text{O}$  of CL-blue and CL-brown quartz using SIMS on Shimanto Belt samples (Raimbourg et al., 2015). The oxygen isotopes show no difference between both types of quartz in any given sample, while slight difference can be seen from one sample to another. In addition, all isotopic ratios are compatible with host-rock buffering, on the basis of literature data on similar metasediments. As a conclusion, oxygen isotopes, probably because of intense dissolution and precipitation of quartz, are systematically reequilibrated with the host rock and lose the original signature of the fluid. They do not constitute therefore an appropriate tool to track fluid circulations in the depths of accretionary prisms.

Another clue to fluid origin is potentially contained in the trace element of quartz, responsible for the cathodoluminescence. A preliminary observation by EPMA has shown that the CL-blue quartz is strongly enriched in aluminum (Raimbourg et al., 2015). This observation is in agreement with other studies of hydrothermal quartz. Al and Li correlate in alpine hydrothermal quartz (Jourdan et al., 2009), and high Al-Li growth rims have a high luminescence contrasting with rims poorer in those elements (Ramseyer et al., 1989).

Nonetheless, the interpretation of trace element concentration in quartz in terms of fluid composition is rather unclear. For example, the incorporation of  $\text{Al}^{3+}$  in the quartz lattice depends not only on its concentration in the fluid but also on the pressure, temperature and quartz growth rate (Rumyantsev and Novozhilov, 1980; Tsinober and Kamentsev, 1964) as well as pH (Merino et al., 1989). The link between Al concentration in quartz and concentration in the fluid and from there on fluid origin is therefore too indirect for any firm conclusion to be drawn.

## **F. Relationship between deformation and fluid flow: the action of pressure solution**

Rates of transfers of the fluid are controlled by the permeability field, which is at first-order dependent of the network of connected fractures. In turn, the network of connected fractures depend on the ability of each individual fracture to heal (e.g. (Renard et al., 2000; Tenthorey and Cox, 2006), as a result of vein precipitation, principally calcite and quartz. Fluid transfers are therefore closely connected, through fracture healing, to the mechanisms of pressure solution.

Pressure solution processes control therefore both the fluid flow, but also bulk rock deformation. The role of pressure solution in macroscopic creep and aseismic deformation has been recently emphasized, using microphysical models combining slip on phyllosilicates and deformation by pressure solution of rigid objects (Den Hartog and Spiers, 2014; Fagereng and Den Hartog, 2017; Niemeijer and Spiers, 2007). The importance of pressure solution is supported by our microstructural observations in rocks from the Hyuga Tectonic mélange in the Shimanto Belt: the rocks are pervasively affected by microfracturing, dissolution and precipitation of quartz, for T conditions around 250°C (Palazzin et al., 2016; Raimbourg et al., 2015) (see also chapter 2). Therefore, bulk rock deformation is accompanied by permanent transfers in quartz that precipitated in cracks at all scales. Conversely, cracks are created throughout the rock evolution and enable the transfer of silica and other solutes. The rock permeability reflects therefore the contribution of these two antagonistic processes: fracturing of competent lenses (sandstones and quartz veins already precipitated) and healing of fractures. Pressure-solution has been studied theoretically (i.e. (Raj, 1982; Raj and Chyung, 1981; Rutter, 1976)) and is the result of a chain of processes, involving dissolution, transport and precipitation. Depending on the conditions considered, either mineral reactions (dissolution/precipitation) or diffusion along the grain boundaries are rate-limiting, yielding distinct creep equations (e.g. (Raj, 1982; Rutter, 1976; Spiers et al., 1989)

It has also been reproduced experimentally, in sand aggregates (Cox and Paterson, 1991; Dewers and Hajash, 1995; Niemeijer et al., 2002) or in compact sandstones (Gratier et al., 2009), i.e. in quartz rich material relevant to the quartz veins from the Shimanto Belt. There, carbonates are minor, as a result of the deposition of many sedimentary units below the CCD (Raimbourg et al., 2018; Taira et al., 1988), and calcite veins are rare. This is also the case in the Kodiak prism in Alaska (Fisher and Brantley, 1992; Fisher et al., 1995) or in the Otago Schist of New Zealand (Fagereng and Harris, 2014), i.e. in the peri-Pacific accretionary prisms. Deformation by pressure solution has been considered to a large extent by the sedimentological community working on the processes of compaction of quartz sediments. Accordingly, many

experiments (Cox and Paterson, 1991) (Dewers and Hajash, 1995; Niemeijer et al., 2002) and models (Oelkers et al., 2000) were designed on quartz sands, i.e. with a large porosity (above 10%). The processes in such low porosity-rock, where there is a large volume of poral water, are different from those active in compacted rocks, where the intergranular water is restricted to thin films around grain boundaries. In addition, the increase in T tends to strongly enhance precipitation/dissolution, while the increase in effective pressure tends to thin the water film along the grain boundaries and to slow down diffusion. As a result, while in shallow, high-porosity rocks the rate limiting process is dissolution (Niemeijer et al., 2002), in deep (typically below a few km), low-porosity rock the rate limiting process is diffusion (Gratier, 1993; Gratier et al., 2009; Gratier et al., 2013; Renard et al., 1997).

As a result, pressure solution creep flow laws relevant for the upper crust and for the seismogenic domain of subduction zones are diffusion-controlled (Gratier et al., 2009; Renard et al., 1997), with typical flow laws of the form (Gratier et al., 2009):

$$\dot{\epsilon} = 8DwcV_s(e^{\frac{3\sigma_n V_s}{RT}} - 1)/d^3$$

where D is the diffusion coefficient, c is the solubility of quartz,  $V_s$  is the molar volume of quartz, R is the gas constant, T is the temperature, w is the thickness of the interface along which diffusion occurs, D is the diffusion constant along the interface,  $\sigma_n$  is the effective deviatoric stress in the solid and d is the transport distance d between dissolution and precipitation sites. The latter parameter has a critical effect on the efficiency pf pressure solution (Gratier et al., 2009). Increase in microfracturing as a result of earthquakes may result in a large decrease in d in post-seismic stages, which in turn strongly activates pressure solution creep. As a result, pressure-solution is envisioned as being activated principally in post-seismic stage and to play a role in healing fractures in the damage zone around zones of seismic slip (Renard et al., 2000).

In deformed rocks from tectonic mélangé, such as Shimanto Belt, the density of fractures is extremely high, which strongly reduces the transport distance and in turn promotes the action of pressure solution. Considering the high density of quartz veins in the Shimanto Belt tectonic mélangé, the spacing between adjacent veins is very small, typically below 1mm. If this spacing represents the transport distance, then very high strain rates can be obtained for pressure solution, which becomes much more efficient than brittle deformation described by Byerlee's law (Figure 52).

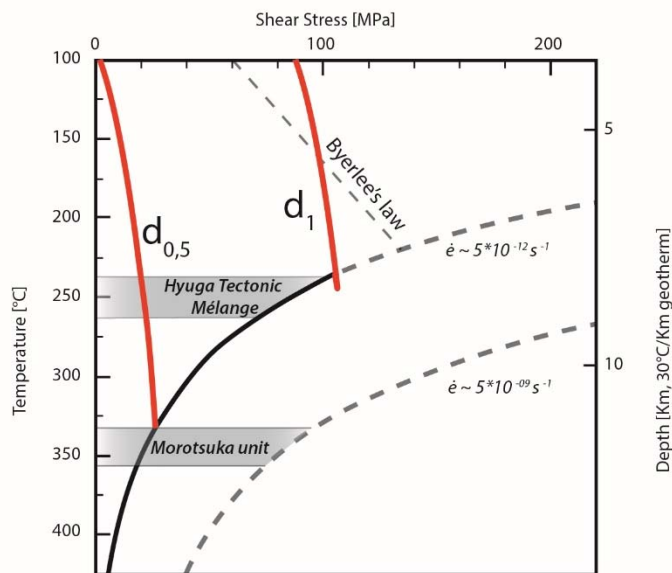


Figure 52 : Stress–depth diagram showing the strength predicted with pressure solution and a small transport distance in pressure solution flow laws (Palazzin et al., 2016). Thick red lines is the strength envelop estimated with pressure solution creep predictions (mean distance  $d_1=1\text{mm}$  and  $d_{0,5}=500\mu\text{m}$ ) for a constant strain rate of  $\sim 10^{-11}\text{s}^{-1}$ , and the flow law for wet quartz by (Hirth et al., 2001) for two distinct strain rates. Pressure solution is active in Hyuga Tectonic mélanges, while plastic deformation is the main deformation process in Morotsuka unit.

### 1. The effect of clays

Additionally, experiments and observations on natural rocks have also shown that pressure solution is more efficient in polymineralic than in monomineralic rocks (Gratier et al., 2013), an effect interpreted as reflecting the easier diffusion of solutes at a grain boundaries between different minerals. This effect is particularly developed when clays are present along the grain boundaries (e.g. (Hickman and Evans, 1995)). A possible explanation lies in their large surface charge of clays, leading to thicker water films along the grain boundaries, which enable quicker elemental diffusion (Renard and Ortoleva, 1997). Furthermore, clays along quartz grain boundaries in sandstones have an effect to enhance quartz dissolution (Bjorkum, 1996).

### 2. The effect of reactions

The effect of diagenetic reactions is not taken into account in pressure solution experiments or in resulting flow laws. On the other hand, many reactions have an effect on the concentrations in solutes, in particular in silica. The smectite-to-illite reaction, active in the T range of 50-150°C, produces  $\text{SiO}_2$  (Velde, 1984). In addition, although there is still some debate on the subject, smectite-to-illite reaction proceeds to a large extent by dissolution of and precipitation (Ferrage et al., 2011; Lanson and Champion, 1991), which is itself activated by deviatoric stress (Casciello et al., 2011). Deformation by pressure solution in metapelitic sediments containing

quartz grains and clays results therefore not simply from quartz dissolution and precipitation, but also from a combination of quartz and clays dissolution and precipitation.

### *3. Diffusion coefficients and the wetted structure of grain boundaries*

Pressure-solution experiments on high porosity material were derived as between 61 and 76kJ/mol in (Schutjens, 1991), with porosity between 45 and 35%, 73kJ/mol in (Dewers and Hajash, 1995), with a porosity of ~35%, 75+/-10kJ/mol in (Niemeijer et al., 2002), with porosities above 15%. Such high values of activation energy, around 70kJ/mol, are relevant for the case where pressure-solution is controlled by mineral reactions processes (Niemeijer et al., 2002; Rimstidt and Barnes, 1980).

At higher temperature and lower porosity, i.e. for conditions more relevant to the Shimanto Belt rocks we are considering here, pressure solution is controlled by diffusion and activation energy is much lower, of the order of ~15-25kJ/mol (Nakashima, 1995). Similarly, (Gratier et al., 2009) also considers a very low value of activation energy (~10kJ/mol) for the indentation of a quartz crystal, i.e. a material with a very low porosity.

These low values of activation energy are valid for diffusion in a free fluid, as in open pore or cracks (Nakashima, 1995). The problems become more complex when considering crystalline or metamorphic rocks, where the diffusion of solutes in a fluid phase is restricted to the grain boundaries. In their review of diffusivity in rocks, (Nakashima, 1995) show that there is a large uncertainty in the diffusion coefficients along the grain boundaries. In novaculite equilibrated with different solution (pure water, a solution with 6mol/L of NaCl, pure H<sub>2</sub>O), “wetted” grain boundaries (equilibrated with 6MNaCl solution) have diffusivity 3 to 4 orders of magnitude higher than partially wetted (=equilibrated with pure water) or non-wetted (=equilibrated with pure CO<sub>2</sub>) material (Farver and Yund, 1992). Additionally, while diffusion in “wetted” grain boundaries of novaculite is characterized by low activation energies between 15 and 30kJ/mol, diffusion in “non-wetted” grain boundaries has a much higher activation energy (~100kJ/mol). There is therefore a very large drop in diffusivity of the grain boundaries from 6M solution (“wetted”) to pure water (“partially wetted”). The values of salinity we have found for the fluid at seismogenic depths is of the order of seawater (Raimbourg et al., 2018), i.e. ~0.6mol/L, much lower than the 6M solution that corresponds in (Farver and Yund, 1991) to “wetted” grain boundary. Even if the abundance of fluids is attested by the large density of fluid inclusions, or of veins themselves, it is still an open question what is the structure (“wetted” vs. “partially wetted”) of the grain boundary in the metasediments at seismogenic depths.

The problem was approached on natural rocks from the Shimanto Belt in Japan (Kawabata et al., 2007; Kawabata et al., 2009). The metasediments show a large density of dark lamellae or

layers, rich in insoluble elements, interpreted as pressure-solution seams (PSS), i.e. as the result of dissolution. PSS density is correlated with the metamorphic grade, which allowed the authors to derive the activation energy of the process, as between 18 and 45kJ/mol. In the framework provided by (Nakashima, 1995), these low values were interpreted as reflecting diffusion along grain-boundary as limiting process of pressure solution.

#### **4. Conclusions**

Pressure-solution and fracturing form a chain of processes that control bulk strain and permeability. Constraining quantitatively these processes, to obtain both the strength and permeability, and their evolution with time, is not possible yet. There is a lack of experimental data on pressure solution creep of highly-strained, low-porosity rocks, where transfers occur along the grain boundaries. The main uncertainties concern the characteristic transport distance, as well as the properties of the fluid film (including its diffusional characteristics), but also the effect of clays, in particular when they are affected by metamorphic reaction, on the efficiency of transport. Assessing the effect of pressure solution is a major challenge to understand both fluid transfer and deformation when considering the seismogenic depth domain.

#### **G. Relationship between deformation and fluid flow: slow slip events**

As seen in chapter 1, the observation of large  $V_p/V_s$  ratio (Audet and Kim, 2016) corresponding to some extent to occurrences of SSE let to postulate a role of high fluid pressure in these deep slip instabilities. The mechanical interpretation is not straightforward. One possible explanation relies on friction laws; the occurrence of slip instabilities similar to what is observed during SSE is possible for very low effective pressures (Liu and Rice, 2007).

Alternatively, models of viscous compaction provide a way to propagate waves of porosity and high fluid pressure (Connolly, 2010), akin to propagating slip instabilities. To mimic what is observed during SSE (amongst other phenomena), (Omlin et al., 2017) developed the mechanical model of porosity wave to add a coupling between devolatilization reaction rates and fluid pressure  $P_f$ . This idea, if interesting, is poorly constrained experimentally, and the authors cite only one experimental work on gypsum (Llana-Funez et al., 2012). First, the latter study shows an effect of  $P_f$  on *reaction rates*, while (Omlin et al., 2017) model uses a linear relationship between  $P_f$  and *mineral-bound water content at equilibrium*. Second, the parameters used in the relationships are not constrained, so that only theoretical cases are considered and the application to actual processes is not possible. Third, it is questionable how a process observed on gypsum can be applied to other dehydration processes, which may result from different elemental mechanisms; for example, for the smectite-to-illite transformation,

several elemental mechanisms may intervene (solid-state transformation, dissolution precipitation) (Bauer et al., 2006; Ferrage et al., 2011).

In addition to the theoretical and modelling approaches exposed above, the question of the generation of SSE has also been tackled using natural fossil examples of veins, considered as remnants of SSE. These studies use principally crack-seal microstructures (e.g. in calcite veins from the shallow subduction channel in the Appenines (Vannucchi et al., 2010)) as evidences of cyclic fluctuations in fluid pressure, tentatively associated with deformation.

The first case study is provided by the Central Belt in the Kodiak Formation, in Alaska. The structural features of the Central Belt (penetrative deformation, recumbent fault, and horizontal cleavage) led to interpret it as an ancient décollement (Fisher and Brantley, 1992, 2014; Fisher et al., 1995), active for P and T conditions of  $260 \pm 40$  MPa and  $270$ - $280^\circ\text{C}$  (Brantley et al., 1997). In addition, the shear zone show a very large density of veins, either as closely spaced ( $<1$  cm), very thin extension veins perpendicular to stretching or as more spaced ( $\sim 500$  cm) array of en-échelon veins. The thinner veins show crack-seal textures with a very reproducible geometry; the spacing between two adjacent bands of phyllosilicates is  $\sim 8 \mu\text{m}$  (Figure 53). Depletion of silica in the host metapelites adjacent to the veins point to a local redistribution of silica by diffusion from the host-rock to the vein, driven by a fluid pressure gradient. The numerous adjacent crack-seal bands point to a cyclic process. The time-scale calculated for the formation of one band by diffusive transport of silica is a few days, in agreement with the characteristic timescale of slow slip events. An interesting point is made in (Fisher and Brantley, 2014) that the cyclic variations in fluid pressure might not be related to deformation, but simply to cycles of fluid pressure build-up – fracturing – fluid escape and fluid pressure drop – fracture sealing – fluid pressure build-up. The relationship to deformation is seducing, but so far not really supported by observations.

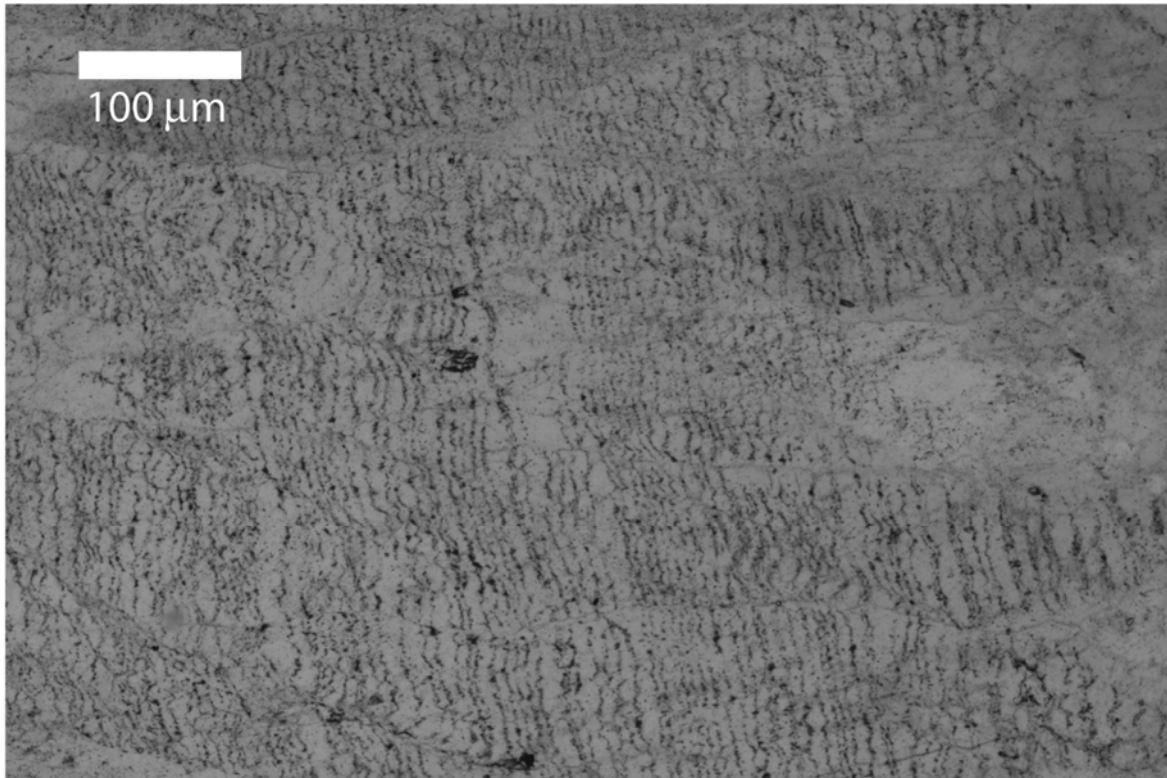


*Figure 53 : Crack-seal textures in quartz veins from the Kodiak Central Belt, from (Fisher and Brantley, 2014).*

A similar example is provided by crack-seal bands in synkinematic veins from the Makimine mélange in the Shimanto Belt, in metapelites buried down to temperatures  $\sim 340^{\circ}\text{C}$  (Palazzin et al., 2016). (Ujii et al., 2018) considers a model of veins formation controlled by precipitation of quartz driven by a fluid pressure drop. (Ujii et al., 2018) study builds on (Saishu et al., 2017)'s one, but for the fact that in the former case the pressure drop is estimated as  $\sim 150$  MPa (lithostatic to hydrostatic pressure), and 10-25MPa in the latter case, from consideration of stress drops in fore-arcs. Similarly to (Fisher and Brantley, 2014), the thickness (20 to  $38\mu\text{m}$ ) of quartz bands in crack-seal textures is used by (Ujii et al., 2018) to deduce the characteristic timescale of the process as 1.6-4.5 years.

The comparison of the Japanese and Alaskan examples are instructive of the lack of constraints on the processes modelled. For crack-seal textures with relatively similar thickness, (Fisher and Brantley, 2014) obtain characteristic timescales two orders of magnitude smaller than (Ujii et al., 2018). The sources of uncertainty are clearly exposed in (Fisher and Brantley, 2014): fluid pressure gradient as well as rates of precipitation (which depend strongly on salt concentration in water). More problematic is the determination of the process itself behind the growth of quartz veins. Both models assume that quartz is redistributed by dissolution from the adjacent host-rock, diffusion in the fluid and precipitation. In this chain of process, precipitation is considered as the rate-limiting process, while all models of pressure solution exposed above

tend to show that diffusion is the limiting process at the large T (relatively to the realm of pressure solution) considered here.

The modelling of the process of vein formation and its connection to deformation, in particular SSE, is therefore unsatisfactory in the present state of knowledge. Additionally, there is complete gap between the large-scale models of viscous/reactive compaction (e.g. (Omlin et al., 2017)) and the natural observations and associated small-scale models, pointing to local-scale redistribution. Further progress, requires clearly better experimental constraints, in particular for the range of temperature and lithology considered. As shown above, the phyllosilicates strongly influence the efficiency of pressure solution. In addition, the metapelites buried down to the SSE source region are affected by extensive reactions, which release or incorporate silica. For example, the metamorphism affecting metapelites from the Shimanto Belt buried down to  $\sim 300^{\circ}\text{C}$  results in the formation of a large amount of chlorite (Kameda et al., 2011), which releases amongst other elements silica (although the balanced reaction is not strongly constrained). The efficiency of pressure solution should therefore be assessed not only for a non-reacting rock but also for a rock in the course of metamorphic transformation.

We also note that in some of these studies of natural microstructures, the geological framework supporting the model is loose and the connection between the microstructures and the subduction is not clear. For example, the quartz veins used to build the model in (Saishu et al., 2017) are contained within the hanging wall of the Nobeoka Thrust and correspond kinematically to a stage of horizontal extension. Based on our geological study of the whole Shimanto Belt on Kyushu, we attributed this particular event, distributed throughout the base of the Cretaceous Belt, to a specific stage of “collapse” of the Belt in the Late Cretaceous-Early Cenozoic, with vertical shortening and horizontal extension (Raimbourg et al., 2014a). This set of veins are therefore completely uncorrelated with typical subduction dynamics, and formed much earlier than the Nobeoka Thrust. The assumption in (Saishu et al., 2017) that extensional veins and Nobeoka Thrust formed contemporaneously during subduction is therefore geologically irrelevant, so that the rest of the conclusions of the article is questionable.

## Chapter V: Research Project

Further progress on the deformation process at seismogenic depths and below, as well as the fluid circulation and the relationship between fluid and deformation, require to combine different approaches on various case studies. I expose in what follows a few axes of research that I intend to pursue in the years to come. Further work on the geology of the deformed zones in the Shimanto Belt and the Kodiak area (axis A) should decipher the structure of mélangé zone and reconstruct the tectonic evolution through time, paying attention to the age of distributed vs. localized deformation. The study of fluid (axis B) is already a mature axis, but more decisive conclusions can be expected from the use of advanced techniques, such as LA-ICP-MS or *in situ* Ar-Ar isotopes. A particular point of interest regards the interaction between fluid flow and deformation during SSE occurring near the base of the seismogenic zone. Finally, another approach to accretionary prism rheology revolves around laboratory experiments. We have developed a project (axis C), submitted already twice to ANR funding, to study in parallel the thermodynamics of smectite dehydration and its influence on frictional properties.

### A. Tectonic evolution and structure of mélangé zones

#### 1. *Further work on the Shimanto Belt*

Whether distributed and localized deformation are contemporaneous, or successive deformation modes, is a key question in fossil subduction zones. The most straightforward answer to this question can be provided by radiometric dating. The first step has already been carried out by dating Mugi and Kure pseudotachylytes (Honda et al., 2011; Tonai et al., 2016). Further examination of this question requires to date mélangé distributed deformation. This is technically challenging, as the minerals composing the foliation (mostly chlorite and illite/muscovite) are extremely small (at best micron size), so dating requires K-Ar dating on carefully sorted granulometric fractions (Clauer, 2013). K-Ar dating facility is in the course of installation at ISTO, making this project readily applicable.

The second objective would be to determine the large-scale internal structure of mélangé zones. The idea that mélanges are composed of individual thrust sheets, each of them soled by a basalt layer and an underlying fault, is more akin to a concept than a data-supported model. In fact, alternative models exist (Kiminami et al., 1992; Kiminami and Miyashita, 1992; Osozawa et al., 1990), such as a “mille-feuille” structure composed of alternation of sediments and basalt lava flow, which would not be tectonic but inherited from pre-subduction, trench volcanism. The repetition of thrust units should be confirmed by dating zircons in tuff layers (Shibata et al., 2008), a task Asuka Yamaguchi and I have started to carry out. To test the alternative model

of trench magmatism, with lava flow on top of trench sediments, Raman analysis of organic matter in sediments in contact with the basalts could be carried out. Preliminary results that I obtained in the Mugi mélange zone tend to show a thermal anomaly in the sediment close to the basalt, in agreement with the model of trench magmatism rather than tectonic duplexing, for this mélange unit.

## 2. *Extension to other case studies- Kodiak accretionary prism*

The relevance of geological observations and hence the models derived from them might always be limited to the domain where they were carried. For the sake of generality, it is necessary to multiply the same observations on various case studies. The accretionary prisms on the island of Kodiak and nearby islands is, beside the Shimanto Belt, another classical example of fossil structures. The geological evolution has been well constrained by numerous structural studies (Byrne, 1984; Connelly, 1978; Fisher and Byrne, 1987; Moore and Wheeler, 1978; Sample and Fisher, 1986; Sample and Moore, 1987), providing a robust framework to analyze, at smaller-scale, deformation and fluid flow processes. In addition, the Kodiak accretionary prism shows the coexistence of distributed and localized deformation, with the description of the a large-scale pseudotachylyte cutting across tectonic mélange (Rowe et al., 2005). Finally, crack-seal textures, interpreted as possibly associated with SSE, were described in the Kodiak Central Belt (Fisher and Brantley, 2014).



*Figure 54 : Pervasive deformation and veining in Waterfall Bay mélange from the Kodiak formation, in the footwall of the Uganik Thrust, from (Rowe et al., 2009). Temperature of deformation is ~200-250°C.*

The Kodiak formation is therefore very similar to the structures we have analyzed in the Shimanto Belt and provide therefore the opportunity to generalize our results on another case

study. One can also note that no precise temperature estimates are available for the area; a first stage of the work would consist in establishing T maps using Raman, in particular across the Uganik Thrust (Rowe et al., 2009), as the structures across it seem to reflect the transition from pressure-solution to plastic deformation. This work shall be initiated in summer 2019, in collaboration and with the help of Pr. Donald Fisher, of Pennsylvania University.

## **B. Fluid properties and its relationship to deformation**

### ***1. Fluid circulation: insights from the composition of fluid inclusions***

As explained in chapter IV, if progressive dehydration of subducting material involves significant flow of fluid, the time- and space-scale of this circulation is not well constrained, for part because of a lack of geochemical signatures of the different sources of fluids. For example, our CL analysis of vein microstructures has unraveled the occurrence of stages of opening of the system, when an “exotic” fluid penetrates the metasediments, but it is so far unclear where this exotic fluid originates from. The next step requires therefore the analysis of the composition of the fluid trapped in the fluid inclusions contained in the two types of quartz, in order to relate it to mineral reactions, hence to identify its source.

The chemical analysis of fluid inclusions was already carried out by LA-ICP-MS in olivine crystals formed after antigorite break-down (Scambelluri et al., 2004e). In our case, such *in-situ* analysis is necessary considering the fact that CL-blue and CL-brown quartz are intricately mixed to the small scale, preventing a bulk approach to the fluid composition, as enabled for example by in vacuum crush-leach techniques (e.g. (Kendrick et al., 2012)). An additional difficulty lies in the fact that the fluid inclusions are of a very small size, unlike the large inclusions analyzed in (Scambelluri et al., 2004e). While in the latter case, the LA-ICP-MS signal related to the quartz matrix can clearly be discriminated from the one related to the inclusion, in our case, we are bound to analyze a mixture of quartz+many small fluid inclusions. To decipher fluid composition, we need first to obtain the composition of the quartz matrix and then subtract it from the mixture signal. We have already carried out a significant number of LA-ICP-MS analyses for major and trace elements, but we are still struggling to get clear analyses of the quartz matrix itself, as clear, inclusion-free quartz is extremely rare. Beside cations, a similar *in situ* analysis will be carried out on irradiated samples, to obtain the composition of the fluid in terms of halogen ratio (Br, I and Cl) from Ar and noble gases isotopes (Kendrick et al., 2006). The latter analysis, technically challenging, will start in early 2019 under the guidance of Stéphane Scaillet, the head of Ar/Ar facility at ISTO.

In parallel of the chemical analysis of the fluid trapped in inclusions, an experimental study of the composition of the fluid produced during dehydration reactions shall be carried out by

Florian Osselin, a postdoc at ISTO. This experimental study is focused on clay dehydration at low temperature and serpentine dehydration at high temperatures.

Finally, the match, in terms of cations and halogens, between the fluid trapped in inclusions and the fluid produced by different mineral reactions, representative of the various materials affected by prograde dehydration reactions, shall provide major insights into the fluid circulation schemes at depth.

## ***2. Fluid pressure as a key factor of solid rock deformation and vein precipitation***

The space- and time-scales of fluid circulation bear a large influence on the fluid pressure field at depth. In turn, as pointed out by mechanical models of friction or by geophysical observations, fluid pressure is supposed to be a major controlling factor of subduction zone dynamics. Unfortunately, direct measurements of fluid pressure, or fluid pressure variations, are very scarce, and the deep fluid pressure field is hardly known.

There are a few pieces of evidences suggesting that fluid pressure varies over time: Crack-seal textures (Fisher and Brantley, 2014; Ujiie et al., 2018) or the alternating compositions of quartz veins or growth rims visible by cathodoluminescence (Raimbourg et al., 2018) point to cyclic variations in vein formation. These cycles are interpreted as reflecting variations in pressure, possibly related to solid rock deformation (either classical earthquakes or SSE). Additionally, some analyses of fluid inclusions contained in euhedral quartz in the Alps (Mullis, 1988a) or in the Kodiak accretionary prism (Vrolijk, 1990) have demonstrated the existence and the amplitude of fluid pressure variations.

Still, there is a missing connection between microstructural observation of syn-tectonic veins and fluid pressure variation estimates, as the latter are not associated directly with deformation, so it is not clear what fluid pressure variations attend the formation of the veins during deformation. An illustration of this point is given by the large range of values considered by (Fisher and Brantley, 2014) in their analysis of the formation of veins with crack-seal textures. Furthermore, there is a large uncertainty in the estimation of the *absolute* fluid pressure along the seismogenic zone and its downdip limit. (Saffer and Tobin, 2011) describe near-lithostatic pore fluid pressure near the down-dip limit of the seismogenic zone, where SSE nucleate, and slightly lower, with respect to lithostatic pressure gradient, fluid pressure along the seismogenic zone. But as we saw in Chapter 1, there is no way to convert seismic attribute into absolute pressure (fluid or effective), and these considerations are principally based on relative evolution with depth of  $V_p/V_s$  ratio. The record of the fluid inclusions tells otherwise; the fluid pressure is systematically much lower than lithostatic pressure (Raimbourg et al., 2018) (Figure 55).

There is therefore a need for more data about fluid pressure (both time-variations and absolute value), on microstructures that can be unambiguously associated with deformation. The CL-unraveled textures are a good candidate, as the two types of quartz formed contemporaneously with deformation, and differences in fluid pressure could be the triggering factor to differential incorporation of Al and Li, responsible for the luminescence. A key point, to derive fluid pressure, is to consider not only water+salt, as is commonly done, but the mixture of water+salt+methane, as we did in (Raimbourg et al., 2014b). This is the correct chemical system to assess the pressure and one of our objective is to apply such a method to well-characterized fluid inclusions in the two types of quartz. We aim through this at associating fluid pressure to the model of cyclic fluid flow we proposed in (Raimbourg et al., 2018) and eventually to connect it to deformation.

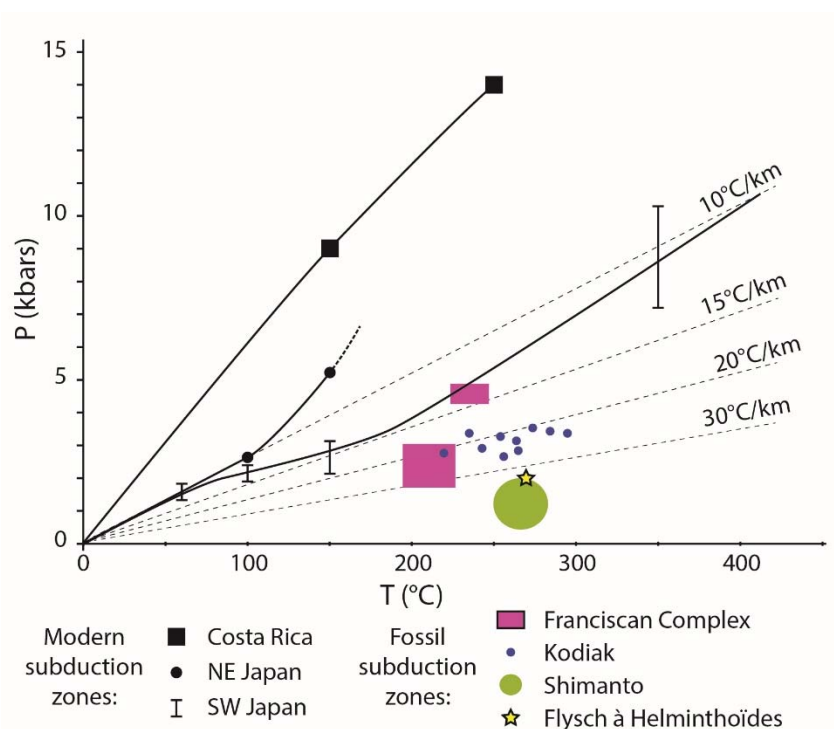


*Figure 55 : Comparison of the P-T record of fluid inclusions in samples corresponding to the seismogenic zone with thermal régimes from modern subduction zones. Fluid inclusions record systematically a lower pressure than along the subduction interface. Reference P-T gradients (dashed lines) were calculated assuming a volumetric mass of 2.65g/cm<sup>3</sup> for metasediments (Tsuji et al., 2006). References for modern subduction zones: Costa Rica – thermal model from Harris et al. (2010) and plate interface depths from Hayes et al. (2012), NE Japan - Kimura et al. (2012), SW Japan - Marcaillou et al. (2012). References for fossil subduction zones: Franciscan Complex - Dalla Torre et al. (1996), Kodiak - Vrolijk et al. (1988), Shimanto - Raimbourg et al. (2014b), Flysch à Helminthoïdes - this study. Fluid types: Franciscan Complex and Kodiak- methane-rich, Shimanto and Flysch à Helminthoïdes-water-rich.*

### 3. Relationships between fluid properties and deep SSE in fossil examples

So far, our work has principally focused on tectonic mélangé rocks that were formed shallower than the BPT, in which most of the strain is taken up by pressure solution. On the other hand, the Shimanto Belt shows examples of deformation at slightly higher temperature (~350°C, the Makimine Group), where plastic deformation is fully active. Within this unit, domains of concentrated fluid flow (as evidenced by abundant quartz veins), have been interpreted as the expression of SSE (Ujiie et al., 2018) (Figure 56).

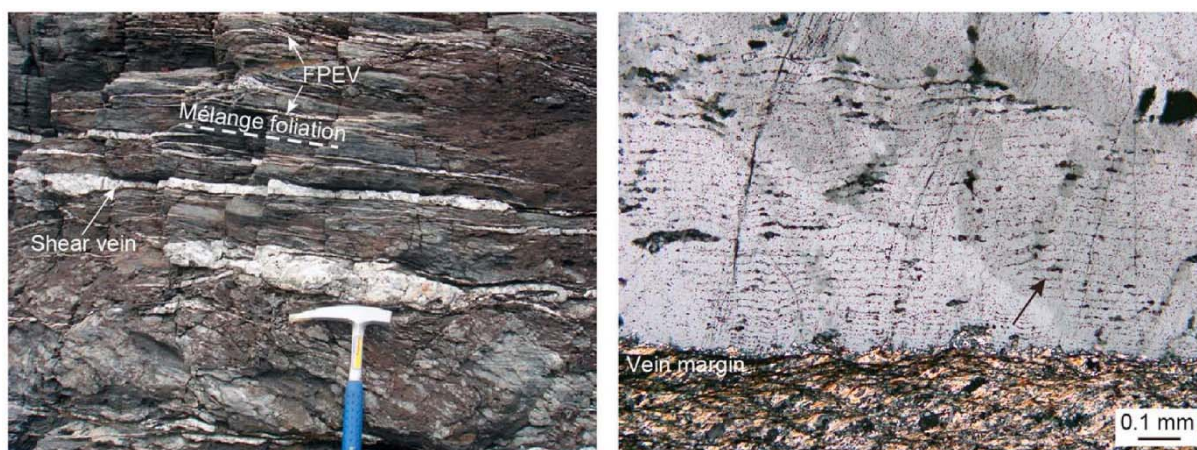


*Figure 56 : (Left): Foliation-parallel and shear veins, the latter showing fibers, very abundant in localized domains of the Makimine unit in the Shimanto Belt.. (Right): Shear vein cut parallel to quartz fibers (=stretching lineation), showing crack-seal bands parallel to vein margins. The two images from (Ujiie et al., 2018).*

These different types of veins should be analyzed using the different tools we have developed so far. While fluid inclusions are probably too small to be analyzed by microthermometry (this is often the case in the plastic realm), cathodoluminescence and chemical analyses with LA-ICP-MS should be applied in order to determine how these veins can be incorporated in the hydrological model we have developed (Raimbourg et al., 2018).

#### **C. Experimental approach to rheology at seismogenic depths – smectite dehydration and its influence on friction**

Another approach to subduction rheology relies on laboratory experiments of deformation, which I have initiated through the Ph.D. of Leslie Gadenne. We have carried out friction experiments at different temperatures on smectite powders, with different interlayer cations, as well as illite and quartz powder. These experiments have shown the large influence of the interlayer cation and temperature on the friction behavior of smectite, through both the absolute value of the friction coefficient and the stability of slip. Slip instabilities were observed only at 300°C and with K-exchanged smectite (Figure 57).

Friction experiments have focused a lot of attention recently, because frictional properties are considered as the key to elucidate the dynamics of subduction zone, from aseismic slip to megathrust earthquakes or slow-slip events. Nonetheless, the results of the experiments are still rather confusing with respect to the geophysical observations. For example, the smectite-to-illite transformation was thought to control the onset of seismic slip in the shallow region of subduction zones (Hyndman et al., 1997; Oleskevich et al., 1999). Friction experiments discarded this hypothesis (Saffer et al., 2012), but a clear and convincing alternative hypothesis is still lacking. Recent experiments with natural samples have shown their complex frictional behavior, controlled by lithology, temperature and slip velocity (Sawai et al., 2017).

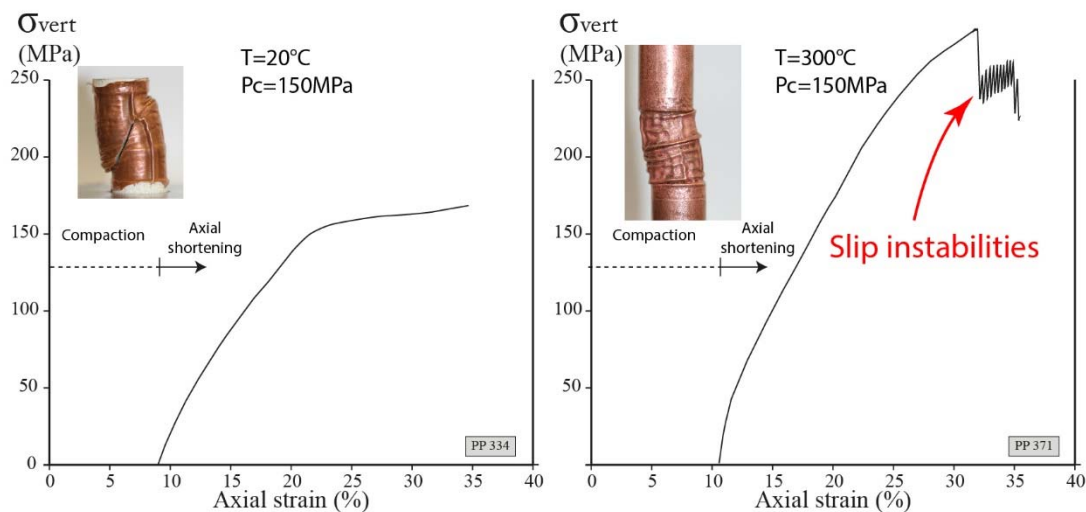


*Figure 57: Triaxial shortening experiments carried out with powders of K-exchanged smectite-rich, natural sediments from Boso Peninsula, Japan, in the Paterson apparatus showing the onset of slip instability only in tests at large temperature.*

The study by (Sawai et al., 2017) and the complexity it reveals actually calls for an approach of friction using simplified systems, as we did in the course of Gadenne's Ph.D.. Smectite is an expandable clay, whose properties varies as a function of the number of water layer in the interlayer space (Ikari et al., 2007) as well as the nature of the interlayer cation (Behnsen and Faulkner, 2013). Dehydration, which is a step-wise process (Ferrage et al., 2005; Huang et al., 1994), potentially affect smectite during burial, as a result of the increase in P, T and deformation. It might have a major effect on smectite friction, by changing the hydration state but also in itself, as it produces pore water.

Yet, only few experiments, carried out with a hydrothermal cell, have characterized dehydration using synchrotron X-ray diffraction at elevated P and T, i.e. the conditions relevant for subduction zones (Basset et al., 1996; Huang et al., 1994; Wu et al., 1997). These experiments did not consider K-smectite, although K is the dominant cation in many instances of marine shales (Buatier et al., 1992; Freed and Peacor, 1992; Merriman and Frey, 1999; Niu et al., 2000)

and diagenesis of pelitic rocks is modelled using K-micas as thermodynamic endmembers (Dubacq et al., 2010). The effect of K as interlayer cation, with a low ionic potential, is to reduce the temperature of dehydration, so that it occurs, according to thermodynamic modelling, at  $T < 100^{\circ}\text{C}$ , i.e. lower than illitisation of smectite and relevant for the upper limit of the seismogenic zone (Vidal and Dubacq, 2009). Other problems of this limited experimental dataset of high pressure dehydration of smectite are (i) the discrepancy with thermodynamic models, as well as low-pressure data (Vidal and Dubacq, 2009), (ii) the lack of precision on reactional volume change  $\Delta_r V$  (hence on potential overpressure during dehydration) and (iii) the limited control on pressure during these experiments.

We propose therefore first to reassess the thermodynamics of dehydration by experiments on sorted (fraction  $< 2\mu\text{m}$ ) and chemically exchanged smectite (where interlayer cation will be K, Na, Ca and Mg). These experiments will monitor *in-situ* the evolution of smectite hydration by X-ray diffraction as a function of P (0.5 to 2kbars) and T (up to  $600^{\circ}\text{C}$ ). The experimental setup involves a HP-HT, semi-transparent vessel at ISTO that will be equipped with X-ray diffraction device (Figure 58). This device is unique and shall allow to follow smectite (and other clays) thermodynamic properties and reactions for in situ conditions, corresponding to subduction zones (or the depth of sedimentary basins).

These static experiments, which will provide the locus, in the P-T grid, of dehydration reaction, form then the starting point of friction experiments to be carried out in the Paterson press. P-T conditions of the deformation experiments will be chosen to test the different hydration states of smectite, as well as dehydration reactions themselves.

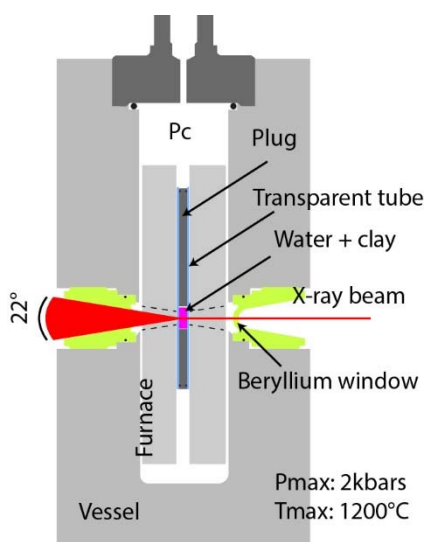


Figure 58 : Sketch of the high-pressure vessel with a transparent window

## References

- Abercrombie, R.E., Antolik, M., Felzer, K. and Ekström, G. (2001) The 1994 Java tsunami earthquake: Slip over a subducting seamount. *J. Geophys. Res.* 106, 6595-6607.
- Abers, G.A., MacKenzie, L.S., Rondenay, S., Zhang, Z., Wech, A.G. and Creager, K.C. (2009) Imaging the source region of Cascadia tremor and intermediate-depth earthquakes. *Geology* 37, 1119-1122.
- Adelinet, M., Fortin, J., Guéguen, Y., Schubnel, A. and Geoffroy, L. (2010) Frequency and fluid effects on elastic properties of basalt: Experimental investigations. *Geophys. Res. Lett.* 37, 1-4.
- Agard, P., Goffé, B., Touret, J.L.R. and Vidal, O. (2000) Retrograde mineral and fluid evolution in high-pressure metapelites (Schistes Lustrés unit, Western Alps). *Contrib. Mineral. Petrol.* 140, 296-315.
- Agard, P., Jolivet, L. and Goffé, B. (2001) Tectonometamorphic evolution of the Schistes Lustrés Complex: implications for the exhumation of HP and UHP rocks in the Western Alps. *Bull. Soc. Geol. France* 172, 617-636.
- Alt, J.C. and et. al. (1996) Hydrothermal alteration of a section of upper oceanic crust in the eastern equatorial Pacific: a synthesis of results from site 504 (DSDP legs 69, 70 and 83 and ODP legs 111, 137, 140 and 148), in: Alt, J.C., Kinoshita, H., Stokking, L.B., Michael, P.J. (Eds.), *Proc. ODP, Sci. Res.*, vol. 148, pp. 417-434.
- Amita, K., Ohsawa, S., Nishimura, K., Yamada, M., Mishima, T., Kazahaya, K., Morikawa, N. and Hirajima, T. (2014) Origin of saline waters distributed along the Median Tectonic Line in southwest Japan: hydrogeochemical investigation on possibility of derivation of metamorphic dehydrated fluid from subducting oceanic plate. *Journal of the Japanese association of hydrological sciences* 44, 17-38.
- Angelier, J., Barrier, E. and Chu, H.-T. (1986) Plate collision and paleostress trajectories in a fold-and-thrust belt: the Foothills of Taiwan. *Tectonophysics* 125, 161-178.
- Angelier, J., Bergerat, F., Chu, H.-T. and Lee, T.-Q. (1990) Tectonic analysis and the evolution of a curved collision belt: The Hsiiehshan Range, northern Taiwan. *Tectonophysics* 183, 77-96.
- Angiboust, S., Langdon, R., Agard, P., Waters, D. and Chopin, C. (2012) Eclogitization of the Monviso ophiolite (W. Alps) and implications on subduction dynamics. *J. Metamorphic Geol.* 30, 37-61.
- Audet, P., Bostock, M.G., Christensen, N.I. and Peacock, S.M. (2009) Seismic evidence for overpressured subducted oceanic crust and megathrust fault sealing. *Nature* 457, 76-78.
- Audet, P. and Kim, Y. (2016) Teleseismic constraints on the geological environment of deep episodic slow earthquakes in subduction zone forearcs: A review. *Tectonophysics* 670, 1-15.
- Audet, P. and Schwartz, S.Y. (2013) Hydrologic control of forearc strength and seismicity in the Costa Rican subduction zone. *Nature Geoscience* 6, 852-855.
- Avouac, J.-P. (2011) The lessons of Tohoku-Oki. *Nature* 475, 300-301.
- Bachmann, R., Oncken, O., Glodny, J., Seifert, W., Georgieva, V. and Sudo, M. (2009) Exposed plate interface in the European Alps reveals fabric styles and gradients related to an ancient seismogenic coupling zone. *J. Geophys. Res.* 114, 1-23.
- Baldwin, B. and Butler, C.O. (1985) Compaction curves. *AAPG Bull.* 69, 622-626.
- Bally, A.W., Gordy, P.L. and Stewart, G.A. (1966) Structure, seismic data and orogenic evolution of southern Canadian Rocky Mountains. *Bull. Can. Pet. Geol.* 14, 337-381.
- Bangs, N.L., Moore, G.F., Gulick, S.P.S., Pangborn, E.M., Tobin, H.J., Kuramoto, S. and Taira, A. (2009) Broad, weak regions of the Nankai Megathrust and implications for shallow coseismic slip. *Earth Planet. Sci. Lett.* 284, 44-49.
- Bangs, N.L.B. and Gulick, S.P.S. (2005) Physical properties along the developing decollement in the Nankai Trough: Inferences from 3-D seismic reflection data inversion and leg 190 and

- 196 drilling data, in: Mikada, H., Moore, G.F., Taira, A., Becker, K., Moore, J.C., Klaus, A. (Eds.), Proc. ODP, Sci. Results, 190/196, p. doi:10.2973/odp.proc.sr.190196.190354.192005.
- Barr, H. (1990) Preliminary fluid inclusion studies in a high-grade blueschist terrain, Syros, Greece. *Mineral. Mag.* 54, 159-168.
- Barrier, E. and Angelier, J. (1986) Active collision in Eastern Taiwan: the Coastal Range. *Tectonophysics* 125, 39-72.
- Basset, D., Sutherland, R. and Henrys, S. (2014) Slow wavespeeds and fluid overpressure in a region of shallow geodetic locking and slow slip, Hikurangi subduction margin, New Zealand. *Earth Planet. Sci. Lett.* 389, 1-13.
- Basset, W.A., Wu, T.-C., Chou, I.-M., Haselton Jr., H.T., Frantz, J. and et al. (1996) The hydrothermal diamond anvil cell (HDAC) and its application. *The Geochemical Society Spec. Pub* 5, 261-272.
- Baudin, F., Tribouvillard, N. and Trichet, J. (2007) *Géologie de la matière organique*, Paris.
- Bauer, A., Lanson, B., Ferrage, E., Emmerich, K., Taubald, H., Schild, D. and Velde, B. (2006) The fate of smectite in KOH solutions. *Am. Mineral.* 91, 1313-1322.
- Bebout, G.E. (1995) The impact of subduction-zone metamorphism on mantle-ocean chemical cycling. *Chem. Geol.* 126, 191-218.
- Bebout, G.E. (2007) Trace element and isotopic fluxes/Subducted slab, 3.20, in: Rudnick, R. (Ed.), *The crust, treatise on geochemistry*. Elsevier-Pergamon, Oxford, pp. 1-50.
- Bebout, G.E., Agard, P., Kobayashi, K., Moriguti, T. and Nakamura, E. (2013a) Devolatilization history and trace element mobility in deeply subducted sedimentary rocks: Evidence from Western Alps HP/UHP suites. *Chem. Geol.* 342, 1-20.
- Bebout, G.E., Agard, P., Kobayashi, K., Moriguti, T. and Nakamura, E. (2013c) Devolatilization history and trace element mobility in deeply subducted sedimentary rocks: Evidence from Western Alps HP/UHP suites. *Chemical Geology* 342, 1-20.
- Bebout, G.E. and Fogel, M.L. (1992) Nitrogen-isotope compositions of metasedimentary rocks in the Catalina Schists, California: implications for metamorphic devolatilization history. *Geochim. Cosmochim. Ac.* 56, 2839-2849.
- Behnken, J. and Faulkner, D.R. (2013) Permeability and frictional strength of cation-exchanged montmorillonite. *J. Geophys. Res.* 118, 2788-2798.
- Bekins, B.A. and Dreiss, S.J. (1992) A simplified analysis of parameters controlling dewatering in accretionary prisms. *Earth Planet. Sci. Lett.* 109, 275-287.
- Bilek, S., DeShon, H.R. and Engdahl, E.R. (2012) Spatial variations in earthquake source characteristics within the 2011 Mw = 9.0 Tohoku, Japan rupture zone. *Geophys. Res. Lett.* 39, 1-5.
- Bilek, S. and Lay, T. (1999) Rigidity variations with depth along interplate megathrust faults in subduction zones. *Nature* 400, 443-446.
- Bilek, S., Lay, T. and Ruff, L.J. (2004) Radiated seismic energy and earthquake source duration variations from teleseismic source time functions for shallow subduction zone thrust earthquakes. *J. Geophys. Res.* 109, 1-14.
- Bilek, S., Rotman, H.M.M. and Phillips, W.S. (2016) Low stress drop earthquakes in the rupture zone of the 1992 Nicaragua tsunami earthquake. *Geophys. Res. Lett.* 43, 10,180-110,188.
- Bilek, S., Schwartz, S. and DeShon, H.R. (2003) Control of seafloor roughness on earthquake rupture behavior. *Geology* 31, 455-458.
- Biot, M.A. (1941) General theory of three-dimensional consolidation. *J. Appl. Phys.* 12, 155-164.
- Bjorkum, P.A. (1996) How important is pressure in causing dissolution of quartz in sandstones? *J. Sed. Res.* 66, 147-154.
- Bodnar, R.J. (2003) Reequilibration of fluid inclusions, in: Anderson, A., Marshall, D. (Eds.), *Fluid inclusions: analysis and interpretation*. Min. Assoc. Canada, Short Course 32, pp. 213-230.

- Bodnar, R.J. and Beane, R.E. (1980) Temporal and spatial variations in hydrothermal fluid characteristics during vein filling in preore cover overlying deeply buried porphyry copper-type mineralization at Red Mountain, Arizona. *Economic Geology* 75, 876-893.
- Boullier, A.M. and Robert, F. (1992) Paleoseismic events recorded in Archean gold-quartz veins networks, Val d'Or Abitibi, Quebec. *J. Struct. Geol.* 14, 161-179.
- Brace, W.F. and Byerlee, J.D. (1966) Stick-slip as a mechanism for earthquakes. *Science* 153, 990-992.
- Brantley, S.L., Fisher, D.M., Deines, P., Clark, M.B. and Myers, G. (1997) Segregation veins: evidence for the deformation and dewatering of a low-grade metapelite, in: Holness, M.B. (Ed.), *Deformation-enhanced fluid transport in the Earth's crust and mantle*. Chapman and Hall, London, pp. 267-288.
- Bray, C.J. and Karig, D.E. (1985) Porosity of sediments in accretionary prisms and some implications for dewatering processes. *J. Geophys. Res.* 90, 768-778.
- Brudzinski, M.R. and Allen, R.M. (2007) Segmentation in episodic tremor and slip all along Cascadia. *Geology* 35, 907-910.
- Buatier, M.D., Peacor, D.R. and O'Neil, J.R. (1992) Smectite-illite transition in Barbados accretionary wedge sediments: TEM and AEM evidence for dissolution/crystallization at low temperature. *Clays and Clay Minerals* 40, 65-80.
- Bürgmann, R., Kogan, M.G., Levin, V.E., Scholz, C., King, R.W. and Steblov, G.M. (2001) Rapid aseismic moment release following the 5 December 1997 Kronotsky Kamchatka earthquake. *Geophys. Res. Lett.* 28, 1331-1334.
- Bürgmann, R., Kogan, M.G., Steblov, G.M., Hilley, G., Levin, V.E. and Apel, E. (2005) Interseismic coupling and asperity distribution along the Kamchatka subduction zone. *J. Geophys. Res.* 110, 1-17.
- Burkhard, M. and Kerrich, R. (1988) Fluid regimes in the deformation of the Helvetic nappes, Switzerland, as inferred from stable isotope data. *Contrib. Mineral. Petrol.* 99, 416-429.
- Burkhard, M., Kerrich, R., Maas, R. and Fyfe, W.S. (1992) Stable and Sr-isotope evidence for fluid advection during thrusting of the Glarus nappe (Swiss Alps). *Contrib. Mineral. Petrol.* 112, 293-311.
- Busigny, V., Cartigny, P., Philippot, P., Ader, M. and Javoy, M. (2003) Massive recycling of nitrogen and other fluid-mobile elements in a cold slab environment: evidence from HP to UHP oceanic metasediments of the Schistes Lustrés nappe (Western Alps, Europe). *Earth Planet. Sci. Lett.* 215, 27-42.
- Byerlee, J.D. (1978) Friction of rocks. *Pure and Applied Geophysics* 116, 615-626.
- Byrne, D.E., Davis, D.M. and Sykes, L.R. (1988) Loci and maximum size of thrust earthquakes and the mechanics of the shallow region of subduction zones. *Tectonics* 7, 833-857.
- Byrne, T. (1984) Structural evolution of melange terranes in the Ghost Rocks Formation, Kodiak Island, Alaska, in: Raymond, L. (Ed.), *Melanges, their origin and significance*. Spec. Pap. Geol. Soc. Am. 198, pp. 21-51.
- Byrne, T. and Fisher, D. (1990) Evidence for a weak and overpressured decollement beneath sediment-dominated accretionary prisms. *J. Geophys. Res.* 95, 9081-9097.
- Casciello, E., Cosgrove, J.W., Cesarano, M., Romero, E., Queralt, I. and Verges, J. (2011) Illite-smectite patterns in sheared Pleistocene mudstones of the Southern Apennines and their implications regarding the process of illitization: A multiscale analysis. *J. Struct. Geol.* 33, 1699-1711.
- Chan, L.H. and Kastner, M. (2000) Lithium isotopic compositions of pore fluids and sediments in the Costa Rica subduction zone: implications for fluid processes and sediment contribution to the arc volcanoes. *Earth Planet. Sci. Lett.* 183, 275-290.
- Chang, C.-P., Angelier, J. and Huang, C.-Y. (2000) Origin and evolution of a melange: the active plate boundary and suture zone of the Longitudinal Valley, Taiwan. *Tectonophysics* 325, 43-62.

- Chapple, W.M. (1978) Mechanics of thin-skinned fold-and-thrust belts. *Geological Society of America Bulletin* 89, 1189-1198.
- Charvet, J. (2013) Late Paleozoic–Mesozoic tectonic evolution of SW Japan: A review – Reappraisal of the accretionary orogeny and revalidation of the collisional model. *J. Asian Earth Sci.* 72, 88-101.
- Charvet, J. and Fabbri, O. (1987) Vue générale sur l'orogénèse Shimanto et l'évolution tertiaire du Japon sud-ouest. *Bull. Soc. Geol. France* 8, 1171-1188 (in french with english abstract).
- Chester, F.M. and Logan, J.M. (1986) Implications for mechanical properties of brittle faults from observations of the Punchbowl Fault Zone, California. *Pure and Applied Geophysics* 124, 79-106.
- Chester, F.M., Rowe, C., Ujiie, K., Kirkpatrick, J., Regalla, C., Remitti, F., Moore, J.C., Toy, V., Wolfson-Schwehr, M., Bose, S., Kameda, J., Mori, J.J., Brodsky, E.E., Eguchi, N., Toczko, S. and Scientists, E.a.T. (2013) Structure and composition of the plate-boundary slip zone for the 2011 Tohoku-Oki earthquake. *Science* 342, 1208-1211.
- Chlieh, M., Mothes, P.A., Nocquet, J.-M., Jarrin, P. and et al. (2014) Distribution of discrete seismic asperities and aseismic slip along the Ecuadorian megathrust. *Earth Planet. Sci. Lett.* 400, 292-301.
- Christensen, N.I. (1984) Pore pressure and oceanic crustal seismic structure. *Geophys. J. Roy. Astron. Soc.* 79, 411-423.
- Christensen, N.I. (1996) Poisson's ratio and crustal seismology. *J. Geophys. Res.* 101, 3139-3156.
- Christensen, N.I. and Wang, H.F. (1985) The influence of pore pressure and confining pressure on dynamic elastic properties of Berea sandstone. *Geophysics* 50, 207-213.
- Clauer, N. (2013) The K-Ar and <sup>40</sup>Ar/<sup>39</sup>Ar methods revisited for dating fine-grained K-bearing clay minerals. *Chem. Geol.* 354, 163-185.
- Cloos, M. (1982) Flow melanges: Numerical modelling and geologic constraints on their origin in the Franciscan complex, California. *Geological Society of America Bulletin* 93, 330-345.
- Cloos, M. and Shreve, R. (1988a) Subduction-channel model of prism accretion, melange formation, sediment subduction, and subduction erosion at convergent plate margins: 1. Background and description. *Pure Appl. Geophys.* 128, 455-500.
- Cloos, M. and Shreve, R. (1988b) Subduction-channel model of prism accretion, melange formation, sediment subduction, and subduction erosion at convergent plate margins: 2. Implications and Discussion. *Pure Appl. Geophys.* 128, 501-545.
- Cloos, M. and Shreve, R. (1996) Shear zone thickness and the seismicity of Chilean- and Mariana-type subduction zones. *Geology* 24, 107-110.
- Collot, J.-Y., Sanclemente, E., Nocquet, J.-M., Leprêtre, A., Ribodetti, A., Jarrin, P., Chlieh, M., Graindorge, D. and Charvis, P. (2017) Subducted oceanic relief locks the shallow megathrust in central Ecuador. *J. Geophys. Res.* 122, 3286-3305.
- Connelly, W. (1978) Uyak Complex, Kodiak Islands, Alaska: A Cretaceous subduction complex. *GSA Bull.* 89, 755-769.
- Connolly, J.A.D. (2010) The mechanics of metamorphic fluid expulsion. *Elements* 6, 165-172.
- Cox, S.F. and Paterson, M.S. (1991) Experimental dissolution-precipitation creep in quartz aggregates at high temperatures. *Geophys. Res. Lett.* 18, 1401-1404.
- Dahlen, F.A. (1990) Critical taper model of fold-and-thrust belts and accretionary wedges. *Annual Review of Earth And Planetary Sciences* 18, 55-99.
- Dalla Torre, M., De Capitani, C., Frey, M., Underwood, M., Mullis, J. and Cox, R. (1996) Very low-temperature metamorphism of shales from the Diablo Range, Franciscan Complex, California: New constraints on the exhumation path. *GSA Bull.* 108, 578-601.
- Den Hartog, S.A.M. and Spiers, C.J. (2014) A microphysical model for fault gouge friction applied to subduction megathrusts. *J. Geophys. Res.* 119, 1510-1529.

- DeShon, H.R., Schwartz, S.Y., Bilek, S., Dorman, L.M., Gonzalez, V., Protti, J.M., Flueh, E.R. and Dixon, T.H. (2003) Seismogenic zone structure of the southern Middle America Trench, Costa Rica. *J. Geophys. Res.* 108, 1-14.
- Dewers, T. and Hajash, A. (1995) Rate laws for water-assisted compaction and stress-induced water-rock interaction in sandstones. *J. Geophys. Res.* 100, 13,093-013,112.
- Dielforder, A., Vollstaedt, H., Vennemann, T.W., Berger, A. and Herwegh, M. (2015) Linking megathrust earthquakes to brittle deformation in a fossil accretionary complex. *Nature Communications* 6, 1-10.
- Dieterich, J.H. (1994) A constitutive law for rate of earthquake production and its application to earthquake clustering. *J. Geophys. Res.* 99, 2601-2618.
- Dominguez, S., Lallemand, S.E., Malavieille, J. and Von Huene, R. (1998) Upper plate deformation associated with seamount subduction. *Tectonophysics* 293, 207-224.
- Dominguez, S., Malavieille, J. and Lallemand, S.E. (2000) Deformation of accretionary wedges in response to seamount subduction: Insights from sandbox experiments. *Tectonics* 19, 182-196.
- Dragert, H., Wang, K. and James, T.S. (2001) A silent slip event on the deeper Cascadia subduction interface. *Science* 292, 1525-1528.
- Dubacq, B., Vidal, O. and De Andrade, V. (2010) Dehydration of dioctahedral aluminous phyllosilicates: thermodynamic modelling and implications for thermobarometric estimates. *Contrib. Mineral. Petrol.* 159, 159-174.
- England, P.C. and Holland, T.J.B. (1979) Archimedes and the Tauern eclogites: the role of buoyancy in the preservation of exotic eclogite blocks. *Earth Planet. Sci. Lett.* 44, 287-294.
- Erickson, S.N. and Jarrard, R.D. (1998) Velocity-porosity relationships for water-saturated siliciclastic sediments. *J. Geophys. Res.* 103, 30,385-330,406.
- Evans, M.A. and Dunne, W.M. (1991) Strain factorization and partitioning in the North Mountain thrust sheet, central Appalachians, U.S.A. *J. Struct. Geol.* 13, 21-35.
- Fagereng, A. and Den Hartog, S.A.M. (2017) Subduction megathrust creep governed by pressure solution and frictional–viscous flow. *Nat. Geo.* 10, 51-60.
- Fagereng, A. and Harris, C. (2014) Interplay between fluid flow and fault–fracture mesh generation within underthrust sediments: Geochemical evidence from the Chrystalls Beach Complex, New Zealand. *Tectonophysics* 612-613, 147-157.
- Fagereng, A., Remitti, F. and Sibson, R.H. (2011) Incrementally developed slickenfibers - geological record of repeating low stress-drop seismic events? *Tectonophysics* 510, 381-386.
- Fagereng, A. and Sibson, R.H. (2010) Mélange rheology and seismic style. *Geology* 38, 751-754.
- Farver, J.R. and Yund, R.A. (1991) Oxygen diffusion in quartz: dependence in temperature and water fugacity. *Chem. Geol.* 90, 55-70.
- Farver, J.R. and Yund, R.A. (1992) Oxygen diffusion in a fine grained quartz aggregate with wetted and nonwetted microstructures. *J. Geophys. Res.* 97, 14,017-014,029.
- Faulkner, D.R., Jackson, C.A.L., Lunn, R.J., Schlische, R.W., Shipton, Z.K., Wibberley, C. and Withjack, M.O. (2010) A review of recent developments concerning the structure, mechanics and fluid flow properties of fault zones. *J. Struct. Geol.* 32, 1557-1575.
- Faulkner, D.R., Lewis, A.C. and Rutter, E.H. (2003) On the internal structure and mechanics of large strike-slip fault zones: field observations of the Carboneras fault in southeastern Spain. *Tectonophysics* 367, 235-251.
- Ferrage, E., Lanson, B., Sakharov, B.A. and Drits, V.A. (2005) Investigation of smectite hydration properties by modeling experimental X-ray diffraction patterns: Part I. Montmorillonite hydration properties. *Am. Mineral.* 90, 1358-1374.
- Ferrage, E., Vidal, O., Mosser-Ruck, R., Cathelineau, M. and Cuadros, J. (2011) A reinvestigation of smectite illitization in experimental hydrothermal conditions: Results from X-ray diffraction and transmission electron microscopy. *Am. Mineral.* 96, 207-223.

- Fisher, D. and Byrne, T. (1987) Structural evolution of underthrust sediments, Kodiak Islands, Alaska. *Tectonics* 6, 775-793.
- Fisher, D. and Byrne, T. (1990) The character and distribution of mineralized fractures in the Kodiak Formation, Alaska: Implications for fluid flow in an underthrust sequence. *J. Geophys. Res.* 95, 9069-9080.
- Fisher, D.M. and Brantley, S.L. (1992) Models of quartz overgrowth and vein formation: deformation and episodic fluid flow in an ancient subduction zone. *J. Geophys. Res.* 97, 20,043-020,061.
- Fisher, D.M. and Brantley, S.L. (2014) The role of silica redistribution in the evolution of slip instabilities along subduction interfaces: Constraints from the Kodiak accretionary complex, Alaska. *J. Struct. Geol.* 69B, 395-414.
- Fisher, D.M., Brantley, S.L., Everett, M. and Dzonik, J. (1995) Cyclic fluid flow through a regionally extensive fracture network within the Kodiak accretionary prism. *J. Geophys. Res.* 100, 12,881-812,894.
- Freed, R.L. and Peacor, D.R. (1989) Variability in temperature of the smectite/illite reaction in Gulf Coast sediments. *Clay Miner.* 24, 171-180.
- Freed, R.L. and Peacor, D.R. (1992) Diagenesis and the formation of authigenic illite-rich I/S crystals in Gulf Coast shales: TEM study of clay separates. *J. Sed. Res.* 62, 220-234.
- Freymueller, J.T. and Beavan, J. (1999) Absence of strain accumulation in the Western Shumagin Segment of the Alaska subduction zone. *Geophys. Res. Lett.* 26, 3233-3236.
- Frezzotti, M.L. and Ferrando, S. (2015) The chemical behavior of fluids released during deep subduction based on fluid inclusions. *American Mineralogist* 100, 352-377.
- Fujiwara, T., Kodaira, S., No, T., Kaiho, Y., Takahashi, N. and Kaneda, Y. (2011) The 2011 Tohoku-Oki earthquake: Displacement reaching the trench axis. *Science* 334, 1240.
- Fukuchi, R., Fujimoto, K., Kameda, J., Hamahashi, M., Yamaguchi, A., Kimura, G., Hamada, Y., Hashimoto, Y., Kitamura, Y. and Saito, S. (2014) Changes in illite crystallinity within an ancient tectonic boundary thrust caused by thermal, mechanical, and hydrothermal effects: an example from the Nobeoka Thrust, southwest Japan. *Earth, Planets and Space* 66:116, 1-12.
- Gadenne, L. (2015) Processus de déformation et diagenèse dans les zones de subduction : Impact sur les propriétés mécaniques des roches, ISTO. Université d'Orléans, p. 235.
- Giaramita, M.J. and Sorensen, S.S. (1994) Primary fluids in low-temperature eclogites: evidence from two subduction complexes (Dominican Republic, and California, USA). *Contrib. Mineral. Petrol.* 117, 279-292.
- Gomberg, J. and Cascadia 2007 and Beyond Working Group (2010) Slow-slip phenomena in Cascadia and beyond: a review. *GSA Bull.* 122, 963-978.
- Gratier, J.P. (1993) Le fluage des roches par dissolution-cristallisation sous contrainte, dans la croûte supérieure. *Bull. Soc. Geol. Fr.* 164, 267-287.
- Gratier, J.P., Guiguet, R., Renard, F., Jenatton, L. and Bernard, D. (2009) A pressure solution creep law for quartz from indentation experiments. *J. Geophys. Res.* 114, 1-16.
- Gratier, J.P., Thouvenot, F., Jenatton, L., Tourette, A., Doan, M.-L. and Renard, F. (2013) Geological control of the partitioning between seismic and aseismic sliding behaviours in active faults: Evidence from the Western Alps, France. *Tectonophysics* 600, 226-242.
- Griggs, D.T. (1967) Hydrolytic weakening of quartz and other silicates. *Geophys. J. Roy. Astron. Soc.* 14, 19-31.
- Gu, J.-C., Rice, J.R., Ruina, A. and Tse, S.T. (1984) Slip motion and stability of a single degree of freedom elastic system with rate and state dependent friction. *J. Mech. Phys. Solids* 32, 167-196.
- Hacker, B.R. (2008) H<sub>2</sub>O subduction beyond arcs. *Geochemistry Geophysics Geosystems* 9, 1-24.
- Hacker, B.R., Abers, G.A. and Peacock, S.M. (2003) Subduction factory 1: Theoretical mineralogy, densities, seismic wave speeds, and H<sub>2</sub>O contents. *J. Geophys. Res.* 108.

- Hara, H. and Kimura, K. (2008) Metamorphic cooling history of the Shimanto accretionary complex, Kyushu, southwest Japan: Implications for the timing of out-of-sequence thrusting. *Island Arc* 17, 546-559.
- Harris, R.N., Spinelli, G., Ranero, C.R., Grevemeyer, I., Villinger, H.W. and Barckhausen, U. (2010) Thermal regime of the Costa Rican convergent margin: 2. Thermal models of the shallow Middle America subduction zone offshore Costa Rica. *Geochem. Geophys. Geosyst.* 11, 1-22.
- Hashimoto, C., Noda, A. and Matsu'ura, M. (2012) The Mw 9.0 northeast Japan earthquake: total rupture of a basement asperity. *Geophys. J. Int.* 189, 1-5.
- Hashimoto, Y. and Kimura, G. (1999) Underplating process from melange formation to duplexing: Example from the Cretaceous Shimanto Subbelt, Kii Peninsula, southwest Japan. *Tectonics* 18, 92-107.
- Hayes, G.P., Wald, D.J. and Johnson, R.L. (2012) Slab 1.0: a three-dimensional model of global subduction zone geometries. *J. Geophys. Res.* 117, B01302.
- Henry, P., Foucher, J.-P., Le Pichon, X., Sibuet, M., Kobayashi, K., Tarits, P., Chamot-Rooke, N., Furuta, T. and Schultheiss, P. (1992) Interpretation of temperature measurements from the Kaiko-Nankai cruise: Modeling of fluid flow in clam colonies. *Earth Planet. Sci. Lett.* 109, 355-371.
- Heuret, A., Lallemand, S., Funiciello, F., Piromallo, C. and Faccenna, C. (2011) Physical characteristics of subduction interface type seismogenic zones revisited. *G-cubed* 12, 1-26.
- Hickman, S.H. and Evans, B. (1995) Kinetics of pressure solution at halite-silica interfaces and intergranular clay films. *J. Geophys. Res.* 100, 113-113,132.
- Hirose, H. and Obara, K. (2006) Short-term slow slip and correlated tremor episodes in the Tokai region, central Japan. *Geophys. Res. Lett.* 33, 1-5.
- Hirth, G., Teyssier, C. and Dunlap, W.J. (2001) An evaluation of quartzite flow laws based on comparisons between experimentally and naturally deformed rocks. *Int. J. Earth Sci.* 90, 77-87.
- Hoffman, N.W. and Tobin, H.J. (2004) An empirical relationship between velocity and porosity for underthrust sediments in the Nankai Trough accretionary prism, in: Mikada, H., Moore, G.F., Taira, A., Becker, K., Moore, J.C., Klaus, A. (Eds.), *Proc. ODP, Sci. Results*, 190/196, pp. 1-23. doi:10.2973/odp.proc.sr.190196.190355.192004.
- Homberg, C., Bergerat, F., Philippe, Y., Lacombe, O. and Angelier, J. (2002) Structural inheritance and cenozoic stress fields in the Jura fold-and-thrust belt (France). *Tectonophysics* 357, 137-158.
- Honda, G., Ishikawa, T., Hirono, T. and Mukoyoshi, H. (2011) Geochemical signals for determining the slip - weakening mechanism of an ancient megasplay fault in the Shimanto accretionary complex. *Geophys. Res. Lett.* 38, 1-5.
- Huang, W.-L., Basset, W.A. and Wu, T.C. (1994) Dehydration and hydration of montmorillonite at elevated temperatures and pressures monitored using synchrotron radiation. *Am. Mineral.* 79, 683-691.
- Hubbert, M.K. and Rubey, W.W. (1959) Role of fluid pressure in mechanics of overthrust faulting 1. Mechanics of fluid-filled porous solids and its application to overthrust faulting. *Geol. Soc. Am. Bull.* 70, 115-166.
- Hüpers, A. and Kopf, A. (2012) Effect of smectite dehydration on pore water geochemistry in the shallow subduction zone: an experimental approach. *Geochem. Geophys. Geosyst.* 13.
- Husen, A., Kissling, E. and Quintero, R. (2002) Tomographic evidence for a subducted seamount beneath the Gulf of Nicoya, Costa Rica: The cause of the 1990 Mw = 7.0 Gulf of Nicoya earthquake. *Geophys. Res. Lett.* 29, 1-4.
- Hyndman, R.D., Yamano, M. and Oleskevich, D.A. (1997) The seismogenic zone of subduction thrust faults. *The Island Arc* 6, 244-260.
- Ide, S., Beroza, G.C., Shelly, D.R. and Uchide, T. (2007) A scaling law for slow earthquakes. *Nature* 447, doi:10.1038/nature05780.

- Ikari, M.J., Marone, C. and Saffer, D. (2011) On the relation between fault strength and frictional stability. *Geology* 39, 83-86.
- Ikari, M.J., Marone, C., Saffer, D. and Kopf, A. (2013) Slip weakening as a mechanism for slow earthquakes. *Nat. Geo.* 6, 468-472.
- Ikari, M.J. and Saffer, D. (2011) Comparison of frictional strength and velocity dependence between fault zones in the Nankai accretionary complex. *Geochem. Geophys. Geosystems* 12(4), 1-16.
- Ikari, M.J., Saffer, D.M. and Marone, C. (2007) Effect of hydration state on the frictional properties of montmorillonite-based fault gouge. *J. Geophys. Res.* 112, 1-12.
- Ikesawa, E., Kimura, G., Sato, K., Ikehara-Ohmori, K., Kitamura, Y., Yamaguchi, A., Ujiie, K. and Hashimoto, Y. (2005) Tectonic incorporation of the upper part of oceanic crust to overriding plate of a convergent margin: An example from the Cretaceous-early Tertiary Mugi Melange, the Shimanto Belt, Japan. *Tectonophysics* 401, 217-230.
- Ikesawa, E., Sakaguchi, A. and Kimura, G. (2003) Pseudotachylyte from an ancient accretionary complex: Evidence for melt generation during seismic slip along a master décollement? *Geology* 31, 637-640.
- Imai, I., Teraoka, Y., Okumura, K. and Ono, K. (1975) Geological Map of Japan, 1:50,000, Mikado. Geological Survey of Japan.
- Issler, D.R. (1992) A new approach to shale compaction and stratigraphic restoration, Beaufort-Mackenzie Basin and Mackenzie Corridor, Northern Canada. *AAPG Bull.* 76, 1170-1189.
- Ito, Y., Tsuji, T., Osada, Y., Kido, M., Inazu, D., Hayashi, Y., Tsushima, H., Hino, R. and Fujimoto, H. (2011) Frontal wedge deformation near the source region of the 2011 Tohoku - Oki earthquake. *Geophys. Res. Lett.* 38.
- Jaeger, J.C., Cook, N.G.W. and Zimmerman, R.W. (2007) Fundamentals of rock mechanics. Blackwell Publishing Ltd, Malden, USA.
- Jarrard, R.D. (2003) Subduction fluxes of water, carbon dioxide, chlorine, and potassium. *Geochem. Geophys. Geosyst.* 4, 1-50.
- Jourdan, A.-L., Vennemann, T.W., Müllis, J., Ramseyer, K. and Spiers, C.J. (2009) Evidence of growth and sector zoning in hydrothermal quartz from Alpine veins. *Eur. J. Mineral.* 21, 219-231.
- Kameda, J., Raimbourg, H., Kogure, T. and Kimura, G. (2011) Low-grade metamorphism around the down-dip limit of seismogenic subduction zones: Example from an ancient accretionary complex in the Shimanto Belt, Japan. *Tectonophysics* 502, 383-392.
- Kameda, J., Shimizu, M., Ujiie, K., Hirose, T., Ikari, M.J., Mori, J., Oohashi, K. and Kimura, G. (2015) Pelagic smectite as an important factor in tsunamigenic slip along the Japan Trench. *Geology* 43, 155-158.
- Kanamori, H. (2008) Earthquake physics and real-time seismology. *Nature* 451, 271-273.
- Kastner, M., Elderfield, H., Jenkins, W.J., Gieskes, J.M. and Gamo, T. (1993) Geochemical and isotopic evidence for fluid flow in the western Nankai subduction zone, Japan, in: Hill, I.A., Taira, A., Firth, J.V. (Eds.), *Proc. ODP, Sci. Results*, 131, pp. 397-413.
- Kastner, M., Elderfield, H. and Martin, J.B. (1991) Fluids in convergent margins: What do we know about their composition, origin, role in diagenesis and importance for oceanic chemical fluxes? *Phil. Trans. R. Soc. Lond.* 335, 243-259.
- Kastner, M., Sample, J.C., Whiticar, M.J., Hovland, M., Cragg, B.A. and Parkes, J.R. (1995) Geochemical evidence for fluid flow and diagenesis at the Cascadia convergent margin, in: Carson, B., Westbrook, G.K., Musgrave, R.J., Suess, E. (Eds.), *Proc. ODP, Sci. Res.*, 146, pp. 1-10.
- Kato, N. and Hirasawa, T. (1997) A numerical study on seismic coupling along subduction zones using a laboratory-derived friction law. *Phys. Earth Planet. Inter.* 102, 51-68.
- Kawabata, K., Tanaka, H. and Kimura, G. (2007) Mass transfer and pressure solution in deformed shale of accretionary complex: Examples from the Shimanto Belt, southwestern Japan. *Journal of Structural Geology* 29, 697-711.

- Kawabata, K., Tanaka, H., Kitamura, Y. and Ma, K.-F. (2009) Apparent activation energy and rate-limiting process estimation from natural shale deformed by pressure solution in shallow subduction zone. *Earth Planet. Sci. Lett.* 287, 57-63.
- Kelleher, J. and McCann, W. (1976) Buoyant zones, great earthquakes, and unstable boundaries of subduction. *J. Geophys. Res.* 81, 4885-4896.
- Kendrick, M.A., Phillips, D. and Miller, J.M. (2006) Part I. Decrepitation and degassing behaviour of quartz up to 1560°C: Analysis of noble gases and halogens in complex fluid inclusion assemblages. *Geochimica et Cosmochimica Acta* 70, 2540-2561.
- Kendrick, M.A., Woodhead, J.D. and Kamenetsky, V.S. (2012) Tracking halogens through the subduction cycle. *Geology* 40, 1075-1078.
- Kerrick, D.M. and Connolly, J.A.D. (2001a) Metamorphic devolatilization of subducted marine sediments and the transport of volatiles into the Earth's mantle. *Nature* 411, 293-296.
- Kerrick, D.M. and Connolly, J.A.D. (2001e) Metamorphic devolatilization of subducted oceanic metabasalts: implications for seismicity, arc magmatism and volatile recycling. *Earth and Planet Sci. Lett.* 189, 19-29.
- Kiminami, K., Kashiwagi, N. and Miyashita, S. (1992) Occurrence and significance of in-situ greenstones from the Mugi Formation in the Upper Cretaceous Shimanto Supergroup, eastern Shikoku, Japan. *Jour. Geol. Soc. Japan* 98, 867-883.
- Kiminami, K. and Miyashita, S. (1992) Occurrence and geochemistry of greenstones from the Makimine Formation in the Upper Cretaceous Shimanto Supergroup in Kyushu, Japan. *J. Geol. Soc. Jpn.* 98, 391-400.
- Kimura, G., Hashimoto, C., Yamaguchi, A., Kitamura, Y. and Ujiie, K. (2016) Cretaceous-Neogene accretionary units: Shimanto Belt, in: Moreno, T., Wallis, S., Kojima, T., Gibbons, W. (Eds.), *The Geology of Japan*. The Geological Society of London, London, pp. 125-137.
- Kimura, G., Hina, S., Hamada, Y., Kameda, J., Tsuji, T., Kinoshita, M. and Yamaguchi, A. (2012) Runaway slip to the trench due to rupture of highly pressurized megathrust beneath the middle trench slope: The tsunamigenesis of the 2011 Tohoku earthquake off the east coast of northern Japan *Earth Planet. Sci. Lett.* 339-340, 32-45.
- Kimura, G. and Mukai, A. (1991) Underplated unit in an accretionary complex: melange of the Shimanto Belt of eastern Shikoku, southwest Japan. *Tectonics* 10, 31-50.
- Kitajima, H. and Saffer, D.M. (2012) Elevated pore pressure and anomalously low stress in regions of low frequency earthquakes along the Nankai Trough subduction megathrust. *Geophys. Res. Lett.* 39, 1-5.
- Kitamura, Y. (2006) A fate of sediments in subduction zones, University of Tokyo. *Univ. of Tokyo, Tokyo*, p. 159.
- Kitamura, Y. and Kimura, G. (2012) Dynamic role of tectonic mélangé during interseismic process of plate boundary mega earthquakes. *Tectonophysics* 568-569, 39-52.
- Kitamura, Y., Sato, K., Ikesawa, E., Ikehara-Ohmori, K., Kimura, G., Kondo, H., Ujiie, K., Onishi, C.T., Kawabata, K., Hashimoto, Y., Mukoyoshi, H. and Masago, H. (2005) Melange and its seismogenic roof decollement: A plate boundary fault rock in the subduction zone - An example from the Shimanto Belt, Japan. *Tectonics* 24, 1-15.
- Kodaira, S., Iidaka, T., Kato, A., Park, J.O., Iwasaki, T. and Kaneda, Y. (2004) High pore fluid pressure may cause silent slip in the Nankai Trough. *Science* 304, 1295-1298.
- Kondo, H., Kimura, G., Masago, H., Ohmori-Ikehara, K., Kitamura, Y., Ikesawa, E., Sakaguchi, A., Yamaguchi, A. and Okamoto, S. (2005) Deformation and fluid flow of a major out-of-sequence thrust located at seismogenic depth in an accretionary complex: Nobeoka Thrust in the Shimanto Belt, Kyushu, Japan. *Tectonics* 24, 1-16.
- Koper, K.D., Hutko, A.R., Lay, T., Ammon, C.J. and Kanamori, H. (2011) Frequency-dependent rupture process of the 2011 Mw 9.0 Tohoku Earthquake: Comparison of short-period P wave backprojection images and broadband seismic rupture models. *Earth Planets And Space* 63, 599-602.

- Lachenbruch, A.H. (1980) Frictional heating, fluid pressure, and the resistance to fault motion. *J. Geophys. Res.* 85, 6097-6112.
- Lallemant, S. and Le Pichon, X. (1987) Coulomb wedge model applied to the subduction of seamounts in the Japan Trench. *Geology* 15, 1065-1069.
- Lallemant, S., Malavieille, J. and Calassou, S. (1992) Effects of oceanic ridge subduction on accretionary wedges: experimental modeling and marine observations. *Tectonics* 11, 1301-1313.
- Lallemant, S., Peyret, M., van Rijsingen, E., Arcay, D. and Heuret, A. (2018) Roughness characteristics of oceanic seafloor prior to subduction in relation to the seismogenic potential of subduction zones. *G-cubed* 19, 2121-2146.
- Lanson, B. and Champion, D. (1991) I/S to illite transformation in diagenesis. *Am. J. Sci.* 291, 473-506.
- Lapusta, N. and Rice, J.R. (2003) Nucleation and early seismic propagation of small and large events in a crustal earthquake model. *J. Geophys. Res.* 108, 1-18.
- Lay, T., Ammon, C.J., Kanamori, H., Xue, L. and Kim, M.J. (2011) Possible near-trench slip during the 2011 Mw 9.0 off the Pacific coast of Tohoku Earthquake. *Earth Planets Space* 63, 687-692.
- Le Pichon, X., Henry, P. and Lallemant, S. (1993) Accretion and erosion in subduction zones: The role of fluids. *Annu. Rev. Earth Pl. Sc.* 21, 307-331.
- Lewis, J.C. and Byrne, T.B. (2003) History of metamorphic fluids along outcrop-scale faults in a Paleogene accretionary prism, SW Japan: Implications for prism-scale hydrology. *Geochem. Geophys. Geosyst.* 4, 1-10.
- Liu, Y. and Rice, J.R. (2005) Aseismic slip transients emerge spontaneously in three-dimensional rate and state modeling of subduction earthquake sequences. *J. Geophys. Res.* 110, 1-14.
- Liu, Y. and Rice, J.R. (2007) Spontaneous and triggered aseismic deformation transients in a subduction fault model. *J. Geophys. Res.* 112, 1-23.
- Llana-Funez, S., Wheeler, J. and Faulkner, D.R. (2012) Metamorphic reaction rate controlled by fluid pressure not confining pressure: implications of dehydration experiments with gypsum. *Contrib. Mineral. Petrol.* 164, 69-79.
- Logan, J.M. and Rauenzahn, K.A. (1987) Frictional dependence of gouge mixtures of quartz and montmorillonite on velocity, composition and fabric. *Tectonophysics* 144, 87-108.
- Loveless, J.P. and Meade, B.J. (2010) Geodetic imaging of plate motions, slip rates, and partitioning of deformation in Japan. *J. Geophys. Res.* 115, 1-35.
- Loveless, J.P. and Meade, B.J. (2011) Spatial correlation of interseismic coupling and coseismic rupture extent of the 2011 Mw=9.0 Tohoku-oki earthquake. *Geophys. Res. Lett.* 38, 1-5.
- Maltman, A., Labaume, P. and Housen, B. (1997) Structural geology of the decollement at the toe of the Barbados accretionary prism, in: Shipley, T.H., Ogawa, Y., Blum, P., Bahr, J.M. (Eds.), *Proc. ODP, Sci. Results*, 156, pp. 279-292.
- Mancktelow, N.S. (1995) Nonlithostatic pressure during sediment subduction and the development and exhumation of high pressure metamorphic rocks. *Journal of geophysical research* 100, 571-583.
- Manning, C.E. (1994) The solubility of quartz in H<sub>2</sub>O in the lower crust and upper mantle. *Geochimica et Cosmochimica Acta* 58, 4831-4839.
- Marcaillou, B., Henry, P., Kinoshita, M. and et al. (2012) Seismogenic zone temperatures and heat-flow anomalies in the To-nankai margin segment based on temperature data from IODP expedition 333 and thermal model. *Earth Planet. Sci. Lett.* 349-350, 171-185.
- Marone, C. (1998) Laboratory-derived friction laws and their application to seismic faulting. *Ann. Rev. Earth Planet. Sci.* 26, 643-696.
- Marone, C., Raleigh, C.B. and Scholz, C.H. (1990) Frictional behavior and constitutive modeling of simulated fault gouge. *J. Geophys. Res.* 95, 7007-7025.

- Matsumura, M., Hashimoto, Y., Kimura, G., Ohmori-Ikehara, K., Enjohji, M. and Ikesawa, E. (2003) Depth of oceanic-crust underplating in a subduction zone: Inferences from fluid-inclusion analyses of crack-seal veins. *Geology* 31, 1005-1008.
- Mazzotti, S., Dragert, H., Henton, J., Schmidt, M., Hyndman, R.D., James, T.S., Lu, Y. and Craymer, M. (2003) Current tectonics of northern Cascadia from a decade of GPS measurements. *J. Geophys. Res.* 108, 1-18.
- Mazzotti, S., Le Pichon, X., Henry, P. and Miyazaki, S.-I. (2000) Full interseismic locking of the Nankai and Japan-west Kurile subduction zones' An analysis of uniform elastic strain accumulation in Japan constrained by permanent GPS. *J. Geophys. Res.* 105, 13,159-113,177.
- Meneghini, F., Di Toro, G., Rowe, C.D., Moore, J.C., Tsutsumi, A. and Yamaguchi, A. (2010) Record of mega-earthquakes in subduction thrusts: The black fault rocks of Pasagshak Point (Kodiak Island, Alaska). *GSA Bull.* 122, 1280-1297.
- Meneghini, F., Marroni, M., Moore, J.C., Pandolfi, L. and Rowe, C.D. (2009) The processes of underthrusting and underplating in the geologic record: structural diversity between the Franciscan Complex (California), the Kodiak Complex (Alaska) and the Internal Ligurian Units (Italy). *Geol. J.* 44, 126-152.
- Meneghini, F., Marroni, M. and Pandolfi, L. (2007) Fluid flow during accretion in sediment-dominated margins: Evidence of a high-permeability fossil fault zone from the Internal Ligurian accretionary units of the Northern Apennines, Italy. *J. Struct. Geol.* 29, 519-527.
- Meneghini, F. and Moore, J.C. (2007) Deformation and hydrofracture in a subduction thrust at seismogenic depths: The Rodeo Cove thrust zone, Marin Headlands, California. *GSA Bull.* 119, 174-183.
- Merino, E., Harvey, C. and Murray, H.H. (1989) Aqueous-chemical control of the tetrahedral-aluminum content of quartz, halloysite, and other low-temperature silicates. *Clays Clay Miner.* 37, 135-142.
- Merriman, R. and Frey, M. (1999) Very low-grade metapelites: mineralogy, microfabrics and measuring reaction progress, in: Frey, M., Merriman, R. (Eds.), *Low-grade metamorphism*. Blackwell Science, pp. 10-60.
- Mingram, B. and Bräuer, K. (2001) Amonium concentration and Nitrogen isotope composition in metasedimentary rocks from different tectonometamorphic units of the European Variscan Belt. *Geochim. Cosmochim. Ac.* 65, 273-287.
- Mittempergher, S., Cerchiari, A., Remitti, F. and Festa, A. (2018) From soft sediment deformation to fluid assisted faulting in the shallow part of a subduction megathrust analogue: the Sestola Vidiciatico tectonic Unit (Northern Apennines, Italy). *Geol. Mag.* 155, 438-450.
- Miyazaki, S., Segall, P., Fukuda, J. and Kato, T. (2004) Space time distribution of afterslip following the 2003 Tokachi-oki earthquake: Implications for variations in fault zone frictional properties. *Geophys. Res. Lett.* 31, 1-4.
- Mochizuki, K., Yamada, T., Shinohara, M., Yamanaka, Y. and Kanazawa, T. (2008) Weak interplate coupling by seamounts and repeating  $M \sim 7$  earthquakes. *Science* 321, 1194-1198.
- Moore, G., Park, J.O., Bangs, N.L., Gulick, S.P., Tobin, H.J., Nakamura, Y., Saito, S., Tsuji, T., Yoro, T., Tanaka, H., Uraki, S., Kido, Y., Sanada, Y., Kuramoto, S. and Taira, A. (2009) Structural and seismic stratigraphic framework of the NanTroSEIZE Stage 1 transect, in: Kinoshita, M., Tobin, H., Ashi, J., Kimura, G., Lallemand, S., Sreaton, E.J., Curewitz, D., Masago, H., Moe, K.T., Expedition 314/315/316 Scientists (Eds.), *Proc. IODP, 314/315/316*. Integrated Ocean Drilling Program Management International, Inc., Washington, DC, pp. 1-46.
- Moore, J.C. (2000) Synthesis of Results: Logging While Drilling, Northern Barbados Accretionary Prism, in: Moore, J.C., Klaus, A., Bangs, N.L., Bekins, B.A., Bruckman, W., Bucker, C.J., Erickson, S.N., Hansen, O. (Eds.), *Proc. ODP, Sci. Results, 171A*, pp. 1-25.
- Moore, J.C., Klaus, A., Bangs, N.L., Bekins, B.A., Bucker, C.J., Bruckman, W., Erickson, S.N., Hansen, O., Horton, T., Ireland, P., Olson Major, C., Moore, G.F., Peacock, S., Saito, S., Sreaton, E.J., Shimeld, J.W., Henry Stauffer, P., Taymaz, T., Teas, P.A. and Tokunaga, T.

- (1998) Consolidation patterns during initiation and evolution of a plate-boundary decollement zone: Northern Barbados accretionary prism. *Geology* 26, 811-814.
- Moore, J.C. and Saffer, D. (2001) Updip limit of the seismogenic zone beneath the accretionary prism of southwest Japan: An effect of diagenetic to low-grade metamorphic processes and increasing effective stress. *Geology* 29, 183-186.
- Moore, J.C. and Wheeler, R.L. (1978) Structural fabric of a mélangé, Kodiak Islands, Alaska. *Am. J. Sci.* 278, 739-765.
- Moreno, M., Haberland, C., Oncken, O., Rietbrock, A., Angiboust, S. and Heidbach, O. (2014) Locking of the Chile subduction zone controlled by fluid pressure before the 2010 earthquake. *Nature Geoscience* 7, 292-296.
- Moreno, M., Rosenau, M. and Oncken, O. (2010) 2010 Maule earthquake slip correlates with pre-seismic locking of Andean subduction zone. *Nature* 467, 198-204.
- Morris, J.D. and Villinger, H.W. (2006) Leg 205 synthesis: subduction fluxes and fluid flow across the Costa Rica convergent margin, in: Morris, J.D., Villinger, H.W., Klaus, A. (Eds.), *Proc. ODP, Sci. Rpts*, vol. 205, p. doi:10.2973/odp.proc.sr.2205.2006.
- Morrow, C., Radney, B. and Byerlee, J.D. (1992) Frictional strength and effective pressure law of montmorillonite and illite clays, in: Evans, B. (Ed.), *Fault mechanics and transport properties of rocks*, San Diego, CA, pp. 69-88.
- Mottl, M., Wheat, C.G., Fryer, P. and Gharib, J. (2004) Chemistry of springs across the Mariana forearc shows progressive devolatilization of the subducting plate. *Geochim. Cosmochim. Ac.* 68, 4915-4933.
- Mukoyoshi, H., Hirono, T., Hara, H., Sekine, K., Tsuchiya, N., Sakaguchi, A. and Soh, W. (2009) Style of fluid flow and deformation in and around an ancient out-of-sequence thrust: An example from the Nobeoka Tectonic Line in the Shimanto accretionary complex, southwest Japan. *Island Arc* 18, 333-351.
- Mukoyoshi, H., Sakaguchi, A., Otsuki, K., Hirono, T. and Soh, W. (2006) Co-seismic frictional melting along an out-of-sequence thrust in the Shimanto accretionary complex. Implications on the tsunamigenic potential of splay faults in modern subduction zones. *Earth Planet. Sci. Lett.* 245, 330-343.
- Mullis, J. (1975) Growth conditions of quartz crystals from Val d'Illiez (Valais, Switzerland). *Schweiz. Miner. Petrog. Mitt.* 55, 419-429.
- Mullis, J. (1988a) Rapid subsidence and upthrusting in the Northern Apennines, deduced by fluid inclusion studies in quartz crystals from Porretta Terme. *Schweiz. Miner. Petrog. Mitt.* 68, 157-170.
- Mullis, J. (1988d) Rapid subsidence and upthrusting in the Northern Apennines, deduced from fluid inclusion studies in quartz crystals from Poretta Terme. *Schweiz. Miner. Petrog. Mitt.* 68, 157-170.
- Mullis, J., Dubessy, J., Poty, B. and O'Neil, J. (1994) Fluid regimes during late stages of a continental collision: Physical, chemical, and stable isotope measurements of fluid inclusions in fissure quartz from a geotraverse in the Central Alps, Switzerland. *Geochim. Cosmochim. Ac.* 58, 2239-2267.
- Murata, A. (1996) Nappe structures of the Shimanto terrane of the Mikado-Osuzuyama area in East Kyushu. *Natural Science Research, Faculty of Integrated Arts and Sciences, The University of Tokushima* 9, 49-61 (in Japanese with English abstract).
- Murata, A. (1997) Geological map of Miyazaki prefecture, 1:200,000. Miyazaki Prefectural Government.
- Murata, A. (1998) Duplexes and low-angle nappe structures of the Shimanto terrane, southwest Japan. *Memoir of Geological Society of Japan* 50, 147-158 (in Japanese with English abstract).
- Nakashima, S. (1995) Diffusivity of ions in pore water as a quantitative basis for rock deformation rate estimates. *Tectonophysics* 245, 185-203.
- Nicholson, T., Bostock, M. and Cassidy, J.F. (2005) New constraints on subduction zone structure in northern Cascadia. *Geophys. J. Int.* 161, 849-859.

- Niemeijer, A.R. and Spiers, C.J. (2007) A microphysical model for strong velocity weakening in phyllosilicate-bearing fault gouges. *J. Geophys. Res.* 112.
- Niemeijer, A.R., Spiers, C.J. and Bos, B. (2002) Compaction creep of quartz sand at 400-600°C: experimental evidence for dissolution-controlled pressure solution. *Earth Planet. Sci. Lett.* 195, 261-275.
- Niu, B., Yoshimura, T. and Hirai, A. (2000) Smectite diagenesis in Neogene marine sandstone and mudstone of the Niigata Basin, Japan. *Clays and Clay Minerals* 48, 26-42.
- Obara, K. (2002) Nonvolcanic deep tremor associated with subduction in southwest Japan. *Science* 296, 1679-1681.
- Obara, K., Hirose, H., Yamamizu, F. and Kasahara, K. (2004) Episodic slow slip events accompanied by non-volcanic tremors in southwest Japan subduction zone. *Geophys. Res. Lett.* 31, 1-4.
- Oelkers, E.H., Bjorkum, P.A., Walderhaug, O., Nadeau, P.H. and Murphy, W.M. (2000) Making diagenesis obey thermodynamics and kinetics: the case of quartz cementation in sandstones from offshore mid-Norway. *Applied Geochemistry* 15, 295-309.
- Ohsawa, S., Amita, K., Yamada, M., Mishima, T. and Kazahaya, K. (2010) Geochemical features and genetic process of hot-spring waters discharged from deep hot-spring wells in the Miyazaki Plain, Kyushu Island, Japan: diagenetic dehydrated fluid as a source fluid of hot-spring water. *Journal of hot spring science* 59, 295-319.
- Okada, Y. (1992) Internal deformation due to shear and tensile faults in a half-space. *Bull. Seism. Soc. Am.* 82, 1018-1040.
- Okumura, K., Teraoka, Y., Imai, I., Hoshizumi, H., Ono, K. and Shishido, A. (2010) Geological Map of Japan, 1:50,000, Nobeoka. Geological Survey of Japan.
- Oleskevich, D.A., Hyndman, R.D. and Wang, K. (1999) The updip and downdip limits to great subduction earthquakes: Thermal and structural models of Cascadia, south Alaska, SW Japan, and Chile. *J. Geoph. Res.* 104, 14965-14991.
- Omlin, S., Malvoisin, B. and Podlachikov, Y.Y. (2017) Pore fluid extraction by reactive solitary waves in 3-D. *Geophysical Research Letters* 44, 9267-9275.
- Onishi, C.T. and Kimura, G. (1995) Change in fabric of mélangé in the Shimanto Belt, Japan: Change in relative convergence? *Tectonics* 14, 1273-1289.
- Onishi, C.T., Kimura, G., Hashimoto, Y., Ikehara-Ohmori, K. and Watanabe, T. (2001) Deformation history of tectonic mélangé and its relationship to the underplating process and relative plate motion: An example from the deeply buried Shimanto Belt, SW Japan. *Tectonics* 20, 376-393.
- Osozawa, S., Sakai, T. and Naito, T. (1990) Miocene subduction of an active midocean ridge and origin of the Setogawa ophiolite, central Japan. *Journal of Geology* 98.
- Ozawa, K., Suito, H. and Tobita, M. (2007) Occurrence of quasi-periodic slow-slip off the east coast of the Boso peninsula, Central Japan. *Earth Planets Space* 59, 1241-1245.
- Ozawa, S., Nishimura, T., Suito, H., Kobayashi, T., Tobita, M. and Imakiire, T. (2011) Coseismic and postseismic slip of the 2011 magnitude-9 Tohoku-Oki earthquake. *Nature* 475, doi:10.1038/nature10227.
- Pacheco, J.F., Sykes, L.R. and Scholz, C.H. (1993) Nature of seismic coupling along simple plate boundaries of the subduction tyoe. *J. Geophys. Res.* 98, 14,133-114,159.
- Palazzin, G. (2016) Brittle-ductile transition in subduction zones: the role of quartz. University of Orléans, p. 188pp.
- Palazzin, G., Raimbourg, H., Famin, V., Jolivet, L., Kusaba, Y. and Yamaguchi, A. (2016) Deformation processes at the down-dip limit of the seismogenic zone: The example of Shimanto accretionary complex. *Tectonophysics* 687, 28-43.
- Palazzin, G., Raimbourg, H., Stünitz, H., Heilbronner, R., Neufeld, K. and Précigout, J. (2018) Evolution in H<sub>2</sub>O contents during deformation of polycrystalline quartz: an experimental study. *J. Struct. Geol.* 114, 95-110.

- Park, J.O., Tsuru, T., Takahashi, N., Hori, T., Kodaira, S., Nakanishi, A., Miura, S. and Kaneda, Y. (2002) A deep strong reflector in the Nankai accretionary wedge from multichannel seismic data: Implications for underplating and interseismic shear stress release. *J. Geophys. Res.* 107.
- Parry, W.T. and Bruhn, R.L. (1990) Fluid pressure transients on seismogenic normal faults. *Tectonophysics* 179, 335-344.
- Perfettini, H., Avouac, J.-P., Tavera, H., Kositsky, A., Nocquet, J.-M., Bondoux, F., Chlieh, M., Sladen, A., Audin, L., Farber, D.L. and Soler, P. (2010) Seismic and aseismic slip on the Central Peru megathrust. *Nature* 465.
- Philippot, P., Agrinier, P. and Scambelluri, M. (1998) Chlorine cycling during subduction of altered oceanic crust. *Earth Planet. Sci. Lett.* 161, 33-44.
- Philippot, P. and Selverstone, J. (1991) Trace-element-rich brines in eclogitic veins: implications for fluid composition and transport during subduction. *Contrib. Mineral. Petrol.* 106, 417-430.
- Plank, T. and Langmuir, C.H. (1998) The chemical composition of subducting sediment and its consequences for the crust and mantle. *Chem. Geol.* 145, 325-394.
- Plank, T. and Ludden, J. (1992) Geochemistry of sediments in the Argo Abyssal Plain at Site 765: a continental margin reference section for sediment recycling in subduction zones, in: Gradstein, F.M., Ludden, J.N. (Eds.), *Proc. ODP, Sci. Results*, vol. 123, College Station, TX (Ocean Drilling Program), pp. 167-189.
- Pognante, U. (1989) Early Alpine eclogitisation in talc/chloritoid - bearing Mg-metagabbros and in jadeite - Fe-omphacite - bearing metatrandhjemetes from the ophiolites of the Western Alps. *Rendiconti della Societa Italiana di Mineralogia e Petrologia* 43, 687-704.
- Pudsey, C.J. (1984) X-Ray Mineralogy of Miocene and Older Sediments from Deep Sea Drilling Project Leg 78A, in: Biju-Duval, B., Moore, J.C., et al. (Eds.), *Proc. DSDP, Init. Repts*, vol 78A, pp. 325-342.
- Pytte, A.M. and Reynolds, R.C. (1989) The thermal transformation of smectite to illite, in: Naeser, N.D., McCulloh, T.H. (Eds.), *Thermal history of sedimentary Basins: Methods and case histories*. Springer-Verlag, New York, pp. 33-40.
- Raimbourg, H., Augier, R., Famin, V., Gadenne, L., Palazzin, G., Yamaguchi, A. and Kimura, G. (2014a) Long-term evolution of an accretionary prism: the case study of the Shimanto Belt, Kyushu, Japan. *Tectonics* 33, 1-24.
- Raimbourg, H., Famin, V., Palazzin, G., Mayoux, M., Jolivet, L., Ramboz, C. and Yamaguchi, A. (2018) Fluid properties and dynamics along the seismogenic plate interface. *Geosphere: Subduction top to bottom* 2 14, 1-23.
- Raimbourg, H., Famin, V., Palazzin, G., Sakaguchi, A., Yamaguchi, A. and Augier, R. (2017a) Tertiary evolution of the Shimanto Belt (Japan): a large-scale collision in Early Miocene. *Tectonics* 36, 1-21.
- Raimbourg, H., Hamano, Y., Saito, S., Kinoshita, M. and Kopf, A. (2011) Acoustic and mechanical properties of Nankai accretionary prism core samples. *Geochem. Geophys. Geosyst.* 12, doi:10.1029/2010GC003169.
- Raimbourg, H., Jolivet, L. and Leroy, Y. (2007b) Consequences of progressive eclogitisation on crustal exhumation, a mechanical study. *Geophys. J. Int.* 168, 379-401.
- Raimbourg, H., Shibata, T., Yamaguchi, A., Yamaguchi, H. and Kimura, G. (2009) Horizontal shortening versus vertical loading in accretionary prisms. *Geochem. Geophys. Geosyst.* 10, 1-17.
- Raimbourg, H., Thiéry, R., Vacelet, M., Famin, V., Ramboz, C., Boussafir, M., Disnar, J.-R. and Yamaguchi, A. (2017j) Organic matter cracking: a source of fluid overpressure in subducting sediments. *Tectonophysics* 721, 254-274.
- Raimbourg, H., Thiery, R., Vacelet, M., Ramboz, C., Cluzel, N., Trong, E.L., Yamaguchi, A. and Kimura, G. (2014b) A new method of reconstituting the P-T conditions of fluid circulation in an accretionary prism (Shimanto, Japan) from microthermometry of methane-bearing aqueous inclusions. *Geochim Cosmochim Acta* 125, 96-109.

- Raimbourg, H., Vacelet, M., Ramboz, C., Famin, V., Augier, R., Palazzin, G., Yamaguchi, A. and Kimura, G. (2015) Fluid circulation in the depths of accretionary prisms: an example of the Shimanto Belt, Kyushu, Japan. *Tectonophysics* 655, 161-176.
- Raj, R. (1982) Creep in polycrystalline aggregates by matter transport through a liquid phase. *J. Geophys. Res.* 87, 4731-4739.
- Raj, R. and Chyung, C.K. (1981) Solution-precipitation creep in glass ceramics. *Acta Metallurgica* 29, 159-166.
- Ramseyer, K., Fisher, J., Matter, A., Eberhardt, P. and Geiss, J. (1989) A cathodoluminescence microscope for low intensity luminescence. *J. Sediment. Petrol.* 59, 619-622.
- Ranalli, G. (1995) *Rheology of the Earth*, 2nd ed. Chapman and Hall, New York.
- Ranero, C.R., Morgan, J.P., McIntosh, K. and Reichert, C. (2003) Bending-related faulting and mantle serpentinization at the Middle America trench. *Nature* 425, 367-373.
- Renard, F., Gratier, J.P. and Jamtveit, B. (2000) Kinetics of crack-sealing, intergranular pressure solution, and compaction around active faults. *J. Struct. Geol.* 22, 1395-1407.
- Renard, F. and Ortoleva, P. (1997) Water films at grain-grain contacts: Debye-Hückel, osmotic model of stress, salinity, and mineralogy dependence. *Geochimica et Cosmochimica Acta* 61, 1963-1970.
- Renard, F., Ortoleva, P. and Gratier, J.P. (1997) Pressure solution in sandstones: influence of clays and dependence on temperature and stress. *Tectonophysics* 280, 257-266.
- Rice, J.R. and Rudnicki, J.W. (1979) Earthquake precursory effects due to pore fluid stabilization of a weakening fault zone. *J. Geophys. Res.* 84, 2177-2193.
- Rimstidt, J.D. and Barnes, H.L. (1980) The kinetics of silica-water reactions. *Geochimica et Cosmochimica Acta* 44, 1683-1699.
- Ring, U., Ratschbacher, L., Frisch, W., Biehler, D. and Kralik, M. (1989) Kinematics of the Alpine plate-margin: structural styles, strain and motion along the Penninic- Austroalpine boundary in the Swiss- Austrian Alps. *J. Geol. Soc.* 146, 835-849.
- Robert, F., Boullier, A.M. and Firdaous, K. (1995) Gold-quartz veins in metamorphic terranes and their bearing on the role of fluids in faulting. *J. Geophys. Res.* 100, 12,861-812,879.
- Rogers, G. and Dragert, H. (2003) Episodic tremor and slip on the Cascadia subduction zone: the chatter of silent slip. *Science* 300, 1942-1943.
- Rowe, C.D., Meneghini, F. and Moore, J.C. (2009) Fluid-rich damage zone of an ancient out-of-sequence thrust, Kodiak Islands, Alaska. *Tectonics* 28, 1-20.
- Rowe, C.D., Meneghini, F. and Moore, J.C. (2011) Textural record of the seismic cycle: strain-rate variation in an ancient subduction thrust. *Geol. Soc. Lond. Spec. Publ.* 359, 77-95.
- Rowe, C.D., Moore, J.C., Meneghini, F. and McKeirnan, A.W. (2005) Large-scale pseudotachylytes and fluidized cataclasites from an ancient subduction thrust fault. *Geology* 33, 937-940.
- Rowe, C.D., Moore, J.C., Remitti, F. and IODP Expedition 343/343T Scientists (2013) The thickness of subduction plate boundary faults from the seafloor into the seismogenic zone. *Geology* 41, 991-994.
- Rubin, A.M. (2008) Episodic slow slip events and rate-and-state friction. *J. Geophys. Res.* 113, 1-18.
- Rubinstein, J.L., Vidale, J.E., Gomberg, J., Bodin, P., Creager, K.C. and Malone, S.D. (2007) Non-volcanic tremor driven by large transient shear stresses. *Nature* 448, 579-582.
- Ruff, L.J. (1989) Do trench sediments affect great earthquake occurrence in subduction zones? *Pure and Applied Geophysics* 129, 263-282.
- Ruff, L.J. and Kanamori, H. (1980) Seismicity and the subduction process. *Phys. Earth Planet. Inter.* 23.
- Ruina, A. (1983) Slip instability and state variable friction laws. *J. Geophys. Res.* 88, 10359-10370.

- Rumyantsev, V.N. and Novozhilov, A.I. (1980) Dependence of concentration of aluminum centers and anomalous pleochroism on certain crystallization parameters in synthetic quartz. *Soviets Physics-Crystallography* 25, 75-78.
- Rutter, E.H. (1976) The kinetics of rock deformation by pressure solution. *Phil. Trans. R. Soc. Lond. A* 283, 203-219.
- Saar, M.O. and Manga, M. (1999) Permeability-porosity relationship in vesicular basalts. *Geophys. Res. Lett.* 26, 111-114.
- Sadofsky, S.J. and Bebout, G.E. (2001) Paleohydrology at 5- to 50-kilometer depths of accretionary prisms: The Franciscan Complex, California. *Geophys. Res. Lett.* 28, 2309-2312.
- Sadofsky, S.J. and Bebout, G.E. (2003) Record of forearc devolatilization in low-T, high-P/T metasedimentary suites: Significance for models of convergent margin chemical cycling. *Geochem. Geophys. Geosyst.* 4, 29.
- Sadofsky, S.J. and Bebout, G.E. (2004) Field and isotopic evidence for fluid mobility in the Franciscan Complex: forearc paleohydrogeology to depths of 30 kilometers. *Int. Geol. Rev.* 46, 1053-1088.
- Saffer, D., Lockner, D.A. and McKiernan, A.W. (2012) Effects of smectite to illite transformation on the frictional strength and sliding stability of intact marine mudstones. *Geophys. Res. Lett.* 39, 1-6.
- Saffer, D. and Tobin, H.J. (2011) Hydrogeology and mechanics of subduction zone forearcs: Fluid flow and pore pressure. *Ann. Rev. Earth Planet. Sci.* 39, 157-186.
- Saffer, D., Underwood, M. and McKiernan, A.W. (2008) Evaluation of factors controlling smectite transformation and fluid production in subduction zones: Application to the Nankai Trough. *Island Arc* 17.
- Saffer, D. and Wallace, L.M. (2015) The frictional, hydrologic, metamorphic and thermal habitat of shallow slow earthquakes. *Nature Geoscience* 8, 594-600.
- Saffer, D.M. and Bekins, B.A. (2006) An evaluation of factors influencing pore pressure in accretionary complexes: Implications for taper angle and wedge mechanics. *J. Geophys. Res.* 111, doi:10.1029/2005JB003990.
- Sagiya, T. (2004) Interplate Coupling in the Kanto District, Central Japan, and the Boso Peninsula Silent Earthquake in May 1996. *Pure Appl. Geophys.* 161, 2327-2342.
- Saishu, H., Okamoto, A. and Otsubo, M. (2017) Silica precipitation potentially controls earthquake recurrence in seismogenic zones. *Scientific Reports* 7, 1-10.
- Saito, M., Kimura, K., Naito, K. and Sakai, A. (1996) Geological Map of Japan, 1:50,000, Shiobamuro. Geological Survey of Japan.
- Saito, T., Ujiie, K., Tsutsumi, A., Kameda, J. and Shibasaki, B. (2013) Geological and frictional aspects of very-low-frequency earthquakes in an accretionary prism. *Geophys. Res. Lett.* 40, 703-708.
- Sakaguchi, A. (1999a) Thermal maturity in the Shimanto accretionary prism, southwest Japan, with the thermal change of the subducting slab: Fluid inclusion and vitrinite reflectance study. *Earth Planet. Sci. Lett.* 173, 61-74.
- Sakaguchi, A. (1999b) Thermal structure and paleo-heat flow in the Shimanto accretionary prism, Southwest Japan. *The Island Arc* 8, 359-372.
- Sakaguchi, A. (2003) Observation of the seismogenic fault in the Okitsu Melange, Shimanto Accretionary Complex and stick-slip of mineral cementation of shear experiment. *J. Geography* 112, 885-896.
- Sakaguchi, A., Hashimoto, Y., Mukoyoshi, H., Yokota, T., Takagi, M. and Kikuchi, T. (2006) Seismogenic fault-rock and fluid flow in ancient subduction zone: Field guide of Okitsu, Kure and Yokonami Mélanges, Cretaceous Shimanto accretionary complex, Shikoku, Japan. *J. Geol. Soc. Japan* 112, 71-88 (in Japanese).
- Sakai, H. (1988) Origin of the Misaki Olistostrome Belt and re-examination fo the Takachiho Orogeny. *J. Geol. Soc. Jpn.* 94, 945-961.

- Sakai, T. (1985) Geology of the Nichinan Group and the process of production of the outermargin olisthostrome belt of the Shimanto terrane, Mem. Symp. on formation of slump facies and their relationship to tectonics, some problems on the deformation of unconsolidated sediments. Tectonic Research Group of Japan, Tsukuba, pp. 95-116 (in Japanese with english abstract).
- Sakai, T., Nishi, H., Saito, T., Nakaseko, K. and Nishimura, A. (1984) Microfossil stratigraphy of the Paleogene system in Kyushu Shimanto Belt, in: Saito, T., Okada, H., Kaiho, K. (Eds.), Biostratigraphy and international correlation of the Paleogene system in Japan. Yamagata University, pp. 95-112 (in Japanese with english abstract).
- Sakamoto, T. (1977) Neogene systems, in: Tanaka, K., Nozawa, T. (Eds.), Geology and mineral resources of Japan. Geol. Survey of Japan, pp. 233-259.
- Sample, J.C. and Fisher, D.M. (1986) Duplex accretion and underplating in an ancient accretionary complex, Kodiak Islands, Alaska. *Geology* 14, 160-163.
- Sample, J.C. and Moore, J.C. (1987) Structural style and kinematics of an underplated slate belt, Kodiak and adjacent islands, Alaska. *GSA Bull.* 99, 7-20.
- Satake, K., Shimazaki, K., Tsuji, Y. and Ueda, K. (1996) Time and size of a giant earthquake in Cascadia inferred from Japanese tsunami records of January 1700. *Nature* 379, 246-249.
- Sawai, M., Niemeijer, A.R., Hirose, T. and Spiers, C.J. (2017) Frictional properties of JFAST core samples and implications for slow earthquakes at the Tohoku subduction zone. *Geophys. Res. Lett.* 44, 8822-8831.
- Scambelluri, M., Fiebig, J., Malaspina, N., Muntener, O. and Pettke, T. (2004a) Serpentinite subduction: implications for fluid processes and trace-element recycling. *Int. Geol. Rev.* 46, 595-613.
- Scambelluri, M., Müntener, O., Ottolini, L., Pettke, T.T. and Vannucci, R. (2004e) The fate of B, Cl and Li in the subducted oceanic mantle and in the antigorite breakdown fluids. *Earth and Planet Sci. Lett.* 222, 217-234.
- Scambelluri, M., Pennacchioni, G. and Philippot, P. (1998) Salt-rich aqueous fluids formed during eclogitization of metabasites in the Alpine continental crust (Austroalpine Mt. Emilius unit, Italian western Alps). *Lithos* 43, 151-167.
- Scambelluri, M. and Philippot, P. (2001) Deep fluids in subduction zones. *Lithos* 55, 213-227.
- Scambelluri, M. and Philippot, P. (2004) Volatile and mobile element recycling during subduction of the oceanic lithosphere. Insights from metasediments and serpentinites of the Alps. *Periodico di mineralogia* 73, 221-233.
- Scambelluri, M., Picardo, G.B., Philippot, P., Robbiano, A. and Negretti, L. (1997) High salinity fluid inclusions formed from recycled seawater in deeply subducted alpine serpentinite. *Earth Planet. Sci. Lett.* 148, 485-499.
- Scambelluri, M., Rampone, E. and Piccardo, G.B. (2001) Fluid and element cycling in subducted serpentinite: a trace elements study of the Erro-Tobbio high-pressure ultramafites (Western Alps, NW Italy). *J. Petrol.* 42, 55-67.
- Schmidt, M.W. and Poli, S. (1998) Experimentally based water budgets for dehydrating slabs and consequences for arc magma generation. *Earth and Planetary Science Letters* 163, 361-379.
- Scholz, C. (1990) *The mechanics of earthquakes and faulting*. Cambridge University Press.
- Scholz, C. (1995) On the mechanism of seismic decoupling and the back arc spreading at subduction zones. *J. Geophys. Res.* 100, 22,105-122,115.
- Scholz, C. (1998) Earthquakes and friction laws. *Nature* 391, 37-42.
- Schutjens, P.M.T.M. (1991) Experimental compaction of quartz sand at low effective stress and temperature conditions. *J. Geol. Soc.* 148, 527-539.
- Scientists, E. (2006) Site 1256, in: Teagle, D.A.H., Alt, J.C., Umino, S., Miyashita, S., Banerjee, N.R. (Eds.), Proc. IODP, 309/312. Integrated Ocean Drilling Program Management International, Inc, Washington, DC, pp. 1-549.
- Segall, P. and Rice, J.R. (1995) Dilatancy, compaction, and slip instability of a fluid-infiltrated fault. *J. Geophys. Res.* 100, 22,155-122,171.

- Segall, P. and Rice, J.R. (2006) Do shear heating of pore fluid contribute to earthquake nucleation? *J. Geophys. Res.* 111, 1-17.
- Shearer, P. and Bürgmann, R. (2010) Lessons learned from the 2004 Sumatra-Andaman Megathrust rupture. *Ann. Rev. Earth Planet. Sci.* 38, 103-131.
- Shelly, D.R., Beroza, G.C. and Ide, S. (2007) Non-volcanic tremor and low-frequency earthquake swarms. *Nature* 446, 305-307.
- Shelly, D.R., Beroza, G.C., Ide, S. and Nakamura, S. (2006) Low-frequency earthquakes in Shikoku, Japan, and their relationship to episodic tremor and slip. *Nature* 442, 188-191.
- Shibata, T., Orihashi, Y., Kimura, G. and Hashimoto, Y. (2008) Underplating of mélange evidenced by the depositional ages: U–Pb dating of zircons from the Shimanto accretionary complex, southwest Japan. *Island Arc* 17, 376-393.
- Shipboard Scientific Party (1984) Site 543: oceanic reference site east of the Barbados Ridge Complex, in: Biju-Duval, B., Moore, J.C., et al. (Eds.), *Init. Repts DSDP, College Station, TX (Ocean Drilling Program)*, pp. 1-72.
- Shipboard Scientific Party (1991) Site 808, in: Taira, A., Hill, I., Firth, J.V., et al. (Eds.), *Proc. ODP, Init. Repts, vol 131*, pp. 71-269.
- Shipboard Scientific Party (1997) Site 1040, in: Kimura, G., Silver, E.A., Blum, P., et al. (Eds.), *Proc. ODP, Init. Repts, College Station, TX (Ocean Drilling Program)*, pp. 1-58.
- Shipboard Scientific Party (2001) Site 1174, in: Moore, G.F., Taira, A., et al. (Eds.), *Proc. ODP, Init. Repts, College Station, TX (Ocean Drilling Program)*, pp. 1-149.
- Shibley, T.H., Stoffa, P.L. and Dean, D.F. (1990) Underthrust sediments, fluid migration paths, and mud volcanoes associated with the accretionary wedge off Costa Rica: Middle America Trench. *J. Geophys. Res.* 95, 8743-8752.
- Shreve, R.L. and Cloos, M. (1986) Dynamics of sediment subduction, melange formation, and prism accretion. *Journal of Geophysical Research* 91, 10229-10245.
- Sibson, R.H. (1973) Interactions between temperature and fluid pressure during earthquake faulting - A mechanism for partial or total stress relief. *Nature* 243, 66-68.
- Sibson, R.H. (1994) Crustal stress, faulting and fluid flow. *Special Publications of the Geological society of London* 78, 69-84.
- Sibson, R.H. (2003) Thickness of the seismic slip zone. *Bull. Seism. Soc. Am.* 93, 1169-1178.
- Simons, M., Minson, S.E., Sladen, A. and et al. (2011) The 2011 magnitude 9.0 Tohoku-Oki earthquake: Mosaicking the megathrust from seconds to centuries. *Science* 332, doi: 10.1126/science.1206731.
- Spiers, C.J., Peach, C.J., Brzesowsky, R.H., Schutjens, P.M.T.M., Liezenberg, J.L. and Zwart, H.J. (1989) Long-term rheological and transport properties of dry and wet salt rocks, EUR 11848 EN. Nuclear Science and Technology, Office for Official Publications of the European Communities, Luxembourg.
- Spinelli, G., Mozley, P.S., Tobin, H.J., Underwood, M.B., Hoffman, N.W. and Bellew, G.M. (2007) Diagenesis, sediment strength, and pore collapse in sediment approaching the Nankai Trough subduction zone. *GSA Bull.* 119, 377-390.
- Spinelli, G. and Saffer, D. (2004) Along-strike variations in underthrust sediment dewatering on the Nicoya margin, Costa Rica related to the updip limit of seismicity. *Geophys. Res. Lett.* 31, 1-5.
- Spinelli, G.A., Saffer, D.M. and Underwood, M. (2006) Hydrogeologic responses to three-dimensional temperature variability, Costa Rica subduction margin. *J. Geophys. Res.* 111.
- Spivack, A.J., Palmer, M.R. and Edmond, J.M. (1987) The sedimentary cycle of the boron isotopes. *Geochim. Cosmochim. Ac.* 51, 1939-1949.
- Staudigel, H., Hart, S.R., Schmincke, H.-U. and Smith, B.M. (1989) Cretaceous ocean crust at DSDP Sites 417 and 418: Carbon uptake from weathering versus loss by magmatic outgassing. *Geochimica et Cosmochimica Acta* 53, 3091-3094.

- Sterner, S.M. and Bodnar, R.J. (1989) Synthetic fluid inclusions - VII. Re-equilibration of fluid inclusions in quartz during laboratory-simulated metamorphic burial and uplift. *J. Metamorphic Geol.* 7, 243-260.
- Stuart, W.D. (1988) Forecast model for great earthquakes at the Nankai Trough subduction zone. *Pure Appl. Geophys.* 126, 619-641.
- Suito, H., Nishimura, T., Tobita, M., Imakiire, T. and Ozawa, S. (2011) Interplate fault slip along the Japan Trench before the occurrence of the 2011 off the Pacific coast of Tohoku Earthquake as inferred from GPS data. *Earth Planets And Space* 63, 615-619.
- Suzuki, K., Hino, R., Ito, Y., Yamamoto, Y., Suzuki, S., Fujimoto, H., Shinohara, M., Abe, M., Kawaharada, Y., Hasegawa, Y. and Kaneda, Y. (2012) Seismicity near the hypocenter of the 2011 off the Pacific coast of Tohoku earthquake deduced by using ocean bottom seismographic data *Earth Planets and Space* in press.
- Taira, A. (1981) The Shimanto Belt of southwest Japan and arc-trench sedimentary tectonics. *Recent Progress of Natural Sciences in Japan* 6, 147-162.
- Taira, A., Katto, J., Tashiro, M., Okamura, M. and Kodama, K. (1988) The Shimanto Belt in Shikoku, Japan-Evolution of Cretaceous to Miocene accretionary prism. *Modern Geology* 12, 5-46.
- Taira, A., Okamura, M., Katto, J., Tashiro, H., Saito, Y., Kodama, K., Hashimoto, M., Chiba, T. and Aoki, T. (1980a) Lithofacies and geologic age relationship within mélangé zones of northern Shimanto Belt (Cretaceous), Kochi prefecture, in: Taira, A., Tashiro, H. (Eds.), *Geology and paleontology of the Shimanto Belt*. Rinyo Kosaikai Press, Kochi, pp. 319-389.
- Taira, A., Tashiro, M., Okamura, M. and Katto, J. (1980d) The geology of the Shimanto Belt in Kochi prefecture, Shikoku, in: Taira, A., Tashiro, H. (Eds.), *Geology and paleontology of the Shimanto Belt*. Rinyo Kosaikai Press, Kochi, pp. 319-389.
- Tajima, F., Mori, J. and Kennet, B.L.N. (2013) A review of the 2011 Tohoku-Oki earthquake (Mw 9.0): Large-scale rupture across heterogeneous plate coupling. *Tectonophysics* 586, 15-34.
- Tanaka, K. (1977) Pre-Neogene tectonic division, in: Tanaka, K., Nozawa, T. (Eds.), *Geology and mineral resources of Japan*. Geol. Survey of Japan, pp. 20-44.
- Tarantola, A., Müllis, J., Vennemann, T.W., Dubessy, J. and De Capitani, C. (2007) Oxidation of methane at the CH<sub>4</sub>/H<sub>2</sub>O-(CO<sub>2</sub>) transition zone in the external part of the Central Alps, Switzerland: Evidence from stable isotope investigations. *Chem. Geol.* 237, 329-357.
- Tembe, S., Lockner, D.A. and Wong, T.-F. (2010) Effect of clay content and mineralogy on frictional sliding behavior of simulated gouges: Binary and ternary mixtures of quartz, illite, and montmorillonite. *J. Geophys. Res.* 115, 1-22.
- Tenthorey, E. and Cox, S.F. (2006) Cohesive strengthening of fault zones during the interseismic period: An experimental study. *J. Geophys. Res.* 111, 1-14.
- Tichelaar, B.W. and Ruff, L.J. (1993) Depth of seismic coupling along subduction zones. *J. Geophys. Res.* 98, 2017-2037.
- Tobin, H.J. and Saffer, D.M. (2009) Elevated fluid pressure and extreme mechanical weakness of a plate boundary thrust, Nankai Trough subduction zone. *Geology* 37, 679-682.
- Tonai, S., Ito, S., Hashimoto, Y., Tamura, H. and Tomioka, N. (2016) Complete <sup>40</sup>Ar resetting in an ultracataclasite by reactivation of a fossil seismogenic fault along the subducting plate interface in the Mugi Mélangé of the Shimanto accretionary complex, southwest Japan. *J. Struct. Geol.* 89, 19-29.
- Toriumi, M. and Teruya, J. (1988) Tectono-metamorphism of the Shimanto Belt. *Modern Geology* 12, 303-324.
- Tse, S.T. and Rice, J.R. (1986) Crustal earthquake instability in relation to the depth variation of frictional slip properties. *J. Geophys. Res.* 91, 9452-9472.
- Tsinober, L.I. and Kamentsev, I.E. (1964) Effect of growth rate on the concentration of smoky color and on the unit cell parameters of synthetic quartz crystals. *Soviets Physics-Crystallography* 9, 374-376.

- Tsuji, T., Kimura, G., Okamoto, S., Kono, F., Mochinaga, H., Saeki, T. and Tokuyama, H. (2006) Modern and ancient seismogenic out-of-sequence thrusts in the Nankai accretionary prism: Comparison of laboratory-derived physical properties and seismic reflection data. *Geophys. Res. Lett.* 33, 1-5.
- Tsuru, T., Park, J.O., Takahashi, N., Kodaira, S., Kido, U., Kaneda, Y. and Kono, Y. (2000) Tectonic features of the Japan Trench convergent margin off Sanriku, northeastern Japan, revealed by multichannel seismic reflection data. *J. Geophys. Res.* 105, 16,403-416,413.
- Ujiie, K. (1997) Off-scraping accretionary process under the subduction of young oceanic crust: The Shimanto Belt of Okinawa, Ryukyu Arc. *Tectonics* 16, 305-322.
- Ujiie, K., Hisamitsu, T. and Soh, W. (2000) Magnetic and structural fabrics of the melange in the Shimanto accretionary complex, Okinawa Island: Implication for strain history during decollement-related deformation. *Journal of Geophysical Research* 105, 25729-25741.
- Ujiie, K., Saishu, H., Fagereng, A., Nishiyama, N., Otsubo, M., Masuyama, H. and Kagi, H. (2018) An explanation of episodic tremor and slow slip constrained by crack-seal veins and viscous shear in subduction mélange. *Geophys. Res. Lett.* 45, 5371-5379.
- Ujiie, K., Tanaka, H., Saito, T., Tsutsumi, A., Mori, J.J., Kameda, J., Brodsky, E.E., Chester, F.M., Eguchi, N., Toczko, S. and Expedition 343 and 343T Scientists (2013) Low coseismic shear stress on the Tohoku-Oki megathrust determined from laboratory experiments. *Science* 342, 1211-1214.
- Ujiie, K., Yamaguchi, H., Sakaguchi, A. and Toh, S. (2007) Pseudotachylytes in an ancient accretionary complex and implications for melt lubrication during subduction zone earthquakes. *J. Struct. Geol.* 29, 599-613.
- Uyeda, S. and Kanamori, H. (1979) Backarc opening and the mode of subduction. *J. Geophys. Res.* 84, 1049-1061.
- Vallée, M., Nocquet, J.-M., Battaglia, J., Font, Y. and et al. (2013) Intense interface seismicity triggered by a shallow slow slip event in the Central Ecuador subduction zone. *J. Geophys. Res.* 118, 2965-2981.
- van Dinther, Y., Gerya, T.V., Dalguer, L.A., Mai, P.M., Morra, G. and Giardini, D. (2013) The seismic cycle at subduction thrusts: Insights from seismo-thermo-mechanical models. *J. Geophys. Res.* 118, 1-20.
- Van Rijnsingen, E., Lallemand, S., Peyret, M., Arcay, D., Heuret, A., Funicello, F. and Corbi, F. (2018) How subduction interface roughness influences the occurrence of large interplate earthquakes. *G-cubed* 19, 2342-2370.
- Vannucchi, P., Remitti, F. and Bettelli, G. (2008) Geological record of fluid flow and seismogenesis along an erosive subducting plate boundary. *Nature* 451, 699-703.
- Vannucchi, P., Remitti, F., Bettelli, G., Boschi, C. and Dallai, L. (2010) Fluid history related to the early Eocene - middle Miocene convergent system of the Northern Apennines (Italy): Constraints from structural and isotopic studies. *J. Geophys. Res.* 115, 1-23.
- Vannucchi, P., Sage, F., Morgan, J.P., Remitti, F. and Collot, J.-Y. (2012) Toward a dynamic concept of the subduction channel at erosive convergent margins with implications for interplate material transfer. *G-cubed* 13, 1-24.
- Velde, B. (1984) Transformations of clay minerals, Thermal phenomena in sedimentary basins. Technip, Paris.
- Velde, B. (1996) Compaction trends of clay-rich deep sea sediments. *Mar. Geol.* 133, 193-201.
- Velde, B. and Vasseur, G. (1992) Estimation of the diagenetic smectite to illite transformation in time-temperature space. *Am. Mineral.* 77, 967-976.
- Vidal, O. and Dubacq, B. (2009) Thermodynamic modelling of clay dehydration, stability and compositional evolution with temperature, pressure and H<sub>2</sub>O activity. *Geochimica et Cosmochimica Acta* 73, 6544-6564.
- Vigny, C., Socquet, A., Peyrat, S., Ruegg, J.-C., Métois, M. and et al. (2011) The 2010 Mw 8.8 Maule megathrust earthquake of Central Chile, monitored by GPS. *Science* 332, 1417-1421.

- Vrolijk, P. (1987) Tectonically-driven fluid flow in the Kodiak accretionary complex, Alaska. *Geology* 15, 466-469.
- Vrolijk, P. (1987) Paleohydrogeology and fluid evolution of the Kodiak accretionary complex, Alaska. University of California, Santa Cruz, p. 232.
- Vrolijk, P. (1990) On the mechanical role of smectite in subduction zones. *Geology* 18, 703-707.
- Vrolijk, P., Chambers, S.R., Gieskes, J.M. and O'Neil, J. (1990) Stable isotope ratios of interstitial fluids from the Northern Barbados accretionary prism, ODP Leg 110, in: Moore, J.C., et al. (Eds.), *Proc. ODP, Sci. Results*, pp. 181-205.
- Vrolijk, P., Myers, G. and Moore, J.C. (1988) Warm fluid migration along tectonic melanges in the Kodiak accretionary complex, Alaska. *J. Geophys. Res.* 93, 10313-10324.
- Wagner, W. and Pruss, A. (2002) The IAPWS formulation 1995 for the thermodynamic properties of ordinary water substance for general and scientific use. *J. Phys. Chem. Ref. Data* 31, 387-535.
- Wakabayashi, J. (2011) Mélanges of the Franciscan Complex, California: Diverse structural settings, evidence for sedimentary mixing, and their connection to subduction processes. *GSA Spec. Paper* 480, 1-6.
- Wallace, L.M. and Beavan, J. (2006) A large slow slip event on the central Hikurangi subduction interface beneath the Manawatu region, North Island, New Zealand. *Geophys. Res. Lett.* 33, 1-4.
- Wallace, L.M. and Beavan, J. (2010) Diverse slow slip behavior at the Hikurangi subduction margin, New Zealand. *J. Geophys. Res.* 115, 1-20.
- Wang, C.-Y., Mao, N.-H. and Wu, F.T. (1980) Mechanical properties of clays at high pressure. *J. Geophys. Res.* 85, 1462-1468.
- Wang, K. and Bilek, S.L. (2016) Do subducting seamounts generate or stop large earthquakes? *Geology* 39, 819-822.
- Wibberley, C. and Shimamoto, T. (2003) Internal structure and permeability of major strike-slip fault zones: the Median Tectonic Line in Mie Prefecture, Southwest Japan. *J. Struct. Geol.* 25, 59-78.
- Williams, L.B. and Hervig, R.L. (2005) Lithium and boron isotopes in illite-smectite: The importance of crystal size. *Geochim. Cosmochim. Ac.* 69, 5705-5716.
- Wood, A.B. (1941) *A textbook of sound*. G. Bell and Sons, Ltd, London.
- Wu, T.-C., Bassett, W.A., Huang, W.-L., Guggenheim, S. and Koster Van Groos, A. (1997) Montmorillonite under high H<sub>2</sub>O pressures: Stability of hydrate phases, rehydration hysteresis, and the effect of interlayer cation. *Am. Mineral.* 82, 69-78.
- Yagi, Y., Kikuchi, M. and Sagiya, T. (2001) Co-seismic slip, post-seismic slip, and aftershocks associated with two large earthquakes in 1996 in Hyuga-nada, Japan. *Earth Planets And Space* 53, 793-803.
- Yamaguchi, A., Cox, S.F., Kimura, G. and Okamoto, S. (2011) Dynamic changes in fluid redox state associated with episodic fault rupture along a megasplay fault in a subduction zone. *Earth Planet. Sci. Lett.* 302, 369-377.
- Yamaguchi, A., Ujiie, K., Nakai, S. and Kimura, G. (2012) Sources and physicochemical characteristics of fluids along a subduction-zone megathrust: A geochemical approach using syn-tectonic mineral veins in the Mugi mélange, Shimanto accretionary complex. *Geochem. Geophys. Geosyst.* 13, 1-22.
- Yamaguchi, D.K., Atwater, B.F., Bunker, D.E., Benson, B.E. and Reid, M.S. (1997) Tree-ring dating the 1700 Cascadia earthquake. *Nature* 389, 923-924.
- Yamanaka, Y. and Kikuchi, M. (2004) Asperity map along the subduction zone in northeastern Japan inferred from regional seismic data. *J. Geophys. Res.* 109, 1-16.
- Yardley, B.W.D. and Graham, J.T. (2002) The origins of salinity in metamorphic fluids. *Geofluids* 2, 249-256.

- Yoshida, K., Hirajima, T., Ohsawa, S., Kobayashi, T., Mishima, T. and Sengen, Y. (2015) Geochemical features and relative B-Li-Cl compositions of deep-origin fluids trapped in high-pressure metamorphic rocks. *Lithos* 226, 50-64.
- You, C.F., Castillo, P.R., Gieskes, J.M., Chan, L.H. and Spivack, A.J. (1996) Trace element behavior in hydrothermal experiments: Implications for fluid processes at shallow depths in subduction zones.
- You, C.F. and Gieskes, J.M. (2001) Hydrothermal alteration of hemi-pelagic sediments: experimental evaluation of geochemical processes in shallow subduction zones. *Applied Geochemistry* 16, 1055-1066.
- You, C.F., Spivack, A.J., Gieskes, J.M., Rosenbauer, R. and Bischoff, J.L. (1995) Experimental study of boron geochemistry: implications for fluid processes in subduction zones. *Geochim. Cosmochim. Acta* 59, 2435-2442.
- Zhao, D., Huang, Z., Umino, N., Hasegawa, A. and Kanamori, H. (2011) Structural heterogeneity in the megathrust zone and mechanism of the 2011 Tohoku - oki earthquake (Mw 9.0). *Geophys. Res. Lett.* 38, 1-5.